Late Holocene environmental change on the NE Tibetan Plateau: a palaeolimnological study of Lake Qinghai and Lake Gahai, China, based on stable isotopes

Thesis submitted for the degree of
Doctor of Philosophy
University College London

ANDREW CHARLES GRAHAM HENDERSON

Department of Geography
University College London
July 2004

ProQuest LLC
789 East Eisenhower Parkway
P.O. Box 1346
Ann Arbor, MI 48106-1346

Abstract

Climate driven hydrologic variability has direct socio-economic impacts on local, regional and global scales. Particularly vulnerable is the region that lies within the boundaries of the East Asian monsoon, which is one of the most pronounced and influential phenomena of Earth's climate system. People within the heavily populated Asian countries have adapted many aspects of their society to the subtleties of monsoon rains, and are thus highly susceptible to small changes in the timing and intensity of monsoon precipitation. This study aims to reconstruct high-resolution late Holocene climatic and hydrologic variability from Lake Qinghai, NE Tibetan Plateau, using stable isotope techniques. The thesis also examines the modern isotope systematics of Lake Qinghai through mass balance methods to understand the modern hydrology of the lake in order to determine which factors are important in influencing lake water isotope composition. The isotopic compositions of Lake Qinghai's modern waters indicate that they have been modified by evaporation, as they plot below the Global Meteoric Water Line (GMWL). Isotope mass balance models quantify this, and demonstrate that 29 to 35% of the waters entering the lake are from direct precipitation and surface runoff, while evaporation from the lake's surface accounts for 44 to 54% of the lakes water loss. This suggests that the balance of precipitation to evaporation (P/E) is an important control on the composition of lake waters and therefore carbonate incorporated into the sediment record will reflect this. Four cores were used in this study and they provide a palaeohydrological history displaying distinct changes in $\delta^{18}O_{auth}$ and $\delta^{13}C_{auth}$ over the past 1500 years. These are interpreted in terms of effective moisture and one particularly pronounced event, between 1600 and 1850 AD has been attributed to decreases in evaporation. This event, when compared to other regional palaeoenvironmental archives is coincident with cold temperatures, synonymous with the Northern Hemisphere Little Ice Age, tentatively suggested to be a result of solar variability.

Acknowledgements

I thank my principal supervisor, Dr. Jonathan Holmes, for his encouragement, motivation, and scientific input, particularly the finer points of isotope geochemistry and for covering teaching duties when not in the country. I would also like to thank Dr. Melanie Leng as her encouragement and gentle prodding has been invaluable throughout the completion of this research. Additionally, I am indebted to Prof. Rick Battarbee who sparked my fascination in the wonders of Lake Qinghai and for his continuing enthusiasm for the subject!

This PhD would have not been possible without the support of a Department of Geography Teaching Assistantship, which I gratefully acknowledge. Funding for fieldwork and analytical work was generously provided by a host of sources: Department of Geography, UCL Graduate School, The British Council, the ENSIS Trust Fund, the Environmental Change Research Centre, the NERC Isotope Geosciences Laboratory, the NERC Radiocarbon Laboratory, the Royal Society Dudley Stamp Memorial Fund, and Dr. Anson Mackay.

While overseas I have been lucky enough to meet and work with a number of people, many of whom I now call friends and their hospitality and generosity helped make my trips to China so enjoyable. In particular, I would like to thank Prof. Fahu Chen, Dr. Jiawu Zhang, Jin Ming, Jinbao Li, Xiahou Guo, Jijun Li, Yan Zhao and Chengjun Zhang. They acted as fabulous hosts and many worked with me in the field acting as translators, logistical support and explained the finer points of Chinese drinking games. Other 'support' in the field came in the form of Tom 'no trousers' Davidson who despite all attempts to wreck a well-oiled machine proved invaluable help. My thanks go to the people who put me on the right tracks in the laboratory. Namely, Melanie Leng, Carol Arrowsmith, and Hilary Sloane at NIGL, Keyworth, Andy Cundy at the University of Sussex, Charlotte Bryant at the NERC-RCL, East Kilbride and Ian Slipper at the University of Greenwich. I would also like to thank Dr. Tim Jull for analysis of modern water for radiocarbon, Prof. Lonnie Thompson for providing the Dunde ice core data, Dr. Achim Brauning for supplying the temperature composite series and Dr. Hong Chun Li for providing me with the Buddha cave dataset.

I am eternally grateful to my friends at UCL, especially to; Gina Clarke, Sally Luckes, Sam Mendelson, Carl Sayer, Ben Goldsmith, Tom Davidson, Martin Kernan, Patrick Rioual, Helen Bennion, Kira Larsen, David Morley and all the others, for their generosity of spirit and for knowing that if all else fails, there is always the Lord John Russell.

Finally, I would like to thank my family and friends at home, who continue to support me despite my nuances and I dedicate this thesis to my Dad, Martyn John Henderson.

Table of contents

List of figures

List of tables

Chapter One
Introduction

Introduction

Climate-driven hydrologic variability has direct socio-economic impacts on local, regional and global scales. Particularly vulnerable is the region that lies within the boundaries of the East Asian monsoon, which is one of the most pronounced and influential phenomena of Earth's climate system. People of the most heavily populated Asian countries have adapted many aspects of their society to the subtleties of monsoon rains, and are thus highly susceptible to small changes in the timing and intensity of monsoon precipitation. A dry monsoon can have disastrous effects, such as agricultural failure, while flooding related to extreme monsoon rains has proven to be one of the deadliest natural catastrophes. These vulnerabilities are likely to increase in the future with continued population growth, intensified land use and sea level rise. Although there is a growing effort to improve seasonal to interannual monsoon prediction, the largest threats to human health and livelihood could come from unanticipated decade to century-scale extremes in monsoon behaviour. An understanding of natural climatic variability is therefore essential for evaluating anthropogenic impacts on recent and future climate (Crowley, 2000; Mann *et al.,* 1998; Jones *et al.,* 1996) and the consequences that they may have for monsoon circulation. Due to the lack of lengthy instrumental records, such information must be gained from natural archives of climate change.

The 20th Century is unusual as it has been dominated by an almost universal warming trend (Bradley *et al.,* 2002) with temperatures at the end of the century being significantly higher than at the beginning (Jones *et al.,* 1999). However, the warming, as widely acknowledged, varies significantly from region to region (Wang *et al.,* 2001). Regional characteristics of the warming have been less well examined in China due to the lack of long and homogeneous temperature series. It is now beginning to be rationally examined in order to assess modern climate warming in context of longer term, pre-anthropogenic global change (e.g. Wang *et al.,* 2001). Although the application of proxy data to reconstruct temperature series on different timescales will improve understanding of modern warming, there is still a lot of doubt over the behaviour of the monsoons, which are so intrinsically linked to these temperature changes.

The current trend in global change shows that regional climate extremes such as droughts and extreme rainfall are becoming more and more important. Global warming is likely to lead to greater extremes of drying and heavy rainfall and increase the risk of droughts and floods that occur with El Niño events in many different regions (Houghton *et al.,* 2001): determining the teleconnections associated with this climate oscillation is vitally important for assessing monsoon stability. Risk assessment, however, is still difficult, because climate models currently lack the spatial and temporal detail required to make confident predictions (Houghton *et al.,* 2001). In

order to model the regional change to be expected in the future, there is a need to put more effort on the detection, quantification and the cause of *past* regional change.

Critical questions facing people living in monsoonal regions is whether, and if so, how, a rapid and significant change in global climate might affect the monsoon system. Enhanced understanding of the factors governing variability of the flux of heat and moisture within these systems is critical, as these are the principal components that drive the monsoon circulation. Therefore past histories of monsoon climates are important in answering these questions, to provide evidence of the past behaviour of the monsoons at times when global climate was different from today and to provide insights into the nature and regional impacts of future climate changes.

1.1 Research aims

Numerical modelling simulations of the East Asian monsoonal precipitation have shown that the arid regions of NW China are very sensitive to climatic change, whereas eastern China displays a diminished response (An *et al.*, 2000). The Tibetan Plateau plays an important role in monsoon generation due to its high-altitude and its position at a critical climatic boundary. However, much of our climatic understanding of the monsoon systems has been established through records derived from the Loess Plateau in central China and from low resolution lake records from the Tibetan Plateau itself. There is a need for much higher resolution records, particularly in the late Holocene to understand past monsoon/climate variability from this region.

The aim of this research is to reconstruct late Holocene (*c.* last 1000 years) climatic and hydrologic variability in the Lake Qinghai drainage basin through isotopic and related analyses of lake sediments. Lake Qinghai (100°E, 37°N, 3194 m a.s.l) (Fig. 1.1) is the largest inland lake in China (4300 km^2). It lies in a hydrologically-closed basin and has a present-day salinity of around 15 ‰ as a result of evaporative enrichment. Lake Qinghai is an important site, as it lies at the climatic boundary of the present-day monsoon, with the pressure system that lies to the southwest, prevailing dry winds from the northwest and a precipitation gradient to the southeast which increases steadily towards the coast, marking a 'triple junction' of climatic influences. Moreover, previous studies have shown the lake to have a continuous sedimentary record stretching back at least to the last glacial maximum (Kelts *et al.*, 1989; Lister *et al.*, 1991), with variations in lake level attributed to changes in the effective moisture balance, reflecting shifts in monsoon circulation. It is therefore ideally located to investigate variations in monsoon circulation during the late Holocene using high-resolution lake sediment records.

Specific research objectives of the project are:

(1) To assess Lake Qinghai's modern hydrology by establishing its isotopic systematics and developing an isotope mass balance model; key questions are:

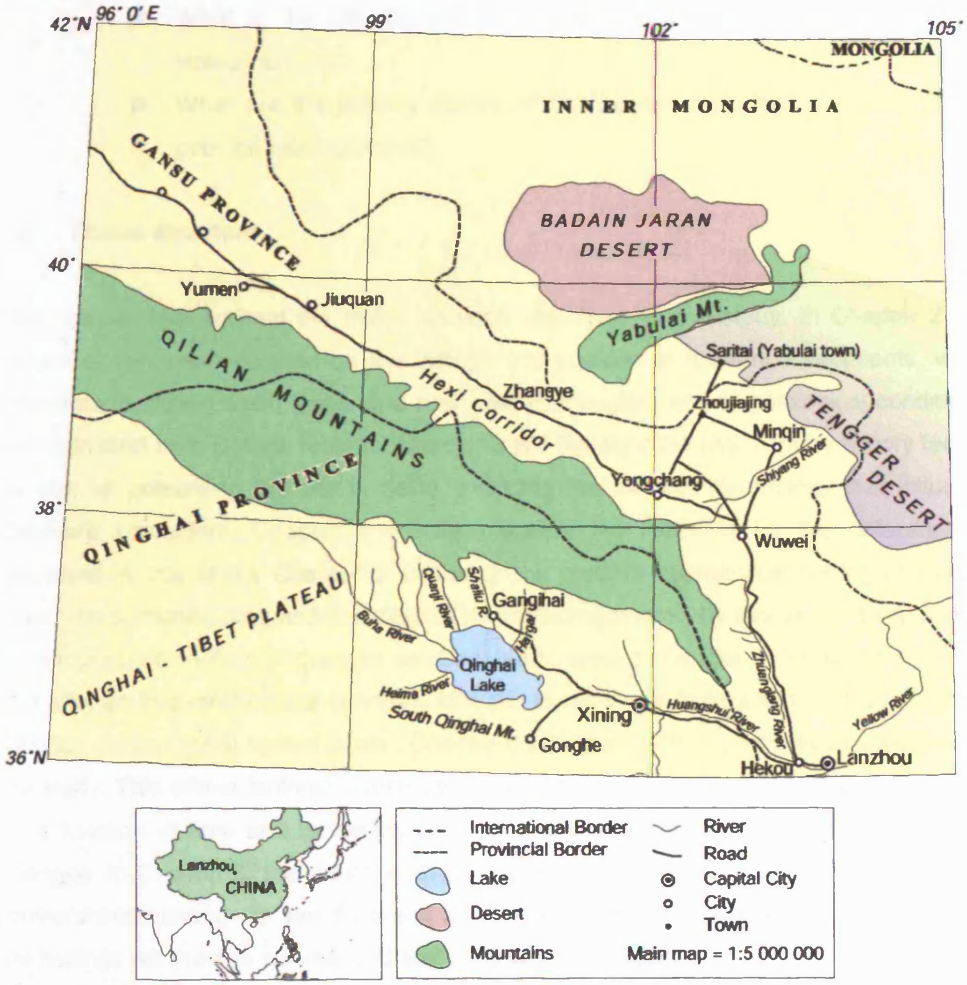

Figure 1.1 – Location map of Lake Qinghai on the NE Tibetan Plateau, China.

i. What is Lake Qinghai's modern lake hydrology?
ii. What factors affect lake water isotope composition?

(2) To construct a chronology to determine sediment accumulation rates using a combination of the radioisotopes namely, ^{210}Pb, ^{137}Cs and ^{14}C;

(3) To reconstruct palaeohydrology from sediment cores using stable isotope composition of authigenic and biogenic lacustrine carbonates ($\delta^{18}O$, $\delta^{13}C$) and isotopic ($\delta^{13}C_{org}$) and elemental (C/N) composition of organic matter;

(4) To evaluate the palaeohydrological record in terms of forcing mechanisms and compare the record from Lake Qinghai with other palaeoclimatic archives, in order to assess whether there is a clear, regionally-synchronous climatic signal (e.g. Thompson *et al.*, 1989); key questions being:

a. What is the climatic and hydrologic history of Lake Qinghai during the late Holocene?

b. What are the primary modes of climatic and hydrologic variability in the region over the late Holocene?

1.2 Thesis structure

This chapter has outlined the major research objectives of the study. In Chapter 2, there is a review of the major controls on the isotopic composition of lacustrine sediments, with specific reference to closed basin lakes, and how past hydrological and climatological conditions can be reconstructed from isotope records. Chapter 3 will highlight the past climate history for NW China as well as presenting the site in detail, including the modern climatology that influences Lake Qinghai's catchment. Chapter 4 will then outline the methods for the different techniques employed in this study. Chapter 5 evaluates the modern hydrological setting of Lake Qinghai, based on published data and limnological information gathered by this study. It will show how the contemporary limnology of the lake can be used to assess changes in the lake's sediment record and attempt to quantify these changes. In order to put these changes in context of other regional records, chronological control is vital; Chapter 6 will develop the age models for each core used in the study. This allows isotopic investigations on the sediment cores (Chapter 7) to be discussed as a function of time and to assess whether there is whole lake response to any hydrological changes. In Chapter 8, the results of these investigations will be compared with other records of environmental change to see if there is a regionally synchronous response to climate forcing. All the findings will then be summarised and concluded in Chapter 9.

Chapter Two
Using stable isotopes to reconstruct past climate

Introduction

Stable isotopes of oxygen and carbon have been become increasingly used in recent decades to reconstruct past climates in a range of hydrological contexts. Lake systems are complex, with many possible-controlling mechanisms on resulting water chemistry and inorganic precipitates. Moreover, inadequate understanding of the isotopic systematics of lakes means that such systems are often underdetermined. The aim of this chapter is to review the processes controlling oxygen and carbon isotope ratios in the lacustrine environment. Firstly, the use of lake sediments, in particular from closed basins, will be discussed (section 2.1), followed by a review of the processes controlling oxygen isotopes in the hydrological cycle (section 2.2) and the processes by which information about such change is inferred to the sediment record, especially the carbonates (section 2.3). Controls on a lake's carbon budget and resulting changes in $\delta^{13}C$ values in both carbonates and organic carbon are also discussed (section 2.4).

2.1 Lakes

Lakes are excellent sensors of environmental change. Their sediment records are abundant in space and time, being found under a wide range of climatic conditions at all latitudes and altitudes. They contain a wealth of multi-proxy information and represent one of the richest geological climate archives. However, climate influences lakes in many different ways (summarised in fig. 2.1) and the direct and indirect linkages between climate and lake water column need to be understood to realise the full potential of lake sediments as palaeoclimate archives (Battarbee, 2000).

Changes in the water balance, particularly in semi-humid to semi-arid environments, have an impact on lake levels and lake-water residence times. Changes in lake level influence the structure of marginal habitats, can re-distribute sediment and significantly alter the ionic composition and salinity of the water body (Eugster and Hardie, 1978). Additional impacts arise from climatically-induced changes in a lake's catchment, not only through modification of catchment hydrology but also through biogeochemical processes like rates of mineral weathering, dissolved organic carbon production and nutrient and alkalinity generation (Battarbee, 2000). Given these counteractive forcings on a lake, the challenge is to determine which processes are important in a lake's environmental history and how these climatically driven changes are recorded in the lake's sediment record.

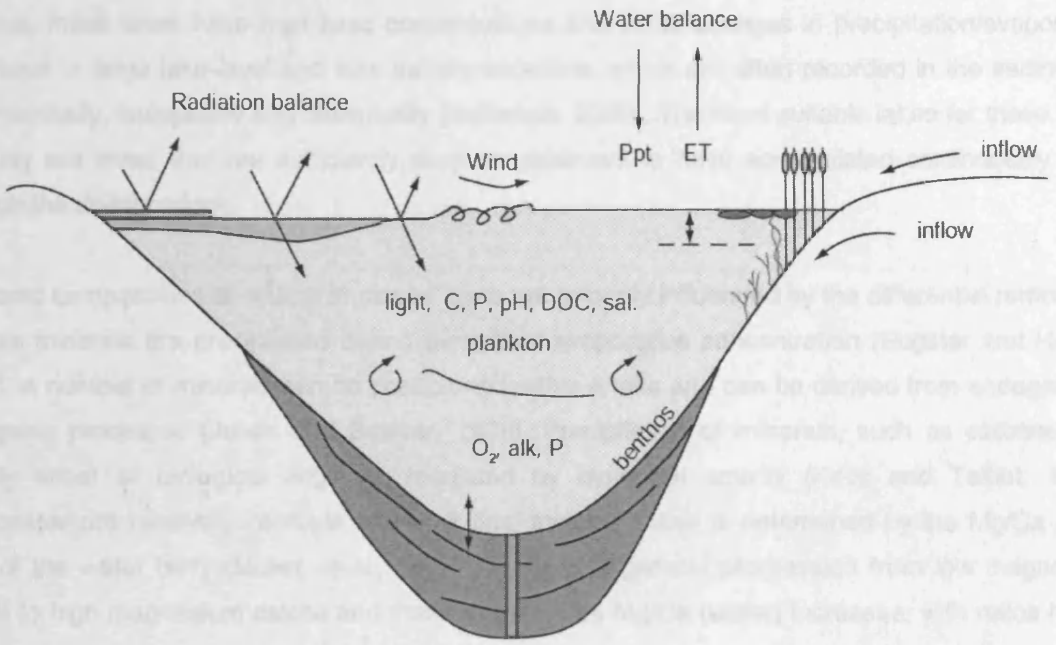

Figure 2.1 – Schematic diagram to show examples of the principal physical, chemical and biological responses of lake systems to changes in climate forcing (from Battarbee, 2000). Ppt = precipitation, ET = evapotranspiration, DOC = dissolved inorganic carbon, C = carbon, P = phosphorous, sal = salinity, O_2 = oxygen and alk = alkalinity.

Palaeolimnological methods have principally been used to reconstruct changes in effective moisture (precipitation/evaporation, P/E) and temperature, although there have been attempts to relate sediment records to a number of other climate variables, such as wind regimes (Bradbury *et al.*, 1993), moisture sources and atmospheric circulation patterns (McKenzie and Hollander, 1993) and atmospheric pCO_2 (Street-Perrott *et al.*, 1997). However, it is often difficult to attribute individual effects as the water body to individual controls. In general, palaeolimnological approaches to climate reconstruction are indirect and require an understanding of the relationship between the sediment record and water-column processes and between water-column processes and climate. The following section will concentrate on how stable isotope techniques, based on authigenic and biogenic carbonates as well as organic carbon, can be used to determine past lake level fluctuations and changes in P/E (or a lake's palaeohydrology), with specific reference to closed-basin lakes and within lake and catchment carbon cycles.

2.1.1 Hydrologically-closed lakes

Hydrologically-closed lakes are commonly found in semi-humid to semi-arid regions. Their annual evaporation exceeds precipitation and since they have little or no outflow, either by surface or via

groundwater, are subsequently responsive to moisture balance changes. Depending on their water balance, these lakes have high ionic concentrations and small changes in precipitation/evaporation can result in large lake-level and lake salinity variations, which are often recorded in the sediments, geochemically, isotopically and biologically (Battarbee, 2000). The most suitable lakes for these kinds of study are those that are sufficiently deep for sediment to have accumulated continuously even through the driest periods.

The ionic compositions of waters in closed lakes are strongly influenced by the differential removal of ions as minerals are precipitated during periods of evaporative concentration (Eugster and Hardie, 1978). A number of minerals can be precipitated within a lake and can be derived from endogenic or authigenic processes (Jones and Bowser, 1978). Precipitation of minerals, such as carbonate, is usually either of biological origin or mediated by biological activity (Kelts and Talbot, 1990). Carbonates are relatively insoluble and their final mineral phase is determined by the Mg/Ca molar ratio of the water body (Muller *et al.,* 1972). There is a general progression from low magnesium calcite to high magnesium calcite and then aragonite, as Mg/Ca (water) increases; with ratios higher than seven generally producing aragonite. Other sedimentary deposits include clastic mineral grains – from a range of organic components derived from lake biota, endogenic minerals precipitated from the water column and diagenetic precipitates from sedimentary pore waters (Kelts and Talbot, 1990). The geochemical signals contained in these authigenic and biogenic carbonates can provide information about past climate changes as they reflect the prevailing environmental conditions in the lake at the time of their precipitation.

2.2 Controls on isotopes in precipitation

Following the formation of the International Atomic Energy Agency (IAEA) global network for isotope in precipitation (GNIP) Craig (1961) and Dansgaard (1964) identified a number of relationships between oxygen and hydrogen isotope ratios in precipitation and physical and climatic factors. These factors include temperature (Rozanski *et al.,* 1992; Rozanski *et al.,* 1993) seasonality, altitude, continentality (Rozanski *et al.,* 1993) and the amount of precipitation and its source (Araguas-Araguas *et al.,* 1998; Araguas-Araguas *et al.,* 2000; Rozanski *et al.,* 1993; Johnson and Ingram, 2004; Hoffmann and Heimann, 1997; Tian *et al.,* 2001; Tian *et al.,* 2003).

During the process of evaporation, water vapour becomes depleted in the heavier ^{18}O (and ^{2}H), while residual water becomes enriched. During precipitation, the heavier isotope condenses first and is enriched in rain and snow, whereas the cloud moisture is subsequently depleted in ^{18}O (and ^{2}H) as the rain out continues. Most of the evaporation occurs in the sub-tropics, from where water is transported to higher latitudes. During this transport, water is lost through precipitation, leaving the

residual water vapour more and more enriched in ^{16}O (and ^{1}H) according to processes approximating a Raleigh distillation model (Araguas-Araguas *et al.,* 2000; Rozanski *et al.,* 1993). As a result a global trend of atmospheric precipitation that shows precipitation becoming progressively depleted in ^{18}O (and ^{2}H) towards the poles. The oxygen isotope composition of mean annual precipitation varies globally (Yurtsever and Gat, 1981) (Fig 2.2) and the covariation in $\delta^{18}O$ and δD defines a global meteoric water line (Craig, 1961).

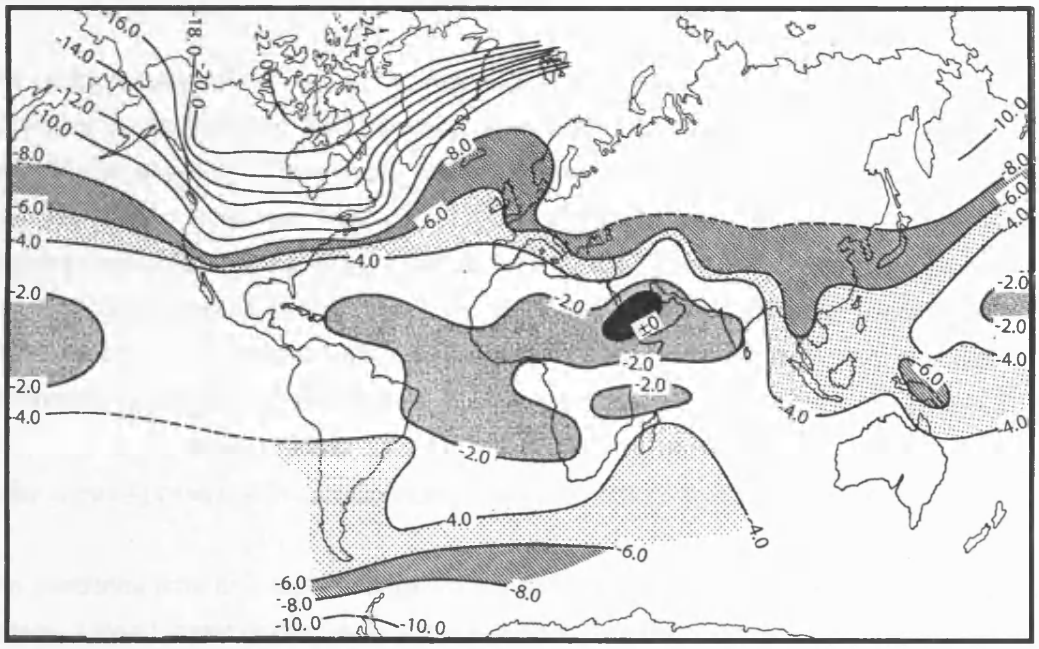

Figure 2.2 – Modern-day global distribution of mean $\delta^{18}O$ (‰ VSMOW) in precipitation (from Leng, 2003 based on Yurtsever & Gat, 1981).

There is a series of additional effects that influences the isotopic composition of precipitation. Outside the tropics, intense precipitation events are more depleted in heavier isotopes than light rains (amount effect), winter precipitation is more depleted than summer precipitation (seasonality effect), while isotopic depletion increases with altitude of precipitation (altitude effect). δp, which is either $\delta^{18}O$ or δD, varies systematically with mean annual precipitation (Clark and Fritz, 1997), thus broadly correlating with latitude and altitude of a site (Bowen and Wilkinson, 2002). This global relationship between δp and temperature ($d\delta p/dT$ ~ 0.2 to 0.7‰/°C) is sometimes referred to as the 'Dansgaard relationship' (Dansgaard, 1964). Therefore, depending on which of these effects is the most important in influencing local precipitation, will have some bearing on the isotope composition of lake water, together with any within lake effects. The isotope values of precipitation over the Tibetan Plateau and Lake Qinghai are discussed later (section 5.2).

2.3 Controls on oxygen isotopes in lake water

The oxygen isotope composition of lake water will reflect the isotopic composition of the precipitation received by the lake, together with subsequent modification of lake water by evaporation and environmental processes occurring within the catchment (Gat and Lister, 1995). In closed-basins, many processes manipulate the isotopic composition of lake water, whereas in an open lake, lake water will predominantly reflect the isotopic composition of precipitation.

The dominant control on the $^{18}O/^{16}O$ ratio in hydrologically-closed lakes is evaporative fractionation, controlled by temperature and humidity. The isotope composition of a lake's water is therefore generally enriched in ^{18}O due to the preferential removal of the lighter isotope ^{16}O, particularly if the lake has a long residence time, (Fig. 2.3). The effect of evaporation on a closed basin can be assessed by comparing the oxygen isotope values from lake waters with a meteoric water line (MWL) (Fig. 2.3). Lake waters that are close to the MWL are isotopically similar to precipitation, whereas lake waters that plot away from the MWL define a local evaporation line and have undergone evaporative enrichment (Gonfiantini, 1986) (Fig. 2.3). During periods of decreased precipitation to evaporation (P/E) lake levels become lower as climate is more arid and the resulting $\delta^{18}O$ composition of lake water is more positive, with corresponding lower $\delta^{18}O$ values in humid phases.

The residence time of a lake is therefore important in the control of the isotope composition of lake waters. Closed basin lakes usually have longer residence times than open lakes. The isotope composition of hydrologically-closed systems will therefore display larger variability as they are generally more sensitive to changes in the P/E ratio. However, if a lake's residence is substantial (*c.* 100s – 1000s of years) the isotope composition of water will be an average of many years flux through the system (Ricketts and Johnson, 1996).

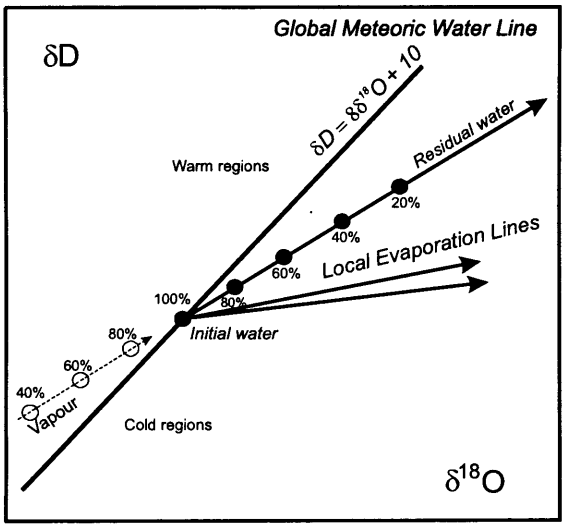

Figure 2.3 – Major controls on the $\delta^{18}O$ vs. δD of precipitation and lake waters. (from Leng and Marshall 2004).

2.3.1 Isotope steady-state

The isotope composition of water in hydrologically-closed lakes will reach steady-state (i.e. a singular isotopic composition) if lake level remains relatively constant, regardless of lake volume. This is because the net evaporation evolves to a value equal to the composition of the inputs during time of constant lake level (Ricketts and Johnson, 1996). Rather than the lake volume defining the direction of isotope shift, it is the increase (or decrease) of input rate relative to the output rate that will effect isotope composition of lake water. If the isotope composition of the inputs or outputs to/from a lake shift abruptly then a new steady-state value for lake water is achieved, although this occurs in approximately 3 – 5 residence times of a closed basin lake (Ricketts and Johnson, 1996).

Short-term lake level fluctuations caused by changes in increased effective moisture (P>E) will cause higher lake levels and a more negative $\delta^{18}O$ composition of lake water. As inputs to the lake return to normal, evaporation becomes the dominant control and the lake returns to its original lake level and its previous steady-state composition (Lister *et al.,* 1991). The magnitude and duration of these excursions will depend on whether they are a single event or an accumulation of events and the ability of the lake water reservoir to dilute the isotope signal. If such events persist then the $\delta^{18}O$ of water establishes a new steady-state. However, different isotope responses occur depending on whether there is an establishment of a new hydrologic or climatic regime (Lister *et al.,* 1991).

Increased regional humidity, for example, may shift both precipitation and evaporation rates leading to greater inputs and decreased outputs creating a change in lake-level. This lake-level change must be reached in order for the new surface area to accommodate both a higher input rate and a decreased evaporation rate (Lister *et al.,* 1991). Increased humidity at an inland location may be considered as decreased continentality, so accompanying $\delta^{18}O$ values for precipitation can be expected to be more positive. There will also be less direct evaporation within the catchment, although an increased vegetation cover (e.g. grass to trees) may in fact initially increase the evapotranspiration loss and attenuate the runoff characteristics. $\delta^{18}O$ values could shift negatively during the transition and then embark on a less severe isotopic enrichment gradient corresponding to the new regime (Lister *et al.,* 1991).

Changes in mean annual air temperature, which may accompany humidity changes, alter both the $\delta^{18}O$ values for precipitation and the evaporation rates, which modify the $\delta^{18}O$ values for runoff. Also a shifting pattern for seasonal rainfall distribution may alter the net $\delta^{18}O$ value for annual lake input. This cumulative isotope effect on lake water $\delta^{18}O$ values is multi-faceted and will reflect different combinations of factors that act in concert. This can effectively preclude the quantification of individual isotopic controls (Lister *et al.,* 1991).

2.4 Controls on oxygen isotopes in lake sediments

The isotopic composition of lacustrine carbonates is a reflection of the isotopic composition of lake water and the temperature at which the carbonate was precipitated, together with any vital or kinetic effects (Fig. 2.4). Perhaps more importantly, since semi-arid environments are subject to strong evaporation, the oxygen isotope compositions of carbonate mostly reflect changes in the oxygen-isotopic composition of the lake water. Consequently, they are potentially very sensitive palaeohydrological indicators, as the isotopic composition of waters is mainly controlled by the composition of the input waters and by evaporation effects i.e. effective moisture. $\delta^{18}O$ records from lakes in semi-arid regions are subsequently interpreted in terms of past changes in precipitation/evaporation ratios.

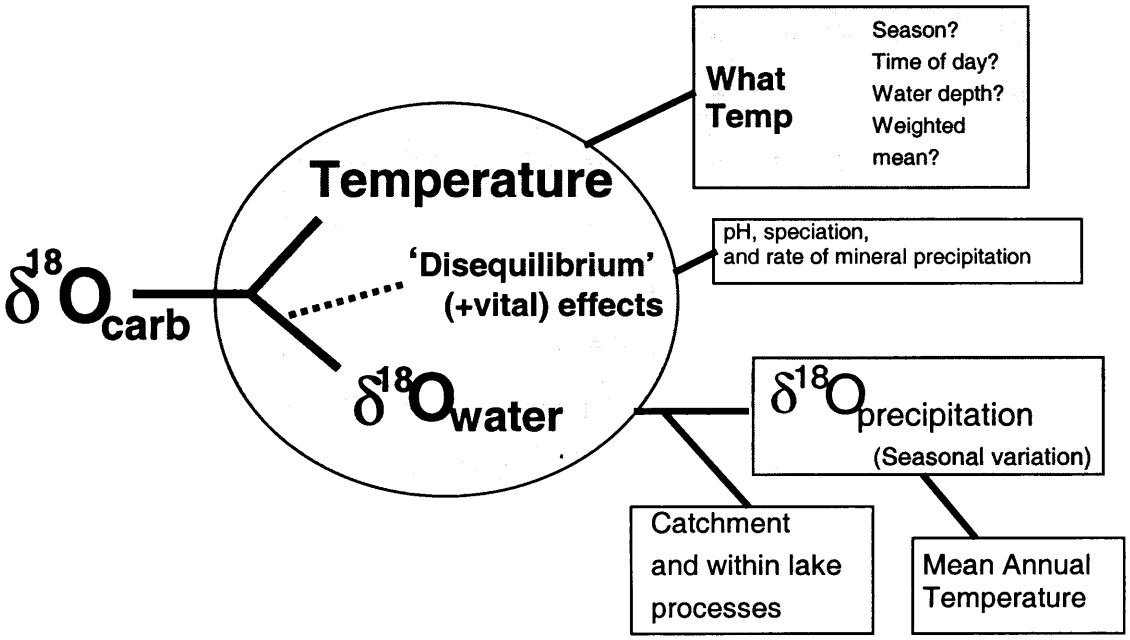

Figure 2.4 – Controls on the oxygen isotope composition of lacustrine carbonates (δ^{18}Ocarb) (from Leng and Marshall, 2004).

2.4.1 Authigenic carbonate

Carbonate precipitation in lakes occurs as bicarbonate is utilised during photosynthesis by aquatic plants and algae (McKenzie, 1985), where:

$$Ca^{2+} + 2HCO_3^- \rightarrow CO_2 + CaCO_3 + H_2O \qquad (2.1)$$

During carbonate precipitation there is a temperature dependent carbonate-water fractionation of oxygen isotopes. Values measured from precipitating carbonate ($\delta^{18}O_{auth}$) are therefore dependent on the temperature of lake water. The value of $\delta^{18}O$ decreases at about 0.24‰/°C (Craig, 1965) as a result of this fractionation.

A number of studies have attempted to determine the empirical relationship between temperature, the oxygen isotope composition of different carbonate minerals and the composition of the water in which they form (e.g. Craig, 1965; Grossman and Ku, 1986; Kim and O'Neil, 1997). The temperature dependence of ^{18}O content in calcite can be expressed as (Craig, 1965):

$$T°C = 16.9 - 4.2(\delta_c - \delta_w) + 0.13(\delta_c - \delta_w)^2 \quad (2.2)$$

Where δ_c is the $\delta^{18}O$ of the carbonate (VPDB) and δ_w is the $\delta^{18}O$ of lake water (VSMOW). Further experimental work by Kim and O'Neil (1997) proposes the following equilibrium fractionation relationship for calcite:

$$1000 \ln \alpha_{(calcite-water)} = 18.03(10^3 T^{-1}) - 32.42 \quad (2.3)$$

Where T is the temperature in Kelvin and α is the fractionation between mineral and water $(^{18}O/^{16}O)_{calcite}/(^{18}O/^{16}O)_{water}$. However, Leng and Marshall (2004) have re-expressed the Kim and O'Neil relationship as:

$$T°C = 13.8 - 4.158(\delta_c - \delta_w) + 0.08(\delta_c - \delta_w)^2 \quad (2.4)$$

Where δ_c is the $\delta^{18}O$ of the carbonate (VPDB) and δ_w is the $\delta^{18}O$ of lake water (VSMOW). The authors suggest that this relationship be adopted as a measure of equilibrium, although as they acknowledge, calculated temperatures for calcite formation will be lower than those derived from the Craig equation.

There is a small fractionation effect on $\delta^{13}C$, with values becoming lighter with increasing temperature, however the effect is small *c.* 0.08‰/°C and largely ignored as it will usually be lost in the overall isotope signal as other factors are more important (Leng and Marshall, 2004).

2.4.2 Biogenic carbonate

Ostracods are small aquatic bivalved crustaceans that form a low-Mg calcite shell that are often well preserved in lake sediments. They moult up to nine times during their lifecycle (De Deckker, 1988), with each stage ('instar') formed rapidly from calcium carbonate in the host waters (Turpen and Angell, 1971). Therefore ostracod shell composition represents only a short period of time, from a few hours to days and subsequently a number of individuals are needed to be analysed from any sample level to show variation in $\delta^{18}O$ of the timeframe represented by that sample.

The carbonate precipitated by ostracods to make shells will form in disequilibrium with lake waters, as additional species-specific fractionation or 'vital effects' occur that will shift isotope values away from equilibrium. These effects are most commonly seen in $\delta^{18}O$ composition of ostracod shells and have been documented by a number of studies (Holmes and Chivas, 2002; von Grafenstein *et al.,* 1999; Xia *et al.,* 1997). Recent research has suggested that the offset between water and ostracod carbonate can be attributed to differences in internal pH and rate of calcification within the organism (Keatings *et al.,* 2002). It has also been demonstrated that different species living at the same time in the same lake yield different $\delta^{13}C$ values (Heaton *et al.,* 1995) probably due to difference in microhabitat water isotope values and seasonal differences in periods of shell growth.

2.5 Indirect controls on oxygen isotope composition of carbonates

2.5.1 pH

The precipitation of carbonate consumes calcium, carbon and oxygen from the host waters, with the isotope composition of the precipitated carbonate largely dependent on the isotopic composition of lake water. However, the relative fraction of inorganic carbon species present in lake water is dependent on pH (Fig. 2.5). At low pH aqueous CO_2 is the dominant species, whereas HCO_3^- is most abundant at intermediate pH, and CO_3^{2-} is the dominant carbonate species in solution at high pH (Zeebe, 1999).

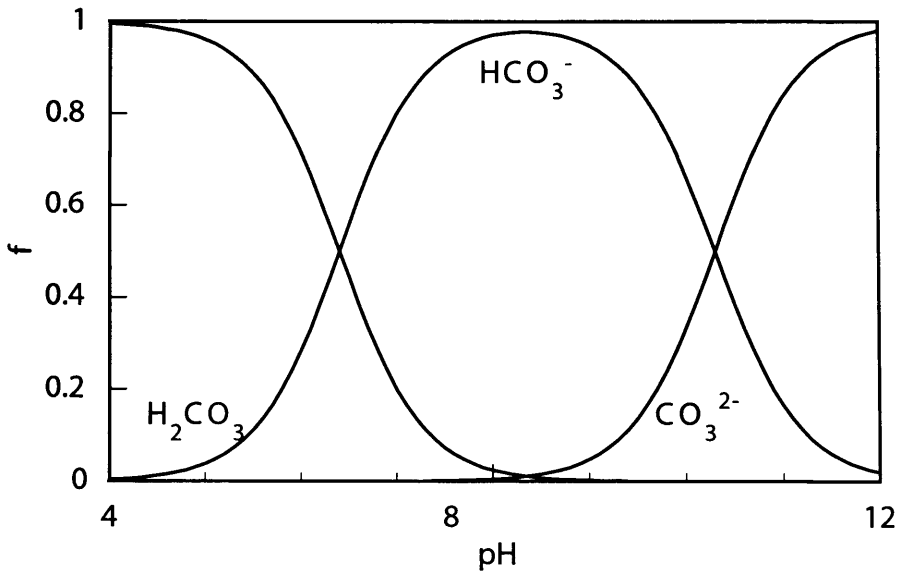

Figure 2.5 – The concentration of the dissolved carbonate species as a function of pH. f refers to the fraction of carbonate species in solution (adapted from Zeebe, 1999).

The interaction between water and atmospheric CO_2 means CO_2 becomes dissolved in water, the subsequent solution contains unhydrated CO_2 at about the same concentration by volume as in the atmosphere, so that:

$$CO_2\ (g) = CO_2\ (aq) + H_2O \tag{2.3}$$

Dissolved CO_2 then hydrates by a slow reaction to yield carbonic acid:

$$CO_2 + H_2O = H_2CO_3 \tag{2.4}$$

This reaction predominates at a pH of less than 8, but H_2CO_3 is a weak acid and dissociates rapidly relative to the hydration reaction:

$$H_2CO_3 = H^+ + HCO_3^- \tag{2.5}$$
$$HCO_3^- = H^+ + CO_3^{2-}$$

These bicarbonate and carbonate ions dissociate to establish equilibrium (Fig. 2.5).

Zeebe (1999) demonstrated that water becomes marginally enriched in ^{18}O as the dominant species in solution changes from CO_2 to HCO_3^- as a result of pH increase, because CO_2 is isotopically heavier than HCO_3^- (Fig. 2.6). Therefore CO_2 is the isotopically heaviest species followed by H_2CO_3 (enriched

in ^{18}O compared to HCO_2^- and CO_3^{2-}), whereas CO_3^{2-} is isotopically the lightest species (Zeebe, 1999) (Fig. 2.6).

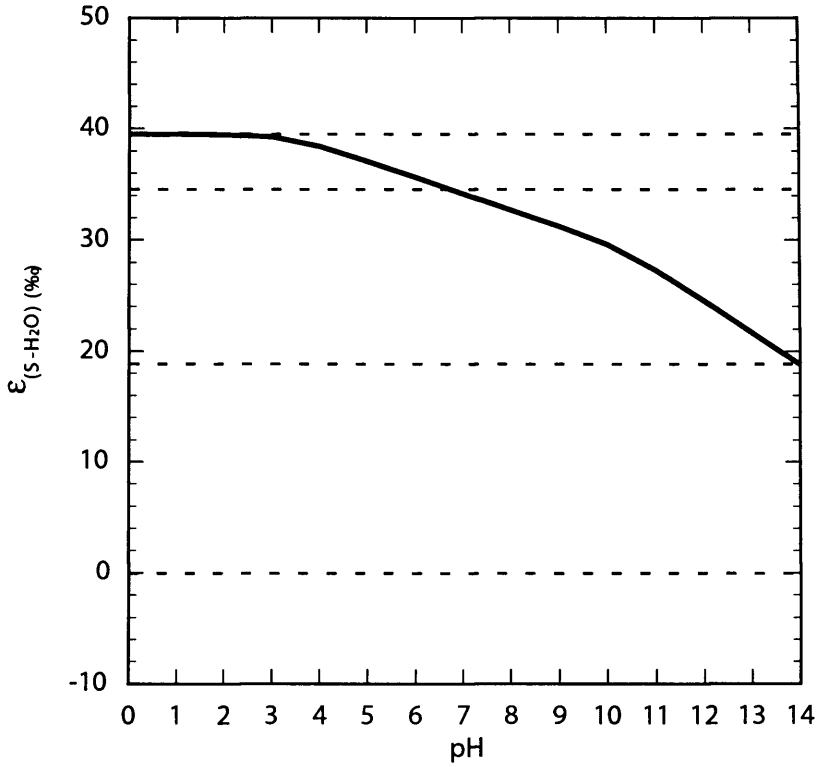

Figure 2.6 – The oxygen isotope partitioning between water and carbonate species as a function of pH (adapted from Zeebe, 1999).

2.5.2 Mineralogy

The mineralogy of the precipitated carbonate can also alter the $\delta^{18}O$ composition of lake sediments. Aragonite and magnesium calcites that precipitate at equilibrium generally have $\delta^{18}O$ values that are higher than low magnesium calcites. Aragonite $\delta^{18}O$ values are typically around + 0.6‰ higher than equivalent calcite (Grossman, 1984; Abell and Williams, 1989). Magnesium calcites typically have $\delta^{18}O$ values that are elevated by 0.06‰/mol% $MgCO_3$ (Tarutani *et al.,* 1969). For both aragonite and high magnesium calcite the magnitude of the offset from the calcite value appears to be independent of temperature (Kim and O'Neil, 1997).

2.6 Controls on carbon isotopes in lake sediments

Controls on the $\delta^{13}C$ values of lake water are complex and dependent on a variety of local limnological conditions. The $\delta^{13}C$ of carbonates is a reflection of the temperature of carbonate

precipitation from the total dissolved inorganic carbon (TDIC) pool and its isotope composition. The isotope composition of a lake's TDIC is influenced by two main processes: photosynthesis/respiration of aquatic plants within the lake and CO_2 exchange between the atmosphere and lake water (Fig. 2.7).

Aquatic photosynthesis results in the preferential uptake of ^{12}C by aquatic plants for assimilation into organic matter. This results in the carbon pool becoming depleted in ^{12}C and consequently it has a higher amount of the heavier isotope ^{13}C. This effect will be countered if organic matter is then oxidised at the lake bed, releasing ^{12}C back into the carbon pool (McKenzie, 1985). Additionally, if terrestrial carbon is incorporated into the lake sediments the amount of ^{12}C released will be greater than that removed by plants resulting in a decreasing $\delta^{13}C$.

Enriched $\delta^{13}C$ values in the TDIC can also occur as a result of exchange with atmospheric CO_2. This is because hydrologically-closed lakes tend to have longer residence times and therefore undergo isotopic equilibration with atmospheric CO_2. Under isotopic equilibrium with atmospheric CO_2, the TDIC pool which normally has a $\delta^{13}C$ value of – 7‰, the lake TDIC would have a $\delta^{13}C$ value of + 1‰ to + 3‰ (VPDB) unless it is modified by photosynthetic activity within the lake (Li and Ku, 1997).

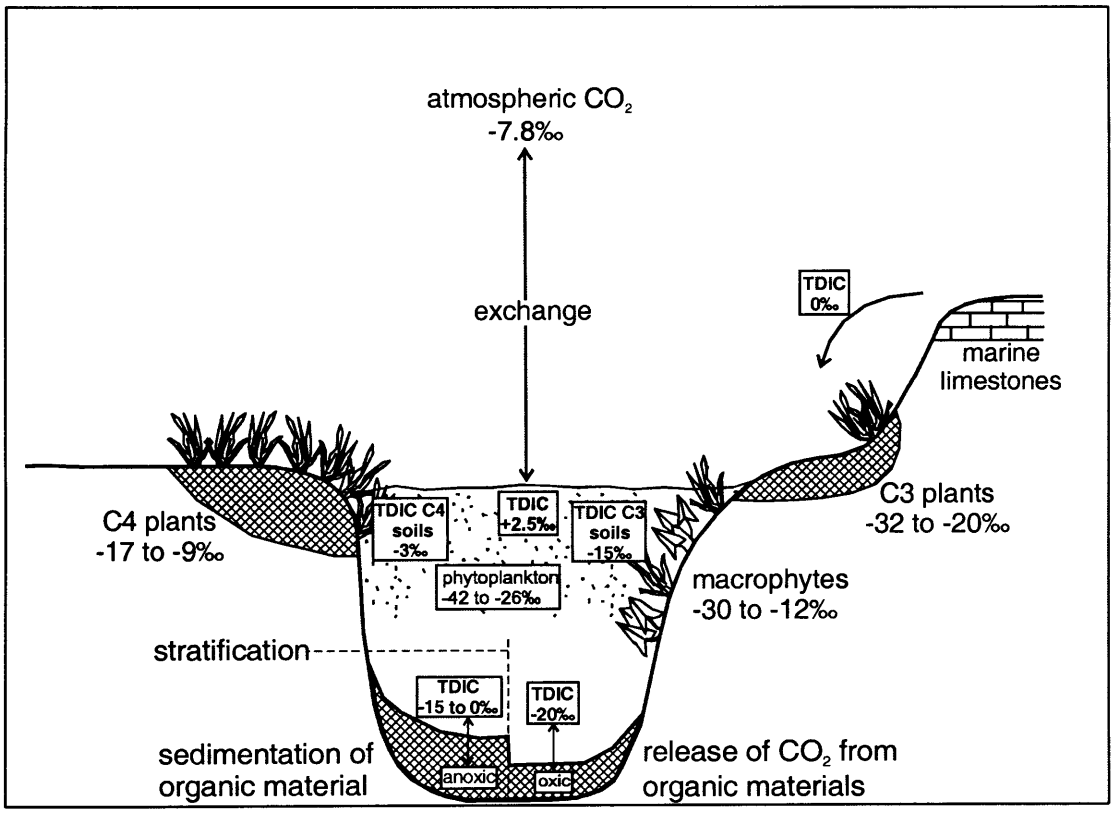

Figure 2.7 – Carbon isotope values for the major sources of carbon into lakes and examples of the range of resulting $\delta^{13}C_{TDIC}$ (from Leng and Marshall (2004).

2.7 Isotope covariance

Isotopic covariance is often a feature of authigenic carbonates formed in closed basin lakes (Talbot, 1990). The presence or absence of a covariant trend in the modern environment is a useful indicator of the strength of isotopic effects in the lake. This type of analysis is restricted to authigenic carbonate as covariance is generally weaker or absent in biogenic carbonates, as $\delta^{13}C$ values are heavily influenced by local habitat effects and are therefore poorly correlated with $\delta^{18}O$. Talbot (1990) suggested that isotope covariance is due to hydrological effects associated with dilution and concentration balances.

If lake volume experiences rapid decline as a result of intense net evaporation, the lake $\delta^{18}O$ will increase rapidly because ^{16}O preferentially goes to the vapour phase. Lake volume decline will also result in an increase of the $\delta^{13}C$ value for the lake TDIC. Therefore a rapidly declining lake will show elevated $\delta^{13}C$ and $\delta^{18}O$ values, giving rise to strong isotopic covariance with heavy δ values for both isotopes. However, as Li and Ku (1997) argue, the increase of $\delta^{13}C$ can be attributed to three effects; (1) since freshwater is usually more depleted in ^{13}C than lake water, under condition of evaporation exceeding precipitation, photosynthetic removal of organic carbon would lead to an increase of lake $\delta^{13}C$, even if the lake productivity remains unchanged, (2) strong evaporation raises pCO_2 of the lake, causing a net loss of CO_2 to the atmosphere, with lighter $\delta^{13}C$ than lake water $\delta^{13}C$, and (3) mixing across the thermocline or chemocline of a lake which supplies nutrients from deep water to the eutrophic zone where phytoplankton grow. Therefore, as lake volume declines due to reduced freshwater input or an intensified evaporation, increased vertical mixing would enhance surface productivity and lead to elevated $\delta^{13}C$ in the lakes TDIC (Li and Ku, 1997).

Usually in lakes that precipitate carbonates with a high $\delta^{18}O$, there is a high $\delta^{13}C$ as vapours exchange between lake water and the atmosphere forces them to approach steady-state values, reflecting a level of equilibration in the TDIC with atmospheric CO_2 and the preferential evaporative loss of ^{16}O. The rate of vapour exchange may go hand in hand with the rate of CO_2 exchange between lake water and the atmosphere. The effect of CO_2 exchange on the carbon isotope fractionation therefore may be a function of lake volume changes, linked to climate controls. A rapid increase in lake volume tends to reduce CO_2 exchange between lake water and the atmosphere, causing the lake $\delta^{13}C$ to approach steady-state more slowly, toward a value that is lighter than under a stable lake volume. The opposite effects, i.e. lake $\delta^{13}C$ is driven toward a heavier steady-state value at a more rapid pace than the stable condition, would characterise the case for a strong decline in lake volume. However, these effects of CO_2 or vapour exchange on lake $\delta^{13}C$ in response to lake-level fluctuations should be relatively minor when compared to the dilution effect and the influence of evaporation (Li and Ku, 1997).

2.8 Organic carbon

The $\delta^{13}C$ of organic matter is dependent on the influences of the TDIC, from which submergent aquatic plants fix their carbon, as well as the difference between different sources of organic matter (Fig. 2.6) (Meyers and Lallier-Verges, 1999; Meyers and Teranes, 2001). Studies of organic matter in lake sediments have demonstrated that carbon isotope ratio can vary considerably. The most important control is the effects associated with different photosynthetic pathways and productivity (Ariztegui *et al.,* 1996). Although different sources of organic matter may have different $\delta^{13}C$ values (Meyers and Lallier-Verges, 1999; Leng and Marshall, 2004), there is considerable overlap in the $\delta^{13}C$ of various plants (Fig. 2.7).

The $\delta^{13}C$ value of organic matter in lake sediments will be derived from a mixture of a number of sources making their interpretation complex. For terrestrial plants, floating and emergent aquatic macrophytes, the $\delta^{13}C$ will reflect the relative input from C_3 plants ($\delta^{13}C$ = – 22‰ to – 33‰) and C_4 plants ($\delta^{13}C$ = – 9‰ to – 16‰) (Smith and Epstein, 1971; Deines, 1980; Holmes *et al.,* 1999). C_4 plants are favoured by aridity, high temperature and/or low partial pressure of atmospheric CO_2 (Holmes *et al.,* 1999). In the case of submerged aquatic macrophytes, their $\delta^{13}C$ depends on the $\delta^{13}C$ of the source carbon (atmospheric CO_2, biogenic CO_2, co-methanogenic CO_2 or HCO_3^-) and on the degree of isotopic fractionation with respect to the source (Holmes *et al.,* 1999; Keeley and Sandquist, 1992). Additionally, the degree of fractionation into aquatic macrophytes and algae is reduced in carbon-limited ecosystems, which give rise to higher $\delta^{13}C$ values. This can include lakes of high pH, salinity and temperature (Holmes *et al.,* 1999).

Carbon/nitrogen (C/N) ratio analysis of the same material can be used to identify the source of organic material (Silliman *et al.,* 1996). C/N ratios are used, in particular, to differentiate between algal and higher plant sources. For example ratios of < 10 indicate lacustrine algae, while values between 10 and 20 indicate submergent and floating aquatic macrophytes or a mixed source, and values > 20 indicate emergent macrophytes and terrestrial plants (Holmes *et al.,* 1997; Holmes *et al.,* 1999; Leng and Marshall, 2004; Meyers and Lallier-Verges, 1999).

2.9 Summary

This chapter has highlighted that there are a number of factors controlling lake stable isotopes, all of which must be taken into account when interpreting sediment records. In general, the $\delta^{18}O$ of precipitated carbonate in hydrologically-closed basins will depend on the $\delta^{18}O$ of lake water, which is likely to have been modified by evaporation, and the temperature of carbonate formation, together with any vital or kinetic effects. The $\delta^{13}C$ composition of precipitated carbonate and organic matter is

perhaps slightly more complex, although the most important control on its value is the lake's TDIC pool. This is primarily due to the degree of equilibration with atmospheric CO_2, particularly important in closed lakes with long residence times, and changes in lake productivity.

Chapter Three
The environmental history of NW China and the Tibetan Plateau

Introduction

The climates of Asia are caused by the extent and height of the Himalayan mountains and the Tibetan Plateau (Brocoli and Manabe, 1992; Kutzbach *et al.,* 1993; Molnar *et al.,* 1993; Kutzbach *et al.,* 1997; An *et al.,* 2001). Uplift of this region began about 50 Myr ago, and further significant increases in altitude of the Tibetan Plateau are thought to have occurred *c.* 10-8 Myr ago (Harrison *et al.,* 1992; Molnar *et al.,* 1993). This region therefore has many sites that potentially have extremely long records of monsoonal evolution, ranging from lake sediments, ice cores, loess deposits and glacial relicts.

Lake Qinghai is located in the northeastern part of the Tibetan Plateau, China (Fig. 3.1) and it lies at the boundary of the most northerly limit of the present-day East Asian Monsoon. Climatologically, monsoon regions are the most convectively active areas on Earth and account for the majority of global atmospheric heat and moisture transport (Clemens *et al.,* 2003). Both modern and palaeo studies have demonstrated that monsoon systems are highly variable over annual to orbital scales (Clemens *et al.,* 1996; Charles *et al.,* 1997; Meehl, 1997; Webster, 1998; Suli *et al.,* 1999; Webster *et al.,* 1999; Clark *et al.,* 2000; Wang *et al.,* 2001). This chapter will therefore outline the major climatic events within NW China since the last glacial maximum, highlighting abrupt events and to characterise the environment of Lake Qinghai and its catchment.

3.1 Uplift of the Tibetan Plateau

The uplift of the Tibetan Plateau is thought to be one of the most significant events in the Earth's recent history, particularly as the vast area of high ground exerts an important influence on regional and global climate (Benn and Owen, 1998). An *et al.,* (2001) identified three stages in the evolution of Asian climates; firstly, enhanced aridity in the Asian interior and onset of the Indian and East Asian monsoons, approximately 9-8 Myr ago; next continued intensification of the east Asian summer and winter monsoons, together with increased dust transport to the North Pacific Ocean (Rea *et al.,* 1998), about 3.6-2.6 Myr ago; last, increased variability and possible weakening of the Indian and east Asian summer monsoons and continued strengthening of the east Asian winter monsoon since 2.6 Myr ago (An *et al.,* 2001).

The importance of the plateau's evolution is firstly due to its mechanical effect on atmospheric circulation. This is most pronounced in winter when the plateau splits the surface westerly winds into northern and southern components (Fig 3.2a) preventing the southward flow of cold continental air towards the Indian Subcontinent. Further effects are the enhancement of the

northern westerly jet stream in the lee of the plateau, overshadowed by the Siberian High. Secondly, heating of the plateau in summer raises air temperatures above the zonal mean for the free atmosphere at the same height, which enhances the pressure gradient that drives the East Asian monsoon (Fig. 3.2b).

A strong climatic gradient exists over China and the Tibetan Plateau due to the decreasing influence of the summer monsoon. Precipitation ranges from *c.* 800 mm per year in the south of Tibet (28°N) to *c.* 300 mm at 33°N (the boundary between Tibet Autonomous State and Qinghai Province) to less than 50 mm per year in the north of China. Along this precipitation gradient, the salinity of lakes changes from fresh to saline in response primarily to reduced effective precipitation (Yang *et al.,* 2003). Corresponding with this precipitation gradient, together with effects of altitude, the vegetation ranges from alpine steppe in the south to alpine steppe-desert and desert in the north.

The modern climate of the Tibetan Plateau is now influenced by three relatively independent subsystems, namely the Indian monsoon, the East Asian monsoon, and the Plateau monsoon (Tao and Chen, 1987; Zhou *et al.,* 1996; An *et al.,* 2000). During the seasonal transition from winter to summer, the East Asian summer monsoon moves gradually northward as Northern Hemisphere insolation increases, causing a strengthening of the thermal contrast between the warmer Asian continent and the colder Pacific Ocean. This leads to the marked pressure gradient between ocean and land. In mid-summer, the East Asian summer monsoon advances to *c.* 40°N, spreading across the eastern part of northwestern China, northern China and most of northeastern China.

3.2 Modern climatology

The present climate of China is characterised by a marked gradient in continentality and aridity from southern and eastern China to western China. The region of northwestern China is particularly arid with a maximum of only 50 – 300 mm of precipitation per year (Fig. 3.3) (Wei and Gasse, 1999). The Tibetan Plateau plays a critical role in the initiation of the Asian monsoon system as discussed above. The Asian monsoon is an important component of atmospheric circulation and plays a significant role in the global hydrologic and energy cycles. It has influenced the geographic environment of the region under its direct influence, as well as its marginal zones. The monsoon region of eastern China differs from other dry, subtropical, and temperate areas of the same latitude in being densely populated. Not only is the livelihood of the people closely linked to the summer monsoon precipitation in agricultural regions, but the monsoon rains also generate devastating floods that can impact tens of thousands of people (An *et al.,* 2000).

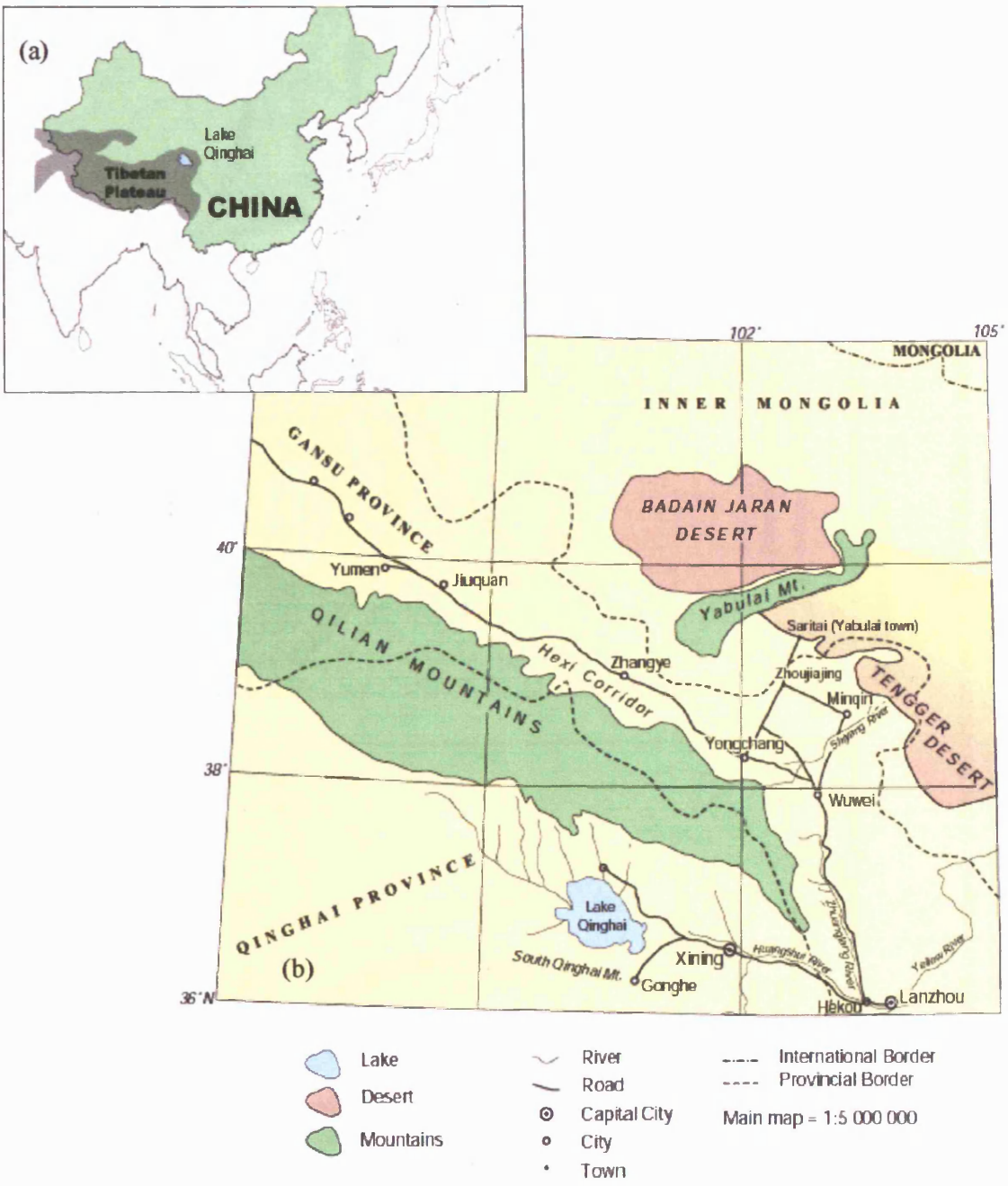

Fig. 3.1 - Location of Lake Qinghai on the NE corner of the Tibetan Plateau. Shaded area in (a) represents land above 3000 m a.s.l.

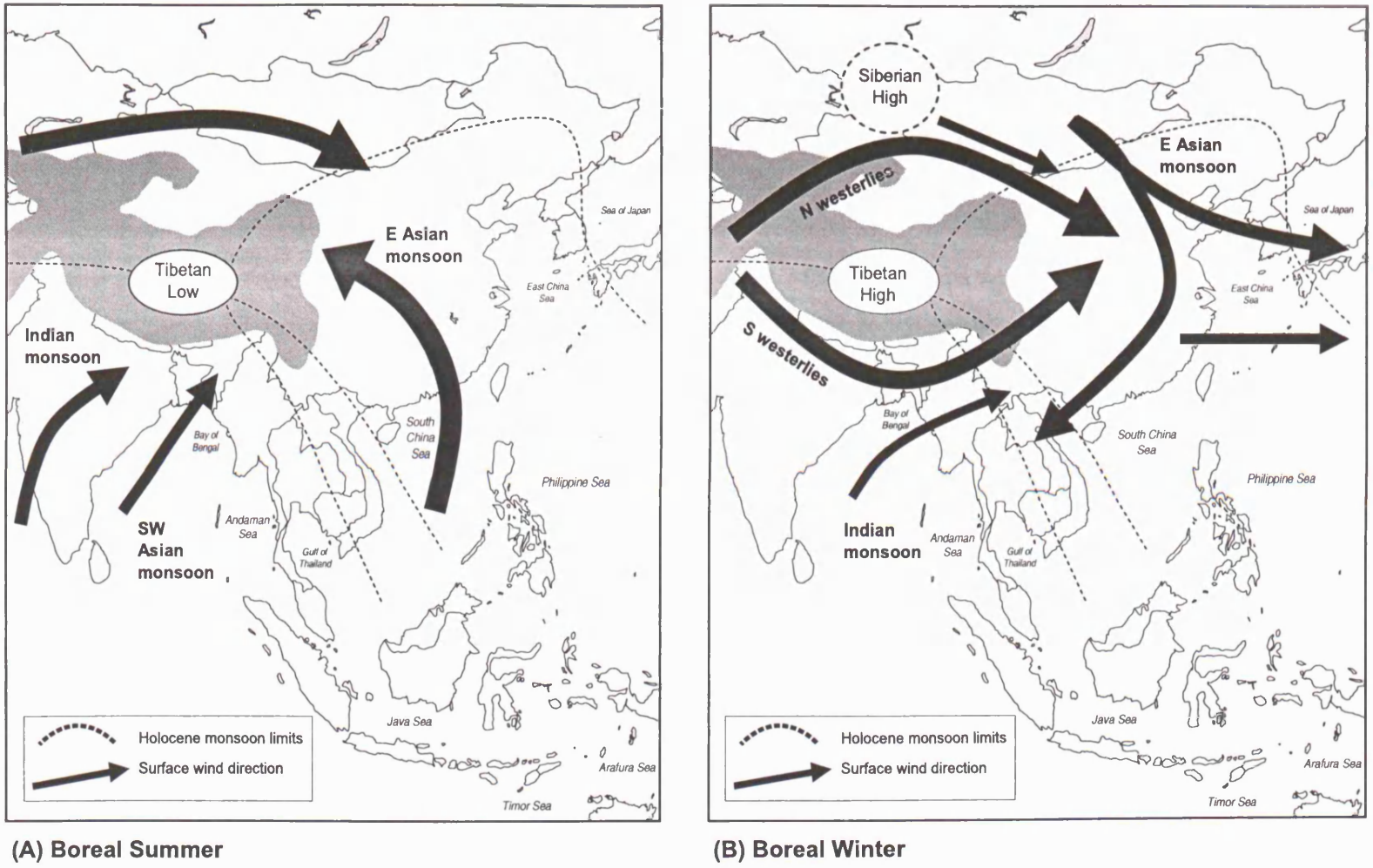

Figure 3.2 – Differences in the major surface circulation patterns of the Monsoon system over Asia during the two main seasons. (a) boreal summer, (b) boreal winter. Dashed lines represent the approximate boundary of modern-day monsoon.

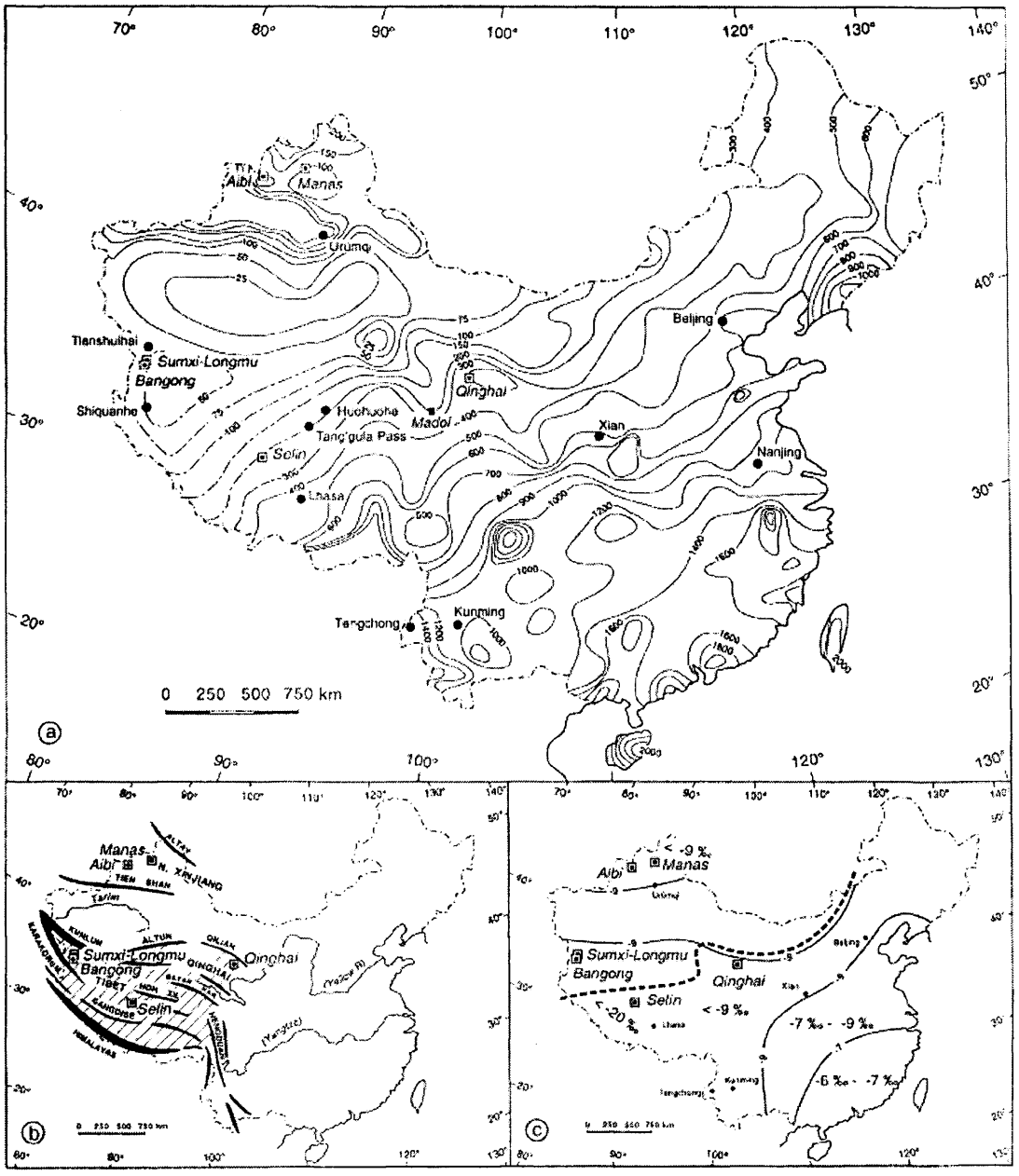

Figure 3.3 – Location of lakes mentioned in the text. Maps of China showing: (a) mean annual precipitation (mm); (b) major topographical features; (c) average annual isotopic composition ($\delta^{18}O$). Coarse dashed line represents the modern limit of the East Asian monsoon (From Wei & Gasse, 1999).

3.3 Climatic history of NW China and the Tibetan Plateau

Our knowledge about the climatic and environmental evolution since the last glacial maximum of the monsoon regimes in NW China and the Tibetan Plateau has been principally derived from marine and loess records (Rea and Leinen, 1988; Pye and Zhou, 1989; Sirocko *et al.,* 1996; Zhou *et al.,* 1996; Guo *et al.,* 1998; Zhou *et al.,* 1999; An *et al.,* 2000; Huang *et al.,* 2000; Porter, 2001; Zhou *et al.,* 2001). Additional information has recently been derived from three ice cores obtained from the Tibetan Plateau, namely, Dunde (Thompson *et al.,* 1989; Yao *et al.,* 1991), Guliya (Thompson *et al.,* 1997; Yao *et al.,* 1997), and Danuspo (Thompson *et al.,* 2000; Thompson, 2000). Extensive work has also been carried out on glacial deposits to reconstruct the glacial history of the Tibetan Plateau (Shi *et al.,* 1993; Shi *et al.,* 1994; Lehmkuhl *et al.,* 1998; Lehmkuhl and Haselein, 2000; Rost, 2000; Shi, 2002; Zheng *et al.,* 2002). There is now an increasing amount of work being conducted on lacustrine sediments (Fig. 3.4), utilising a number of climate proxies, at varying timescales to great effect (Kelts *et al.,* 1989; Gasse *et al.,* 1991; Lister *et al.,* 1991; Fontes *et al.,* 1993; Van Campo and Gasse, 1993; Yang *et al.,* 1995; Fan *et al.,* 1996; Fontes *et al.,* 1996; Gasse *et al.,* 1996; Van Campo *et al.,* 1996; Wei and Gasse, 1999; Yan *et al.,* 1999; Wang *et al.,* 2002; Henderson *et al.,* 2003).

In order to discuss the environmental evolution of this climatically sensitive region a number of records from key sites will be used to examine major changes since the Last Glacial Maximum (LGM). A number of reviews of monsoon variability have focussed on determining how and why the Asian monsoon varies on interannual and millennial times (Zhou *et al.,* 1991; Winkler and Wang, 1993; Webster, 1998), while recent work has highlighted the importance of abrupt changes in the monsoon that occur at the centennial scale (Morrill *et al.,* 2003). To evaluate the most recent interglacial monsoon history, a number of specific events identified in the record will be assessed, namely, the deglaciation and late glacial (including the Younger Dryas and the Bølling-Allerød), the Holocene Optimum, and the most recent millennium, up to and including the instrumental period.

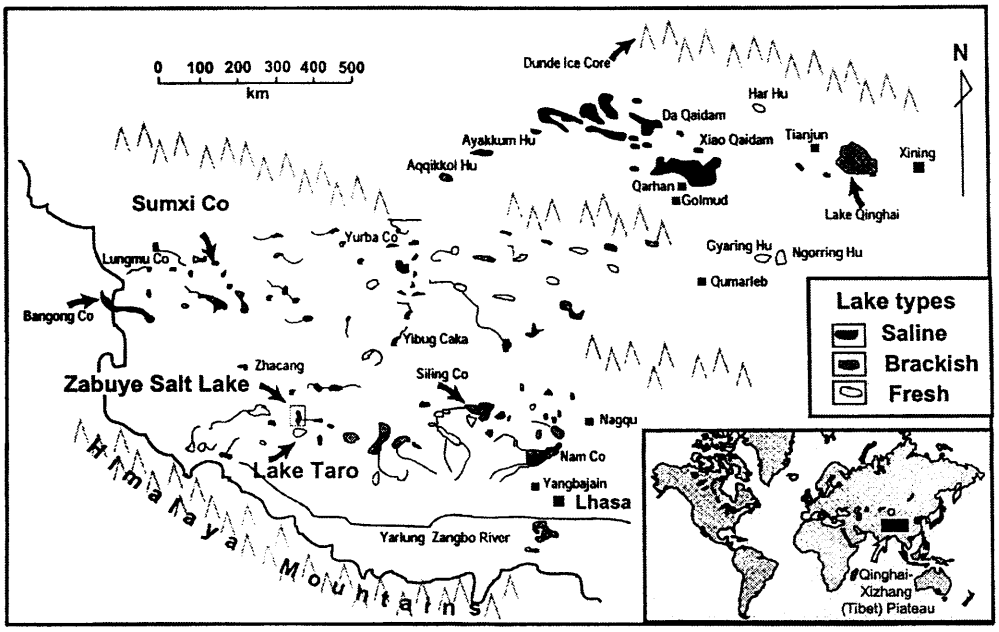

Figure 3.4 – Map showing the major water bodies and their type on the Tibetan Plateau. Named lakes are where palaeoclimate records exist. (After Wang *et al.*, 2002).

3.3.1 Glacial-Holocene transition

Globally, the last deglaciation was a period of intense and rapid change (Broecker *et al.*, 1988) and these fluctuations have been well documented in deep-sea cores (Karpuz and Jansen, 1992; Rochon *et al.*, 1998) and Greenland ice cores (GRIP Project Members, 1993; Grootes *et al.*, 1993; Taylor *et al.*, 1993). Mounting evidence is now supporting the existence of a number of short-lived climatic fluctuations, particularly from the desert-loess transitional belt in China highlighting an abrupt change equivalent to the Younger Dryas, reflecting cold-dry to cool-wet conditions that return to cold-dry century-scale fluctuations (Zhou *et al.*, 1996). Comparative data of sufficiently high-resolution are only now being examined in detail, but are corroborating these findings (An *et al.*, 1993; Porter and An, 1995; Zhou *et al.*, 1999; Huang *et al.*, 2000; Porter, 2001; Zhou *et al.*, 2001; Zhou *et al.*, 2001b).

Zhou *et al.*, (1999) presented a record from the Midiwan loess section, in central China, using organic carbon isotopes ($\delta^{13}C_{org}$) to reflect changes in environmental conditions since deglaciation until the onset of the Holocene. The profile they present is compared to two other loess sections (Baxie and Yangtaomo) and all these show a three phase component coeval with the European Younger Dryas, preceded by a Bølling-Allerød climatic event. The $\delta^{13}C_{org}$ values of the Midiwan profile change rapidly, consistent with a change to slightly warmer, wetter conditions, peaking at 14,500 yr B.P. A period of sharp, minor fluctuations occurred until an excursion at 14,100 yr B.P. Following this climate transition, the Younger Dryas period is reflected by a shift to more negative $\delta^{13}C_{org}$ values, suggesting increased precipitation. This mid-Younger Dryas peak found in the

Midiwan record also correlates well with higher summer temperatures and low sea ice cover in the North Sea (Zhou *et al.,* 1999).

However, these short-lived fluctuations have yet to be seen in lacustrine records and although the Younger Dryas period has been well documented, the existence of a lake Bølling-Allerød transition has not been detected. Evidence from Lake Qinghai suggests an abrupt event at ~10,700 – 10,000 ^{14}C yr BP that is characterised by arid conditions with enhanced evaporation and reduced catchment inflow leading to the formation of a carbonate playa environment (Yu and Kelts, 2002). This arid event is chronologically synchronous with the European Younger Dryas (Lister *et al.,* 1991) and represents a return to cold and arid conditions. This event might also be linked to the cold and dry episode at ~11,000 – 10,000 ^{14}C yrs B.P. as interpreted from the Lake Sumxi record from western Tibet (Gasse *et al.,* 1991) and to the δ^{18}O reversal event seen in the Guliya ice core (Thompson *et al.,* 1997). Yu & Kelts, (2002) suggest there is no clear evidence for a return to cold climatic conditions during the Younger Dryas period, but rather carbonate production and organic productivity during this period is indicative of intensified summer evaporation, which is distinctly different to the cold and arid period preceding this (Lister *et al.,* 1991; Yu and Kelts, 2002). The data suggest an abrupt increase in summer temperature, requiring monsoon moisture penetration to the Tibetan Plateau to lag behind the change in inland surface conditions by approximately 700 years (Yu and Kelts, 2002). Summer temperature increases, due to increased summer insolation and regional deglaciation, brought about the enhancement of summer evaporation and aridification of the lake, but a further enhancement of monsoonal rainfall did not occur until 10,000 ^{14}C yrs B.P. Yu & Kelts (2002) suggest a step-wise pattern of climatic change across the late-glacial/Holocene transition along with abrupt shifts in effective moisture on the NE Tibetan Plateau.

During the late glacial, the East Asian monsoon climate variations were mainly controlled by changing solar radiation and surface boundary conditions of the Northern Hemisphere (Prell and Kutzbach, 1987; An *et al.,* 1993). During the Younger Dryas stadial, summer insolation over the northern hemisphere was close to its maximum, which led to a strengthening of the summer monsoon circulation (Zhou *et al.,* 1996). Conversely, fluctuations could have been a response to changes in the Siberian High as a result of alternating periods of strengthening and weakening of the cold air masses in high latitudes. Zhou *et al.,* (1996) infer that varying strengths of these cold air masses caused oscillations in the East Asian monsoon climate producing detectable changes in the position of the summer monsoon front and change in the precipitation regime of east-central China. This would account for the apparent discrepancies in the signals in the seen during the Younger Dryas in loess records (Zhou *et al.,* 1999) and lake records from the Tibetan Plateau (Gasse *et al.,* 1991; Lister *et al.,* 1991; Yu and Kelts, 2002).

The abrupt events seen in these records and the onset of the Holocene therefore cannot be attributed directly to orbital forcing. Porter & An (1995) suggest there is a close connection

between North Atlantic Heinrich events and the Asian winter monsoon via the Siberian High pressure system as indicated by increased loess deposition on the Chinese loess plateau. Simulations of Northern Hemisphere winter sea level pressures and dominant wind direction for the last glacial maximum (Kutzbach *et al.,* 1993) suggest strong storm tracks would have travelled through Europe into Central China, providing cold surges. Teleconnections between Asia and the high latitudes have also been suggested to occur during the summer (Sirocko *et al.,* 1996) and the interaction between cold high latitude air masses and moist air masses from the Pacific Ocean, are presumed to be closely related to climate forcing from the polar high latitude North Atlantic (Zhou *et al.,* 1996).

It has been proposed that enhanced North Atlantic deep-water formation at the start of the Holocene (Boyle and Keigwin, 1987; Marchitto *et al.,* 1998; Hughen *et al.,* 2000) and subsequent changes in atmospheric circulations influenced these observed changes, borne out by the North Atlantic-Central Asian teleconnections. An increase in deep-water formation could produce warm anomalies in the North Atlantic that could be advected by the westerlies over the Eurasian continent (Overpeck *et al.,* 1996). Warmer temperatures over the continent would reduce snow accumulation, increasing land temperatures in the spring and summer and enhancing the land-to-sea temperature gradients that drive the Asian monsoon.

Synchronous changes in North Atlantic circulation and Asian monsoon provides evidence of the proposed teleconnection, within the limits of precision of radiocarbon dating (Morrill *et al.,* 2003). This similarity makes it likely that the events are related and also suggests that any teleconnections between the two regions would have occurred rapidly and through changes in the atmosphere. The abrupt changes observed in these two regions were of large magnitude. With the temperature increase in the North Atlantic region at this time larger than any other observed during the Holocene (Morrill *et al.,* 2003).

Alternatively, it has also been suggested that a strengthened Asian monsoon could cause a warming in the North Atlantic by increasing atmospheric methane concentration due to the expansion of tropical wetlands (Gasse and Van Campo, 1994) or strengthening the hydrologic cycle and resultant sea-level fall that would stabilize coastal glaciers in the North Atlantic region and allow for a strong thermohaline circulation (Kudrass *et al.,* 2001). Severinghaus *et al.,* 1998 suggest that the increase in atmospheric methane concentrations at the start of the Holocene lags the temperature increase in the North Atlantic by several decades and Fairbanks, 1989 documents a sea-level rise, rather than fall, at the start of the Holocene. Therefore, the mechanism as described by Overpeck *et al.,* (1996) is the likely teleconnection between the North Atlantic and the Asian monsoon during the late glacial (Kutzbach *et al.,* 1993; Porter and An, 1995; Sirocko *et al.,* 1996; Morrill *et al.,* 2003).

3.3.2 The Holocene optimum

The existence of a warm and stable mid-Holocene climate is the considered view typical for this interglacial period, and a mode that is generally used in climatic modelling. However recent studies are suggesting that the mid-Holocene period was a time of profound change in low latitudes, with land and air temperatures, together with wind speeds declining across much of the globe, and distinct regional differences in precipitation (Steig, 1999). The mid-Holocene in China is traditionally thought to have been warmer than present with high precipitation as a result of a strong Asian summer monsoon (Shi *et al.,* 1993). This concept of a 'Megathermal' or climatic optimum from *c.* 8500 to 3000 ^{14}C yr BP still persists in Chinese Quaternary and palaeoclimate communities and it is only now that this is beginning to be reassessed (e.g. An *et al.,* 2000; Chen *et al.,* 2003; Chen *et al.,* 2003). An *et al.,* (2000) refined proxy data and demonstrated an asynchronous feature in the East Asian monsoon during the mid-Holocene optimum over central and northern China, with the maximum extent of the summer monsoon shrinking to southern and eastern China after the early Holocene.

A mid-Holocene dry interval has been documented in a number of records from arid northwest China, contrary to the traditional view held for this time period (An *et al.,* 2000; Mischke, 2001; Chen *et al.,* 2003; Chen *et al.,* 2003; Mischke *et al.,* 2003). In addition to the apparent asynchrony of the optimum across mainland China (An *et al.,* 2000), it is thought that an optimum existed prior to 7000 ^{14}C yr BP ago in the early Holocene in the arid and semi-arid regions of NW China, while other records demonstrate a prolonged interval of aridity (5600-7000 ^{14}C yr BP) (Guo *et al.,* 2000). Huang *et al.,* (2000) reported that Holocene soil development in the Guanzhong Basin of the central Chinese Loess Plateau was interrupted by high dust deposition at 5700 to 6800 ^{14}C yr BP, indicating regional aridity. Therefore it is conceivable that this mid-Holocene dry event affected a large region in NW China along the present limits of the Asian monsoon. That such a large area was affected by drought conditions may also explain the paradox of maximum dust flux in the Pacific Ocean sediments (Rea and Leinen, 1988; Pye and Zhou, 1989) during a supposedly warm and humid climatic optimum in China.

Chen *et al.,* (2003b) suggest two possible explanations for lake desiccation and dry climates in the Southern Mongolian Plateau – (1) less rainfall due to a weakened Asian summer monsoon, (2) lower effective precipitation due to a relatively higher temperature. They present data supporting the former explanation that a monsoonal weakening is the main reason for the environmental change at this time. Low pollen concentrations and plant diversity in a dried-lake that was fed by the Shiyang River, which flows from the Qilian Shan on the NE Tibetan Plateau (Zhu, 2001; Zhu *et al.,* 2001) indicate that vegetation change in the entire Shiyang River catchment during the mid-Holocene. Upland vegetation (conifer and shrubby grassland) in the Qilian Mountains declined dramatically *c.* 7000 years ago, indicating mid-Holocene vegetation was not only degraded in the lower catchment, but also in the upper reaches of the drainage

basin. In semi-arid and arid regions, like NW China, vegetation coverage is more sensitive to precipitation (humidity) than to temperature. Therefore, degradation of vegetation cover in both mountain and desert areas suggest reduced precipitation during mid-Holocene. In addition, precipitation reconstructions for central Inner Mongolia indicate lower precipitation during the mid-Holocene (Shi and Song, 2003; Chen *et al.,* 2003). Therefore, lakes that were recharged by local precipitation (in the Badain Jaran Desert to the north, see Fig. 3.1) and lakes that are recharged by large river systems that originate from mountainous areas (Shiyang drainage basin) all experienced dessication, indicating a regional decrease in effective moisture. Stabilised dune fields in the early- and late-Holocene (Yang *et al.,* 2003) also imply low rainfall in this region during the mid-Holocene.

Patterns of temperature during the mid-Holocene are complicated by conflicting data, as some records suggest a temperature increase (particularly in East China) (Shi *et al.,* 1993), with cold events being noted (Shi *et al.,* 1994). However, other records indicate that the mid-Holocene was cooler, especially on the Tibetan Plateau where glacial advances have been frequently reported at different sites (the so-called second Neoglaciation) (Zhou *et al.,* 1991; Shi *et al.,* 1994). A study of a core taken from Lake Qinghai show both high arboreal and total pollen concentrations, which appeared before *c.* 7400 cal yr BP Liu *et al.,* 2002) contrary to the hypothesised mid-Holocene megathermal. Evidence from the Guliya ice core (Thompson *et al.,* 1997; Yao *et al.,* 1997) highlight temperature changes after the early-Holocene, which rapidly decreased after *c.* 7000 ^{14}C yr BP, remaining at a minimum and then increased to present day values.

The mechanism for these observed changes during the mid-Holocene has been linked to monsoon strengthening (Morrill *et al.,* 2003). An abrupt shift towards drier conditions could have resulted from cold temperature anomalies in the North Atlantic. These cold surges could have been advected over Eurasia, similar to the mechanism described for the start of the Holocene, but they would have worked oppositely. However, this abrupt change observed in the North Atlantic is one of many that occurred at this time and are of smaller magnitude and duration than the cold surges seen at the beginning of the Holocene. There are also discrepancies between the timing of events in the North Atlantic, with the record of Bond *et al.,* 1997) that showed cold events out-of-phase with those observed by Jennings *et al.,* 2002) and Keigwin, 1996).

Alternatively, mid-Holocene climate fluctuations may be related to changes in the state of the El Niño Southern Oscillation (ENSO). An increase in the frequency of strong El Niño events could have caused a decrease in monsoon precipitation observed during the mid-Holocene by altering the location of convection in the Pacific Ocean (Morrill *et al.,* 2003). During El Niño events, warmer sea surface temperatures (SSTs) in the central and eastern equatorial Pacific cause surface convergence to occur further east, away from the region of the Asian monsoon (Yang, 1996). This is thought to draw moisture away from Asia and cause a weaker summer monsoon. However, there are several uncertainties that need to be resolved. For example, the exact timing

of the change in ENSO is not well defined and the mechanism responsible for less intense and less frequent warm events in the middle Holocene is also not clear (Morrill *et al.,* 2003).

The final possibility of the cause of the abrupt event in the mid-Holocene in China is that it originated from within the monsoon region itself as a result of a non-linear land-atmosphere process responding to insolation change. Such a response is seen in the African monsoon, where an abrupt decrease in precipitation at this time period has been related to a decrease in vegetation cover in the Sahara, which is though to respond slowly to varying insolation changes (Clausen *et al.,* 1999). It is possible that regional land-atmosphere interactions may not have been the primary driver of the abrupt shift in Africa, but they were still an important factor (Morrill *et al.,* 2003). This is supported by other studies that indicate ocean feedbacks may also have played an important role in the circulation of the African monsoon (Kutzbach and Liu, 1997; Hewitt and Mitchell, 1998). A similar land-atmosphere interaction could have occurred in Asia, but is unlikely to have occurred synchronously in both Africa and Asia. Changes in either the North Atlantic or the tropical Pacific therefore appear to be the most likely cause of observed abrupt change (Morrill *et al.,* 2003).

3.3.3 Last Millennium

Global climate warming has been broadly identified in the latter part of the 20th Century, but this warming varies significantly from region to region over the globe. This warming has been less well examined in China due to the lack of long and homogeneous temperature series. Even though proxy data can enable us to reconstruct climate, and sometimes temperature indirectly, this time period is still relatively understudied at a sufficient resolution to be particularly useful. Exceptions to this are a number of ice cores taken from the Tibetan Plateau (Yao *et al.,* 1997; Thompson *et al.,* 2000; Thompson *et al.,* 2003) and lake sediments (Henderson *et al.,* 2003; Zhang *et al.,* 2003).

Syntheses of a number of records have identified an abrupt event at AD 1300 within a time period sometimes described as the transition between the 'Medieval Warm Period' and 'Little Ice Age' (Morrill *et al.,* 2003). Records show several decadal to multi-decadal warm and cold temperature anomalies but they disagree with one another regarding the timing of these climatic changes (Grove, 1988; Bradley and Jones, 1993; Hughes and Diaz, 1994; Mann *et al.,* 1999; Crowley and Lowery, 2000). Despite the climatic heterogeneity of this period, several high-resolution records show a convincing shift in climatic regimes at AD 1300, which has also been shown globally by other proxy records (e.g. Laird *et al.,* 1996; Woodhouse and Overpeck, 1998; Verschuren *et al.,* 2000).

Wang *et al.,* (2001) employed proxy and documentary data to reconstruct different temperature time series in China. Figure 3.5 shows annual mean temperature anomalies for the time period

1880-1998 with respect to the norm of 1961-1990. It indicates that warming in the 20th Century started in the 1920s and was interrupted in the 1950/60s by a cooling, but temperature has persistently increased since 1969 with a maximum temperature anomaly of + 1.36°C recorded in 1998.

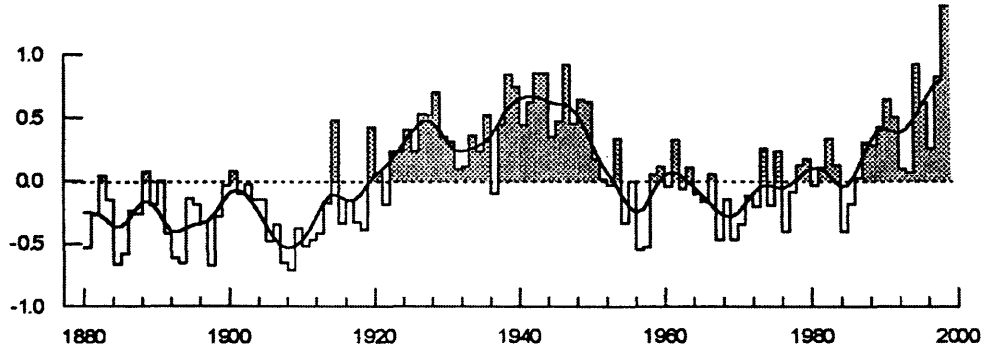

Figure 3.5 – Annual mean temperature anomalies for China (reference period is 1961-1990). (From Wang *et al.*, 2001).

In order to determine whether the 20th Century was the warmest of the last millennium, documentary evidence of mean temperature anomalies was used in conjunction with available proxy data (Wang *et al.*, 2001). Figure 3.6 highlights three cold spells (I, II & III) in this time period which clearly characterise the Little Ice Age, additionally there appears to be two definable cold stages (1 & 2) within these cold events. This suggests that the 20th Century is significantly warmer than the previous 5 centuries in China. It also highlights the existence of a short warm spell at the beginning of the 20th Century, the 1920s-1940s, which was about 1°C higher than those for the cold stage (AD 1620-99) during the Little Ice Age. It has already been highlighted that the Medieval Warm Period probably occurred during AD 900-1300 over a large area of the globe, but the intensity and timing of warming climate is still debated (Hughes and Diaz, 1994). Therefore assessment of the characteristic of modern warming in China is fundamental for determining whether the 20th Century was the warmest period of the last 1000 years.

It is worth noting that the last millennium has not been the warmest period (on average) of the whole Holocene in China, with the so-called Megathermal having been considerably warmer than the present. However, as discussed previously, the spatial extent and timing of this phenomenon is currently being debated. The climatic warming of the 20th Century still lies within the limits of natural variability, no matter whether the warming is attributed to anthropogenic or natural causes (Wang *et al.*, 2001). Therefore in order to determine whether dry conditions predominated when the climate was warm the relationship between temperature and precipitation anomalies in climatic change has been examined using observational and reconstructed climatic series. Figure 3.7 shows the correlation with annual mean temperature and total precipitation calculated from a 160-station data set between 1951-98 (Wang *et al.*, 2001). It highlights that a negative correlation dominates in the northern part of China, suggesting warm-dry conditions persisted over warm-wet

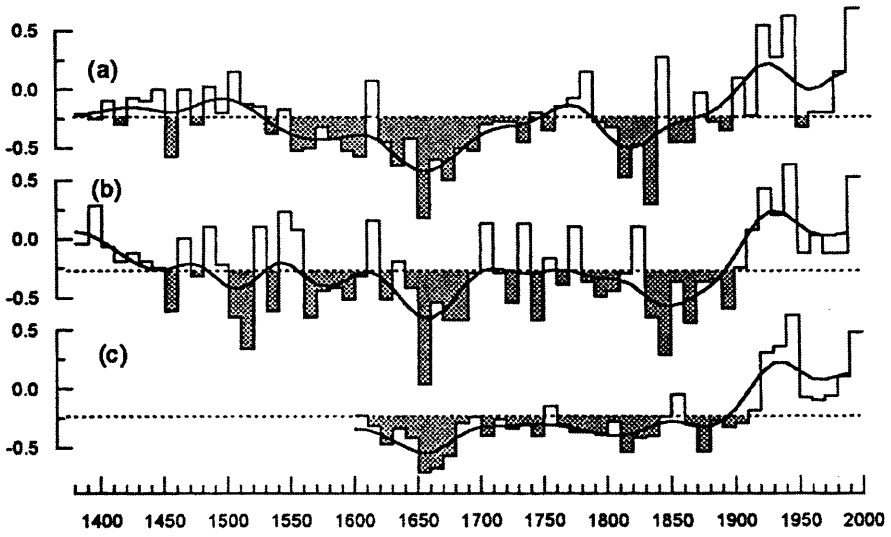

Figure 3.6 – Temperatures (°C) in China since AD 1380; (a) Northern China; (b) Eastern China; (c) whole of China. The means of the whole series are shown as dotted lines (From Wang *et al.*, 2001).

conditions. The correlation found in the southern part of the country is positive and suggests predominantly warm-wet conditions. This present day relationship can be tested by using climatic data for earlier periods. For example, figure 3.5 showed a 30-year period 1920-49 was the warmest during the 1880-1990s, and 1880-1909 was the coldest. Therefore by using 30-year mean anomalies of annual total precipitation for both warm (1920-49) and cold (1880-1909) periods and the difference between them, shows warm-dry and cold-wet predominates in the north of country but warm-wet in the south east (Fig. 3.9).

The evidence for some of the changes seen in the last thousand years has been based on instrumental and documentary data, but a lot of our understanding of recent climate changes is gained through proxy records. Presently, three ice core records exist from the Tibetan Plateau covering the last millennium, namely; Dasuopu (7200 m a.s.l.), Guliya (6200 m a.s.l.) and Dunde (5325 m a.s.l.). Dasuopu is dominated by advection of moisture from the Indian Ocean with possible contributions from the Arabian Sea. Dunde and Guliya receive monsoon precipitation traversing the Tibetan Plateau from the south, but snowfall is also likely to arrive from westerly flow at times during the winter (Thompson *et al.*, 2003). Decadal averages of $\delta^{18}O_{ice}$ from the three Tibetan ice cores (Fig. 3.9) display major differences on both decadal and century scales. This is not surprising given the diverse regional settings that contribute to the various sources of precipitation and post-depositional processes.

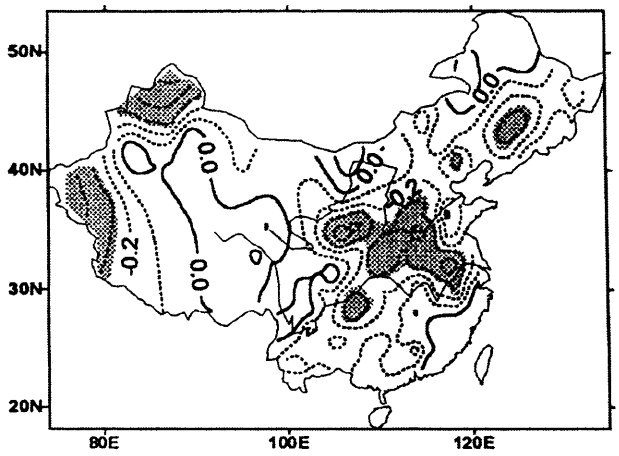

Figure 3.7 – Correlation between annual temperature and annual precipitation. Areas within 95% confidence limits are shaded. Data for 160 stations are used for the period 1951-98 (From Wang *et al.*, 2001)

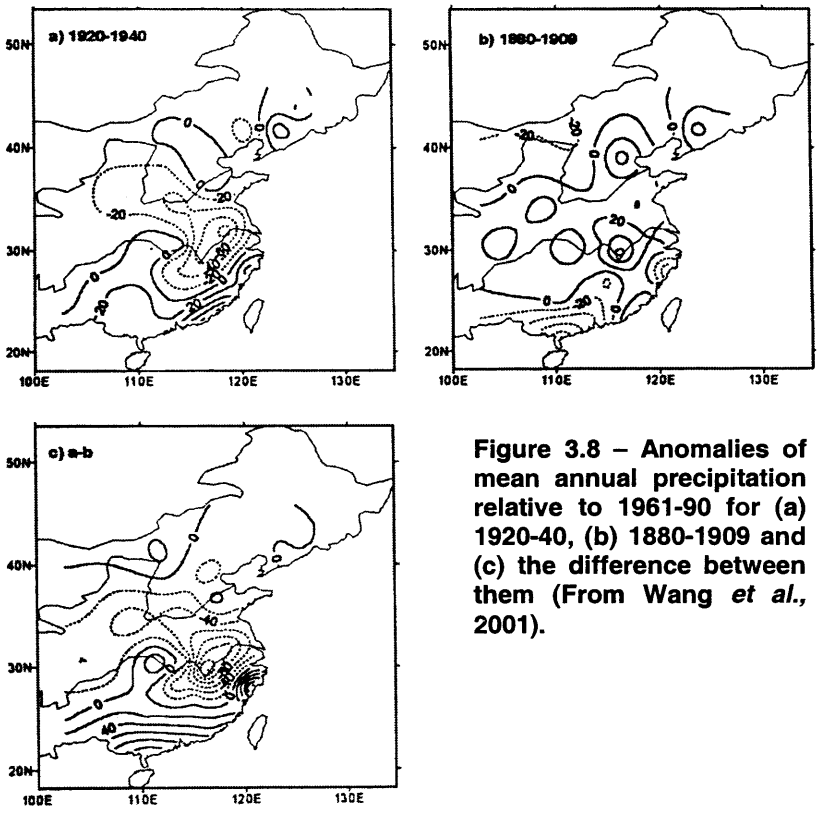

Figure 3.8 – Anomalies of mean annual precipitation relative to 1961-90 for (a) 1920-40, (b) 1880-1909 and (c) the difference between them (From Wang *et al.*, 2001).

Millennial $\delta^{18}O_{ice}$ histories from Dasuopu and Dunde contain broadly similar trends, while the Guliya record appears largely disconnected from that of Dunde (Thompson *et al.*, 2000). However, since AD 1800 all three $\delta^{18}O_{ice}$ histories show a consistent increasing trend suggesting large spatial-scale warming has affected the region. Also $\delta^{18}O_{ice}$ in Dunde deposited since 1950 has increased by 0.99‰ relative to the millennial mean, with similar enrichments seen in Guliya and Dasuopu (1.05‰ and 1.84‰ respectively), suggesting temperatures in the second half of the 20th Century on both Dunde and Dasuopu have been the warmest of the millennium (Thompson *et al.*, 2003). Warming is the most pronounced at the highest elevation site (Dasuopu), suggesting that regional temperature increases are greatest at higher altitudes.

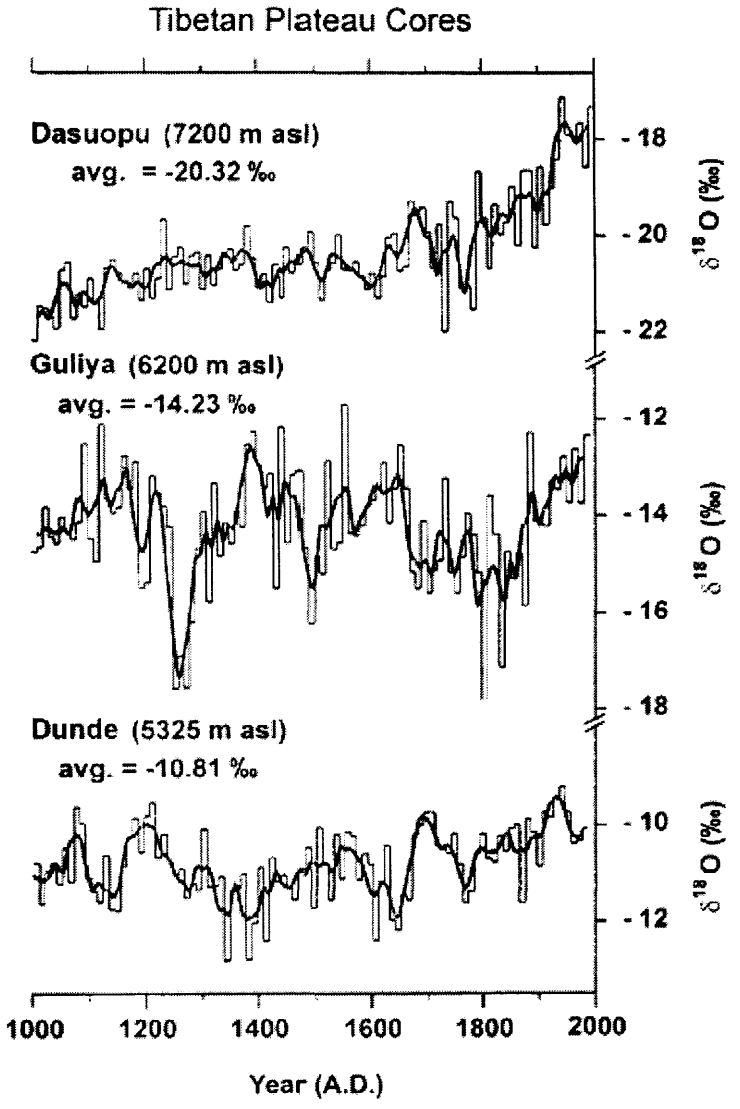

Figure 3.9 – Decadal averages of $\delta^{18}O_{ice}$ (histogram) for the last millennium from three Tibetan ice cores (Dunde, Guliya and Dasuopu) are shown along with their respective elevations and millennial averages. The darker, smooth curve is a 3 decade running mean (from Thompson *et al.*, 2003).

A composite record of the Tibetan Plateau $\delta^{18}O_{ice}$ records show greater $\delta^{18}O_{ice}$ values between 1140 to 1250 AD, possibly reflecting the Medieval Warm Period and lower values *c.* 1300 to 1850 AD, correlative with the Little Ice Age. However, the dominant signal in the $\delta^{18}O_{ice}$ composite is the ^{18}O enrichment in the 20th Century (Fig. 3.10). The similarities between ice core $\delta^{18}O_{ice}$ composite and the best Northern hemisphere temperature record over the last millennium provide strong evidence that over large distances and decadal (and longer) timescales, the dominant control on ice core $\delta^{18}O_{ice}$ record is temperature (Thompson *et al.,* 2003). The composites therefore illustrate that 20th Century $\delta^{18}O_{ice}$ increase is a dominant longer-term feature common to these regions that are geographically quite separate. Ice core records therefore support meteorological evidence (Jones *et al.,* 1999) of a significant 20th Century warming, but have added value of placing the observations within longer-term perspectives that seem to be signalling large and unusual warming that is underway at high elevation (Thompson *et al.,* 2003).

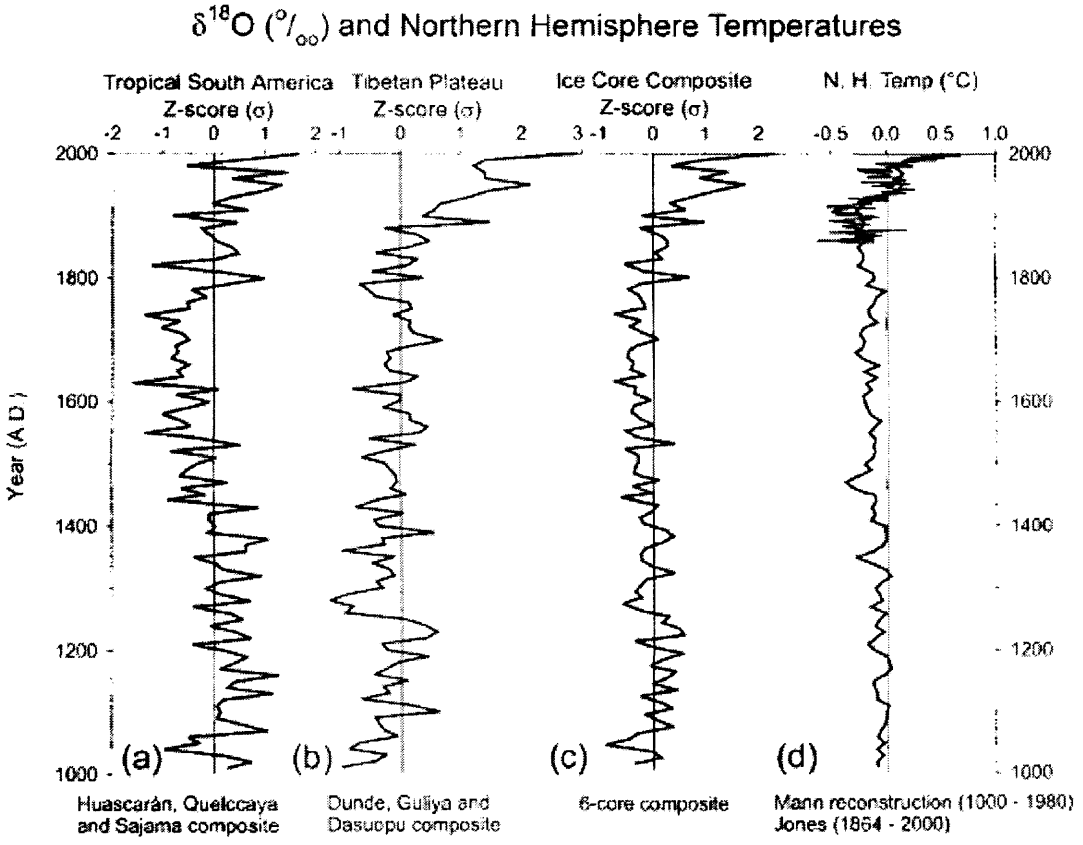

Figure 3.10 – Regional composites, shown as z-scores, for the last millennium were constructed from decadal averages of $\delta^{18}O_{ice}$ from three Andean ice cores (a) and three Tibetan ice cores (b). The composite of all six low latitude cores is shown in (c). The measured (Jones *et al.,* 1999) and reconstructed (Mann *et al.,* 1999) Northern Hemisphere temperatures are shown in (d) and are plotted as deviations (°C) from their respective 1961-1990 means. Note that decadal average of for $\delta^{18}O_{ice}$ 1991 to 1997 annual values for the Dasuopu core drilled in 1997 and on the 1991-1997 annual values for the Sajama drilled in 1997. The Quelccaya $\delta^{18}O_{ice}$ history has been updated to 2000 by drilling new shallow cores (From Thompson *et al.,* 2003).

Additional evidence comes from mountain glaciers. Mountain glaciers are sensitive to climatic change and their advance and retreat is a response to temperature and precipitation fluctuations. 20th Century warming has greatly reduced glacier coverage since the Little Ice Age and has increased the equilibrium line altitudes (ELAs) of many glaciers, particularly those in temperate China (Su and Shi, 2002). The Little Ice Age contained three severe cold periods (Yao *et al.,* 1997; Wang *et al.,* 2001; Thompson *et al.,* 2003); the second, which was most severe, occurred in the 17th Century and was coincident with the Maunder Minimum of solar irradiance (1645-1715) (Shi and Liu, 2000). Since the maximum of the Little Ice Age the mean annual air temperature has increased by 0.8°C and the glacier area has decreased by 3921.2 km^2, an amount equivalent to 30% of the modern glacier area (Su and Shi, 2002). This decrease in glacier area is larger than that of sub-polar and polar type glaciers in China but smaller than that of temperate glaciers in the European Alps.

There are few meteorological stations on the Tibetan Plateau and available time series are short. Liu and Chen (2000) using a monthly surface air temperature data from meteorological stations on the Plateau report linear increasing temperature of *c.* 0.16°C per decade between 1955 and 1996 and an increasing winter trend of *c.* 0.32°C. Moreover, the rate of warming has increased with elevation, and the greatest rate of warming (*c.* 0.35°C per decade) occurs at the highest elevation (Liu and Chen, 2000). Variations in monsoon strength (particularly) at AD 1300 are more spatially heterogeneous than at the other time periods, perhaps because this climatic change was smaller than during other time periods. Recent patterns of precipitation change have been attributed to an increase in winter snow cover over Eurasia (Yang and Xu, 1994; Qian *et al.,* 2003), although more data is needed to determine if an increase in snow cover could have caused the change in monsoon strength at AD 1300.

In summary, the climatic history of northwest China and the Tibetan Plateau highlights that: (1) teleconnections with other parts of the climatic system, in particular the North Atlantic and the tropical Pacific, are likely to have been important in determining the timing and direction of climate changes; (2) gradual changes in forcing (e.g. insolation) may trigger abrupt shifts in monsoon strength, either directly or through these teleconnections; and (3) changes in monsoon precipitation have shown both homogeneous and heterogeneous spatial patterns during the Holocene. The size of the climatic change might determine which of these spatial patterns occurs. Most importantly, it highlights the potential for future major abrupt changes in the Asian monsoon, some of which can take place on time scales of 100 years or less.

3.4 Lake Qinghai

3.4.1 Geological setting and catchment characteristics

Active tectonics and geophysical profiles indicate that Lake Qinghai is tectonically a piggyback basin behind the Qinghai Nan Shan which is moving southward (Fig. 3.11). The lake consists of the northern and southern sub-basins separated by a normal faulting horst in the middle of the lake. The northern sub-basin has been disturbed by a few active faults, whereas the southern one shows relatively simple structure and continuous stratigraphic sequences, implying a stable depositional environment (An, 2003). The southern sub-basin can be further divided into eastern and western depressions, in which *c.* 700 m of unconsolidated sediment have been detected.

The eastern part of the lake catchment, which is drained by the Buha River, is dominated by Late Paleozoic marine limestones and sandstones (Fig. 3.2). Triassic volcanics and Mesozoic granodiorites are common in catchments of smaller tributaries surrounding Lake Qinghai in the west (Yan *et al.,* 2001). Most of the catchment is covered by grazing land, alpine shrubs and meadows. The permafrost is wide-spread above 3600 m (which includes nearly half of the total catchment area). There are virtually no forests in the basin, only a limited area of desert, and some irrigated farmland to the north and northeast of the lake (Qin and Huang, 1998). The highest part of the basin is located in the northwest and reaches more than 5000 m a.s.l.

3.4.2 Hydrological setting of Lake Qinghai

In spite of a cold semi-arid climate, the large catchment provides annual surface runoff of more than 1.6×10^9 m^3 along with an estimated 0.64×10^9 m^3 of groundwater input per year (Yu and Kelts, 2002), maintaining a perennial lake of *c.* 4400 km^2 and a maximum depth 27 metres. Table 3.1 summarises the basic characteristics of Lake Qinghai and its catchment. Of the total annual catchment runoff today, about 1% is from melt water of modern glaciers in the lake's upper catchment at altitudes above 4800 km^2. The annual precipitation is approximately 400 mm, of which 65% falls in the summer from June – September (see Fig. 3.13). The lake is currently at the outer margin of the Asian summer-monsoon influence, but past changes in monsoon circulation undoubtedly influenced the precipitation to evaporation balance (effective moisture) of the lake and its catchment, resulting in substantial changes in lake-level and water chemistry (Yu and Kelts, 2002). Six of the inflows contribute *c.* 75% of the total runoff; with the longest and greatest river is the Buha River, which discharges a volume equivalent to almost half of the total runoff.

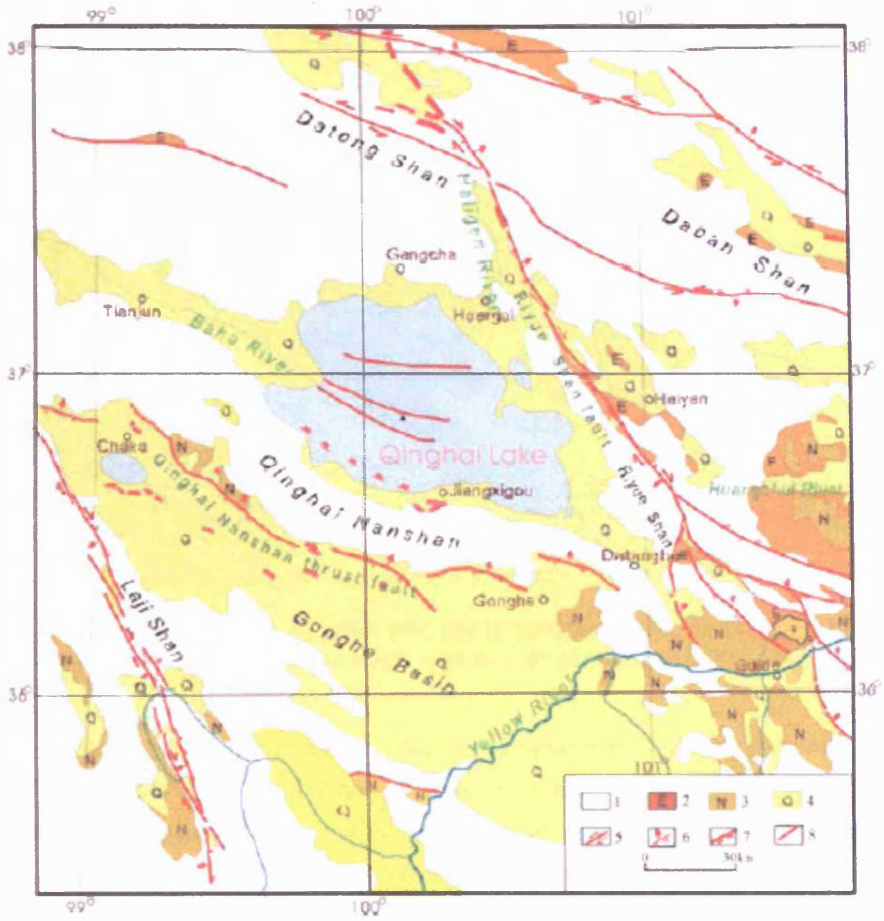

Figure 3.11 – Map of active tectonics in the Lake Qinghai region. (1) pre-cenozoic bedrock; (2) Paleogene red beds; (3) Neogene red beds; (4) Quaternary loess and other sediments; (5) active strike slip faults (arrows indicate direction of motion); (6) active thrust fault or reverse faults (arrows indicate direction of dip of fault plane); (7) active normal faults with ticks indicating dips of fault planes; (8) active fault with unknown sense of motion (An, 2003).

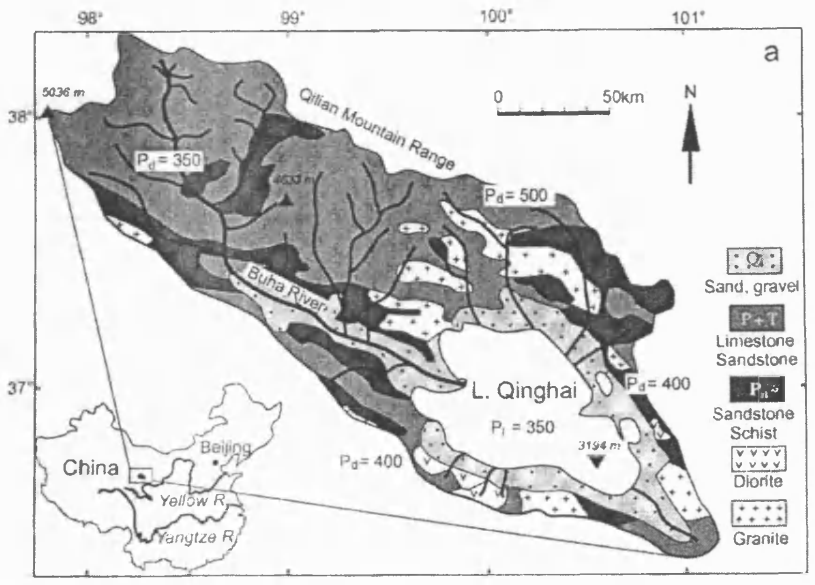

Figure 3.12 – Location of Lake Qinghai and the lithologies in its drainage basin, P_l and P_d mean annual precipitation in the drainage area and over the lake (After Yan, 1998).

Since the beginning of the century, the area of Lake Qinghai has shrunk: from 4980 km^2 in 1908, 4568 km^2 in 1957 to 4474 km^2 in 1972 and 4304 km^2 in 1986. This rapid shrinkage of the surface area reflects the long-term deficit in the water budget of Lake Qinghai. Water balance studies (1958-1990) show that evaporation exceeded the water input resulting in the drop in the lake's level. Additional moisture conditions of the lake basin shows a slight decrease of precipitation over the catchment (333.3 mm/yr in 1958-1967, 293.8 mm/yr in 1968-1977 and 288.9 mm/yr in 1978-1986 (Qin and Huang, 1998). The total catchment runoff has declined considerably during the period of 1958 to the end of 1980s – discharge of Buha River was 30.88 m^3/s in 1958-1967, 25.38 m^3/s in 1968-1977 and 19.47 m^3/s in 1978-1986. This reflects the arid conditions that have persisted for a considerable time, compounded by a decline in the soil water content.

The river waters entering Lake Qinghai reflect the dominance of the carbonate-rich sedimentary rocks in the Buha River basin (67% inflow), and are Ca-(Na)-HCO_3-type (Table 3.2). They are poor in dissolved silica (ranging from 1.9 to 5.7 mg/l); their content of total dissolved solids is between 300 and 400 mg/l and pH between 8 and 9. The (Ca+Mg)/HCO_3 molar ratio is about 0.47. The present-day lake water is of magnesium-sulphate-subtype and exhibits a salinity of 14.1 g/l (pH 9.2) (Yan *et al.,* 2001). The lake water has evolved since the basin became closed *c.* 9800 years ago. Sodium and chloride are the dominant ions; the lake is currently saturated with respect to aragonite and hydromagnesite. Mirabilite has also been found at times of low water temperature (Sun *et al.,* 1992). During the warm season, the lake becomes thermally stratified (epilimnion 12-15°C, hypolimnion <6°C), whereas during the cold season (from October to April) the lake mixes and becomes ice covered.

Location	Lake Qinghai
Climate (precipitation, mm/a)	cold continental
Drainage area	350-550
Lake surface	350-400
Drainage area	
Surface area (km^2)	30,000
Lithology	limestone, sandstone, shale
Total denudation rate, DR_t (mm/ka)	40
Chemical denudation rate, DR_c (mm/ka)	20
Lake basin	
Lake area (km^2)	4400
Altitude (m a.s.l.)	3194
Lake volume (km^3)	77.5
Maximum depth (m)	27
Lake closure time (ka BP)	10
Hydrological leakage[a]	leaky
Basin capacity for sediments (with respect to overflow, km^3)	500
Subsidence rate (m/ka)	0.2
Estimated basin lifetime (ka)[b]	300
Inflow water	
TDS (g/l)	350
SiO_2/HCO_3 (mmol/mmol)	0.01
Ca/HCO_3 (mmol/mmol)	0.32
pH	8.3
Lake water (present-day)	
TDS (g/l)	14.5
Composition (principal ions)	Na-(Mg)-(K)-Cl-SO_4
SiO_2 (mg/l)	0.35
Temperature (°C)	7.5
pH	9.2

Table 3.1 - Basic characteristics of Lake Qinghai (Yan *et al.*, 2001). [a]inferred from long-term Cl budget (Yan, 1998), [b]inferred from present sediment input

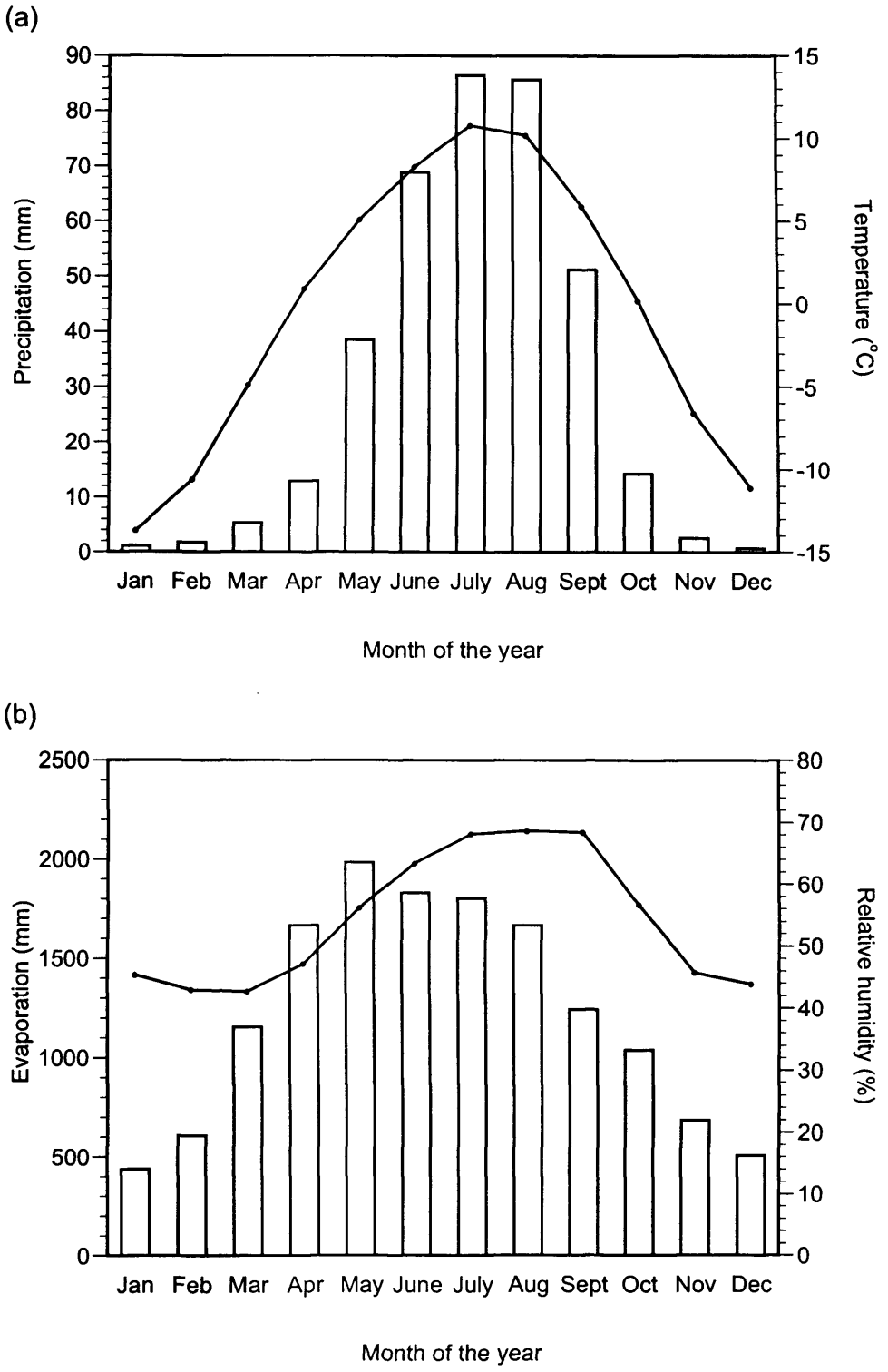

Figure 3.13 – (a) averaged precipitation (bar) and temperature (line) (1958-1999); (b) averaged evaporation (bar) and humidity (line) from Gangcha County meteorological station, northern margin of Lake Qinghai.

	Water type	K	Na	Mg	Ca	Cl	SO_4	HCO_3	SiO_2	TDS
Lake Qinghai	inflow	1	27.4	13.9	46	13.3	23.9	220	2.5	350
	lake	157.8	3973	798	13	5850	2380	1200	0.35	14,380

Table 3.2 - inflow and lake water composition of Lake Qinghai. Data in mg/l (From Yan *et al.*, 2001)

3.4.3 Catchment geomorphology and environmental history

The area around the lake has shore features that offer evidence of past highstands, while sediments in shore from the lake include evidence of periglacial conditions during the last glacial age, as well as subsequent aeolian sedimentation and soil formation (Porter, 2003). Of particular note is a large terraced outwash fan that provides evidence of several episodes of late Quaternary alpine glacier advance and retreat (Porter *et al.*, 2001). A large field of active dunes lies to the East of the lake, where recent erosion has exposed buried soil complexes that stand out in relief and appears as a dark-brownish band within the enclosing light-coloured sand. Features on the southern margin of the lake include pit exposures of alluvium (pebble-cobble-gravel) capped by loess and a palaeosol (Fig. 3.14). The gravel underlies a broad bajada surface (coalescing alluvial fans) formerly at the northern base of the Qinghai Nan Shan (Porter *et al.*, 2001). There are also a number of wedge features that penetrate into the gravels and are overlain by a loess-palaeosol section (Fig. 3.14).

A large alluvial fan heads into steep valleys that drain glaciated drainage basins along the western Qinghai Nan Shan. The northern flank of the range is indented by cirques and glaciated valley heads excavated by small glaciers during the most recent glacial age. Most of the glaciers faced north to northeast and ranged in length from 1 to 5 km. The most recent glaciers (MIS 2) had an average equilibrium-line altitude (ELA) of 4250 ± 50 m (Porter *et al.*, 2001). The cirques now are ice free, but extrapolation of present ELAs from nearby glacierized mountains suggest that the present ELA lies at *ca.* 5000 m (Shi *et al.*, 1992). Snowline depressions during the last glaciation therefore have been about 750 ± 50 m.

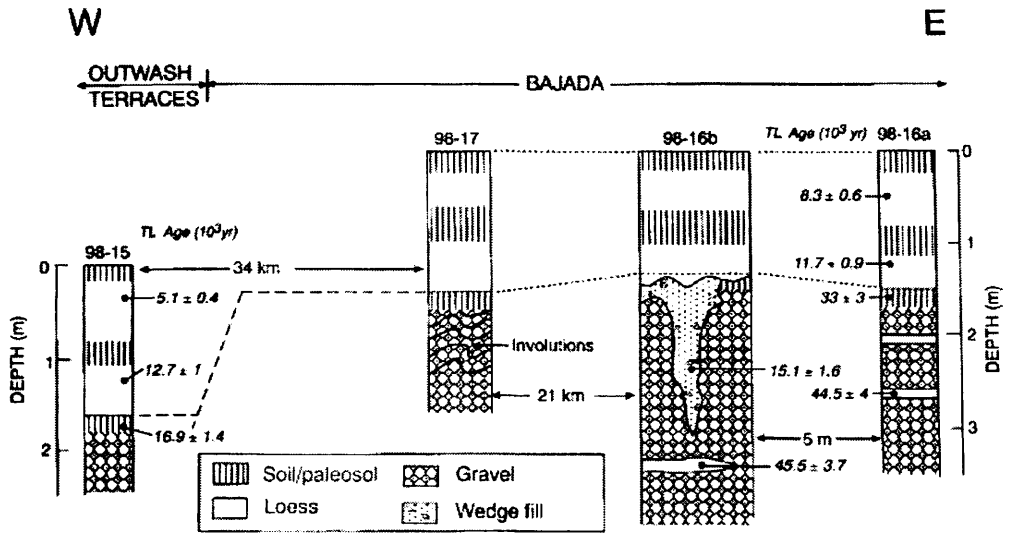

Figure 3.14 – Stratigraphic sections showing the relationship of the ground wedge at locality 98-16b to adjacent alluvial and aeolian units to involutions in a gravel section to the west, and to loess and palaeosol units overlying outwash terraces beyond the bajada surface (After Porter *et al.*, 2001).

3.5 Previous records of environmental change from Lake Qinghai

Preliminary scientific investigations during the 1960s and 1970s provided initial data on the biology, chemistry and hydrology of the lake. A comprehensive study was then undertaken by a Sino-Swiss limnogeological expedition in 1985 (Kelts *et al.*, 1989; Lister *et al.*, 1991), recovering seismic profiles and piston cores to calibrate palaeoclimatic models of monsoon and insolation fluctuations over the NE Tibetan Plateau since the last glacial maximum. This study demonstrated that the past lake levels of Lake Qinghai have responded to changing climatic conditions, especially the Asian monsoon. Lake level fluctuations were primarily caused by atmospheric precipitation/evaporation balances and histories of lake level shifts were proxies for past regional climatic development (Lister *et al.*, 1991).

Lister *et al.*, (1991) produced a $\delta^{18}O$ record from ostracod valves in order to determine changing lake levels since the latest Pleistocene (summarised in Fig. 3.15). They showed that Lake Qinghai has responded to changes in effective moisture since the last glacial and that lake levels fluctuate in response to small changes in the climatic/hydrologic regime. The authors noted that the rate of isotopic enrichment of lake water is a function of input- and evaporative-loss rates and for a given characteristic lake level, under a stable climatic/hydrologic regime, isotope composition will remain constant. A changed climatic/hydrologic regime may alter the mean lake level (surface area) and its long-term ^{18}O enrichment rate ($\delta^{18}O$ gradient). Short-term excursions however, are superimposed on the long-term $\delta^{18}O$ gradient for a given closed-basin lake and can result from periods of unusually dry or wet conditions; a lowering of the lake to below its mean stable level increases the ^{18}O enrichment rate, whereas a rise to above stable level will decrease or

negatively override the ^{18}O enrichment rate. Return to a mean stable lake-level tends to restore $\delta^{18}O$ values back to a pre-event track. Eventually an isotopic steady-state is reached between the lake water and atmosphere and the lake water $\delta^{18}O$ will not increase further under the given climatic/hydrologic regime. Once that stage has been reached, only short-term events leading to periodic isotopic dilution of the lake waters may leave a signal. A shift in isotopic steady-state can result from climatic or hydrologic change, but is not directly interpretable in terms of lake-level change.

Further work by Yu and Kelts (2002) on the same set of cores focussed on the late-glacial/Holocene transition. They showed that the climate was unstable, showing three abrupt shifts in hydro-climatic conditions on time scales of less than a millennium. Correlation with the Sumxi Lake record (Gasse *et al.,* 1991), Guliya ice core (Thompson *et al.,* 1997) and the Baxie loess-palaeosol section (An *et al.,* 1993) demonstrates that this late-glacial climatic instability is a regional phenomenon (Yu and Kelts, 2002), as a result of increasing seasonality of insolation and changing surface boundary conditions accompanying deglaciation. The authors suggest that two distinct hydro-climatic regimes existed during this period, (1) ~ 11600 to 10700 ^{14}C yr BP, where increased seasonal inflow occurred during relatively cool climate with lower summer evaporation, and (2) ~10700 to 10000 ^{14}C yr BP, which is characterised by arid conditions with enhanced evaporation and reduced catchment inflow, leading to the formation of a carbonate playa environment. This arid event is chronologically synchronous with the European Younger Dyras (Lister et al. 1991, Yu and Kelts, 2002). However, the proxy record from Lake Qinghai presented by Yu and Kelts (2002) provides no clear evidence for a return to cold climatic conditions during the Younger Dryas time. Increases in both carbonate production and organic productivity suggest intensified summer evaporation, which is distinctly different from the cold arid period noted in the record from ~12500 to 11600 ^{14}C yr BP (Lister *et al.,* 1991; Fig. 3.15).The authors suggest that increased summer temperature, as a result of increased summer insolation and regional deglaciation, brought about the enhancement of summer evaporation and aridification of the lake, but a further enhancement of monsoonal rainfall did not come along until about 10000 ^{14}C yr BP. This suggests a step-wise pattern of climatic change across the late-glacial/Holocene transition along with abrupt shifts in effective moisture on the NE Tibetan Plateau.

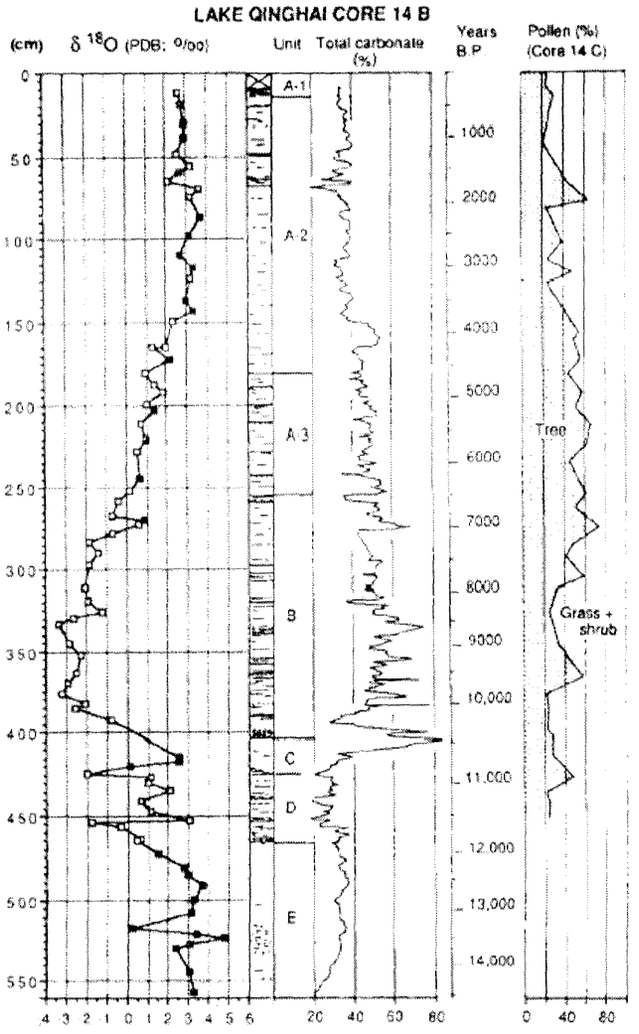

Stages in the evolution of Lake Qinghai since the latest Pleistocene

~ **3000 yr BP** - isotopic steady-state obscures the climatic/hydrologic regime-dependent $\delta^{18}O$ gradient, there is little stratigraphic evidence to suggest that lake level has been significantly below present level during that time. Three negative shifts at ~ 2800, 1700, and 1300 yr BP may correspond to Plateau glacier advances at ~3000, 2000 and 1500 yr BP during China's neoglacial. Questions whether negative $\delta^{18}O$ excursions reflect lake-level or colder mean air temperature for annual precipitation

~ **6800-3000 yr BP** - corresponds to China's climatic optimum, $\delta^{18}O$ values show the least short-term variations (< ± 0.5‰) for the whole record, characteristic of a large stable lake system with uniform environmental conditions

~ **10200-6800 yr BP** - the modern climatic regime has existed in the Qinghai region since ~ 10000 yr BP and at ~10200 yr BP the basin began filling towards modern lake dimensions. Substantial lake-level rises probably characterised the periods ~10200 to 9800, 9500-8500, 8300-7200 yr BP and through perhaps a century at ~6800 yr BP. Decreasing lake-levels probably characterised the intervening intervals.

~ **10800 yr BP** - a possible weakening of an incipient monsoon system for several centuries leading to increased aridity, a drop in lake level and a cessation of river-silt influx into the southwestern basin

~ **11800 yr BP** - river transported silts first reach the centre of the southwestern basin

~ **12500 yr BP** - regional climate remained arid until this time when the first post-Glacial strengthening of monsoonal circulation may have occurred. The lake had a total surface area considerably smaller than that of today, sedimentation was dominated by loess, water depths cannot have exceeded a few metres and surfaces were probably frozen for much of the year

Fig. 3.15 - Evolution of Lake Qinghai since the latest Pleistocene (Lister *et al.*, 1991). $\delta^{18}O$ (VPDB ‰) values for *Limnocythere inopinata* (filled squares) and *Eucypris inflate* (open squares) versus sediment depth in Lake Qinghai core 14B. Interpolated ages are based on AMS ^{14}C dates. Pollen percentages are for core 14C (site adjacent to core 14B). For tree pollen *Betula* percentages are about double that of *Pinus* for the early Holocene but only about half for *Pinus* through the rest of the Holocene.

More recently, a high-resolution study by Henderson *et al.,* (2003) demonstrated that isotope composition of authigenic and ostracod carbonate provides an indication of lake-level change and evaporative history over the past ~ 300 years and testifies to marked climatic variability over NE Tibetan Plateau during the past few centuries. Comparisons of the $\delta^{18}O$ curves with recorded lake level suggest that Lake Qinghai has responded to variations in effective precipitation as shifts in $\delta^{18}O$ values reflect changing lake level which is primarily a response to effective precipitation change. As these fluctuations are accompanied by changes in water salinity, an independent palaeosalinity indicator was investigated (Sr/Ca and Mg/Ca ratios of ostracods) as a check on the interpretation of the stable isotopes. However, the use of trace elements (Sr and Mg) was not possible in Lake Qinghai's sediments due to water chemistry conditions and diagenetic effects on the sub-fossil ostracod shells (Henderson, 1999).

3.6 Summary

Climate in NW China has shown some large-scale variations since the last glacial maximum. The observed changes have been linked to the onset of monsoon strengthening as the Tibetan Plateau received increased insolation. As a result, most records show a change towards more humid climates and it appears to have been a regional phenomenon. The occurrence of a mid-Holocene megathermal is the accepted climate pattern for NW China, but new evidence is suggesting that this might not be the case. More recently, attention has begun to focus on changes in climate over the past 2000 years. The studies suggest abrupt changes in the climate of NW China, most notably at 1300 AD, with the recent climate warming of the 20th Century apparent in high-altitude ice cores.

Chapter Four
Methods

Introduction

This study is based on four radiometrically-dated short cores (*c.* 80 cm), coupled with analysis of modern lake sediments and catchment material and surface waters from the lake and other parts of the catchment hydrological cycle. Lake Qinghai was cored over two successive field seasons in May 2001 and October 2001, while additional material had been recovered in May 1999. Extensive water and surface sediment sampling was carried out during these trips in order to characterise the contemporary hydrology of the lake and establish links between the lake and its sediment record. Isotopic analysis of sediment and waters were performed at the NERC Isotope Geosciences Laboratory (NIGL), British Geological Survey, Nottingham, UK (contract no. IP/679/1100), while radiocarbon analysis was undertaken at the NERC Radiocarbon Laboratory, East Kilbride, UK (contract no. MHG/1004.1002/700). ^{210}Pb and ^{137}Cs determinations were carried out at the School of Chemistry, Physics and Environmental Science, University of Sussex, UK and x-ray diffraction analysis was undertaken at the Department of Earth Sciences, Birkbeck College, UK and Department of Earth and Environmental Sciences, University of Greenwich, UK. The following sections will discuss the methods used for water chemistry analysis, including the locations they were taken, followed by surface and core sediment analysis and radiometric dating.

4.1 Water analysis

4.1.1 Collection of modern waters

Modern water samples were collected from the main body of the lake at the surface and at 5 metre depth intervals from the same point using a van Dorm sampler at the sampling locations shown in figure 4.1. Water samples were also taken from major river inflows, nearby lakes, springs, plus some isolated rainwater events (Tables 4.1 and 4.2). Samples were collected in acid-washed, leak-tight polyethylene bottles, rinsed several times with the water to be sampled and sealed with PVC tape. All samples were kept refrigerated at 4°C prior to laboratory analysis.

60 ml of untreated water was collected for oxygen ($^{18}O/^{16}O$) and hydrogen (*D*/H) isotope ratios and 100 ml for carbon ($^{13}C/^{12}C$) isotope ratios, taking care not to include any organic or calcareous particulate material. For carbon isotope ratios, the total dissolved inorganic carbon (TDIC) was precipitated on site as $BaCO_3$ by replacing 15 ml of the sample with $BaCl_2.2H_2O$ + NaOH solution after sampling. The solution was prepared in the laboratory by adding 500g of $BaCl_2.2H_2O$ and 35g of NaOH pellets slowly to 800 ml of distilled water placed in an acid-washed glass bottle. The solution was allowed to stand for several days to allow $BaCO_3$ to settle. The clear solution above was then decanted into 100 ml plastic bottles for use in the field.

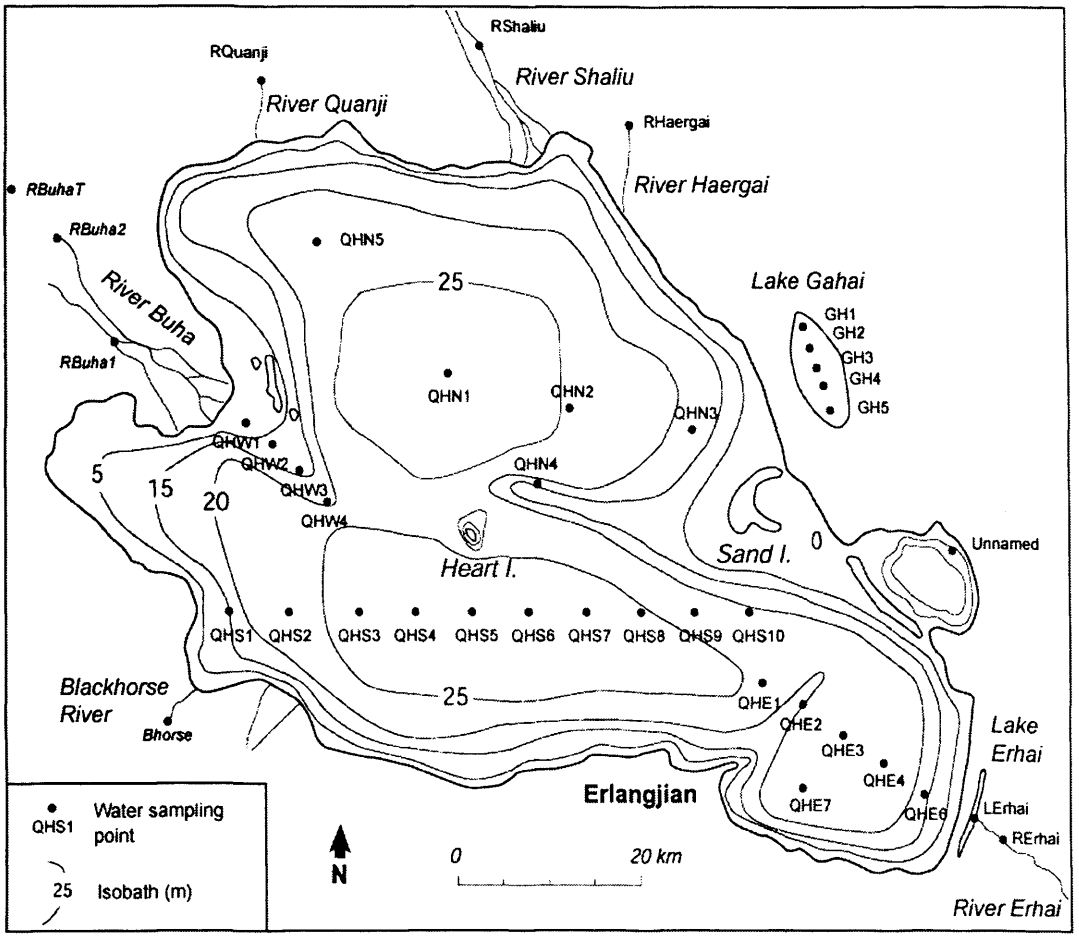

Figure 4.1 - Water sampling framework for Lake Qinghai (May and October 2001)

4.1.2 Physical limnology

pH measurements were conducted in the field, on unfiltered samples using a Hanna instruments® pH meter with a general purpose combination electrode. The electrode was allowed to stand in the sample for several minutes before the pH value was recorded. Values were recorded to the nearest 0.1 pH unit. The pH was calibrated using pH buffer 7 and 4 solutions prior to measurement. Test measurements were made on distilled water samples before each run.

Temperature measurements were conducted in the field, on unfiltered samples using a Hanna instruments® thermometer. The thermometer was allowed to stand in the sample for several minutes before the temperature was recorded.

Sample	Water depth (m)					Sediment taken
	0	5	10	15	20	
QHE1	✓	✓	✓	✓		+, Δ,
QHE2	✓	✓	✓			+
QHE3	✓	✓	✓	✓		+, Δ
QHE4	✓	✓	✓	✓		+, Δ
QHE6	✓					+
QHE7	✓	✓	✓	✓		+, Δ
QHS1	✓					+, Δ
QHS2	✓					+
QHS3	✓	✓	✓	✓	✓	+, Δ
QHS4	✓	✓	✓	✓	✓	+
QHS5	✓	✓	✓	✓	✓	+
QHS6	✓	✓	✓	✓	✓	+, Δ
QHS7	✓	✓	✓	✓	✓	+
QHS8	✓	✓	✓	✓		+
QHS9	✓	✓	✓	✓		+
QHS10	✓	✓	✓	✓		+, Δ
QHW1	✓					+, Δ
QHW2	✓	✓				+
QHW3	✓	✓				+
QHW4	✓	✓	✓	✓		+, Δ
QHN1	✓	✓	✓	✓	✓	+
QHN2	✓	✓				+
QHN3	✓	✓				+
QHN4	✓	✓	✓			+, Δ
QHN5	✓					+, Δ
GH1	✓					+
GH2	✓					+
GH3	✓					+, ϕ
GH4	✓					+
GH5	✓					+

Table 4.1 – Location of water samples ($\delta^{18}O$, δD and $\delta^{13}C_{TDIC}$) from Lake Qinghai and Lake Gahai (May and October, 2001). + surface sediment taken, Δ mini-Mackereth taken, ϕ Livingstone taken.

Sample	Description	Comments
Counter Flow River	Small permanent river (does not flow into main lake)	Flowing
Counter Flow Lake	Small lake 10m from Lake Qinghai	Macrophyte dominated
Unnamed Lake	Cut off lake from Lake Qinghai	
Black Horse River	Small permanent river	Flowing
River Buha (1)	Major river flowing into Lake Qinghai.	Flowing
River Buha (2)	Major river flowing into Lake Qinghai.	Flowing
River Buha (3)	Tributary to River Buha	Flowing
River Quanji	Perennial river	Flowing
River Shaliu	Perennial river	Flowing
River Haergai	Small permanent river	Flowing
QH2	Edge of Lake Qinghai	Marsh area
QH4	Edge of Lake Qinghai	Marsh area
Precipitation	Single event in May 2001	Rain lasted *c.* 4 hours
Spring	Single source in October 2001	Nr. Counter Flow Lake

Table 4.2 – Location of water samples ($\delta^{18}O$, δD and $\delta^{13}C_{TDIC}$) from around Lake Qinghai (May and October, 2001).

4.1.3 Isotopic analysis of modern waters

4.1.3.1 Oxygen isotope analysis ($\delta^{18}O_{water}$) and hydrogen isotope analysis (δD_{water})

2 ml of untreated water was pipetted into a sample vessel with any air remaining in the vessel pumped away through a capillary tube to minimise water vapour loss. Dry CO_2 is then emitted into each flask and is mixed with the sample water by shaking for six hours at a constant temperature of 23°C. Once the CO_2 is fully equilibrated with the sample it is admitted directly to the mass spectrometer for analysis (Arrowsmith, 1998).

4 µl of untreated water sample was reacted with 100 mg of zinc turnings at a constant 500°C (Heaton, 1992). The hydrogen gas liberated was collected for analysis. Measurements were made on a VG SIRA 10, split-flight mass spectrometer. Isotope values ($\delta^{18}O$ and δD) are reported as per mil (‰) deviations of the isotopic ratios ($^{18}O/^{16}O$ and D/H) from Standard Mean Ocean Water (SMOW).

4.1.3.2 Carbon isotope analysis ($\delta^{13}C_{TDIC}$)

Precipitated $BaCO_3$ from the water samples (see section 4.1.1) were filtered using cellulose nitrate filter papers (Whatman no. 14) and washed several times with deionised distilled water. The TDIC samples were then analysed for $\delta^{13}C$ using a VG Optima mass spectrometer.

4.2 Methods for sediment analysis

4.2.1 Collection of surface and core sediments

4.2.1.1 Surface sediments

These were collected using a Glew gravity corer (Glew, 1991) at the water sampling sites shown in figure 4.1 and table 4.1. The top 0.5 cm of each core was extruded from each site, being replicated three times in order to retrieve enough material. Samples were then stored in sealed Whirlpack® plastic bags and refrigerated at 4°C.

4.2.1.2 Core sediments

A total of fifteen cores were taken from Lake Qinghai (Fig. 4.2) using a pneumatic mini-Mackereth corer (Mackereth, 1969), with an undisturbed sediment-water interface being preserved in each core that was taken (Fig 4.3). The cores were extruded at 0.5 cm intervals for the upper 30 cm section and then at 1 cm intervals to the bottom of the core. Sediments were stored in sealed Whirlpack® plastic bags and refrigerated at 4°C. Core lengths ranged from 58 to 83 cm.

For Lake Gahai, a core was retrieved using a modified piston Livingstone corer (Cushing and Wright, 1965), with an undisturbed sediment-water interface preserved in the core. The core was extruded at 0.5 cm intervals and sediments were stored in sealed Whirlpack® plastic bags and refrigerated at 4°C. Total core length was 105 cm.

4.1.2.3 Core selection

Cores selected for the present study were chosen from a number that were taken (Fig. 4.2), as well as utilising material previously retrieved in 1999 by the author. The following cores are to be used in this study: QHE2/01, QHS3/01, QING6, QING10 and GAHA1/01. They were chosen to be representative of the different sub-basins that occur in Lake Qinghai.

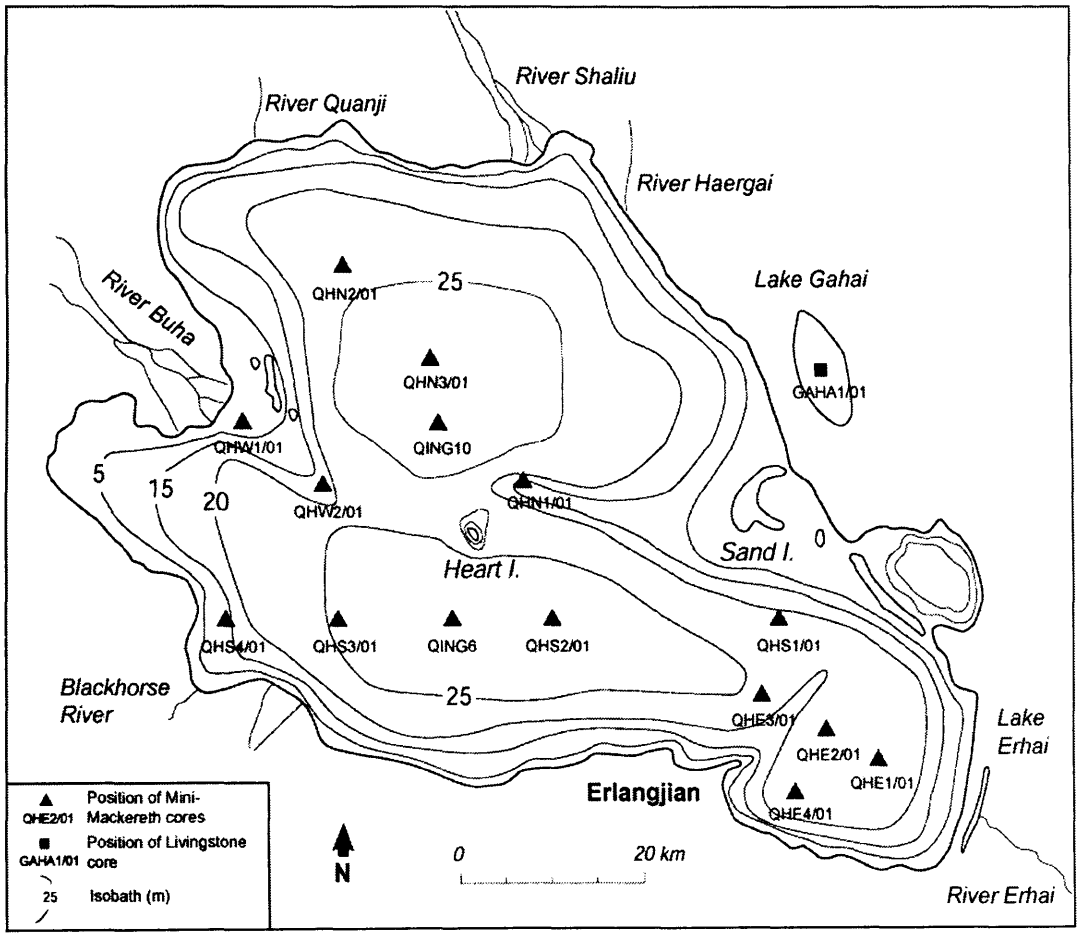

Figure 4.2 – Cores retrieved from Lake Qinghai (May, 1999; May and October, 2001)

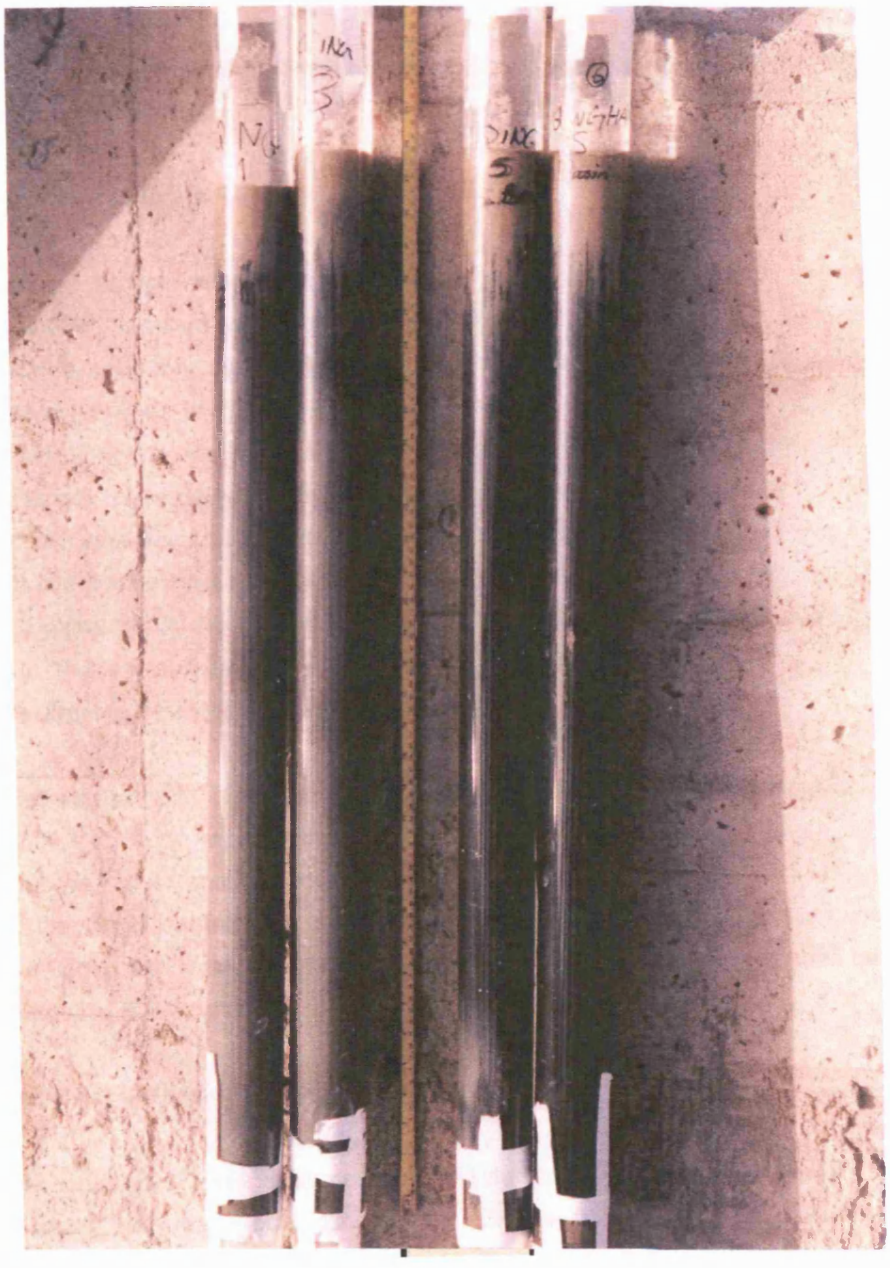

Figure 4.3 – Example of mini-Mackereth cores take from Lake Qinghai

4.2.2 Sediment analysis

A number of analyses were undertaken on contiguous sediment samples from the selected cores and the surface sediments.

4.2.2.1 Sediment analysis – loss on ignition

The percentage organic matter and carbonate is one of the simplest core characteristics to determine and is estimated by using a loss on ignition process (Dean, 1974). An empty crucible was weighed to 3 decimal places and between 1 and 2 grams of wet sediment was added. The crucible was re-weighed and placed in the oven for at least 12 hours or overnight. The crucibles were then removed from the oven and allowed to cool in a dessicator (to prevent re-absorption of moisture) before re-weighing. The percentage weight remaining after drying can then be calculated. The same sample can also be used for loss on ignition analysis. The dried (overnight at 105°C) sediment samples in crucibles were placed back in the furnace and kept at 550°C for 2 hours. After slight cooling the samples were placed in a dessicator and allowed to cool fully before re-weighing. The percentage of the dry weight lost on ignition was then calculated, with the remaining ash sample being used for carbonate analysis.

The weighed ash samples (see method for loss on ignition) were placed back in the furnace and heated to 950°C for 2 hours. After this the crucibles were removed and placed in a dessicator as described above. When cool, the samples were re-weighed and the difference between the ash weight and the weight lost at 925°C was multiplied by 1.36 (to allow for the difference between the molecular weights of CO_2 and CO_3) to derive the carbonate content which can then be expressed as a percentage of the dry weight.

4.2.2.2 Sediment analysis – x-ray diffraction

X-ray diffraction analysis was determined on a Siemens D500 difffractometer with K710 X-ray generator under the tube operating conditions of 40Kv and 40mA. Scan parameters were 1 degree two theta per minute, scanning from 25 to 35 degrees two theta. Approximately 1g of ground sample (as prepared for authigenic carbonates) was loaded into circular holders and stacked into a multi-sample changer with rotation of sample to enable homogeneity. Data was gathered through the DACO_MP interface into the DiffracPlus software suite.

4.2.2.3 Sediment analysis – scanning electron microscope

In order to look at carbonate provenance, sediments that were prepared for isotope analysis were sieved onto a SEM stub and coated with gold. These stubs were then placed into a scanning microscope (JEOL JSM-6301F) with digital image capture via SemAfore (version 4.0).

4.2.2.4 Isotope analysis – authigenic carbonates

Wet sediment samples were wet sieved through an 80μm sieve cloth and the >80 μm fraction retained for ostracod analysis (see next section) whereas the <80 μm was collected in beakers and allowed to settle overnight. The supernatant was then poured off and the remaining residue oven dried at 105°C. The dried residue was gently disaggregated in 5% sodium hypochlorite (NaOCl) solution (12% Chlorox) overnight to oxidise any remaining organic matter. Samples were washed three times in deionised distilled water and filtered through quartz-mirco filter paper (Whatman QM-A), dried at 40°C and ground and homogenised using a pestle and mortar. These isolated carbonates were reacted with anhydrous phosphoric acid *in vacuo* overnight at a constant 25°C. The CO_2 liberated was separated from water vapour and collected for isotope analysis. Measurements were made on a VG Optima mass spectrometer.

Isotope results are expressed in the usual delta (δ) notation as the per mil (‰) difference to the Vienna Pee Dee Belemnite (VPDB) marine carbonate standard for carbon and oxygen:

$$\delta\,‰ = [(R_{sample}/R_{VPDB}) - 1] \times 10^3 \qquad (4.1)$$

where R is the ratio ($^{13}C/^{12}C$) or ($^{18}O/^{16}O$). Ratios were based on the calibration of the laboratory standard NSB-19.

Errors calculated from the standard deviation of laboratory standards used throughout the analyses show that analytical error is ± 0.1‰ for □^{18}O and □^{13}C of authigenic carbonate.

4.2.2.5 Isotope analysis – organic material

Isotopic analysis of sedimentary organic carbon was conducted on three cores – QING6, QHS3/01 and GAHA1/01 and on surface sediments. Contiguous samples were taken and reacted with 5% HCl overnight to remove carbonate. Samples were then washed three times in deionised distilled water and filtered through quartz-mirco filter paper (Whatman QM-A), dried at 40°C, ground and homogenised in a pestle and mortar. 5-10 μg of the remaining organic material was loaded into buckets and the precise weight (three decimal places) was recorded. $^{13}C/^{12}C$ analyses were performed by combustion using a Carlo Erba 1500 on-line to a VG Triple Trap and Optima dual-inlet mass spectrometer. $\delta^{13}C_{organic}$ values were reported relative to the VPDB scale using a within-run laboratory standard (cellulose, Sigma Chemical prod. No. C-6413) calibrated against NBS-19 and NBS-22. Percentage carbon and nitrogen, used to calculate C/N, were measured using a Carlo Erba elemental analyser, calibrated through an internal acetanilide standard.

Errors from the standard deviation of standards used throughout the analyses show that analytical error for $\delta^{13}C_{org}$ were ± 0.1‰ and ± 0.2‰ for C/N ratios.

4.2.2.6 Isotope analysis – biogenic carbonate

Ostracod analysis was performed on surface sediments and cores QING6 and GAHA1/01. Ostracod concentrations within the sediments were generally high, with enough valves present to perform isotopic analysis (*c.* 50 μg of calcium carbonate). Residue retained from the authigenic carbonate preparation (see section 4.2.2 – Isotope analysis – authigenic carbonates) was dried at 105°C and used for ostracod extraction. The > 80 μm fraction was spread on a picking tray and ostracods were selected using a fine paint brush (0000) and de-ionised water under a low power binocular microscope (x120) and stored on microfossil slides for subsequent isotopic analysis. The sediments of Lake Qinghai are dominated by assemblages of *Limnocythere inopinata* (in the upper parts), while Lake Gahai was dominated by *Eucypris inflata*; shells of both species selected for analysis lacked obvious signs of diagenesis such as surface pitting, cracking and overgrowths.

$^{18}O/^{16}O$ and $^{13}C/^{12}C$ analysis was performed on samples of *L. inopinata* (~ 40 valves per sample) and *E. inflata* (~10 valves per sample). Cleaned samples were placed in small glass buckets and similar weights of laboratory standard Carrara marble ('KCM' calibrated against NBS-18 and NBS-19), were loaded into the carousel mechanism of the VG Isocarb™. Samples were subsequently dropped into a reaction vessel containing 100% phosphoric acid at 90°C, and $^{13}C/^{12}C$ and $^{18}O/^{16}O$ ratios of liberated CO_2 analysed on-line in a VG Optima™ mass spectrometer. Due to the lack of sufficient *L. inopinata* in a number of levels of QING6, *E. inflata,* which was abundant at these sample levels were used. Paired analyses of both species were undertaken at levels where they both occurred in order to quantify differences in isotopic vital effects (von Grafenstein *et al.,* 1999).

Errors from the standard deviation of standards used throughout the analyses show that analytical error for $\delta^{18}O$ and $\delta^{13}C$ of ostracod carbonate were ± 0.1‰.

4.3 Methods for chronological analysis

Lake sediments naturally contain radioactive elements (radionuclides), which decay at a known rate. As long as their initial concentrations are known, measurements of radionuclides provide a geological clock, allowing age determinations to be made. The decay of radionuclides can be expressed using the radioactive decay equation:

$$A = A_0 e^{-\lambda t} \qquad (4.2)$$

where A = activity (whose standard units are Bq/kg, where 1 Bq = 1 atomic disintegration per second); A_0 = initial activity; λ = the decay constant, or the probability that any particular atom will disintegrate in unit time; and t = time.

4.3.1 ^{210}Pb and ^{137}Cs dating

^{210}Pb (half-life = 22.3 years) is a naturally-produced radionuclide that has been extensively used in the dating of recent sediments (El-Daoshy, 1988). Dating is based on determination of the vertical distribution of ^{210}Pb derived from atmospheric fallout (termed unsupported ^{210}Pb, or $^{210}Pb_{excess}$), and the known decay rate of ^{210}Pb (Appleby and Parish, 2003). ^{137}Cs (half-life = 30 years) is an artificially produced radionuclide, introduced to the study area by atmospheric fallout from nuclear weapons testing and nuclear reactor accidents.

4.3.1.1 ^{210}Pb dating

^{210}Pb reaches sediments by 2 routes: (1) deposited material contains ^{210}Pb derived from radioactive decay of ^{226}Ra (termed "supported" ^{210}Pb); (2) ^{226}Ra in rocks and soils decays to ^{222}Ra (a gas). Some of this diffuses into the atmosphere, and some decays to ^{210}Pb. This is then washed out of the atmosphere by precipitation and incorporated into sediments (termed "excess" ^{210}Pb).

The annual deposition of "excess" ^{210}Pb is relatively constant, and once it is incorporated into sediments this excess ^{210}Pb gradually decays away. After 22.3 years, half the original amount is left. Measurement of the vertical distribution of excess ^{210}Pb in accumulating sediments therefore provides a "radiometric clock" and allows dates to be ascribed to sedimentary layers based on this known decay rate.

The ^{210}Pb measured in any environmental samples is thus a sum of 2 components:

$$^{210}Pb_{measured} = {}^{210}Pb_{supported} + {}^{210}Pb_{excess} \quad (4.3)$$

In contrast to the excess ^{210}Pb, the supported activity remains constant, because the ^{226}Ra in the sediment is constantly decaying to replace the $^{210}Pb_{supported}$ lost by radioactive decay. The supported activity can be determined by a range of methods (Appleby and Oldfield, 1992), but often it is taken as being equal to the ^{210}Pb activity in sediment that is greater than 200 years old i.e. in sediment older that 200 years almost all excess ^{210}Pb has decayed away and so $^{210}Pb_{measured} = {}^{210}Pb_{supported}$.

In this study, core sub-samples were counted for 24 hours on a Canberra well-type ultra-low background HPGe gamma ray spectrometer to determine the activities of ^{137}Cs, ^{210}Pb and other gamma emitters (cores QHE2, QING10 and GAHA1). Detection limits were ~5Bq/kg. ^{210}Pb data were unreliable in core GAHA1, due to the extremely low sample masses (< 0.5g). In core QING6, ^{210}Pb activity was determined by a proxy method, through alpha spectrometric measurement of its grand daughter nuclide ^{210}Po. The method employed is based on Flynn

(1968), using double acid leaching of the sediment with ^{209}Po as an isotopic tracer followed by autodeposition of the Po isotopes in the leachate on to silver discs. Discs were counted for a minimum of 400000 seconds, and detection limits are 0.1Bq/kg. The $^{210}Pb_{excess}$ activity was estimated by subtraction of the average value of ^{210}Pb activity in deep core samples (0.025 Bq/g, QING6), or by subtraction of the value of ^{210}Pb activity in the deepest core sample (0.018 Bq/g, QHE2, and 0.024 Bq/g, QING10). This is clearly an estimated value for the latter two cores, and may be a slight overestimate, although downward adjustment of the supported activity value has minimal effect on the sediment accumulation rates determined. These values could be checked by measuring deeper samples until the ^{210}Pb activity is clearly constant with depth, but this was not attempted due to limited resources.

4.3.1.2 ^{137}Cs dating

^{210}Pb dating is often corroborated using ^{137}Cs dating. ^{137}Cs is an artificial radionuclide, with a half life of 30 years, which is present in the environment due to nuclear weapons testing and nuclear reactor accidents. Global release of ^{137}Cs began in 1952, with peak input to the environment in 1958/59 and 1963 (due to pre-treaty increases in above-ground nuclear testing), 1971 (southern Hemisphere) and 1986 (in some regions, from Chernobyl). ^{137}Cs may show discrete concentration "spikes" in accumulating sediments corresponding to 1963 and 1986 (1958/59 and 1971, being smaller inputs, are more difficulty to identify). In favourable conditions, periods of peak fallout/discharge provide subsurface activity maxima in accumulating sediments, which can be used to derive rates of sediment accumulation (e.g. Cundy and Croudace, 1996).

4.3.2 Radiocarbon dating

In order to establish a radiocarbon chronology, a combination of authigenic carbonate and bulk organic samples were extracted from the four cores under investigation. Terrestrial plant macrofossils would have been the most suitable material for radiocarbon dating. However, none were found in the cores investigated, probably because they were taken from relatively deep (>25 m) water. Accelerated Mass Spectrometry (AMS) radiocarbon dating techniques were then used to date the cores QING6, QING10, QHE2/01 and GAHA1/01 (Table 4.2). For authigenic carbonate, 5% sodium hypochlorite solution (Chlorox) was added to bulk samples from specific core levels to remove organic material overnight. Samples were then washed three times in deionised distilled water and sieved at 80 μm to separate out ostracod valves (the >80 μm fraction was retained). The <80 μm fraction was filtered through quartz-micro filter paper (Whatman QM-A), dried at 40°C, ground and homogenised. For organic samples, 5% HCl solution was added to bulk samples from specific core levels to remove carbonate material overnight. Samples were then washed three times in deionised distilled water and filtered through quartz-micro filter paper (Whatman QM-A), dried at 40°C, ground and homogenised.

Carbonate samples were hydrolysed to CO_2 using 85% orthophosphoric acid at 25°C. The gas was converted to graphite by Fe/Zn reduction. Organic camples were digested in 2M HCl (80°C, 8 hours), washed free from mineral acid with distilled water then dried and homogenised. The total carbon in known weight of the pre-treatment samples was recovered as CO_2 by heating with CuO in a sealed quartz tube. The gas was converted to graphite by Fe/Zn reduction. $^{12}C/^{13}C$ ratios were measured on the SUERC AMS during ^{14}C determination and used to model $\delta^{13}C$ values by comparison to the Craig (1957) $^{13}C/^{12}C$ value for PDB. These values were considered the most appropriate to normalise ^{14}C data to $\delta^{13}C_{PDB}‰ = -25$, but are not necessarily representative of the $\delta^{13}C$ in the original sample material. $\delta^{13}C$ values were additionally measured on a dual inlet stable isotope mass spectrometer (VG Optima™) and are representative of $\delta^{13}C$ in the original, pre-treated sample material.

No.	Core	Depth (cm)	Material dated	Justification
1	QING6	78-79	calcite	Provide a basal age for the sequence
2	QING6	47-48	calcite	Provide an upper bracketing age on low-amplitude $\delta^{18}O$ variation
3	QING6	36-37	calcite	Provide a date on the peak in $\delta^{18}O$
4	QING6	78-79	organic carbon	Provide a basal date for the sequence, while trying to determine any hard-water effect
5	QING10	75-76	calcite	Provide a basal age for the sequence
6	QING10	49-50	calcite	Provide an upper bracketing age on the large-amplitude $\delta^{18}O$ variation between 66 and 50 cm
7	QING10	37-38	calcite	Provide an upper bracketing age on the excursion referred to above
8	QING10	49-50	organic carbon	Provide an upper bracketing age on the large-amplitude $\delta^{18}O$ variation between 66 and 50 cm, while trying to determine any hard-water effect
9	QHE2/01	81-82	calcite	Provide a basal age for the sequence
10	QHE2/01	57-58	calcite	Provide a date on the peak in $\delta^{18}O$ values
11	QHE2/01	41-42	calcite	Provide a date on the peak in $\delta^{18}O$ values
12	QHE2/01	41-42	organic carbon	Provide a date on the peak in $\delta^{18}O$ values, while trying to determine any hard-water effect
13	GAHA1/01	92-93	calcite	Provide a basal age for the sequence
14	GAHA1/01	57-58	calcite	Constrain a proposed ^{210}Pb & ^{137}Cs chronology with the basal date
15	GAHA1/01	92-93	calcite	Provide a basal age for the sequence, while trying to determine any hard-water effect
16	GAHA1/01	57-58	organic carbon	Constrain a proposed ^{210}Pb & ^{137}Cs chronology with the basal date, while trying to determine any hard-water effect

Table 4.2 – Samples selected for AMS radiocarbon dating and their justification

Chapter Five
Modern lake hydrology and sediments

Introduction

The isotopic composition of lake water, at a given point in time, is a function of the volume-weighted isotopic values for each component of the lake's hydrologic balance. The aim of investigating the isotopic composition of modern lake-waters is to establish their relationship to modern climate and any other non-climatic processes. This is an important question since the isotopic composition of lake-water can be recorded in precipitates such as authigenic and biogenic carbonates. Thus, if authigenic and/or biogenic precipitates are preserved in lake sediments then measurement of their isotopic composition can be useful for palaeolimnology and, if the relationship between lake-water composition and climate is understood, also for palaeoclimatology. However, to calibrate lake-water response to climate it is necessary to acquire knowledge of the baseline conditions for isotopes (O and H) in the meteoric and surface-water components of the hydrological cycle.

For instance, the oxygen isotope composition of water in a hydrologically open lake will predominantly reflect the isotopic composition of the precipitation received by the lake and therefore it is the controls on the isotopic composition of the meteoric water that will be reflected in a lake's isotopic composition. However, in hydrologically closed lakes, such as Lake Qinghai, the isotopic composition of the lake water is under the influence of a number of inter-related environmental processes. Not only is the isotopic composition of precipitation important, but evaporation, which has a major influence on the water's isotopic composition, is a significant control of water loss and isotope change in closed basin lakes. This chapter aims to present Lake Qinghai's modern isotope hydrology and to assess quantitatively the contemporary water balance of the lake using isotopic mass balance models. It will also look at the carbon cycle within the lake and its catchment.

5.1 Modern Isotope Hydrology of Lake Qinghai

The present climate of China is characterised by a marked gradient in continentality and aridity from southern/eastern to western China and a pronounced feature of its climate is the monsoon circulation, which brings summer rain over a large part of the country (see Chapter 3). The isotopic composition of Lake Qinghai, which lies close to the maximum extent of the modern day monsoon, is therefore influenced by the monsoon rains, but to what extent these are more important than local convective rainfall is still unclear. Many studies have demonstrated that the oxygen isotope composition of mean annual precipitation varies globally (Yurtsever and Gat, 1981) and covariation in $\delta^{18}O$ and δD defines a Global Meteoric Water Line (GMWL) (Craig, 1961). Moreover, remarkably good positive correlations between long-term surface temperature

and the oxygen and hydrogen isotope ratios of precipitation have been established globally (Dansgaard, 1964), which generally correlate well with latitude and altitude of a site (Bowen and Wilkinson, 2002). However, this is not applicable to areas that are significantly affected by monsoonal circulation, (Rozanski *et al.,* 1992; Rozanski *et al.,* 1993; Hoffmann and Heimann, 1997) as discussed below.

5.1.1 Isotope composition of precipitation – China

The modern distribution of stable isotopes in precipitation over China is significantly affected by the East Asian monsoon during the summer, which brings moisture-bearing winds over the continent of Southeast Asia (see Chapter 3). The monsoon also leads to changes in air pressure, wind, and temperature gradients over East and Southeast Asia. This means that the stable isotope systematics of China are highly complex due to the combined influence of temperature, precipitation and circulation changes. The global $\delta^{18}O_p$-temperature relationship is weak in low latitudes, suggesting that there is a different mechanism of moisture transport predominating (Rozanski *et al.,* 1993). In convectively active regions a negative relationship between $\delta^{18}O_p$ in precipitation and amount of precipitation has been observed, where air mass trajectories have a large vertical component, leading to the progressive depletion of ^{18}O and *D* in precipitation (Johnson and Ingram, 2004). Based on this assumption, Hoffman and Heiman (1997) determined an $\delta^{18}O_p$-P relationship for the Asian monsoon region that suggested 'amount effect' was a significant factor influencing the $\delta^{18}O$ of precipitation in China.

The modern-day distribution of $\delta^{18}O$ for Southeast Asia shows a progressive heavy isotope depletion as the monsoon evolves from June to August every year, illustrating its seasonal importance in influencing $\delta^{18}O$ in precipitation and a possible amount effect (Fig. 5.1). This is particularly evident over the Tibetan plateau (30° - 40°N, 80° - 100°E) in the months of July and August (Fig. 5.1). The presence of the Tibetan Plateau intensifies the uplift and cooling of warm air masses generated by the monsoons, leading to increased precipitation over the continent. During the cold season (December – February), this depletion is not seen due to the dominance of the westerly air mass in winter (Fig. 5.1). However, the controls on the isotopic composition of $\delta^{18}O_p$ over China are more complex, as during the summer months both temperature and precipitation are at their highest. Hence, the temperature effect (positive $\delta^{18}O_p/\delta T$) and the amount effect (negative $\delta^{18}O_p/\delta P$) partially cancel each other out (Johnson and Ingram, 2004). Therefore, a different effect may be contributing to the $\delta^{18}O_p$ depending on location.

An investigation into the relationship between temperature, precipitation and $\delta^{18}O_p$ at ten IAEA/GNIP stations across the country (Fig. 5.2) highlighted the different controls on $\delta^{18}O_p$ across China (Johnson and Ingram, 2004). This found that southern China is strongly influenced by summer monsoon precipitation, which is linked to the western Equatorial Pacific, primarily due to

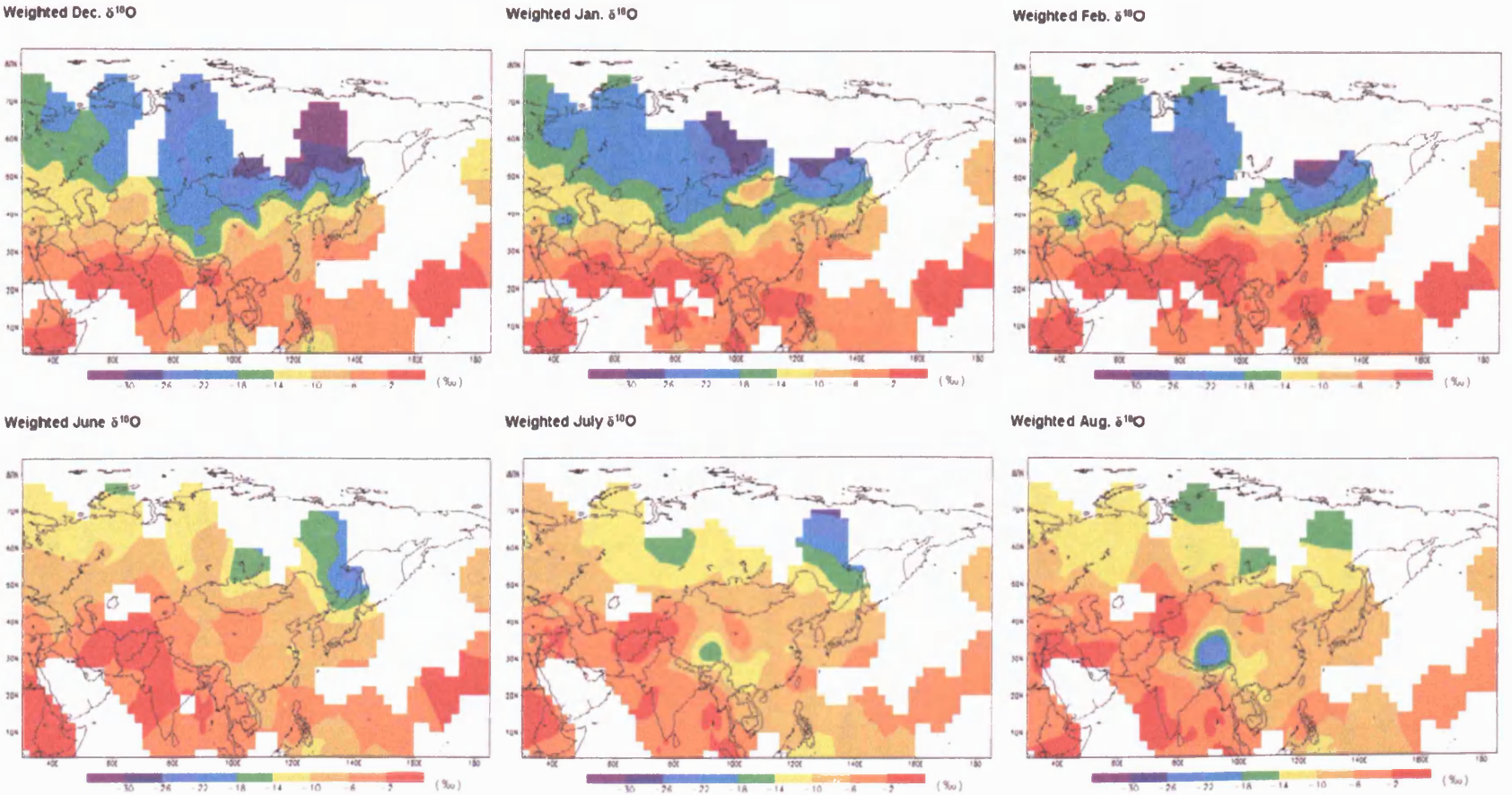

Fig. 5.1 – Modern spatial distribution of weighted $\delta^{18}O$ in precipitation over Central and SE Asia. (adapted from IAEA, 2001)

its location, to the south of the intertropical convergence zone for much of the year (Perry and Walker, 1977; Johnson and Ingram, 2004). The amount effect control was also found to be the dominant control of $\delta^{18}O_p$ in this region in a previous study (Araguas-Araguas *et al.*, 1998). In northern China, where IAEA/GNIP stations are near the limit of the modern-day monsoon, increased precipitation during the summer is linked to a large proportion of locally-derived convective storms, rather than monsoonal rains.

This is supported by a positive relationship between temperature and $\delta^{18}O_p$. The same relationship is found in north-central China, but is further complicated by a positive relationship between precipitation amount and $\delta^{18}O_p$, which Johnson and Ingram (2004) suggest is a multi-colinearity artefact that is larger than the amount effect.

In western China, the majority of precipitation falls in the summer months, and both IAEA/GNIP station records are characterised by very strong positive relationships between $\delta^{18}O_p$ and temperature, as well as a negative relationship with precipitation amount. This reflects different controls at each site. One site, Hetian (Fig. 5.2), is located in the arid northwest of China and is not under monsoon influence, while the other site, Lhasa (Fig. 5.2) is located on the Tibetan Plateau and is under a strong monsoon influence. Precipitation at Hetian is derived from small convective storms, with temperature the dominant control, while the annual $\delta^{18}O_p$ pattern at Lhasa is similar to that of southern China, which is controlled by an amount effect. The $\delta^{18}O_p$ systematics at Lhasa are further complicated by the interaction of the southeast Asian monsoon and the Indian monsoon circulation.

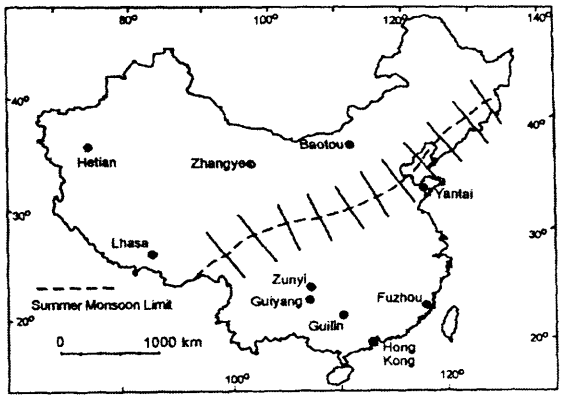

Fig. 5.2 – Map indicating the locations of 10 sites in the IAEA/GNIP database selected for use in Johnson and Ingram (2004). The cross-hatched area denotes the approximate northern limit of the summer monsoon (from Johnson and Ingram, 2004)

5.1.2 Isotope composition of precipitation – on the Tibetan Plateau

Further studies have begun to focus on the isotope systematics of precipitation on the Tibetan Plateau in order to understand the effects of moisture recycling, which is thought to be a major factor in localised rain events (Tian *et al.*, 2001; Zhang *et al.*, 2002; Tian *et al.*, 2003). In the northern Tibetan Plateau there is a clear correlation between air temperature and $\delta^{18}O$ in

precipitation, most likely reflecting a homogenous moisture source at this location (Tian *et al.,* 2003). In the middle of the Tibetan Plateau, the pattern of $\delta^{18}O$ is more complex due to the influence of both continental air masses and monsoon precipitation. In the southern Tibetan Plateau, monsoon activity has an overwhelming impact on the temporal and spatial variation of $\delta^{18}O$ in precipitation resulting in very low $\delta^{18}O$ in summer precipitation, linked to the amount effect (Tian *et al.,* 2003). The high $\delta^{18}O$ values in winter and spring precipitation are most likely related to different moisture sources (Aizen *et al.,* 1996), i.e. the dominance of winter and local convective precipitation rather than summer monsoon rainfall.

5.2 Lake Qinghai and catchment

5.2.1 $\delta^{18}O$ v δD

Oxygen and hydrogen isotopic measurements of precipitation and stream water in the Lake Qinghai catchment and lake surface and sub-surface water from May 2001 to October 2001 are plotted in Figure 5.3. These data allow evaluation of processes that introduce an isotopic signal to the lake water, including the main signal imposed by the isotopic composition of precipitation and local evaporative modification. Lake waters plot below the Global Meteoric Water Line (GMWL) indicating that they have undergone evaporation resulting in the enrichment of ^{18}O and ^{2}H (Fig. 5.3) and they define a Local Evaporation Line (LEL). River waters and a single spring and precipitation sample plot on or close to the GMWL, suggesting that the isotope composition of precipitation is an important control on the isotope composition of input waters. This is the case for both periods of collection, pre-monsoon in May and post-monsoon in October. Unfortunately samples were not collected during the peak of monsoonal activity. Surface and sub-surface waters from the lakes (Qinghai and Gahai) cluster around a single well-defined local evaporation line (LEL) described by the equation $\delta D = 6.05\ (\delta^{18}O) - 2.70$ (May) and $\delta D = 6.07\ (\delta^{18}O) - 3.40$ (October) respectively.

The intersection of the GMWL and the LEL reflects the weighted mean isotopic composition of precipitation in the catchment (δp), corresponding to $\delta^{18}O = -6.1‰$ and $\delta D = -41‰$ (May) and $\delta^{18}O = -6.4‰$ and $\delta D = -42‰$ (October), suggesting little seasonal variation in isotopic composition of precipitation. However, this observation is constrained by few data, with the monsoon season missed due to the timing of the field seasons. Even so, it still provides an indication of meteoric water isotope composition and is useful in determining the main influence on lake water isotope composition.

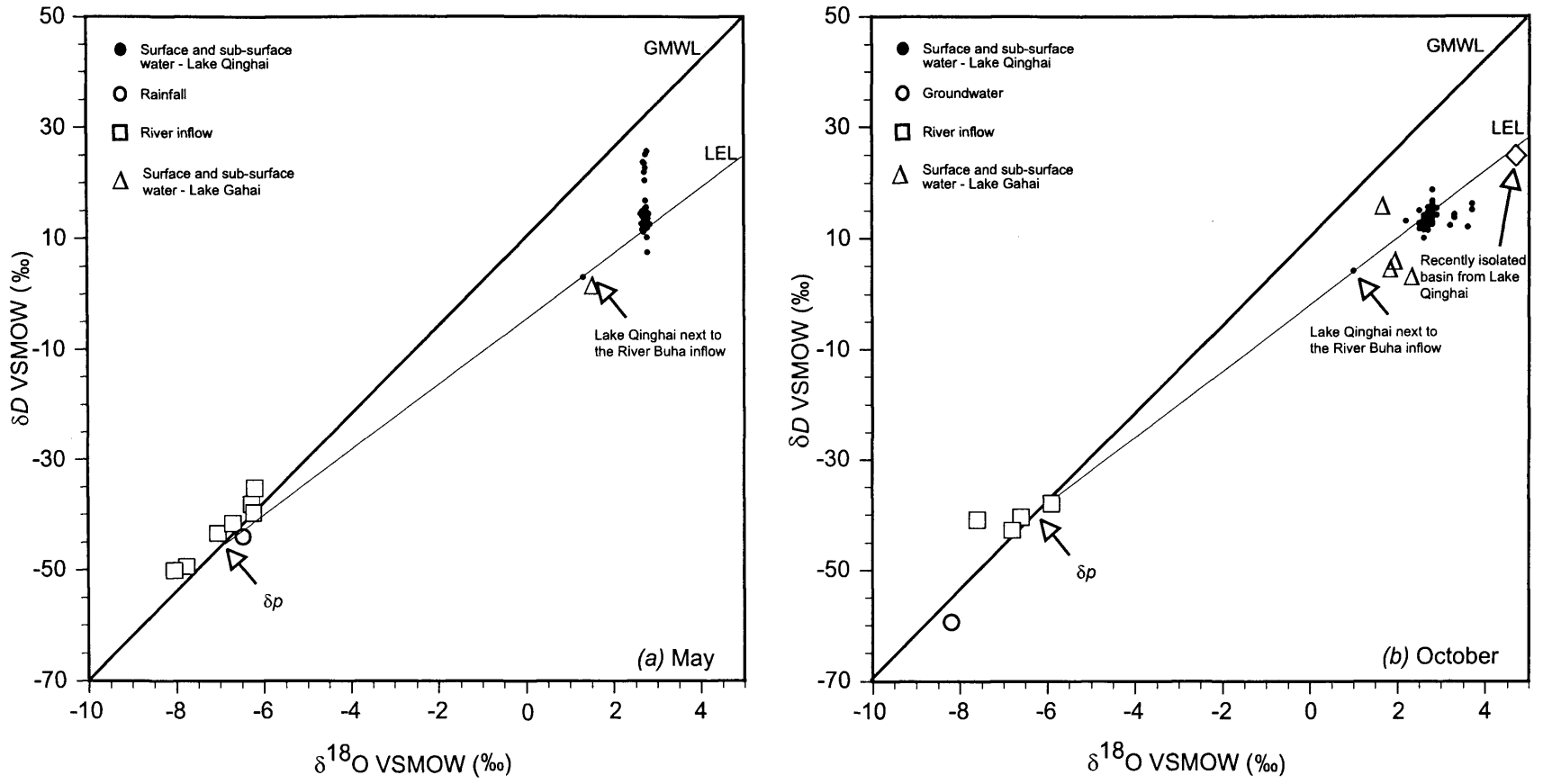

Fig. 5.3 – Bi-plot of $\delta^{18}O$ and δD over different seasons (a) May, (b) October from Lake Qinghai catchment. Data points represent the measured isotopic composition for all water samples. The GMWL determined as $\delta D - 8\delta^{18}O + 10$ (Craig, 1961). The LEL is determined from a linear regression of all meteoric, surface and lake water data. Equation for the LEL is $\delta D = 6.05(\delta^{18}O) - 2.70$ (May) and $\delta D = 6.07\ (\delta^{18}O) - 3.40$ (October).

Displacement along the LEL from δp varies with the degree of evaporative enrichment that the water mass has undergone. Inflowing waters into Lake Qinghai reflect meteoric water. Therefore, the progressive displacement of lake water $\delta^{18}O$ and δD along the LEL reflects overall evaporative enrichment, the gradient of which is a function of humidity (Gonfiantini, 1986). No isotopic stratification with depth was observed, although if this occurs in the lake it may have been missed, as evaporative enrichment of surface waters due to summer insolation is likely to have occurred between sampling seasons. One lake sample has distinctly isotopically more negative values than the rest of the lake and is located near where the River Buha enters the lake. This river has isotopic composition of $\delta^{18}O = -7.05‰$ and $\delta D = -43.4‰$ (May) and $\delta^{18}O = -6.80‰$ and $\delta D = -42.8‰$ (October), while the lake water is $\delta^{18}O = +1.32‰$ and $\delta D = +3.1‰$ (May) and $\delta^{18}O = +1.0‰$ and $\delta D = +4.3‰$ (October) compared with a lake average of $\delta^{18}O = +2.72‰$ and $\delta D = +13.40‰$ (May) and $\delta^{18}O = +2.74‰$ and $\delta D = +13.09‰$ (October), suggesting that the river input influences the lake water composition at this location. Given that $\delta^{18}O$ of precipitation is even lower still, it indicates that some degree of evaporative enrichment of lake water has still occurred.

5.2.2 $\delta^{18}O$ v $\delta^{13}C$

Oxygen isotope values are plotted against carbon isotope values of lake and river DIC for the Lake Qinghai catchment (Fig. 5.4). These data allow evaluation of processes that control the isotopic signal of lake and river water; in particular, it sheds light on the carbon cycle within the lake and catchment.

Mean isotopic composition of inflowing waters to Lake Qinghai is $\delta^{18}O = -6.8‰ \pm 0.9$, $\delta^{13}C = -9.95‰ \pm 1.1$ (May) and $\delta^{18}O = -7.54‰ \pm 0.8$, $\delta^{13}C = -8.56‰ \pm 1.4$ (October), while mean composition of lake water is $\delta^{18}O = 2.73‰ \pm 0.8$, $\delta^{13}C = -3.0‰ \pm 1.0$ (May) and $\delta^{18}O = -2.75‰ \pm 1.4$, $\delta^{13}C = 0.23‰ \pm 1.0$ (October).

What is clear from the oxygen and carbon isotope bi-plots (Fig. 5.4) for the sampling periods of October and May is that the inflowing waters and spring samples that interact with catchment bedrock and vegetation are isotopically distinct from the lake water. They are isotopically lighter in both and are enriched in ^{12}C. A single groundwater sample is similar in value to that of the river inflows, suggesting that little or no alteration is occurring through subsurface inflows. However, more detailed sampling would be needed to verify this suggestion.

The $\delta^{18}O$ and $\delta^{13}C$ composition of lake water is significantly higher when compared to the input waters (Fig. 5.4) indicating alteration of the isotope values of water and DIC through environmental processes. Some alteration is likely to be due either to aquatic productivity or equilibrium exchange with atmospheric CO_2 (see Chapter 2). Moreover, the mean values for $\delta^{13}C$

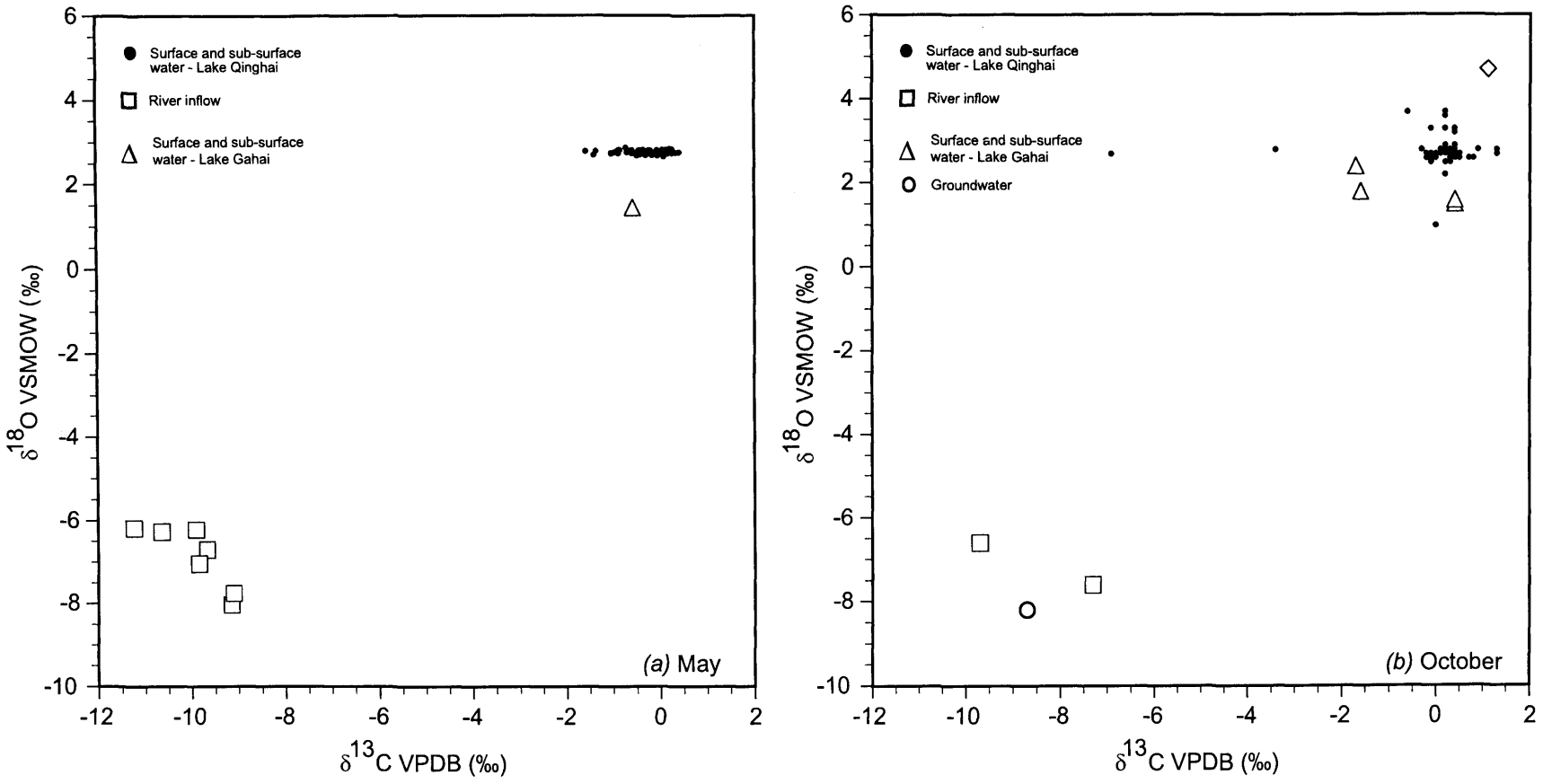

Fig.. 5.4 - Bi-plot of $\delta^{18}O$ and $\delta^{13}C$ isotope values over different seasons (a) May, (b) October from the Lake Qinghai catchment. Data points represent the measured isotopic composition for all water samples.

demonstrate an enrichment of + 3.23‰ from – 3.00‰ to + 0.23‰ over the two sampling periods, indicating that a seasonal alteration of the TDIC is occurring, suggesting that productivity is an important control.

When a closed lake undergoes volume change, there will be changes in its $\delta^{18}O$ and $\delta^{13}C$ values, especially where there is a difference in $\delta^{18}O$ and $\delta^{13}C$ between lake water and input water, as in the case of Lake Qinghai (Fig. 5.4). Fresher waters entering the lake will reduce its $\delta^{13}C$ and $\delta^{18}O$ values as well as carbonate alkalinity and salinity. Linear decreases in $\delta^{18}O$ have been demonstrated in other saline systems e.g. Mono Lake (Li and Ku, 1997) resulting from river input.

However, the $\delta^{13}C$ value of the water is additionally affected by the total CO_2 concentrations ($\sum CO_2$) or carbonate alkalinity (CA), which are also linearly related. Where $\sum CO_2$ in a lake is much higher than in the input waters, the dilution effect on $\delta^{13}C$ is much smaller than that on $\delta^{18}O$. This mechanism has been suggested as a reason for weak isotopic covariance between $\delta^{18}O$ and $\delta^{13}C$ (see Chapter 2) in Lake Qinghai's sediments in a previous study (Henderson *et al.,* 2003), an observation that is counter to the expected pattern of strong covariance in a closed lake (Talbot, 1990).

The two dominant processes affecting the carbon isotope composition of Lake Qinghai are atmospheric CO_2 exchange and aquatic primary productivity. Vapour exchange between lake water and the atmosphere forces the isotopic value of the lake to reach steady-state values. Carbon isotopic fractionation between dissolved inorganic carbon and CO_2 is 8 to 10‰ at 25°C. Under isotopic equilibrium with the atmospheric CO_2, which normally has a $\delta^{13}C$ of about – 7‰; the lakes would have a $\delta^{13}C$ values of between – 3.16 to – 2.2‰ (at 12°C epilimnion temperature). This value brackets the average carbon isotope composition of Lake Qinghai in May, suggesting the fundamental signal from the lake water is exchange with atmospheric CO_2, at this time. In contrast the average composition of $\delta^{13}C$ in October is + 0.23‰, suggesting that lake water has undergone seasonal modification due to photosynthetic activity in the lake water during the summer.

5.3 Hydrologic and isotopic mass balance models

The hydrological budget and isotopic composition of a lake is the sum of its sources and sinks, as well as the effects of environmental processes acting on lake water, such as the amount of evaporation and the isotopic composition of water vapour leaving the lake. Lake sediment records therefore present a complex integration of elements of climate change as well as, in some case, influence of very local processes. In order to unravel the climate history from the $\delta^{18}O$ record from lake sediments it is important to acknowledge that lake systems, particularly large ones as in this case, are underdetermined. Therefore, to make sense of any approximations of climate shifts, a

number of assumptions must be made regarding the nature of the climate system and a lake's response to changes in it.

An increasing number of studies are beginning to utilise isotopic mass balance models, coupled with hydrologic balance models, to analyse $\delta^{18}O$ shifts in a quantitative way (e.g. Rosenmeier *et al.,* in press; Benson and White, 1994; Li and Ku, 1997; Cross *et al.,* 2001; Wolfe *et al.,* 2001; Benson and Paillet, 2002; Yuan, 2003).

5.3.1 Hydrologic mass balance model

The standard hydrological mass balance model describes the balance of inputs and outputs of water for a lake over a given time period and its subsequent volumetric change. Therefore the hydrologic balance of a lake (ΔV_L) at steady-state, i.e. if environmental conditions are considered stable for some time, is controlled by the transfer of water to and from the catchment according to the equation:

$$\Delta V_L = \sum I + P - \sum O - E \tag{5.1}$$

where $\sum I$ and $\sum O$ are the total surface and sub-surface inflows to (I) and outflows (O) from the lake, P is direct precipitation over the lake, and E is the evaporative loss from the lake (Rosenmeier *et al.,* in press; Dincer, 1968; Gat, 1981). This can be further explained by delineating the individual components of the hydrological budget of a lake (e.g. Ricketts and Johnson, 1996):

$$\frac{\Delta V_L}{\Delta t} = S_i + G_i + P - S_O - G_O - E \tag{5.2}$$

where V_L is lake volume; t is time (therefore $\Delta V_L/\Delta t$ is the change in volume per unit time); P is direct precipitation over the lake, S_i is surface inflow, G_i is groundwater (or sub-surface) inflow, and E is the evaporative loss over the lake, S_o is surface outflow and G_o is groundwater outflow. At steady state:

$$\frac{\Delta V}{\Delta t} = 0 \tag{5.3}$$

Some of these values have been measured directly for Lake Qinghai, for example, precipitation, surface inflow and evaporation, but others need to be estimated (G_i, G_o). A water balance model is then used to estimate all unknown values in equation 5.1. The model assumes no temporal lag

between surface and sub-surface components of catchment runoff. Runoff was derived using the following equation:

$$Q = RA_d P_d \tag{5.4}$$

where Q is the mean annual runoff; R is the runoff coefficient (a value of 0.18 is used here, see Yan, 1998); A_d is drainage area and P_d is the precipitation in the drainage area.

Variable	Value	Comments
P	1.667 x 10^6 m^3	Amount of rainfall that enters the lake directly from precipitation each year (lake area (4400 km^2) x mean annual rainfall (376.9 mm))
E	5.354 x 10^6 m^3	Amount of water lost from the lake each year through evaporation (lake area (4400 km^2) x mean annual evaporation (1217 mm))
$\sum O$	unknown	No surface outflow. Groundwater outflow has to be estimated using mass balance techniques (see equation 5.17 and 5.18).
$\sum I$	1.746 x 10^6 m^3	This amount combines the river input and catchment runoff **without** estimated groundwater inputs. Runoff was derived from equation (5.5). Groundwater inflow needs to be estimated using mass balance techniques (see equation 5.19 and 5.20)

Table 5.1 – Summary values used in hydrological mass balance model

The values known for Lake Qinghai (Table 5.1), together with estimation of runoff allow calculation of the current water balance of Lake Qinghai so that

$$Gi - Go = 1.94 \times 10^6 \ m^3 \tag{5.5}$$

5.4 Isotope mass balance model

Given the water balance in equation 5.1, a similar expression can be made for an oxygen isotope mass balance of a lake (δ_L):

$$\Delta V_L \delta_L = S_i \delta_{S_i} + G_i \delta_{G_i} + P\delta_p - S_o \delta_{S_o} - G_o \delta_{G_o} E\delta_E \tag{5.6}$$

where δ is the oxygen isotope composition of the various inputs and outputs. The mass balance modelling will only be concerned with oxygen isotopes, since this study will has no records of hydrogen isotopes within the palaeoenvironmental records. Therefore δ values in this section will refer exclusively to $\delta^{18}O$.

When a lake is in steady state it is assumed that change in volume with change over time is equal to 0. Since there is no surface outflow the balance of Lake Qinghai at steady state can be stated as:

$$S_i\delta_{S_i} + G_i\delta_{G_i} + P\delta_p = G_o\delta_{G_o} + E\delta_E \quad (5.7)$$

From the hydrological variables P, S_i and E are known, with some of their isotopic compositions known through measurements (see Fig. 5.3).

Var	Comments
δ_I	runoff waters to Lake Qinghai can be separated into groundwater (δ_{Gi}) and surface input (δ_{Si})
δ_{Gi}	spring waters collected from the catchment have $\delta^{18}O$ values of – 8.2‰
δ_{Si}	surface waters flowing into the lake range from $\delta^{18}O$ = - 6.80‰ to - 7.07‰
δ_P	only a spot sample of rainwater was taken and its $\delta^{18}O$ value was - 6.47‰ with calculated precipitation, defined as the intercept of the local evaporation line and the LMWL (see section 5.2.1) has a value of – 6.1 to – 6.4 ‰
δ_E	this is very difficult to measure directly and is usually calculated through mass balance methods
δ_{Go}	this is assumed to be equivalent to lake water composition ~ + 2.6‰

Table 5.2 – Isotopic composition of components in the mass balance model

5.4.1 Determining δ_E

Accurate estimation of the isotopic composition of evaporative flux from the lake is crucial for realistic modelling of the isotopic composition of the lake reservoir, albeit extremely difficult to monitor in the field. The isotopic mass balance model is therefore used to calculate the isotopic composition of evaporative waters based on the Craig-Gordon model of evaporation (Craig and Gordon, 1965):

$$\delta_E = \frac{((1+10^{-3}\varepsilon^*)\delta_L - h_n\delta_A - \varepsilon)}{(1-h_n+10^{-3}\varepsilon_k)} \quad (5.8)$$

where ε^* and ε_k represent the respective equilibrium and kinetic fractionation factors, expressed as per mil (‰) separations between liquid and vapour phases, $\varepsilon = \varepsilon^* + \varepsilon_k$, and *h* is the atmospheric relative humidity normalised to the saturation vapour pressure at the temperature of the air-water interface. The equilibrium fractionation ε^* value for oxygen can be estimated from derived empirical relationships (e.g. Horita and Wesolowski, 1994).

$$\varepsilon^* = - 7.685 + 6.7123(10^3/T) - 1.6664(10^6/T^2) + 0.3504(10^9/T^3) \quad (5.9)$$

where T is the interface temperature (in K) and ε_k values for typical natural conditions can be approximated as a function of relative humidity deficit (Gonfiantini, 1986; Araguas-Araguas *et al.*, 2000).

$$\varepsilon_k = 14.2\,(1-h) \tag{5.10}$$

Normalised relative humidity is calculated from the saturation vapour pressure of the overlying air ($e_{s\text{-}a}$) and the saturation vapour pressure ($e_{s\text{-}w}$) at the surface water temperature:

$$h_n = h \times \frac{e_{s-a}}{e_{s-w}} \tag{5.11}$$

Saturation vapour pressure (millibars) is calculated from the following equation (Murray, 1967):

$$e_{s-w} \; and \; / \; or \; e_{s-a} = 6.108 \; EXP\left[\frac{17.27T}{T+237.7}\right] \tag{5.12}$$

where T is the temperature (°C) of the lake surface water ($e_{s\text{-}w}$) or overlying air ($e_{s\text{-}a}$).

Atmospheric moisture (δ_A) is assumed to be in isotopic equilibrium with precipitation (Zuber, 1983; Gibson *et al.*, 1993; Gibson *et al.*, 1999):

$$\delta_A = \delta_p - \varepsilon^* \tag{5.13}$$

Therefore by simultaneously solving all parts to Eq. (5.8) the weighted isotopic composition of vapour leaving Lake Qinghai can be calculated. For Lake Qinghai the following values are used (Table 5.3):

Variable	Value	Comments
δ_L	2.60‰	Average $\delta^{18}O$ of lake water in May 2001
h_n	0.46	Average humidity over the catchment is 0.57 (averaged over 1958-2001), with average air temperature taken for summer months as 9.6°C (averaged over 1958-2001). Lake temperature taken as 12°C average surface water temperature for summer months.
δ_A	-16.92‰	Calculated using h_n above
ε^*	10.47‰	Lake temperature taken as 285.15 K.
ε_k	7.66‰	Calculated using h_n above
ε	18.13‰	Total of $\varepsilon^* + \varepsilon_k$.

Table 5.3 – Summary values used in estimating δ_E based on the Craig-Gordon model of isotopic evaporation

Working through Eq. 5.8 gives an δ_E value of – 14.1‰.

There are however, alternative ways of determining δ_E, although they are largely based on the original Craig-Gordon work. One such alternative was developed by Benson and White (1994) based on observations from Pyramid Lake, Nevada. This has been used by a number of other authors (e.g. Ricketts and Johnson, 1996; Benson and Paillet, 2002; Yuan, 2003). The expression derived by Benson and White (1994) deviates from Craig and Gordon (1965) in four ways. Firstly, the basic set of ratios of isotopic species ($\mathbf{R}_i$) are used instead of isotopic fraction. Secondly, the derivation includes an expression for the ^{18}O:^{16}O ratio of evaporating moisture in terms of the fractions of advected and lake-derived moisture ($\mathbf{R}_{evap}$). Thirdly, equilibrium and kinetic fractionation of ^{18}O and ^{16}O are treated separately, allowing the use of Merlivat and Jouzel (1979) determination of the dependence of kinetic effects on wind speed. Finally, Benson and White (1994) also derived an expression for the net vapour flux (Benson and Paillet, 2002).

According to Benson and White (1994), the $^{18}O/^{16}O$ ratio in water vapour released from the lake surface during evaporation ($\mathbf{R}_{evap}$) is given by:

$$\mathbf{R}_{evap} = \frac{\mathbf{R}_{lake} / \alpha_{eq} - RHf_{ad}\mathbf{R}_{ad}}{(1 - RH / \alpha_{kin}) + RH(1 - f_{ad})} \tag{5.14}$$

Where $\mathbf{R}_{lake}$ and $\mathbf{R}_{ad}$ are the isotopic ratios in lake water and advected water vapour, f_{ad} is the fraction of advected water vapour in the boundary layer, and α_{eq} and α_{kin} are the equilibrium and kinetic fractionation factors respectively. If all the water vapour overlying the lake is derived by evaporation, $f_{ad} = 0$ and equation 5.14 becomes:

$$\mathbf{R}_{evap} = \mathbf{R}_{lake} \frac{\alpha_{kin}}{\alpha_{eq}} \left(\frac{1}{1 - RH + RH\alpha_{kin}} \right) \tag{5.15}$$

Isotope ratios can then be converted to delta (δ) values using:

$$\delta_i = (\mathbf{R}_i - 1)10^3 \tag{5.16}$$

where $\mathbf{R}_i$ is the isotopic ratio of a sample (R_i) divided by the corresponding isotopic ratio of standard (R_{std}) and values of the equilibrium fractionation factor, α_{kin}, can be calculated from Eq. (5.8). For wind speeds < 6.8 m s^{-1}, $\alpha_{eq} = 0.994$ and for wind speeds between 6.8 and 12.5 m s^{-1}, values of α_{eq} range from 0.9955 to 0.9975 (Merlivat and Jouzel, 1979; Benson and Paillet, 2002).

Given that f_{ad} is unknown, values of δ_E from equation 5.14 can be calculated for all values of f_{ad} showing that δ_E will lie between – 10.6 ‰ and – 3.3 ‰ (Fig. 5.5). However, it is clear that δ_E is

susceptible to changes in both the temperature of evaporating water (Fig. 5.5a), but perhaps more significantly on the relative humidity of the atmosphere (Fig. 5.5b).

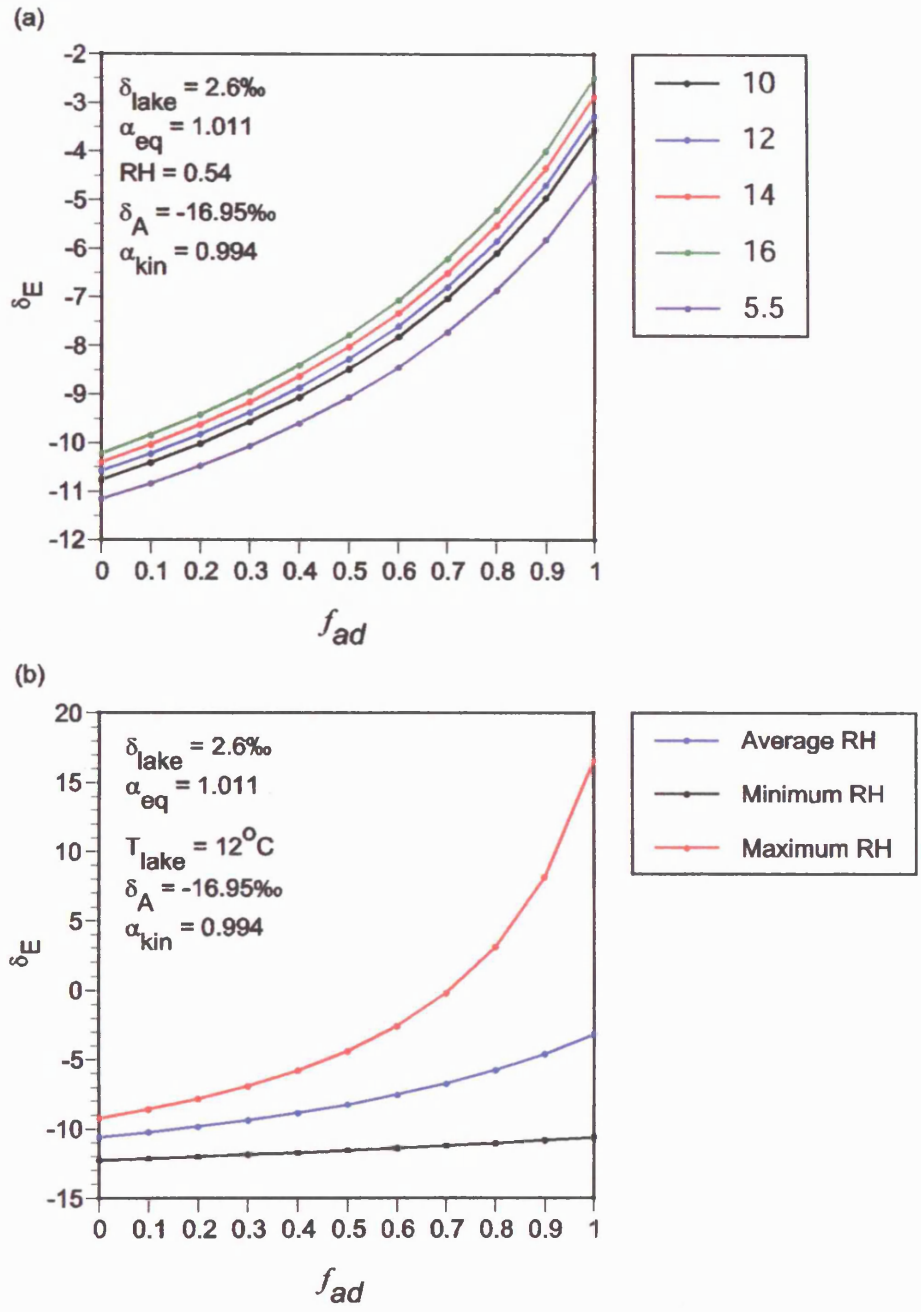

Fig. 5.5 – Calculated values of δ_E from equation 5.16 for all values of f_{ad}. (1) Values of δ_E over a range of temperatures (10 – 16 °C) and the mean annual temperature (5.5 °C), (2) Values of δ_E using over a range of different relative humidity's.

Variable	Value	Comments
R_{lake}	1.0026	Conversion of lake water average from May 2001 = 2.6‰.
α_{kin}	0.994	Average wind speed is 3.7 m/s (Qin and Huang, 1998)
RH	0.54	The average relative humidity for the catchment (1958-2001).
f_{ad}	0 to 1	Unknown and lies between 0 and 1.
R_{ad}	0.98305	The isotopic ratio of advected water vapour *cf.* δ_A
α_{eq}	1.010704	*cf.* $\varepsilon^* = 10.41$

Table 5.4 – Summary of values used in estimating δ_E based on the Benson & White model of isotopic evaporation

Using the known values in equation 5.5 it can be shown that, if δ_E = - 13.5‰, then:

$$-8.2G_i - 2.6G_o = 52.5 \times 10^6 \text{ m}^3 \quad (5.17)$$

Alternatively, if δ_E = -10.6‰, then

$$-8.2G_i - 2.6G_o = 33.6 \times 10^6 \text{ m}^3 \quad (5.18)$$

Therefore, depending on which evaporation model is adopted very different mass balances are achieved, suggesting there are big uncertainties in the evaporation models.

Assessment of the two different models

In order to calculate the relative proportion of G_o the amount of groundwater inflow (G_i) needs to be calculated. Equation 5.19 describes a lake budget in which groundwater can be determined independent of the groundwater outflow (Kebede *et al.*, 2002):

$$G_i = \frac{\left[P(1+k)(\delta_L - \delta_p) + E(\delta_E - \delta_L)\right]}{\left[\delta_{G_i} - \delta_L\right]} \quad (5.19)$$

Where P is precipitation, E is evaporation, k is a runoff coefficient, δ_L, δ_p, δ_E and δ_{Gi} are the isotope composition of these components. By solving equation 5.6 and 5.19 using 5.17 or 5.18 allows calculation of the proportion of G_o (Table 5.5).

		Value (x 10^6 m^3)		Percentage	
		δ_E = - 14.1‰	δ_E = - 10.57‰	δ_E = - 14.1‰	δ_E = - 10.57‰
Inputs					
Precipitation	1.66			14%	17%
Runoff	1.75			15%	18%
Groundwater		8.73	6.42	71%	65%
Outputs					
Evaporation	5.35			44%	54%
Groundwater		6.79	4.48	56%	46%
Total flux		12.14	9.83		
Residence time		6.38 yrs	7.88 yrs		

Table 5.5 – Summary of Lake Qinghai hydrology

5.5 Other isotope mass balance techniques

Another commonly employed technique, which is relatively simple, is based on an isotope mass balance to provide an index of water balance that can be quantified in terms of a evaporation/inflow ratio (E/I) (Edwards *et al.*, 2004) as summarised below:

$$E/I = \frac{(\delta_i - \delta_L)}{(\delta_E - \delta_L)} \tag{5.20}$$

where δ_i is the isotope composition of the inflow waters, δ_L, is the isotope composition of the lake water and δ_E is the isotope composition of the evaporating lake waters and is derived using the linear resistance model of Craig and Gordon (1965) in equation 5.8. This is preferred by Edwards *et al.*, (2004) as it accounts for differing volatilities of water isotopes as a combination of mass-dependent variation in equilibrium vapour processes (equilibrium effects), together with variation in molecular diffusivities arising from the combination of differing absolute mass and its distribution within water molecules (kinetic effects).

Taking measured values and those previously calculated (see section 5.4.1) the E/I ratio of Lake Qinghai is:

$$\frac{(\delta_i - \delta_L)}{(\delta_E - \delta_L)} = 0.56 \tag{5.21}$$

confirming that the lake is heavily influenced by evaporative flux from the lake, which is similar to the percentage flux of evaporation derived from mass balance techniques (Table 5.5).

5.6 Modern lake sediments

Lake surface sediments were collected in October 2001 and analysed for $\delta^{18}O$ and $\delta^{13}C$ of authigenic carbonate, $\delta^{18}O$ and $\delta^{13}C$ of ostracod carbonate and $\delta^{13}C$ and CN ratio of organic carbon (Fig. 5.6).

The authigenic carbonate in the surface sediments show a strong covariance (r^2 = 0.94, p = <0.001) (Fig. 5.6a) between $\delta^{18}O$ and $\delta^{13}C$, reflecting the fact that Lake Qinghai is a closed basin and is precipitating carbonate as a response to summer photosynthetic activity and evaporation. Ostracod carbonate shows a weak negative covariance (r^2 = 0.34, p = <0.01) (Fig. 5.6b), which is expected as ostracods precipitate their shells in a micro-habitat and over a short period. They are therefore more susceptible to very local and short-term changes in both oxygen and carbon isotope compositions. Isotopic analysis of modern organic matter from surface sediments (Fig. 5.6c) shows that within Lake Qinghai the dominant isotope signal is from algae. Lake Gahai shows a strong algal component according to its C/N ratio, but the $\delta^{13}C_{org}$ is much heavier than expected for this group, this may reflect an increasing contribution from C3 plants, or more likely, a result of carbon limitation (Holmes *et al.,* 1999). Lake Gahai is much more saline than Lake Qinghai (33 g/l compared to 14 g/l) and although the pHs are similar, the salinity difference suggests that algae are unable to discriminate against the heavier ^{13}C isotope in the lake TDIC and therefore its $\delta^{13}C_{org}$ is higher.

To further investigate the isotope composition of modern organic matter, living plants from within the catchment and the lake itself were collected and analysed to get a better understanding of the controls on $\delta^{13}C$ and C/N ratios. A number of samples were taken in October 2001, and included submerged and emergent macrophytes, terrestrial plants and marsh species; unfortunately no samples of lake algae were recovered. The results are shown in figure 5.7.

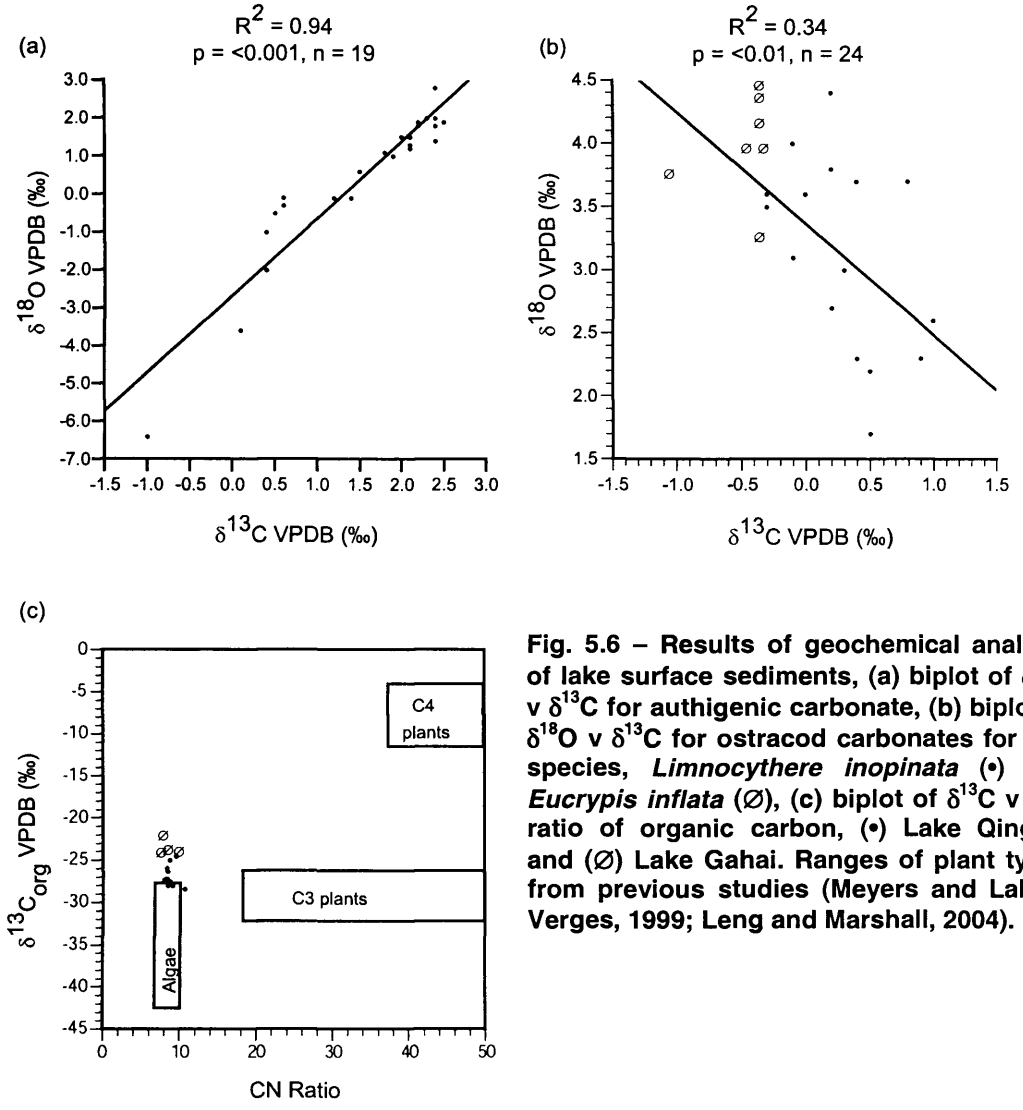

Fig. 5.6 – Results of geochemical analysis of lake surface sediments, (a) biplot of $\delta^{18}O$ v $\delta^{13}C$ for authigenic carbonate, (b) biplot of $\delta^{18}O$ v $\delta^{13}C$ for ostracod carbonates for two species, *Limnocythere inopinata* (•) and *Eucrypis inflata* (Ø), (c) biplot of $\delta^{13}C$ v C/N ratio of organic carbon, (•) Lake Qinghai and (Ø) Lake Gahai. Ranges of plant types from previous studies (Meyers and Lallier-Verges, 1999; Leng and Marshall, 2004).

There is a large amount of variation in the modern organic matter of Lake Qinghai. However, aquatic plants that are submerged (*Hippurus vulgaris*) show good agreement with the proposed sources of organic matter (Fig. 5.7) while the emergent form of this species whose predominant carbon source is from the atmosphere, shows association with terrestrially based plants (elevated C/N ratio). The marsh species, although unidentified, are terrestrially-based and their $\delta^{13}C_{org}$ and C/N ratio suggests this. This is also the case for *Festuca* sp. which is abundant within the catchment, dominating the surrounding environment.

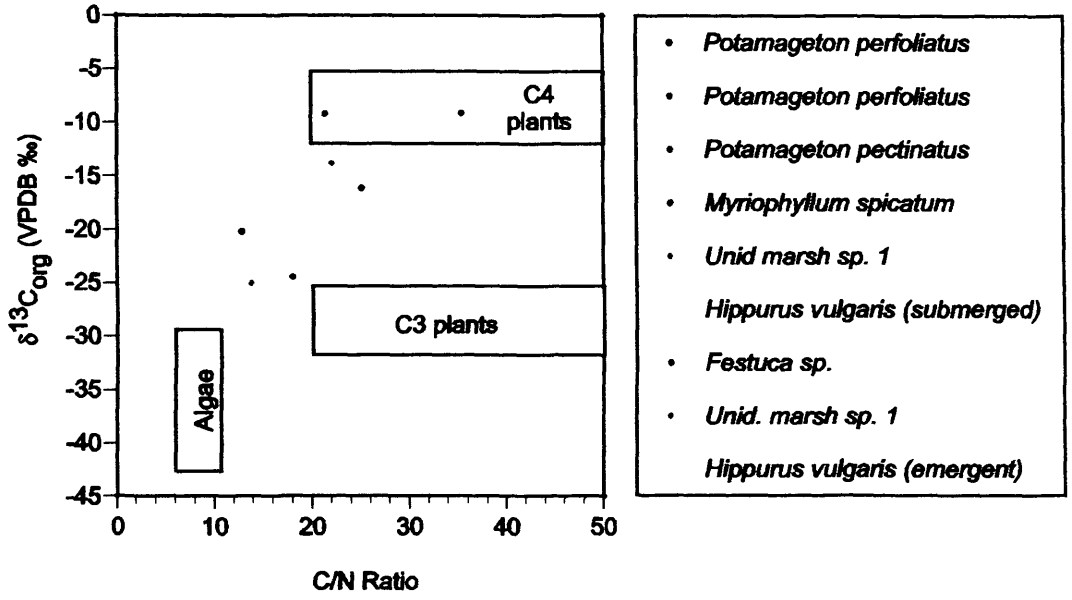

Fig. 5.7 – Bi-plot of $\delta^{13}C$ v C/N for modern plant matter within the catchment and lake body.

5.6.1 Carbonate mineralogy

X-ray diffraction analysis of core sediments indicates that the principle carbonate mineral is a low-Mg calcite. However, high-Mg calcite and aragonite also occurs, be it in low amounts compared to low-Mg calcite (see appendix).

5.6.2 Modern carbonate geochemistry

Carbonates are assumed to precipitate in equilibrium with lake waters and based on this its oxygen isotope composition can be estimated using the following equation (Kim and O'Neil, 1997):

$$\delta^{18}O_{calcite(SMOW)} - \delta^{18}O_{water(SMOW)} = 18.03(10^3T^{-1})-32.42 \quad (5.22)$$

where T is the temperature in Kelvin.

Using water data collected from 2001 and measured $\delta^{18}O$ values of carbonate precipitates from surface sediments it is possible to check when carbonates are precipitated using equation 5.22. Both carbonate and water values must be given against the same standard i.e. SMOW and so carbonate values measured against PDB must be corrected to SMOW such that (Coplen *et al.*, 1983):

$$\delta^{18}O_{calcite(SMOW)} = 1.0309\delta^{18}O_{calcite(PDB)} + 30.91 \quad (5.23)$$

Given average lake water values over 2001 of + 2.66‰ and lake surface water temperatures of *c.* 12°C, assuming isotopic equilibrium a value of + 3.5‰ is calculated using equation 5.23 for $\delta^{18}O$ (VPDB) for lake carbonate. This compares to measured average values for surface sediments of + 1.3‰. However, water isotope and temperature data was taken from May 2001 and this is unlikely to have been the time of carbonate precipitation as maximum temperatures and productivity occur during July and August. An additional error is introduced as the surface sediments (*c.* top 0.5 cm of sediment) represent an integrated signal of approximately 5 years. Therefore, the $\delta^{18}O$ of carbonate in the "surface sediments" is unlikely to represent that preceding summer's precipitation, but more likely to be a sum of a number of previous years carbonate. This is could be further compounded by differential sedimentation rates throughout the whole lake basin (see Chapter 6). Using values for the measured mean air temperature by the shore of the lake and by estimating monthly lake water values, which are likely to be similar throughout the summer given the slope of the LEL for May (δD = 6.05 ($\delta^{18}O$) – 2.70) and October (δD = 6.07 ($\delta^{18}O$) – 3.40), monthly calculations of the $\delta^{18}O$ composition of carbonate can be made (Fig. 5.8).

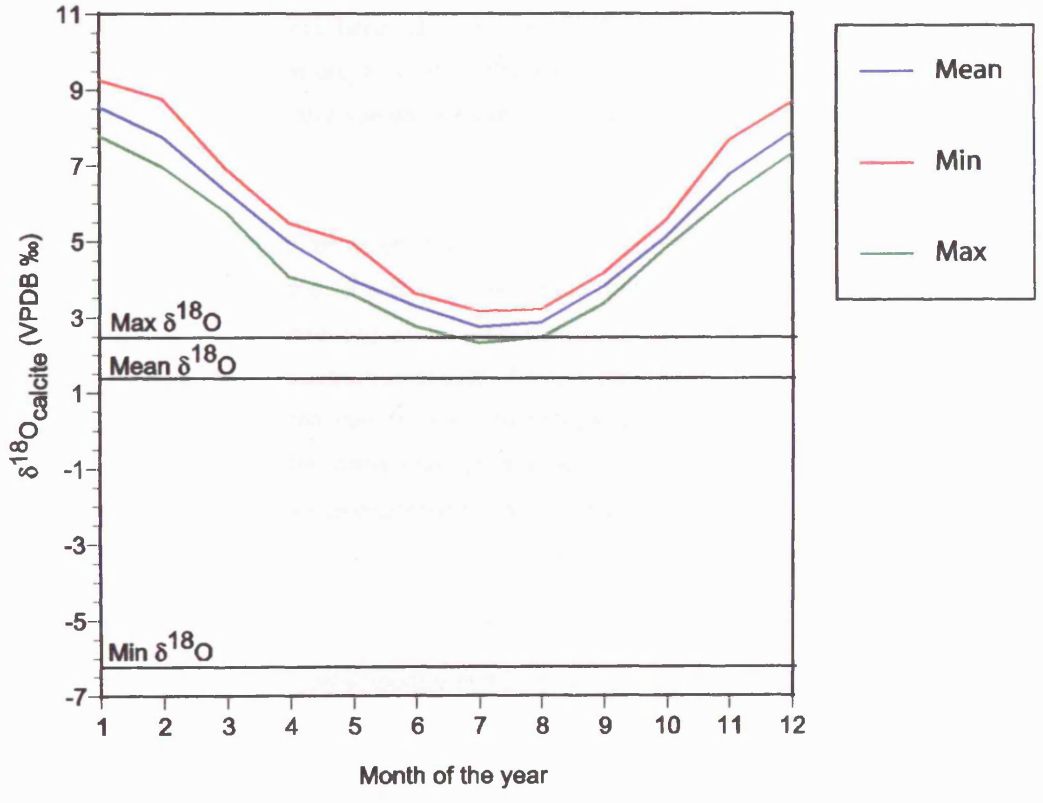

Fig. 5.8 – Calculations of $\delta^{18}O$ of equilibrium precipitated calcite for each month at Lake Qinghai with mean, minimum and maximum air temperatures. Shaded area represents time when the lake is ice free. Waters influenced by river inflow are not included in the calculation.

The oxygen isotope compositions calculated for equilibrium are notably higher than the measured surface sediment carbonate (Fig. 5.8). The relationship between calculated equilibrium $\delta^{18}O$ and measured $\delta^{18}O$ could be affected by a number of factors. The implicit assumption is that carbonates form in equilibrium, so the observed difference between calculated $\delta^{18}O$ and measured $\delta^{18}O$ could be a disequilibrium effect. This disequilibrium could arise due to a number of reasons. Firstly, the mineralogy of the precipitated carbonate would alter the $\delta^{18}O$ composition of carbonate. However, the lake sediments are largely low-Mg calcite, although high-Mg and aragonite do occur in small amounts. Even if there was a change in mineralogy this would enrich the precipitated sediment in ^{18}O by *c.* + 0.6‰ compared to $\delta^{18}O$ of equilibrium calcite. Therefore this effect is rejected as a cause for the observed difference as the precipitated carbonate is lower than calculated equilibrium carbonate.

A second reason for the observed relationship is that rapid precipitation of carbonate in waters can cause a disequilibrium effect. During the summer, lake waters may become supersaturated in carbonate which would cause ^{18}O-depletion in corresponding carbonates. Thirdly, the pH of the lake could cause the apparent disequilibrium; Kim and O'Neil (1997) argue that 'equilibrium' $\delta^{18}O$ is achieved at pH 7.8. Therefore a substantially higher pH than this could theoretically lower the fractionation (i.e. more negative values of equilibrium) as the fraction of carbonate species varies with pH (Zeebe, 1999).

Rather than the difference between calculated $\delta^{18}O$ and measured $\delta^{18}O$ being a result of disequilibrium, it could be due to a bias in the temperature values used to calculate equilibrium $\delta^{18}O$. The temperatures used are an approximation of the actual temperature when calcite precipitation (given the data available) occurs. If this is correct, the implication is that precipitation occurs at higher temperatures than implied, meaning less fractionation, therefore more negative $\delta^{18}O$. Bias could also be in the water composition, but if there is bias in the temperature of calcite precipitation then water would be expected to be more positive, causing higher $\delta^{18}O$ carbonate.

5.7 Summary

By studying Lake Qinghai's contemporary hydrology it has been demonstrated that the governing environmental control on lake isotope composition is seasonal evaporation. The position of lake waters with respect to the GMWL supports this notion of an evaporatively enriched lake and it is consistent between May to October, 2001. The influence of evaporation on Lake Qinghai's waters is further demonstrated by hydrological and isotope mass balance methods. Table 5.5 shows that between 29 to 35% of the waters entering Lake Qinghai is from direct precipitation or surface runoff. The remainder of the water entering the lake is therefore from groundwaters. Depending on which δ_E model is employed, evaporation from the lake accounts for between 44 to 54% of the water leaving the lake.

Composition of calculated $\delta^{18}O$ of carbonate is higher than measured $\delta^{18}O$ of surface sediments this difference could be due to disequilibrium effects, but is more likely to be a result of bias in the temperature data used. Even so, the maximum observed $\delta^{18}O$ of surface sediments is similar to the minimum calculated $\delta^{18}O$, suggesting that carbonates in Lake Qinghai precipitate during the summer months over a relatively short period of time. This is important for interpreting palaeolimnological records, as it suggests down core $\delta^{18}O$ of carbonate is linked to summer water conditions.

Chapter Six
Chronology

Introduction

Fundamental to the success of any palaeolimnological study is the attainment of good chronological control, so that inferred environmental changes can be presented in terms of absolute age and compared with other palaeoenvironmental records. Two of the most routinely used techniques for establishing lake sediment chronologies are ^{210}Pb and radiocarbon (^{14}C) dating. ^{210}Pb dating has become a widely applied procedure in palaeolimnological research for dating recent sediments (up to *c.* 150 years) (Appleby, 2001), while for older sediments, radiocarbon (^{14}C) dating is commonplace and was one of the earliest radiometric methods available (Björck and Wohlfarth, 2001). However, although both techniques have become routine, they are not without their limitations, which will be discussed in turn in the following sections along with the results from cores.

6.1 ^{210}Pb and ^{137}Cs dating

Two ^{210}Pb-dating models have come into general use – the constant initial concentration (CIC) and the constant rate of supply (CRS) models. The CIC model assumes lake water has a substantial reservoir excess of unsupported ^{210}Pb. The CRS model assumes that the input of excess ^{210}Pb to the sediments has remained constant through time (Brenner *et al.,* 2004). However, in the case of Lake Qinghai and Lake Gahai, it was decided to adopt the 'simple model' for calculating sediment accumulation rates. This model is surprisingly robust and is particularly applicable where $^{210}Pb_{excess}$ shows a uniform exponential decline with depth indicating that there have been no prolonged or large-scale variations in sediment accumulation rate over time. The sedimentation rate is given by the slope of the least squares fit for the natural log of $^{210}Pb_{excess}$ activity versus depth. The ^{210}Pb dates were then checked using ^{137}Cs activity down core.

6.1.1 Lake Qinghai

Figure 6.1a, b, c shows the $^{210}Pb_{excess}$ activity of cores from cores QING6, QING10 and QHE2 and they show a broadly exponential decline, confirming that the simple model of sedimentation rate can be used. When this model is employed it gives a calculated sediment accumulation rate of 1.0 mm/yr (2σ = 0.9 - 1.2 mm/yr) for QING6 (Fig. 6.2a), 1.3 mm/yr (2σ = 1.0 - 1.7 mm/yr) for QING10 (Fig. 6.2b) and 1.4 mm/yr (1.1 - 1.8 mm/yr) for QHE2 (Fig. 6.2c). ^{137}Cs activity for cores QING6, QING10 and QHE2 (Fig. 6.1d, e, f) show a clear subsurface maximum. Below this maximum, activities decline to undetectable values at 10 to 15 cm depth. In the absence of large-scale local or regional inputs from nuclear establishments, the main subsurface maximum most likely corresponds to 1963, the year of peak ^{137}Cs fallout from above ground nuclear weapons testing. This gives ^{137}Cs-derived sediment

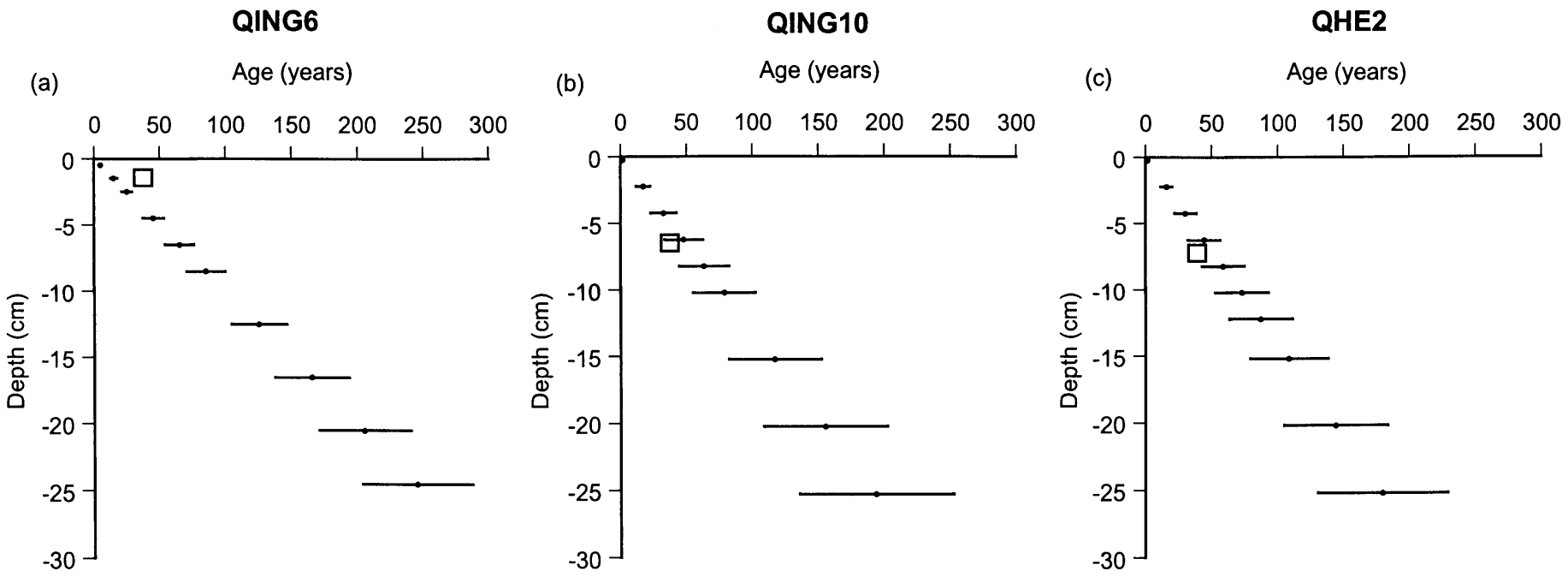

Figure 6.1 – ^{210}Pb activity (Bq/g) versus depth (cm) for cores Qing 6 (a), Qing 10 (b) QHE2 (c) and ^{137}Cs activity (Bq/g) versus depth (cm) for cores Qing 6 (d), Qing 10 (e) and QHE2 (f)

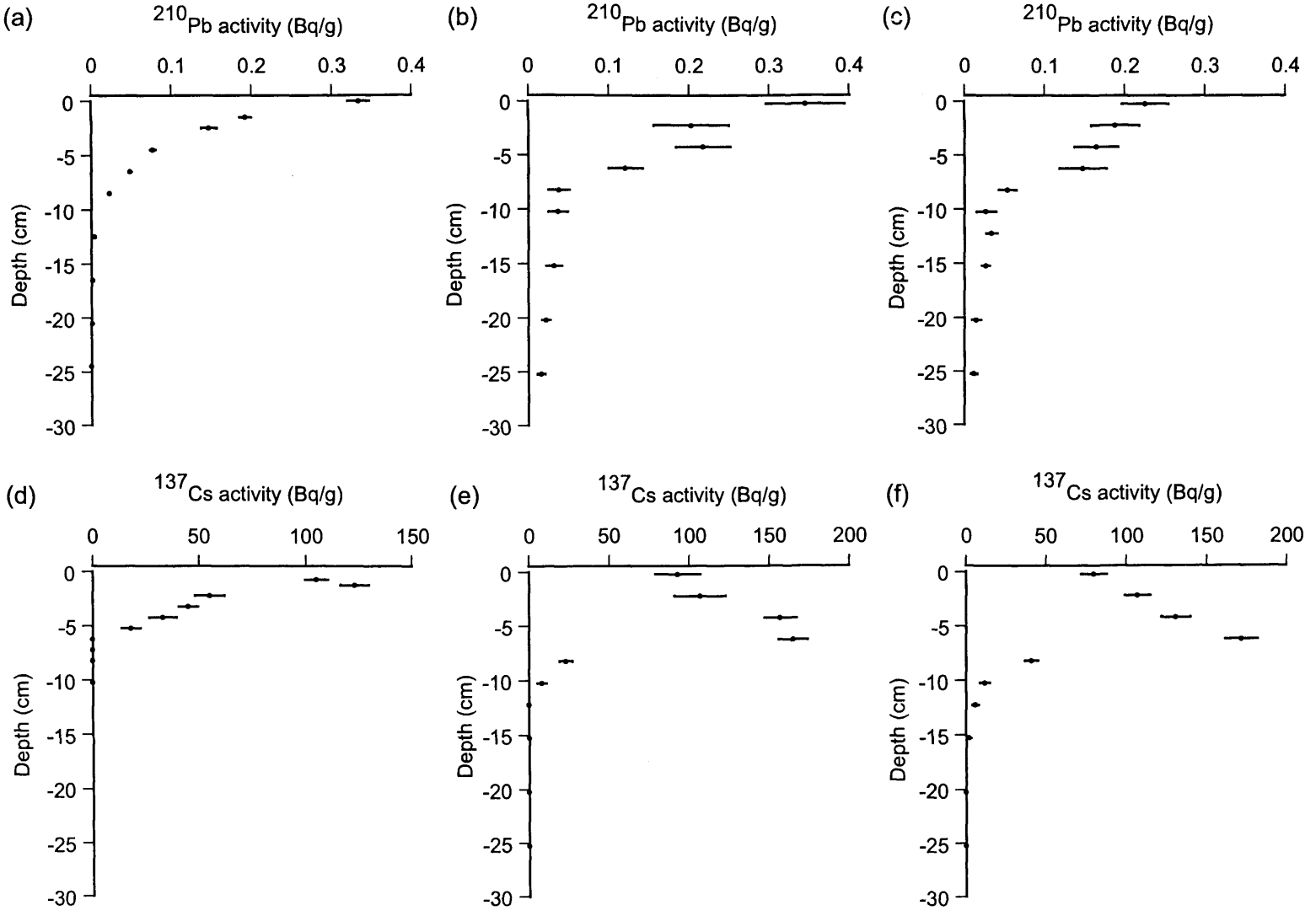

Figure 6.2 - Age vs. depth graph for core QING6 (a), QING10 (b) and QHE2/01 (c) based on the simple model of ^{210}Pb dating (error bars shown are calculated using the standard error on the gradient of the linear regression fit of $\ln ^{210}Pb_{excess}$ vs. depth). The rectangle indicates the ^{137}Cs-derived age.

accumulation rates of 0.4 mm/yr for QING 6, 1.5 mm/yr for QING 10 and QHE2. The sediment accumulation rates for QING10 and QHE2 show extremely good agreement with sedimentation rates calculated from ^{210}Pb, whereas the sediment accumulation rates for ^{210}Pb and ^{137}Cs are significantly different in QING6 (Fig. 6.2).

Figure 6.2 shows the age models for the three cores from Lake Qinghai, and it suggests sedimentation rates for the north (QING10) and east (QHE2) basins of the lake are very similar based on ^{210}Pb dating models and these are independently corroborated by the ^{137}Cs. Problems exist for core QING6 from the south basin as the ^{210}Pb model estimates an sedimentation rate of 1.0 mm/yr, while ^{137}Cs activity suggests a sediment accumulation rate of 0.4 mm/yr. The lack of exact agreement may be a consequence of sediment mixing.

^{137}Cs in QING6 shows a considerable amount of penetration down core below the peak at 1.5cm (to a depth of ca. 6cm), which may indicate that some form of bioturbation has taken place and mixed the ^{137}Cs (and ^{210}Pb) deeper than it would otherwise be. If this were the case, the ^{210}Pb sedimentation rate quoted above would be a maximum value. However, there is no obvious evidence of bioturbation or mixing in this core, based on its lithology. Since the ^{137}C date is derived via a dating peak in activity, it is less affected by any mixing effects than ^{210}Pb.

With such low accretion rates, even slight mixing can displace ^{210}Pb downwards by a couple of centimetres and give an erroneously high rate (Cundy *pers. comm.)*. The same mixing will merely broaden out the ^{137}Cs peak slightly, and so a fairly reliable rate can still be achieved.

6.1.2 Lake Gahai

Figure 6.3a shows the $^{210}Pb_{excess}$ activity of core GAHA1, which shows a weak exponential decline with depth, although the uppermost samples show a reversal in activity. This could be a result of physical mixing in the top sediments within Lake Gahai or that the sediments haven't fully equilibrated with atmospheric ^{210}Pb (Binford, 1994). Sediment accumulation rates were determined using the simple model and gives a calculated rate of 1.2 mm/yr (2σ range = 1.0 - 1.4 mm/yr). ^{137}Cs activity for GAHA1 shows a clear subsurface maximum at 4.5 cm (Fig. 6.3b). Below this maximum, activities decline to undetectable values at 10 to 15 cm depth. In the absence of large-scale local or regional inputs from nuclear establishments, the main subsurface maximum most likely corresponds to 1963, the year of peak ^{137}Cs fallout from above ground nuclear weapons testing. This gives a ^{137}Cs-derived sediment accumulation rate of 1.0 mm/yr which shows good agreement with the sedimentation rate calculated by ^{210}Pb (Fig. 6.3c)

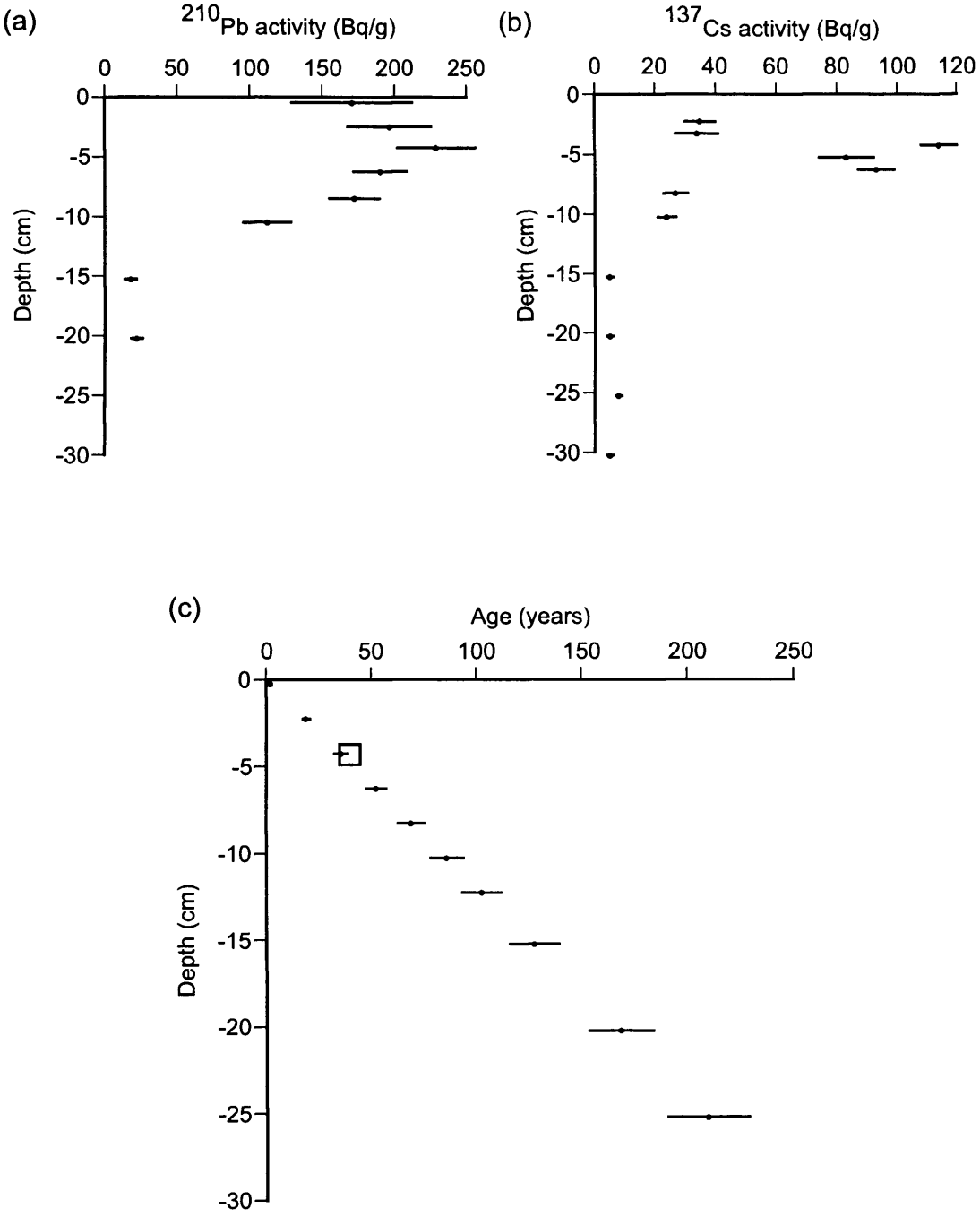

Figure 6.3 – ^{210}Pb (Bq/kg) versus depth (cm) for core GAHA1 (a); ^{137}Cs (Bq/kg) versus depth (cm) for core GAHA1/01 (b); and age vs. depth graph for core GAHA1, based on the simple model of ^{210}Pb dating (error bars shown are calculated using the standard error on the gradient of the linear regression fit of ln^{210}Pb$_{excess}$ vs. depth). The rectangle indicates the ^{137}Cs-derived age.

The sediment accumulation rates for the four cores used in the study, cores QING6, QING10, QHE2 and GAHA1 are summarised in Table 6.1 below. These accumulation rates will be used in conjunction with radiocarbon dating (section 6.2), which has been applied to obtain sediment accumulation rates beyond the dating range of ^{210}Pb (i.e. pre-1850).

Core	^{210}Pb derived sediment accumulation rate (simple model) (mm/yr)	^{137}Cs derived sediment accumulation rate (mm/yr)
QING 6	1.0 (2σ = 0.9 – 1.2)	0.4
QING10	1.3 (2σ = 1.0 – 1.7)	1.5
QHE2/01	1.4 (2σ = 1.1 – 1.8)	1.5
GAHA1/01	1.2 (2σ = 1.0 – 1.4)	1.0

Table 6.1 – Sediment accumulation rates as derived from ^{210}Pb and ^{137}Cs.

6.2 Radiocarbon AMS dating

The background and principles of radiocarbon dating have been well established, outlined and discussed in detail previously (e.g. Björck and Wohlfarth, 2001; Lowe, 1991; Smart and Frances, 1992; Lowe and Walker, 1997 Olsson, 1986; Olsson, 1991). ^{14}C is produced in the Earth's upper atmosphere by the interaction of cosmic ray particles with nitrogen, and is then rapidly oxidised to carbon dioxide ($^{14}CO_2$), becoming mixed throughout the atmosphere, and absorbed by oceans and by living organisms during tissue building. This carbon dioxide is in isotopic equilibrium with its contemporaneous living tissue, where upon death, uptake of CO_2 stops, while the decay of ^{14}C in organic tissues continues. Radiocarbon measurements of fossil organic matter are based on this decay process and allow, together with the internationally agreed fixed half-life of the ^{14}C isotope of 5568 years (Mook, 1986), determination of the age of the fossil material.

Radiocarbon dates in this study were undertaken at the NERC-RCL, East Kilbride and performed on authigenic inorganic carbonates (fraction <63 μm) and carbonate-free bulk organic fractions. All radiocarbon results are presented in Table 6.2 with their associated calibrated age. In general, the radiocarbon ages fall in stratigraphic order for most of the cores, except QING10, which has an age reversal. It is also worth noting that two dates fall within 5 cal ^{14}C year of each other in QING6, even though there they are 10 cm apart in the sediment, which would represent a massive shift in sedimentation not seen in other cores from Lake Qinghai.

However, the ages of the radiocarbon dates obtained from authigenic carbonate in all of the cores are consistently old compared to the dates on total organic carbon. The ages based on the organic fraction are much younger (*c.* 1000 cal ^{14}C years) than those of their carbonate counterparts, in some cases this differences even greater. This apparent offset in radiocarbon ages may be due to several

causes (Fontes *et al.,* 1993; Fontes *et al.,* 1996): (1) contribution of older detrital carbonate to the measured calcite; (2) supply of total dissolved inorganic carbon (TDIC) resulting from the dissolution of old carbonate in the catchment; (3) supply of old TDIC due to a long residence time in an aquifer; (4) oxidation of old organic matter from bottom sediments or from catchment; (5) rise of deep CO_2 into the lake of crustal origin.

Hypothesis (2) seems highly probable as the catchment area contains calcareous bedrock and/or soils, producing alkaline lake water rich in bicarbonate ions. Solid carbonates in the upper reaches of the catchment are thus dissolved by infiltrating, waters which are drained by the main rivers feeding Lake Qinghai. This hard-water effect will result in considerably older radiocarbon dates compared to the actual time of deposition and such dissolution of 'dead' carbonate could be the cause of the observed older age of the authigenic dates. This will also affect the $\delta^{13}C$ of calcite but not its $\delta^{18}O$ composition. Attempts to quantify the hard-water effect in sediment sequences in Lake Qinghai were the thinking behind parallel dating of the authigenic and organic fractions of the sediment. This has certainly highlighted the potential of dissolved inorganic carbon from old carbonate in the catchment in influencing the radiocarbon ages of the authigenic fraction.

In order to validate this hypothesis as a mechanism for causing old radiocarbon dates, the TDIC of modern water can be analysed, as dissolution of 'dead' carbonate from the catchment would cause low ^{14}C in the modern TDIC of surface water (Fontes *et al.,* 1996). Dissolution of old carbonate by modern CO_2 occurs according to the reaction:

$$CaCO_3 + CO_2 + H_2O = Ca^{2+} + 2HCO_3^- \qquad (6.1)$$

However, as a result of this reaction, ^{14}C activity in surface TDIC will not be lower than 50% for the resulting bicarbonate. Analysis of the TDIC of modern waters from Lake Qinghai (Table 6.3) shows that its radiocarbon age is modern (*c.* 5 to 10 years old). Therefore, a simple contribution of 'dead' carbonate according to Eq. (6.1) cannot account for the observed ^{14}C content of the modern TDIC of lake surface water. The ^{14}C enrichment (% modern) of TDIC in Lake Qinghai is very similar to that of modern atmospheric CO_2, presently 108% (Jull *pers. comm.*), suggesting that this hard-water error does not have a significant role in ageing the lake's TDIC and thereby effecting the radiocarbon age of authigenic carbonate.

Core	Depth (cm)	Material	^{14}C enrichment (%modern)	^{14}C age (yr BP)	□^{13}C (VPDB ‰)	Calibrated (2σ cal BP			Lab no.
						min	intercept	max	
GAHA1	57-58	BO	87.63 ±0.34	1061 ± 31	- 20.6	927	967.5	1008	SUERC-1694
	92-93	BO	77.25 ±0.32	2073 ± 34	- 24.0	1948	2035.5	2123	SUERC-1695
	57-58	AC	73.93 ± 0.24	2426 ± 26	1.7	2352	2422	2492	SUERC-1696
	92-93	AC	69.78 ±0.31	2890 ± 36	2.2	2921	3001	3081	SUERC-1915
QING6	78-79	BO	76.06 ±0.31	2199 ± 33	- 28.6	2216	2265	2314	SUERC-1697
	36-37	AC	69.51 ±0.26	2921 ± 30	2.7	2958	3020.5	3083	SUERC-1700
	47-48	AC	69.48 ±0.21	2925 ± 24	2.6	2969	3025.5	3082	SUERC-1702
	78-79	AC	66.55 ±0.23	3272 ± 28	2.2	3439	3505.5	3572	SUERC-1703
QING10	49-50	BO	72.48 ±0.26	2586 ±29	-29.0	2709	2741.5	2774	SUERC-1711
	37-38	AC	62.68 ±0.20	3753 ± 26	2.2	4071	4114	4157	SUERC-1704
	49-50	AC	65.47 ±0.25	3402 ± 30	2.3	3565	3042.5	3720	SUERC-1705
	75-76	AC	60.28 ±0.25	4067 ± 33	2.2	4437	4534	4631	SUERC-1706
QHE2	41-42	BO	85.25 ±0.33	1282 ± 31	n/a	1169	1228.5	1288	SUERC-1707
	41-42	AC	69.54 ±0.23	2918 ±26	4.5	2959	3020.5	3082	SUERC-1713
	57-58	AC	63.80 ±0.29	3611 ± 36	4.0	3829	3909	3989	SUERC-1714
	81-82	AC	62.95 ±0.22	3718 ± 28	4.0	3979	4040.5	4102	SUERC-1715

Table 6.2 – AMS radiometric data for Lake Qinghai and Lake Gahai. Graphite sources for AMS analyses were prepared and measured at the NERC-RCL, East Kilbride, UK. Radiocarbon dates were calibrated using CALIB v4.4 (Stuiver and Reimer, 1993) using calibration dataset INTCAL98 (Stuiver *et al.*, 1998). BO = Bulk organic, AC = Authigenic carbonate. Error values represent one standard deviation (1σ range).

Lab no.	Material	^{14}C enrichment (% modern)	^{14}C yrs B.P.	$\delta^{13}C$ (VPDB ‰)
AA57409a	DIC	111.66 ± 0.0042	post-bomb	1.75
AA57409b	DOC	92.10 ± 0.0037	661 ±32	-23.72

Table 6.3 – Apparent radiocarbon ages for DIC and DOC for modern surface waters from Lake Qinghai, sampled in October 2003. Analysis performed at NSF Arizona AMS Laboratory by A.J.T. Jull.

Hypothesis (3) seems unlikely as the hydraulic gradients upstream in the mountainous upper reaches of the lake's catchment, implies fast groundwater circulations (Fontes *et al.,* 1996). Also, both river and groundwater carbonate $\delta^{13}C$ are similar, reflecting interactions with bedrock and vegetation within the catchment surface, highlighting the lack of any major input from a long residence-time aquifer.

Hypothesis (4) is rejected as a significant contribution of old carbon derived from oxidation of organic matter to the TDIC would have led to a much lower values of the $\delta^{13}C$ in modern lake waters (see Chapter 5). Additionally, hypothesis (5) is compatible with the high alkalinity values of Lake Qinghai's modern water, but there is no evidence apparent that CO_2 other than from the atmosphere is present in the current TDIC pool. Crustal CO_2 has $\delta^{13}C$ values ranging between 0 and – 9 (VPDB ‰) (Fontes *et al.,* 1996) and atmospheric CO_2 falls within this range, but the values of modern TDIC of Lake Qinghai is around 1.0‰.

This leaves hypothesis (1) as the most likely cause for the difference seen between the radiocarbon dates of the two fractions. The existence of detrital material has a number of implications, not only for the radiocarbon dates, but also for other proxies of environmental change most notably the stable isotopes. As Lake Qinghai's surface water TDIC is 'post-bomb' it suggests that the dissolution of old carbonate is having a minimal effect on the age of the water. This is important as the authigenic carbonate fraction is precipitated in surface waters during the summer and if the TDIC was significantly old this age then it would effect the age of calcite and therefore would not be representative of the time of carbonate precipitation. However, modern dissolved organic carbon (DOC) has a notable radiocarbon age of 661 ± 32 yrs BP (Table 6.2). This difference in age between modern TDIC and DOC suggest that old carbon, rather than carbonate, is being incorporated into the lakes sediments.

The likely source of older carbon is therefore likely to be from lake shoreline deposits, as radiocarbon dates from authigenic carbonate, even though older than the organic dates, are not significantly old given the potential source of old carbonate in the catchment - Late Paleozoic marine limestones (see Fig. 3.12). Therefore, any reworking of older material from the lake's shoreline would probably have a similar mineralogy to the lake sediments, as well as similar isotopic composition. This is supported by

the x-ray diffraction analysis (see section 7.1.2), which shows that the major minerals produced are calcite and aragonite, both minerals that are produced within lake. Based on this assumption, 1% of old detrital carbon coming from these shore deposits would alter the carbonate dates by approximately 80 – 100 years (Lowe and Walker, 1997), suggesting the offset between bulk organic and authigenic carbonate dates would require up to 10 – 15% detrital input.

The dates from bulk organic carbon are clearly younger (than carbonate ones) and are assumed to be from within the lake as the C/N and $\delta^{13}C_{org}$ profiles suggest a dominant aquatic source (see Chapter 7). However, the dates obtained do not extrapolate to present day ages at the top of the core (based on ^{210}Pb modelling), showing some influence of 'dead' carbon in aquatic photosynthesis. This is could be due to the fact that aquatic photosynthesis utilises the DOC of lake water, which has an apparent age of 661 ± 32 yrs BP in Lake Qinghai. Therefore the age of organic dates are much younger than their carbonate equivalents, but are still too old and if they are to be used in an age model, need to be corrected using the age of the lake's DOC.

6.3 Age modelling

Many procedures exist for constructing age-depth relationships, with the majority developed using linear interpolations, splines and linear regression models (Bennett, 1994). However the different approaches can give contrasting answers (Bennett, 1994; Bennett and Fuller, 2002; Telford *et al.,* 2004), both for age at depth and the uncertainty attached to that estimate and it is therefore difficult to determine which is the most accurate (Telford *et al.,* 2004). Age-depth models are only meaningful and useful when calculated using calibrated radiocarbon dates (Bartlein *et al.,* 1995; Bennett and Fuller, 2002; Telford *et al.,* 2004).Therefore all models used here are based on calibrated dates, but this introduces an added error as the ^{14}C age has a non-linear relationship with calendar age (Bennett, 1994, Blaauw, 2003).

The construction of age-depth relationships for cores from Lake Qinghai and Lake Gahai is particularly difficult given the large uncertainty of their radiocarbon dates. However, it is possible to construct a simple relationship based on the ^{210}Pb and ^{137}Cs chronologies and the corrected radiocarbon dates for the bulk organic fraction.

6.3.1 Correction of ^{14}C ages

Correction of the apparent ages of bulk organic dates is based on the following considerations: (1) the bulk organic fraction has been significantly less affected by detrital input, producing significantly younger ages than its carbonate counterparts. Given that there is no way of gaining control on the age of the detrital component, the carbonate dates are rejected as too complex to be included in any models; (2) the modern DOC of water is significantly old and this is the carbon available to aquatic

plants during photosynthesis, thereby creating a much older age than in the DIC. Corrected ages for the organic dates are obtained by subtracting 661 (radiocarbon age of modern DOC) from the measured ages of the bulk organic fractions in the four cores. Table 6.4 summaries the corrected ages to be used in the age models for all cores.

Core	Depth (cm)	Lab no.	^{14}C age (yr BP)	^{14}C age (yr BP) corrected	^{14}C cal age (yr BP)
GAHA1	57-58	SUERC-1694	1061 ± 31	400 ± 31	471 ± 43
	92-93	SUERC-1695	2073 ± 34	1412 ± 34	1314 ± 41
QING6	78-79	SUERC-1697	2199 ± 33	1538 ± 33	1434 ± 84
QING10	49-50	SUERC-1711	2586 ±29	1925 ± 29	1882 ± 65
QHE2	41-42	SUERC-1707	1282 ± 31	621 ± 31	582 ± 32

Table 6.4 – Corrected radiocarbon ages for bulk organic dates to be used in age models for the four cores used in the study.

6.3.2 Lake Qinghai and Lake Gahai age models

The ^{210}Pb derived sediment accumulation rate for each core was plotted with the ^{137}Cs inferred date used as a fixed point, together with the corrected bulk organic AMS date (Table 6.4) and a simple linear curve fit applied, with the intercept set at 0 cm, as the surface of the core is assumed to be modern sediment. This is justified as the ^{210}Pb analyses of the upper sediments of all three Lake Qinghai cores suggest that there are no obvious fluctuations in sedimentation rate, and core lithology has shown no hiatuses in deposition. In the case of Lake Gahai, the activity reversal at the top of the core is thought to be due to either physical mixing in the upper-most sediments or the sediments not being fully equilibrated with the modern atmosphere (Binford, 1994). The ^{137}Cs date partially corroborates the ^{210}Pb age, but any age model should be treated with caution.

Figure 6.4 shows the linear age-depth relationships for all four cores. Even though the relationships are statistically significant (r^2 = 0.80 - 0.97, p = <0.001) for all the cores, it is obvious that the linear curves do not fit well with all the data points and the radiocarbon ages are still too old or there has been a change in sedimentation rate. An alternative approach, which would take into account the difference in age and any possible change in sediment accumulation, is to fit a second order polynomial to the data (Fig. 6.5). This allows calculation of a sediment accumulation that takes into account changes in sedimentation and provides a stronger relationship for the data (r^2 = 0.96 - 0.99, p = <0.001).

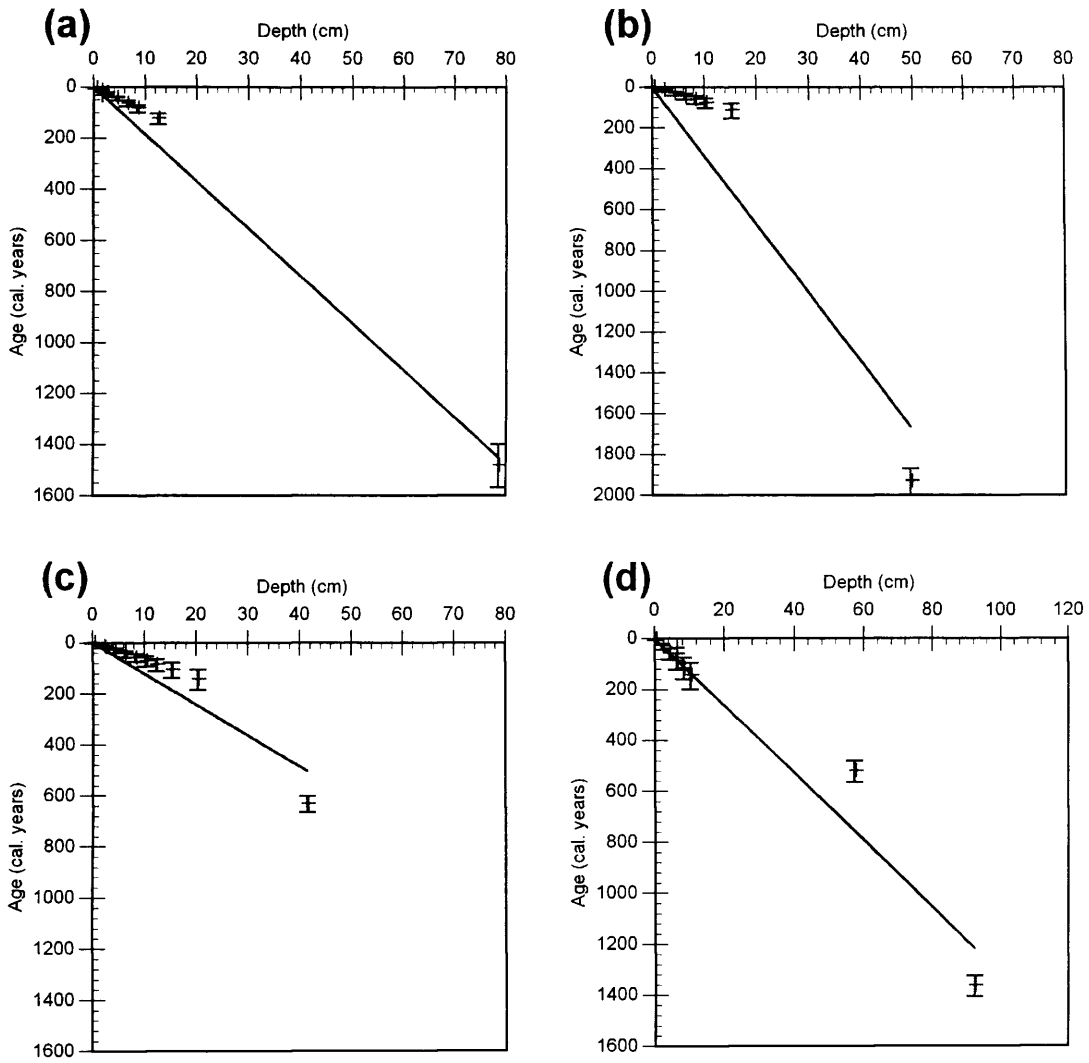

Figure 6.4 – Age-depth relationships of four cores used in the study. Representing the following cores – QING6 (a); QING10 (b); QHE2/01 (c); GAHA1/01 (d). Model constructed using the ^{210}Pb derived chronologies, ^{137}Cs inferred dates and corrected bulk organic AMS date, with a linear fit.

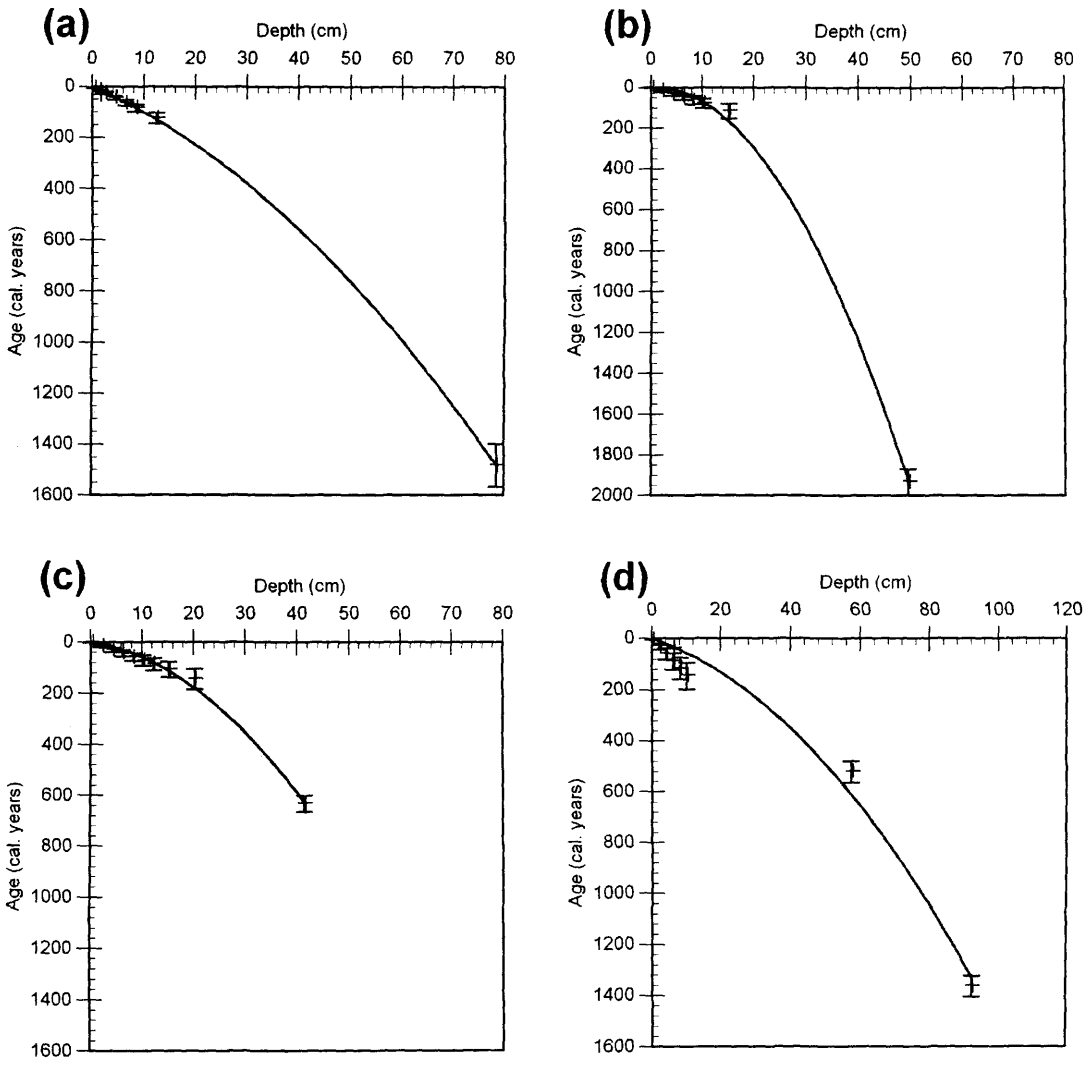

Figure 6.5 – Age-depth relationships of the four cores used in the study. Representing the following cores – QING6 (a); QING10 (b); QHE2/01 (c); GAHA1/01 (d). Model constructed using the ^{210}Pb derived chronologies, ^{137}Cs inferred dates and corrected bulk organic AMS date, with a second order polynomial fit.

Based on this relationship (see Fig. 6.5) a model of sediment accumulation can be applied to the four cores. However, for core QING10, even though there is a strong relationship, the polynomial fit suggests negative accumulation in the upper sediments (covering the ^{210}Pb time period). This is not possible given the robustness of the ^{210}Pb model derived for the upper sediments of this core, suggesting that this relationship is dependent on the ^{210}Pb model and is being skewed by the apparent age of the radiocarbon date. Therefore, in order to overcome this problem it is suggested that the ^{210}Pb model be applied for the upper sediments and then the polynomial relationship be used below this. Any comparisons between records and their apparent timings must therefore be treated with caution.

6.4 Discussion of dating evidence

The ^{210}Pb data, together with the ^{137}Cs inferred ages suggest that the sediments in present-day Lake Qinghai are accumulating at a rate of 0.1 – 0.15 cm/yr, whereas in Lake Gahai, the sediments are accumulating at a rate of *c.* 0.1 cm/yr. The recent sediment accumulation within Lake Qinghai appears to relatively coherent for three different sub-basins, with no evidence of physical mixing. Whereas, in Lake Gahai, the ^{210}Pb inventory suggests some physical mixing in the upper most sediment, although it could be due to non-equilibration with atmospheric (background) ^{210}Pb.

Unfortunately there is no independent way of examining the accuracy of the radiocarbon ages used in this study, since no clearly definable event horizons exist in the core material. However, for two cores from Lake Qinghai (Qing6, QHE2) and for Lake Gahai (Gaha1) the radiocarbon derived ages are at least compatible with the ^{210}Pb and ^{137}Cs constraints on the upper sediments. In addition, it was possible to apply a single correction to the radiocarbon ages, allowing the use of bulk organic dates in the age model. However, the radiocarbon ages derived from carbonate were too old, especially given present-day water dissolved inorganic carbonate was determined to be modern. The reasons for these anomalous dates are thought to due to detrital input of older carbonate from the catchments and lakeshore, rather than a hard water error *per se.* Therefore these dates were excluded from the age modelling process.

The age-depth plots for three of the cores used in this study (Qing6, QHE2, Gaha1) are remarkably similar in shape (Fig. 6.6), suggesting that sediment accumulation rates at these sites have responded to similar forcing. However, this may simply be an artefact, since their chronologies are only secured by one or two AMS dates, which would strongly influence the model produced.

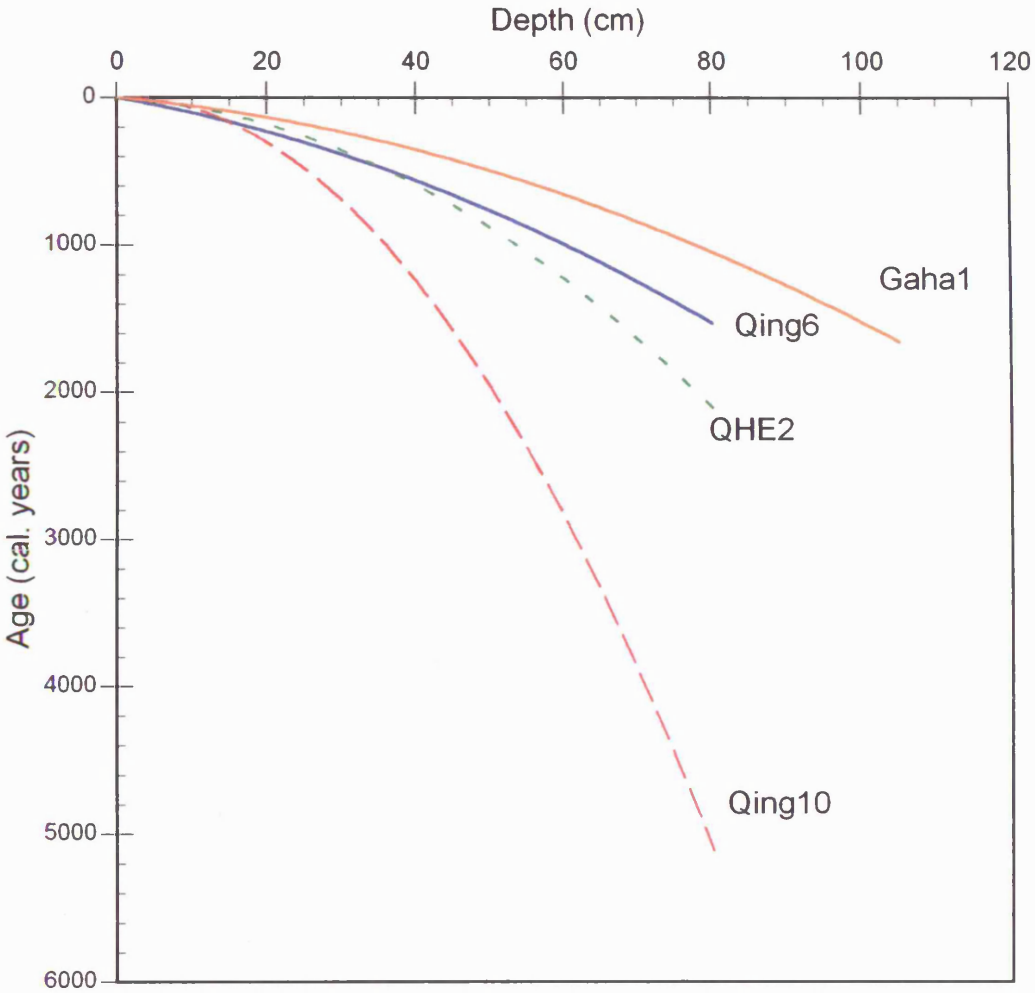

Figure 6.6 – Comparison of the Age-depth relationships of the four cores used in the study. Representing the following cores – QING6 (a); QING10 (b); QHE2/01 (c); GAHA1/01 (d). Model constructed using the ^{210}Pb derived chronologies and corrected bulk organic AMS date, with a second order polynomial fit.

6.5 Summary

Even with the problems that have been encountered with dating the cores of Lake Qinghai and Lake Gahai, it is still possible to obtain some form of chronological control based on the age models developed. It is not ideal that they are based on solely the ^{210}Pb time series, the ^{137}Cs inferred age and one bulk organic AMS date, but it is obvious that there is too much unquantifiable detrital contamination in the authigenic carbonate dates (as discussed previously).

The ^{210}Pb and ^{137}Cs derived age models for Lake Qinghai and Lake Gahai are particularly robust, with strong age-depth relationships. Although there is a difference between ^{137}Cs and ^{210}Pb for QING6, it is still a useful estimate of maximum accumulation rate for this core. The accumulation

estimates they provide suggest a relatively high sedimentation rate, which is significantly higher that those at greater depth in the core, possibly reflecting increased catchment disturbance due to human occupation, although this is uncertain as the age of the bottom of the core is only based on one date. This suggests that deeper sediments are more compacted than surface sediments, so even if there is a completely constant rate of sediment input over time, there is still an apparent increase or acceleration in accumulation rate. These deeper sediments are simply more vertically compacted than the near-surface sediments. Table 6.5 shows a summary of the sediment accumulation rates derived from the ^{210}Pb and ^{14}C age models for all four cores used in the study. It shows that accumulation rates derived from the radiocarbon dates are much lower than those derived from ^{210}Pb. Radiocarbon accumulation rates are broadly consistent with Lister *et al.,* (1991) who studied a Holocene core from the southern basin of Lake Qinghai. Their radiocarbon dates, based on the seed cases and stalks of the brackish water plant *Ruppia* established average sedimentation of 0.3 – 0.5 mm/yr throughout the Holocene. Unfortunately, their dates are restricted to the early Holocene, but they provide a likely indicator of much lower sedimentation rates in the recent past.

Core	Age model	Average sedimentation rate (mm/yr)
QING 6	^{210}Pb model	1.0 mm/yr
	^{14}C model	0.5 mm/yr
QING10	^{210}Pb model	1.3 mm/yr
	^{14}C model	0.15 mm/yr
QHE2/01	^{210}Pb model	1.4 mm/yr
	^{14}C model	0.42 mm/yr
GAHA1/01	^{210}Pb model	1.2 mm/yr
	^{14}C model	0.6 mm/yr

Table 6.5 – Summary of sediment accumulation rates used to develop a chronological framework for the four cores – QING6, QING10, QHE2 and GAHA1

Chapter Seven
The palaeolimnological history of Lake Qinghai and Lake Gahai

Introduction

This chapter presents the data of the sedimentological and geochemical analyses conducted on the four sediment cores used in the study; QING6, QING10, QHE2 and GAHA1. Summary diagrams of the results will be presented first, with the major changes seen in the sediment records outlined. All diagrams are plotted against depth with ages indicated for initial description. The data are then plotted as a function of age (cal. a BP) using the age models developed for the individual cores (see Chapter 6) in order to derive a palaeolimnological history of Lake Qinghai and Lake Gahai.

7.1 Results

7.1.1 QING6

Sediment properties

The lake sediments from core QING6 (Fig. 7.1), situated in the south basin of Lake Qinghai, are composed of quartz, low- to high-Mg calcite, aragonite, clays and organic matter (see appendix). They contain low organic carbon content (5 – 14 %) and relatively abundant carbonate (13 – 22%); both properties display low-magnitude variation in the lower part of the core (25 – 80 cm). Organic carbon then decreases (to 6%) and carbonate increases markedly (to 22%) and these values persist to the uppermost sediments.

Authigenic carbonate

$\delta^{18}O$ and $\delta^{13}C$ values of authigenic carbonate ($\delta^{18}O_{auth}$, $\delta^{13}C_{auth}$) range from -0.5‰ to +1.7‰ (mean = +0.8‰) and from +1.7‰ to +3.4‰ (mean = +2.5‰) respectively (Fig. 7.1). Both records show little isotope variation between depths of 80 – 32 cm, but above this they exhibit increased stratigraphic variability.

This section of the core (32 – 15 cm) displays an initial drop in isotope values not previously seen in the sediment record, for both $\delta^{18}O$ and $\delta^{13}C$ and marks a distinct change in the isotope stratigraphy. This variability is punctuated with a number of negative excursions in both oxygen and carbon.

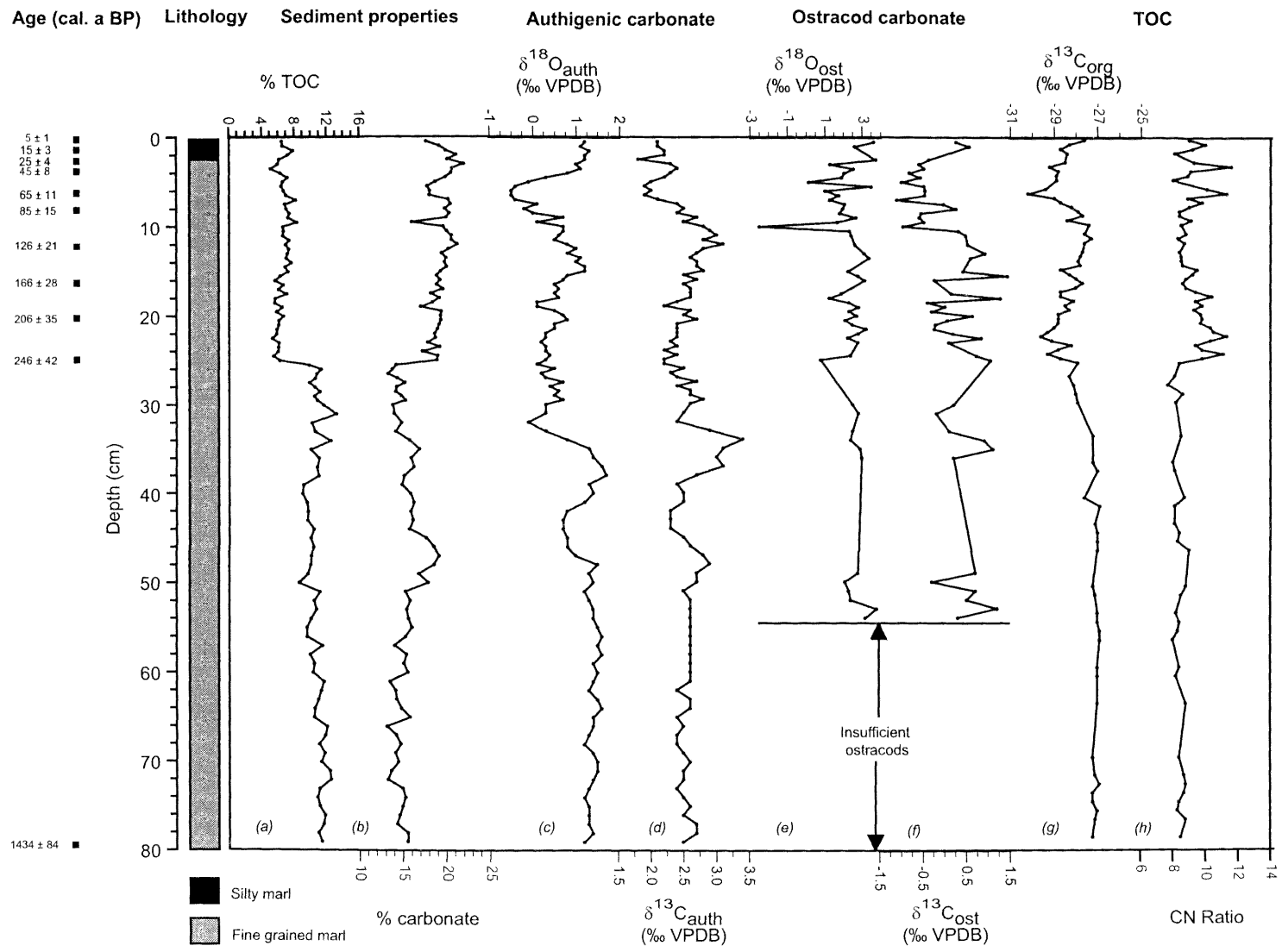

Figure 7.1 – Summary diagram of geochemical proxies for core QING6, south basin, Lake Qinghai. Sediment properties: (a) % carbon (b) % carbonate. Isotopic composition of authigenic carbonate: (c) carbon-isotope values (d) oxygen-isotope values. Isotopic composition of ostracod carbonate: (e) carbon-isotope values (f) oxygen-isotope values. Composition of the total organic carbon: (g) carbon-isotope values (h) carbon/nitrogen ratio.

The upper sediments (15 – 0 cm) show a large amplitude oscillation, most notably in the $\delta^{18}O$ where values fall to their lowest (-0.5‰) before increasing to surface sediment values of *c.* + 1‰. In contrast, the $\delta^{13}C$ values begin to decrease at the same point as in the $\delta^{18}O$ record, but there is an overall decreasing trend with no recovery back to initial values.

Ostracod carbonate

Although ostracods are present throughout the length of the core, they were only abundant enough for isotopic analyses in the upper sections, and sporadically at lower intervals. $\delta^{18}O$ and $\delta^{13}C$ of ostracod carbonate ($\delta^{18}O_{ost}$, $\delta^{13}C_{ost}$) range from -3‰ to +2.6‰ (mean = 1.8‰) and from -1.4‰ to +1.5‰ (mean = 0.7‰) respectively (Fig. 7.1). Overall, the ostracod record shows a greater degree of stratigraphic variability than the authigenic record. Isotope values, where they are available, in the middle of the record are intermediate, compared to the rest of the record. $\delta^{18}O_{ost}$ values remain intermediate while the $\delta^{13}C_{ost}$ decreases before recovering back to initial values. There is no discernable variation in the $\delta^{18}O$ after this point until 25 cm depth, while $\delta^{13}C$ shows a positive excursion (34 – 30 cm) but this is superimposed on an overall decreasing trend. Above this point the record shows increased inter-sample variability on a slightly decreasing trend up to 10 cm depth. A notable feature of the $\delta^{18}O$ record is the large negative excursion at 9.5 cm with an amplitude of *c.* 4‰. A similarly large negative excursion occurs in the $\delta^{13}C$ record at the same point, although it is not as large (*c.* 1.5‰). The upper part of the record (10 – 0 cm) displays an increasing trend in both $\delta^{18}O$ and $\delta^{13}C$ values with much reduced variability.

Organic carbon

The $\delta^{13}C$ value and C/N ratio of organic carbon ($\delta^{13}C_{org}$, CN) range from -30.2‰ to -26.9‰ (mean = -27.9‰) and from 7 to 12 (mean = 9), respectively, with total organic carbon predominantly derived from algae (Fig. 7.2). Both records show limited or no stratigraphic variability in much of the lower part of the core (80 – 25 cm) but above this there are some minor oscillations in $\delta^{13}C_{org}$ and CN. $\delta^{13}C$ increases slightly to a maximum value of *c.* -27‰ and this increasing trend is followed by a large negative excursion to -30‰ after which, there is a return to $\delta^{13}C_{org}$ values of *c.* -27‰. The CN ratio shows an initial increase that is replaced by a decreasing trend before showing larger amplitude changes in the most recent sediments (8 – 0 cm).

7.2.2 QING10

Sediment properties (Fig. 7.3a, b)

The lake sediments from core QING10, located in the north basin of Lake Qinghai, are similar to QING6. They contain organic carbon (7 - 22%) and relatively high carbonate content (15 - 45%) and, like QING6, display some distinct events in the sediment profile. Total organic carbon is generally invariant, with only some minor fluctuations (78 - 36 cm).

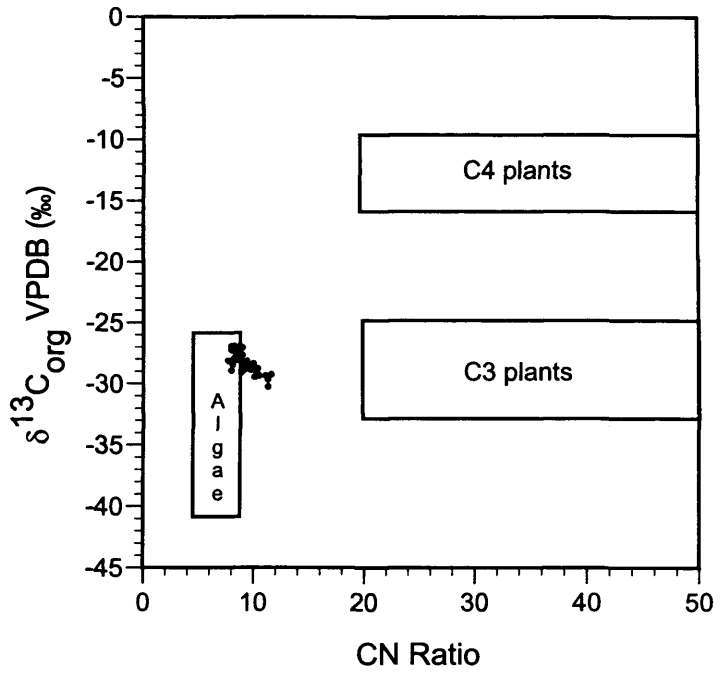

Fig. 7.2 – Stratigraphic variation in $\delta^{13}C_{org}$ against CN ratios for QING6 from Lake Qinghai, compared to ranges of plant types from previous studies (Meyers and Lallier-Verges, 1999; Leng and Marshall, 2004; Meyers and Teranes, 2001).

Organic carbon then increases to their maximum values for the whole record (36 - 26 cm) above which there is a sharp decrease in carbon content, with a slightly increasing trend to the core top.

The carbonate record is marked by a couple of distinct events: an initially decreasing trend is interrupted by large increase to much higher values (54 - 42 cm). This persists until a decrease of equal magnitude occurs (42 - 40 cm). Following this, a large increase is seen again, representing maximum carbonate content for the whole record at 34 - 26 cm (up to 45%). The carbonate record then becomes relatively invariant up to the core top.

Authigenic carbonate (Fig. 7.3c, d)

The $\delta^{18}O$ and $\delta^{13}C$ values of authigenic carbonate range from - 0.1‰ to 2.6‰ (mean = +1.5‰ ± 0.5) and + 1.3 to + 3.5 (mean = +2.6‰ ± 0.3) respectively. The isotope record shows little or no variation in the bottom-most sediment, but undergoes a large magnitude negative shift, followed by a positive and then another negative excursion (60 - 50 cm). $\delta^{18}O$ and $\delta^{13}C$ values then revert to pre-event values but have a slightly increasing trend (50 - 38 cm). Both records display then display a slight decreasing trend, which is enhanced in the $\delta^{13}C$, but superimposed on this general trend are a number of large fluctuations, most notably in the $\delta^{18}O$ curve at 16 cm and 7 cm and in $\delta^{13}C$ at 16 cm, 12 cm and 7 cm.

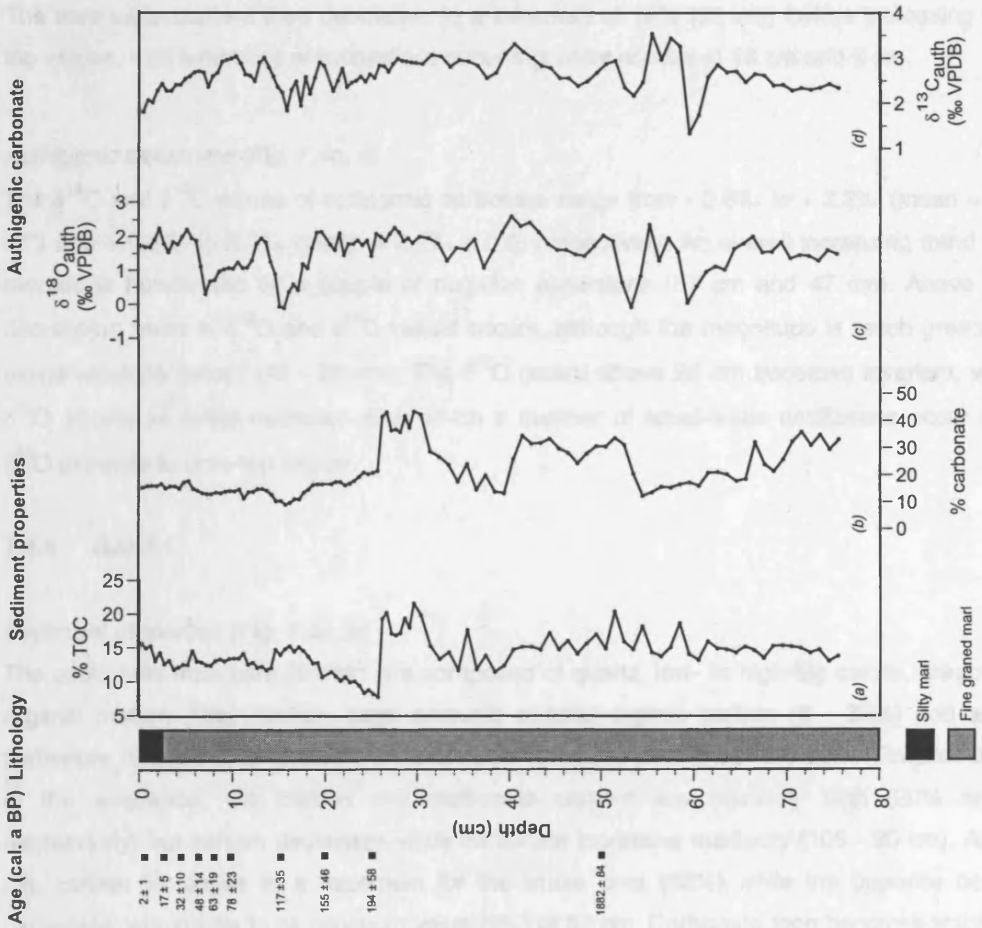

Figure 7.3 – Summary diagram of geochemical proxies for core QING10, north basin, Lake Qinghai. Sediment properties: (a) % carbon (b) % carbonate. Isotopic composition of authigenic carbonate: (c) carbon-isotope values (d) oxygen-isotope values.

7.2.3 QHE2

Sediment properties (Fig. 7.4a, b)

The lake sediments of core QHE2, located in the eastern basin of Lake Qinghai, are similar to QING6 and QING10; they contain low organic carbon content (5 - 13%) and relatively high percentage of carbonate (12 - 22%). Organic carbon is invariant throughout much of the core with only a limited number of oscillations. The carbonate content shows much more variation, with bottom core values constant until an increasing trend (82 - 42 cm).

The carbonate content then decreases to a minimum of 12% (25 cm) before increasing to core-top values, with a number of fluctuations occurring, most notably at 18 cm and 8 cm.

Authigenic carbonate (Fig. 7.4c, d)

The $\delta^{18}O$ and $\delta^{13}C$ values of authigenic carbonate range from - 0.6‰ to + 2.3‰ (mean = 0.8‰ ± 0.7) and + 0.8‰ to 3.2‰ (mean = 2.2‰ ± 0.5) respectively. An overall increasing trend for both records is punctuated by a couple of negative excursions (57 cm and 47 cm). Above 47cm a decreasing trend in $\delta^{18}O$ and $\delta^{13}C$ values occurs, although the magnitude is much greater in the oxygen-isotope record (40 - 26 cm). The $\delta^{13}C$ record above 26 cm becomes invariant, while the $\delta^{18}O$ shows an initial decrease after which a number of small-scale oscillations occur until the $\delta^{18}O$ increase to core-top values.

7.1.4 GAHA1

Sediment properties (Fig. 7.5a, b)

The sediments from core GAHA1 are composed of quartz, low- to high-Mg calcite, aragonite and organic matter. They contain large amounts of total organic carbon (8 - 38%) and abundant carbonate (6-30%) and display high amplitude variability throughout the core. Towards the base of the sequence, the carbon and carbonate content are relatively high (20% and 10% respectively) but carbon decreases while carbonate increases markedly (105 - 90 cm). Above 90 cm, carbon increases to a maximum for the whole core (38%) while the opposite occurs for carbonate, which falls to its minimum value (6%) at 82 cm. Carbonate then becomes stable with a number of oscillations occurring between 82 and 14 cm. Total organic carbon on the other hand, initially decreases back to intermediate values but there is an abrupt change and a return to high values between 58 and 39 cm. Above 39 cm there is an increasing trend with minor fluctuations to core-top values.

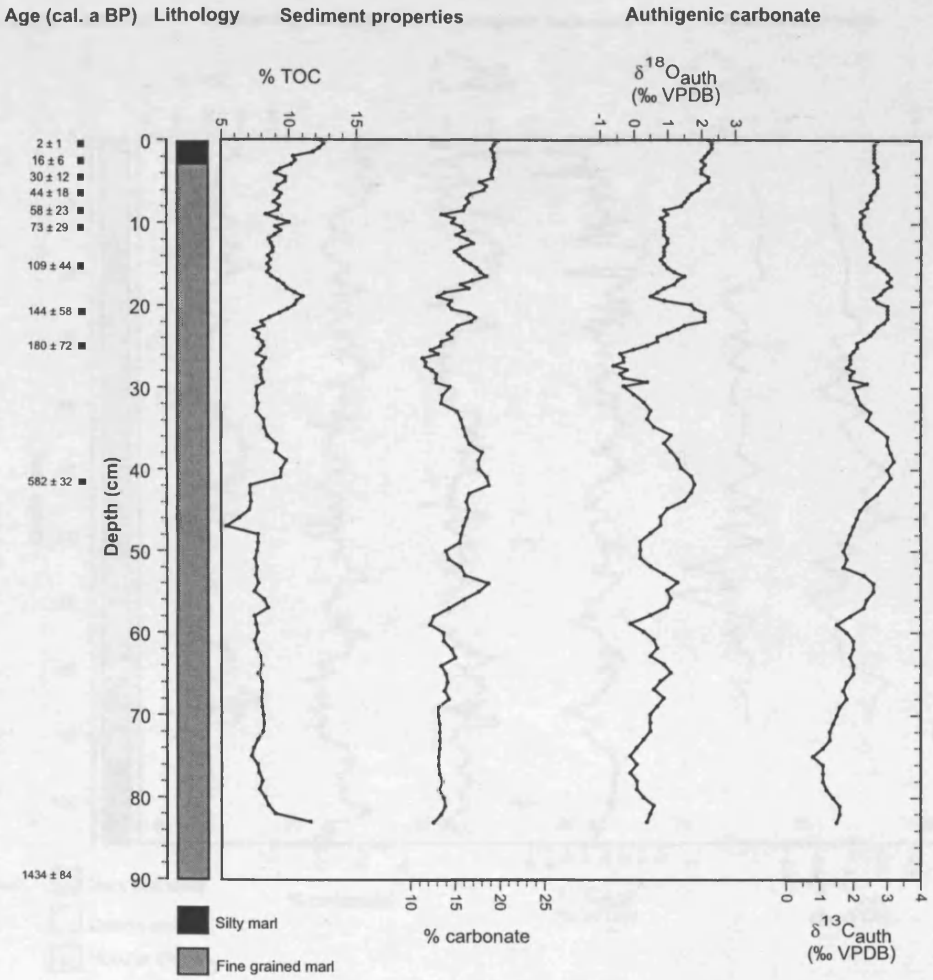

Figure 7.4 – Summary diagram of geochemical proxies for core QHE2, eastern basin, Lake Qinghai. Sediment properties: (a) % carbon (b) % carbonate. Isotopic composition of authigenic carbonate: (c) carbon-isotope values (d) oxygen-isotope values.

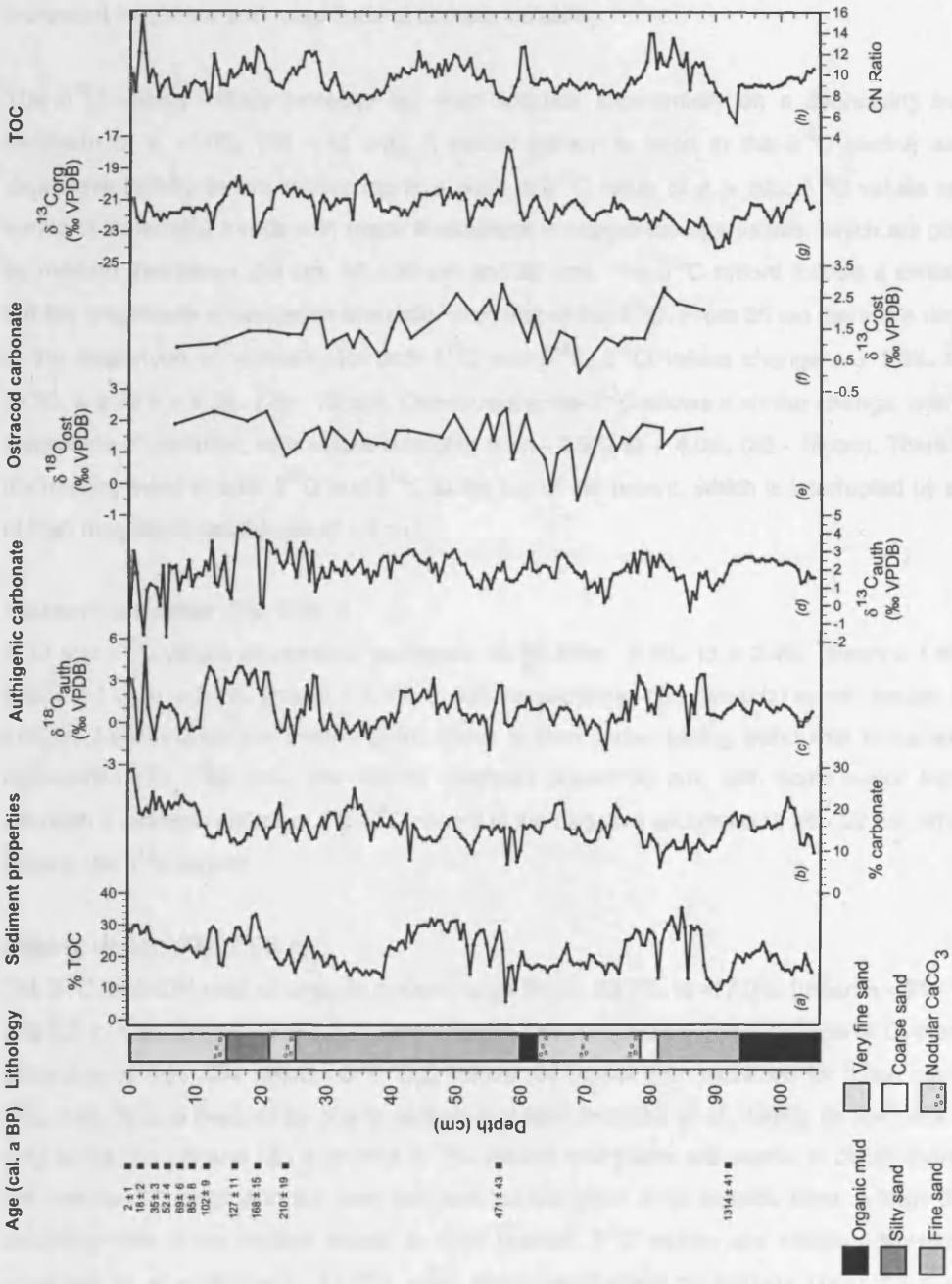

Figure 7.5– Summary diagram of geochemical proxies for core GAHA1, Lake Gahai. Sediment properties: (a) % carbon (b) % carbonate. Isotopic composition of authigenic carbonate: (c) carbon-isotope values (d) oxygen-isotope values. Isotopic composition of ostracode carbonate: (e) carbon-isotope values (f) oxygen-isotope values. Composition of the total organic carbon: (g) carbon-isotope values (h) carbon/nitrogen ratio.

Authigenic carbonate (Fig. 7.5c, d)

$\delta^{18}O$ and $\delta^{13}C$ values of authigenic carbonate ranges from - 1.9‰ to + 5.4‰ (mean = + 1.1‰ ± 1.3) and - 1.7‰ to + 4.3‰ (mean = + 2.0‰ ± 0.9) respectively. Both records show little variability at the bottom of the core (105 - 90 cm), with values at intermediate level. Above this there is increased frequency and magnitude of isotopic variability.

The $\delta^{18}O$ values initially increase but then fluctuate substantially on a decreasing trend to a minimum of *c.* -1.0‰ (88 - 75 cm). A similar pattern is seen in the $\delta^{13}C$ record, although it decreases initially before recovering to a peak in $\delta^{13}C$ value of *c.* + 3‰. $\delta^{18}O$ values undergo a series of increasing trends with major fluctuations in oxygen-isotope values, which are punctuated by marked decreases (55 cm, 40 - 30 cm and 25 cm). The $\delta^{13}C$ record follows a similar pattern but the magnitude of oscillation is smaller than that of the $\delta^{18}O$. From 25 cm there is a distinct shift in the magnitude of variability for both $\delta^{18}O$ and $\delta^{13}C$. $\delta^{18}O$ values change *c.* - 1.5‰ to over + 3.0‰, a shift ≈ + 4.5‰ (25 - 12 cm). Concurrently, the $\delta^{13}C$ shows a similar change, with a similar magnitude of variation, with values changing from - 0.5‰ to + 4.0‰ (22 - 16 cm). There is then a decreasing trend in both $\delta^{18}O$ and $\delta^{13}C$ to the top of the record, which is interrupted by a number of high magnitude oscillations (6 - 0 cm).

Ostracod carbonate (Fig. 7.5e, f)

$\delta^{18}O$ and $\delta^{13}C$ values of ostracod carbonate range from - 0.5‰ to + 2.4‰ (mean = 1.5‰ ± 0.6) and + 0.1‰ to + 2.7‰ (mean = 1.5‰ ± 0.6) respectively. The ostracod record begins at *90 cm* and the initial values are intermediate. There is then a decreasing trend with some large-scale fluctuations (75 - 50 cm). The record stabilises above 50 cm, with some minor fluctuations, although a notable feature of the $\delta^{18}O$ record is the negative excursion at 28 - 22 cm, which is not seen in the $\delta^{13}C$ record.

Organic carbon (Fig. 7.5d, h)

The $\delta^{13}C$ and C/N ratio of organic carbon range from - 23.7‰ to -17.0‰ (mean = - 21.4‰ ± 0.9) and 5.5 to 15.6 (mean = 9.6 ± 1.4) respectively. Total organic carbon is of algal or C_3 plant origins according to their C/N ratios, but $\delta^{13}C_{org}$ values are higher than expected for these plant groups (Fig. 7.6). This is likely to be due to carbon-limitation (Holmes *et al.,* 1999), as the Lake Gahai is very saline (33 g/l) and has a pH of 8.9. This means that plants are unable to discriminate against the heavier ^{13}C isotope in the total inorganic carbon pool. Both records show a large degree of variability with some distinct events in their profiles. $\delta^{13}C$ values are initially intermediate, but decrease to a minimum (- 23.7‰) after which small-scale oscillations occur on a generally increasing trend, which are terminated by a large positive excursion (60 cm). $\delta^{13}C$ values quickly return to pre-event values with a number of marked negative excursions (at 48 cm, 34 cm, 28 cm, 19cm and 12cm). The C/N ratio is invariant until a negative excursion is followed by a pronounced positive event (90 - 76 cm), ratios reach *c.* 14. Following this there is a return to ratios of <10 and

little variation occurs until a sharp, short-lived positive excursion (60 cm). Values return to ratios of <10 and 10 to 12 (60 - 27 cm). There is then a broadly overall decreasing tend to the core top, although there is increasing variability in C/N ratio with a distinct and short positive excursion at 2 cm.

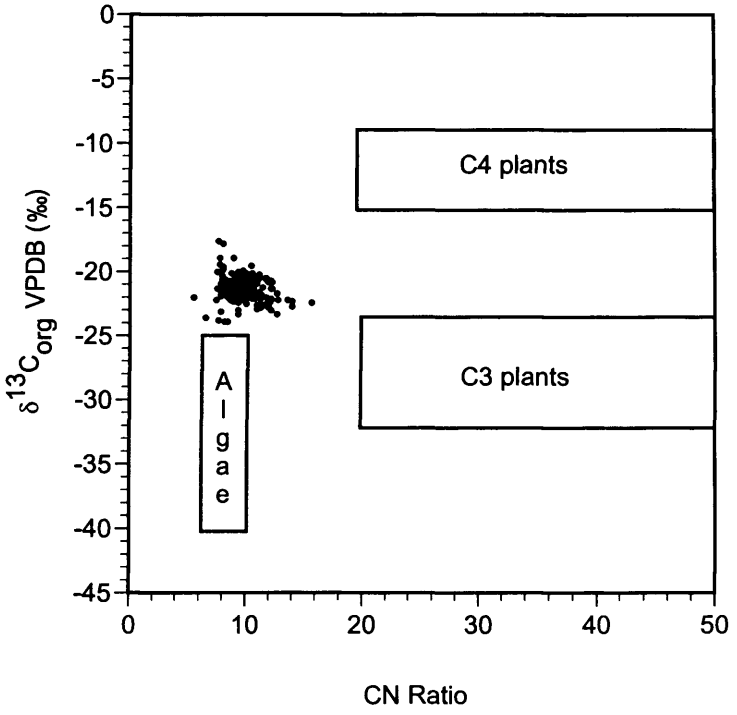

Fig. 7.6 – Stratigraphic variation of $\delta^{13}C_{org}$ against C/N ratios for GAHA1 from Lake Gahai, compared to ranges of plant types from previous studies (Meyers and Teranes, 2001; Meyers and Lallier-Verges, 1999; Leng and Marshall, 2004).

7.2 Interpretation of palaeolimnological indicators

7.2.1 Oxygen isotopes

The oxygen-isotope ratio of lacustrine carbonates is controlled by the temperature and, more importantly in closed lakes like Lake Qinghai and Gahai, the isotope composition of the water at the time of carbonate precipitation (see Chapter 2). In closed lakes the isotopic composition of water is controlled by the precipitation-evaporation ratio (P-E) and, to a lesser extent, by the composition of precipitation and the amount of runoff (see Chapter 5) (Leng and Marshall, 2004). An additional control on authigenic carbonates ($\delta^{18}O_{auth}$) is mineralogy (Grossman, 1984; Romanek *et al.*, 1992; Kim and O'Neil, 1997), which may also affect isotope values. For example, aragonite has an $\delta^{18}O$ value that is 0.6 ‰ greater that calcite precipitated under identical conditions (Grossman and Ku, 1986) and an increase in Mg content of calcite will also affect the $\delta^{18}O$ value, with a *c.* 0.06 ‰ increase in $\delta^{18}O$ recorded for a 1% rise in the mole% Mg in calcite observed by Tarutani *et al.*, (1969). However, minor variations in the proportions of calcite and

aragonite will not significantly affect the $\delta^{18}O_{auth}$ curve. The presence of significant amounts of dolomite may theoretically have a much greater effect on the $\delta^{18}O_{auth}$ record than the presence of aragonite, since dolomite may be enriched by up to 4‰ to 6‰ in ^{18}O compared to calcite formed under the same conditions (Land, 1983; Tucker and Wright, 1990). In practice, however, if the amount of dolomite is low (<10%) then it is probably not a problem, for example, 10% of a mineral that is 6‰ different will only effect the overall $\delta^{18}O_{auth}$ by an increase in 0.6 ‰ if there is a total reaction of dolomite (which there would not be at 25°C for 8 hours) (Leng *pers. comm.*). Biogenic carbonates, such as ostracods ($\delta^{18}O_{ost}$), often have isotopic values that are offset from standard equilibrium values obtained from inorganic carbonates (see Chapter 2) as a result of vital effects. These 'vital effects' must be considered since they are often species- or genus-specific (von Grafenstein *et al.,* 1999; Holmes and Chivas, 2002).

7.2.2 Inorganic carbon isotopes

The carbon isotope ratio of lacustrine carbonate ($\delta^{13}C_{auth}$, $\delta^{13}C_{ost}$) provides an indication of the $^{13}C/^{12}C$ of the total dissolved inorganic carbon (TDIC) in the lake water, which in turn is controlled by catchment and within lake processes (see Chapter 2). Catchment sources include carbonate bedrock and soil carbon. Within the lake, the long-term balance of photosynthesis and respiration by aquatic plants and algae (which involves the preferential uptake of ^{12}C, leaving the TDIC relatively enriched in ^{13}C) and organic decay (which leads to the release of isotopically-light carbon into the TIDC pool) is often the most important control (McKenzie, 1985; Kelts and Talbot, 1990). However, for a lake like Qinghai, which has a water residence time of 33 years (Lister *et al.,* 1991), the equilibration of lake water with atmospheric CO_2 ($\delta^{13}C$ = - 8 to -7 ‰) through gas exchange likely to be the dominant process, especially in lakes where $\delta^{18}O$ and $\delta^{13}C$ co-vary (Kelts and Talbot, 1990).

7.2.3 Organic carbon isotopes

The carbon isotope ratio of lacustrine organic matter ($\delta^{13}C_{org}$) and its carbon-nitrogen ratio (C/N) is an indication of carbon source (see Chapter 2). The dominant effect on its composition is associated with different sources of organic material and productivity (Ariztegui *et al.,* 1996). Where terrestrial plant material gets incorporated into the lake, and there are both C_3 and C_4 plants in the catchment, the carbon-isotope ratio tends to reflect the proportion of input from C_3 plants ($\delta^{13}C$ = - 22 to -33 ‰) and C_4 plants ($\delta^{13}C$ = - 9 to - 16 ‰) (e.g. Smith and Epstein, 1971; Deines, 1980; Holmes *et al.,* 1997). All plants have different $\delta^{13}C$ values (Meyers and Lallier-Verges, 1999), and there can be considerable overlap in the $\delta^{13}C$ values (Holmes *et al.,* 1997), so C/N ratio analysis of the same material can help to define the source of the organic matter. C/N ratios are used, in particular, to differentiate between algal and higher plants. For example ratios of < 10 are common for lacustrine algae, values between 10 and 20 for submergent and floating

aquatic macrophytes or a mixed source, and values > 20 for emergent macrophytes and terrestrial plants (Meyers and Lallier-Verges, 1999; Leng and Marshall, 2004).

7.2.4 Authigenic vs. ostracod carbonate

In deciding which factors are most important in any one lake, it is necessary to consider the source of the carbonate. Authigenic calcite and aragonite are thought to precipitate from surface water through algal photosynthetic uptake of CO_2 during the growing/summer season, which reduces the partial pressure of CO_2 and causes $CaCO_3$ super-saturation in the surface water (Kelts and Talbot, 1990). Therefore the oxygen-isotope composition of the authigenic carbonate reflects average water composition and temperature near the lake surface during summer months. In contrast, ostracods form their shells rapidly over a period of hours to days and provide more of a 'snapshot' of lake conditions. Both *Limnocythere inopinata* and *Eucypris inflata* are benthic taxa and therefore provide a record of bottom-water composition and temperature, although since modern water isotope data indicate that the lake is not isotopically stratified during the summer (see Chapter 5), any differences between the ostracod values and those from authigenic carbonates are best explained by differences in summer water temperature, together with offsets from equilibrium in the ostracod values. *L. inopinata* tends to be present during the late spring to early autumn, whereas little is known about the seasonal preference of *E. inflata*. Shells of *L. inopinata* have $\delta^{18}O$ values of + 0.8‰ greater than authigenic calcite precipitated under the same conditions (von Grafenstein *et al.,* 1999). Such effects have not been quantified for *Eucypris*; Lister *et al.,* (1991) analysed specimens of *L. inopinata* and *E. inflata* from the same level in a short core from Lake Qinghai and found that the $\delta^{18}O$ value of the former was on average 0.4‰ lower than that of the latter. However, as they acknowledge, it is unclear whether this difference is the result of differing 'vital effects' or the fact that the two species calcified in different seasons.

7.3 Palaeolimnological interpretation of Lake Qinghai

Before any emphasis is placed on the palaeolimnological interpretations and because of the problems with imprecise dating it is perhaps pertinent to independently match isotopic excursions in the cores (Fig. 7.7). This will be based on $\delta^{18}O_{auth}$, as this is thought to be influenced by the same controls, whereas $\delta^{13}C_{auth}$ is influenced by many more local factors. There are obvious similarities between the isotope profiles with the most prominent represented by the shaded bar and the labelled peaks and troughs (Fig. 7.7). These are more apparent in the cores from Lake Qinghai, while similarities in Lake Gahai are not as obvious largely due to it being a smaller, independent lake. However, comparison of the cores highlights there are some similar features of the records presented here, suggesting that there may have been an overall climatic or other forcing on the lake.

To support this notion, the cores were then compared after the age model had been applied (Fig. 7.8) since any forcing should have been synchronous. When the age model has been applied, the similarities noted in figure 7.7 are not as apparent. The disparity between the cores could be due to real differences or the imprecise dating could influence them. The greatest similarity is seen in the upper part of the core, probably due to the ^{210}Pb chronology that is fairly robust (Fig. 7.8). Suggesting that any climatic inferences from within the last 150 years derived from the records are more reliable than in the older sediments. Therefore, inferring climate changes over the last 2000 years from the Lake Qinghai and Lake Gahai records should be made with caution, and realized in the full knowledge that the age models derived are limited.

Even so, the stratigraphic changes in isotope values provide a record of limnological history of Lake Qinghai. Three zones have been assigned for QING6 and QHE2 based on changes seen in the $\delta^{18}O_{auth}$ stratigraphy as this is thought to be an appropriate proxy of palaeohydrological and climatological change (see Chapter 2). No zones have been assigned to QING10 due to the uncertainty in the core's chronology as discussed above and in Chapter 6. Figures 7.9, 7.10 and 7.11 show the sediment records for the three cores from Lake Qinghai plotted as a function of age, in calendar years BC/AD. Changes in QING10 are discussed below within the chronostratigraphic framework of the other cores, but interpretations must be viewed with caution owing to the uncertainty in the QING10 chronology (see Chapter 6).

Lake Qinghai is a closed basin lake and undergoes seasonal evaporation, which leaves its waters enriched in ^{18}O relative to input waters. Subsequently, carbonate precipitation within the waters reflect the isotope composition of lake water at that time, which is controlled by effective precipitation (P-E) (see Chapter 5). Lake Qinghai is thought to have reached steady-state *c.* 3000 yrs BP (Lister *et al.*, 1991) after substantial shifts (~ 6‰) in isotopic composition of waters related to the onset of the interglacial and monsoon strengthening. The steady-state isotopic composition for closed-basin lake waters is given by the equation (Ricketts and Johnson, 1996):

$$\delta^{18}O_{ss} = \frac{\left[\left(\delta_{inputs}Q_{inputs} - \delta_{outputs}Q_{outputs}\right) - \delta_L \Delta V_L\right]}{V_L} \qquad (7.1)$$

Where the δ values are relative to SMOW for inputs or outputs, Q is the total flux for inputs or outputs and V_L is the volume of the lake. Using modern meteorological data and measured δ values from this study (see section 5.4) the steady state value $\delta^{18}O_{ss}$ = 0‰. At 12°C (equivalent to summer water temperatures) the corresponding $\delta^{18}O_{auth}$ (VPDB) for $\delta^{18}O_{ss}$ = - 0.1‰, which is *c.* 1‰ more negative than the most recent sediments of QING6, QING10 and QHE2. The difference between the calculated and observed isotope composition of sediment could be due to large-scale uncertainties in the catchment hydrology that define this model or arise as a result of temperature bias, as discussed in section 5.8. Alternatively, it could mean that the lake isn't in steady-state, with some major perturbations in recent times.

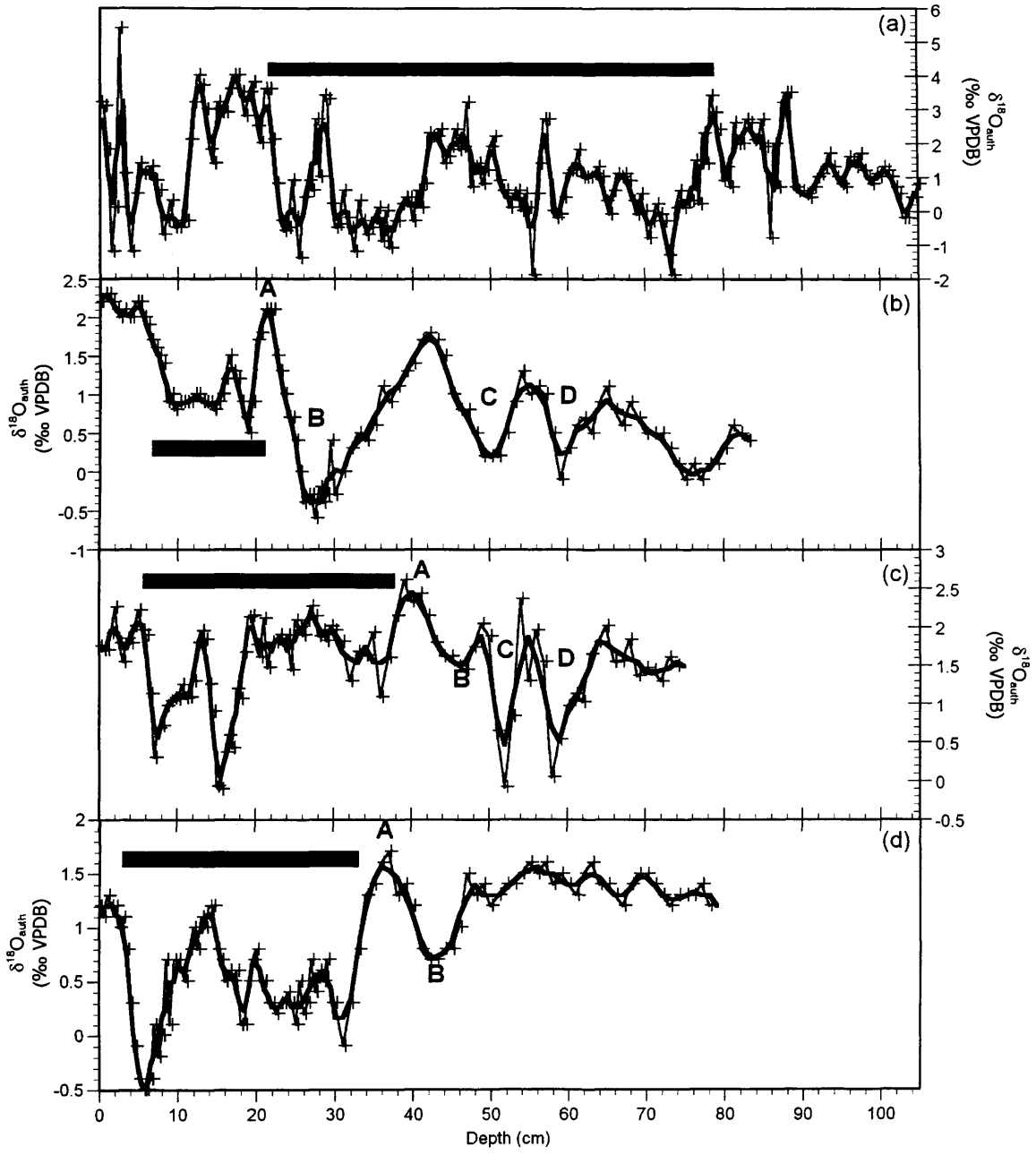

Figure 7.7 – Comparison of $\delta^{18}O_{auth}$ of all four cores used in this study. (a) GAHA1, (b) QHE2, (c) QING10 and (d) QING6. The shaded bar corresponds to the same time span for all the cores based on similarities in the isotope profile. This is based on correlation of peaks and troughs in the isotope records, with A, B, C and D corresponding to 'synchronous' events in the lake's history.

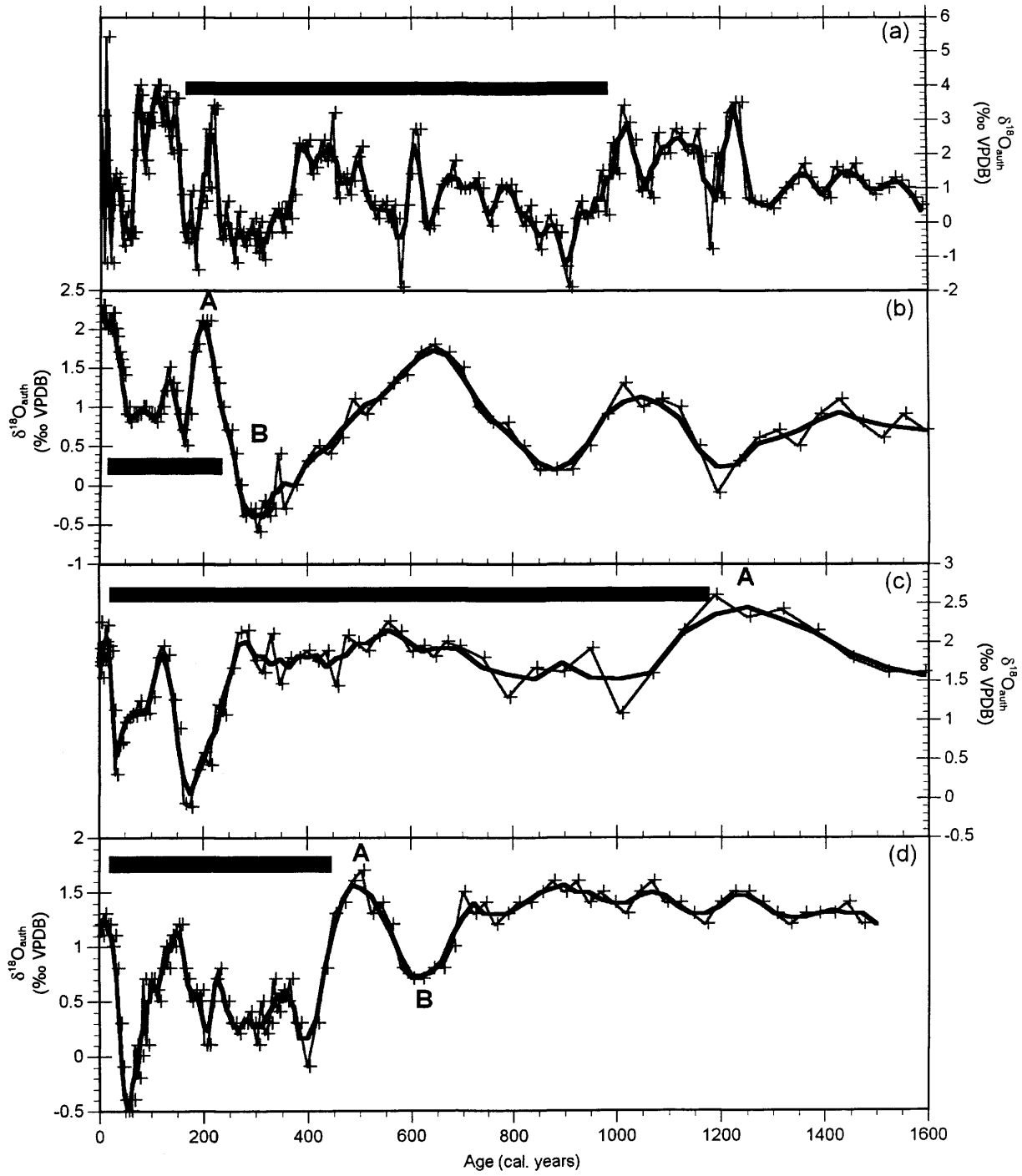

Figure 7.8 – Comparison of $\delta^{18}O_{auth}$ against calendar years for all four cores used in this study. (a) GAHA1, (b) QHE2, (c) QING10 and (d) QING6.

Once isotope steady-state has been reached, only short-term events leading to periodic isotope dilution of lake waters may leave a signal. Table 7.1 shows the extent of isotope change under different scenarios of change in precipitation and evaporation in Lake Qinghai. It shows that changes in evaporation are likely to have a greater influence on the resulting $\delta^{18}O$ of lake water, which further corroborates evaporation as the main control on the isotope composition of water in Lake Qinghai.

Using equation 7.1 the precipitation was adjusted, while all other fluxes remained constant, to determine the amount of volume change under a certain hydrological change. Once the extent of volume change had been established the lake water $\delta^{18}O$ and therefore the $\delta^{18}O$ of carbonate (precipitation at 12°C) could be calculated for Lake Qinghai (Table 7.1). The same exercise was also undertaken for evaporation, with the other fluxes kept constant (Table 7.1).

		Percentage change					
		+ 10%	**+ 20%**	**+ 30%**	**+ 40%**	**+ 50%**	**+ 100%**
PPT	**Vol (m^3)**	341403	682806	1024209	1365612	1707016	3414032
	$\delta^{18}O$ (‰)	-0.05	-0.08	- 0.12	- 0.16	- 0.2	- 0.4
Evap	**Vol (m^3)**	-535480	-	-	-	-	-
			1070960	1606440	2141920	2677400	5354800
	$\delta^{18}O$ (‰)	0.2	0.3	0.4	0.6	0.7	1.5

Table 7.1 – Changes in lake volume and $\delta^{18}O$ composition of lake water (‰ VSMOW) under different percentage changes in precipitation and evaporation

The records from the current study show small oscillations with the maximum isotope change of only *c.* 2‰. This could be related to small changes in the catchment climate. The greatest isotopic variability occurs within the last 500 years (from *c.* 1450 AD), which is a trend seen in all cores (Fig. 7.7, 7.8, 7.9). The palaeolimnological history of Lake Qinghai will now be discussed in calendar years using the modelled isotope changes (Table 7.1).

7.3.1 Zone C (*c.* 2500 BC to 1500 AD)

In this period the $\delta^{18}O_{auth}$ values are relatively stable in all records apart from QING10 which shows a large event at 750 BC to 150 BC, although this may be an artefact of the dating model employed for this core (see section 7.5). $\delta^{18}O_{auth}$ values for both QING6 and QHE2 are above calculated $\delta^{18}O_{ss}$, suggesting that the lake may have been at a different isotopic steady-state since there is minimal variation, apart from a small negative excursion at 1300 AD (QING6) and at 1100AD (QHE2). Isotope values quickly return to pre-event conditions supporting the suggestion of a short-term change in local climate conditions effecting the lake's effective precipitation.

Relatively high $\delta^{13}C_{auth}$ values at this time in QING6, QING10 and QHE2 reflect a TDIC controlled by atmospheric exchange as surface waters would be undergoing no or slow changes in lake level or productivity (Li and Ku, 1997). This supports the hypothesis that the lake is at isotopic

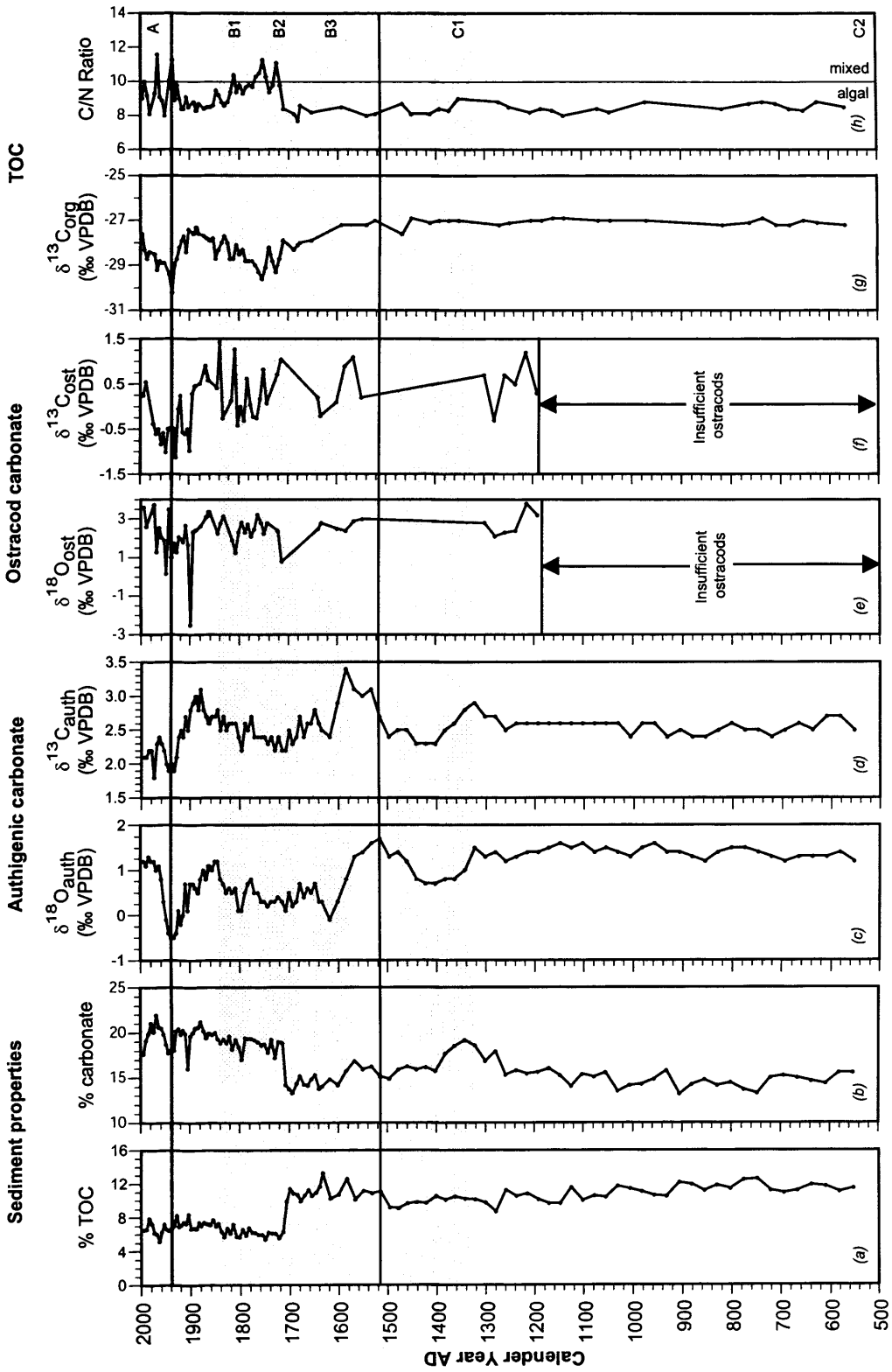

Figure 7.9 – Summary diagram of geochemical proxies plotted using the age model for core QING6. Sediment properties: (a) % carbon (b) % carbonate. Isotopic composition of authigenic carbonate: (c) carbon-isotope values (d) oxygen-isotope values. Isotopic composition of ostracode carbonate: (e) carbon-isotope values (f) oxygen-isotope values. Composition of the total organic carbon: (g) carbon-isotope values (h) carbon/nitrogen ratio.

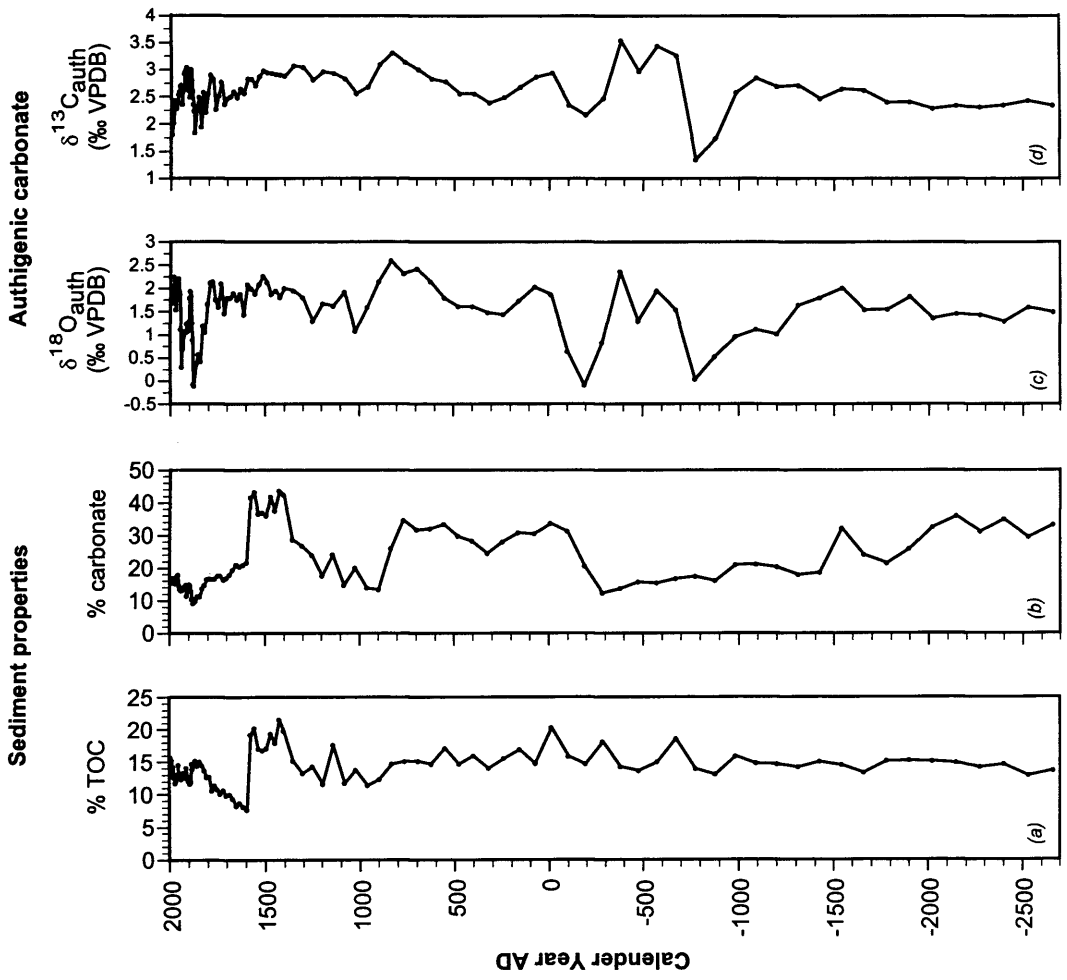

Figure 7.10 – Summary diagram of geochemical proxies plotted using the age model for core QING10. Sediment properties: (a) % carbon (b) % carbonate. Isotopic composition of authigenic carbonate: (c) carbon-isotope values (d) oxygen-isotope values.

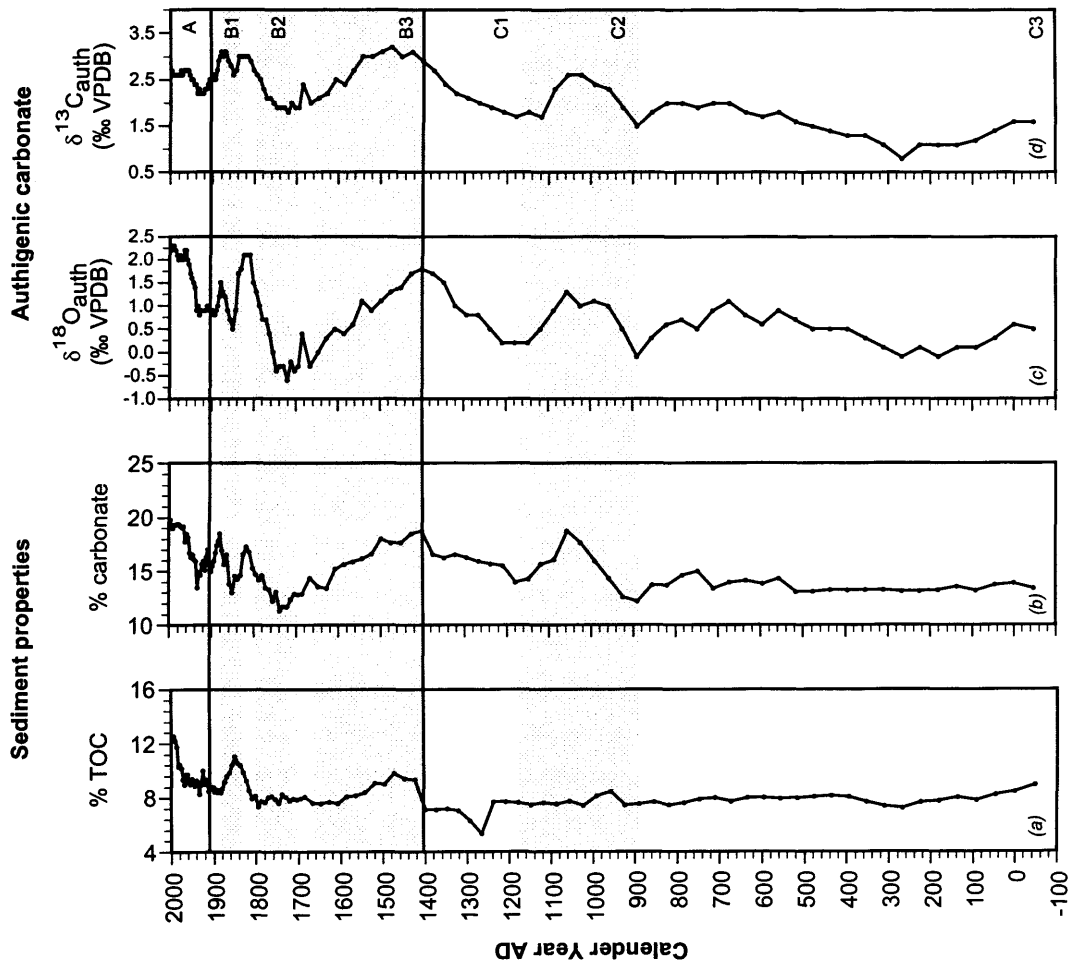

Figure 7.11 – Summary diagram of geochemical proxies plotted using the age model for core QHE2. Sediment properties: (a) % carbon (b) % carbonate. Isotopic composition of authigenic carbonate: (c) carbon-isotope values (d) oxygen-isotope values.

steady-state as $\delta^{13}C_{auth}$ approaches equilibrium with atmospheric CO_2. At this time the lake was dominated by algal productivity as suggested by the $\delta^{13}C_{org}$ (– 27‰ to – 28‰) and CN ratio (< 10) from QING6. The dominance of the algal component suggests that there is minimal catchment in-wash, which is consistent with reduced effective precipitation at this time, as shown by the $\delta^{18}O_{auth}$. Therefore the lakes level was comparable to or lower than the water levels seen in the modern Lake Qinghai.

7.3.2 Zone B (1500 AD to 1920 AD)

As already indicated this period shows the greatest isotopic variability in all the records, which could be a result of varying lake levels, water temperature change or fluctuations in effective precipitation. The latter seems the most likely cause as evaporation is the dominant control on isotope composition of lake water (see Chapter 5). There are three prominent negative excursions in $\delta^{18}O_{auth}$ and $\delta^{13}C_{auth}$ (labelled B1, B2, B3 on Fig. 7.9, 7.11), which are particularly pronounced in the QING6 record. B3 (*c.* 1600 AD) shows a large shift in isotope values with a negative excursion from isotope steady-state. The change, in order of *c.* 2‰, indicates an increasing effective moisture balance and a freshening of the lake which would likely have caused higher lake levels. This magnitude of change could be due to a number of causes. Firstly, increased precipitation received by the catchment. However, even with a doubling of precipitation amount (from 0.4 $m^3\ yr^{-1}$ to 0.8 $m^3\ yr^{-1}$), where other factors remain constant this would produce $\delta^{18}O_{auth}$ = 1.1‰, which is too high compared to the lowest value of $\delta^{18}O_{auth}$ = – 0.25‰ to – 0.5‰ seen in QING 6 and QHE2 within B3. Secondly, a reduction in direct evaporation from the lake. Keeping all inputs and other factors constant a reduction in evaporation by 50% produces a predicted $\delta^{18}O_{auth}$ = 0.6‰, which is extremely close to the sedimentary values of $\delta^{18}O_{auth}$ at this point in the record for QING6 and QHE2. This suggests that the effect of evaporation is a dominant control on the $\delta^{18}O_{auth}$ record from Lake Qinghai. Although it is unlikely that one single factor will be controlling the balance of effective moisture, temperature is a key component as it determines the amount of evaporation, which in turn determines the amount of locally derived convective precipitation (see section 5.1). Additionally, as the lake is ice covered between December and March a decrease in temperature may prolong the ice cover period reducing the time the lake is subject to seasonal evaporation. Additionally, a reduced air temperature would reduce lake water temperatures causing ^{18}O enrichment in precipitated carbonate (and higher $\delta^{18}O_{auth}$ values), which would offset the effects of reduced evaporation to some extent. However, the extent and direction to lower $\delta^{18}O$ values at this time support the notion that a reduction in evaporation linked to reduced air temperatures and ice cover is the dominant control.

From this initial decrease, isotope values show little variation, especially in the QING6 record. The changes seen in QING6 and QHE2 are not concurrent, which could be due to the difference in the age model rather than specific changes in the lake. However, between 1600 AD and 1850 AD in both records the $\delta^{18}O_{auth}$ values are lower with minimal isotope fluctuation (~ 0.5‰ amplitude) in

QING6, while QHE2 shows a much larger shift in isotope values (~ 2‰ amplitude), indicating a prolonged change in the effective moisture regime. The cause of this would be due to increased effective moisture (either decreased evaporation or increased precipitation). Mean $\delta^{18}O_{auth}$ values during this period for QING6 is 0.6‰, which are most likely due to a reduction in evaporation by 600 - 700 mm yr^{-1}, which would produce $\delta^{18}O_{auth}$ = 0.8‰. However, the relative humidity and wind-speed within the catchment will also play an important role in determining the rate of change as. At 1850 AD $\delta^{18}O_{auth}$ values become more positive, moving close to 1500 AD values, signifying a return to pre-event conditions. Following this, a return to less positive $\delta^{18}O_{auth}$ values is shown, which finishes *c.* 1920 AD. From which point there is an increase in $\delta^{18}O_{auth}$ to recent sedimentary values at the top of the core.

The $\delta^{13}C_{auth}$ record indicates that $\delta^{13}C_{auth}$ values are likely to be in equilibrium with atmospheric CO_2 and shows an increase concurrent with an increase in effective precipitation (*c.* 1500 AD) probably as a result of lake freshening. This is seen in both QING6 and QHE2, after which there is a decrease in $\delta^{13}C_{auth}$ values (B3). Changes in $\delta^{13}C_{auth}$ then broadly mirror $\delta^{18}O_{auth}$, displaying a covariant trend (to be discussed in detail later). There is minimal isotopic variation during this period, with values oscillating around 2.5‰ in QING6 and 1.75‰ in QHE2. The $\delta^{13}C_{org}$ and C/N ratios suggest aquatic macrophytes (C/N > 10) developed during this period or there was some catchment inwash. After 1850 AD, where the $\delta^{18}O_{auth}$ decreases again, productivity initially increases, reflecting a pattern similar to that seen in B3.

The $\delta^{18}O_{auth}$ and $\delta^{13}C_{auth}$ records therefore reflect changing moisture balances in the catchment and subsequent changes in surface waters. However there is a large difference between these values and the $\delta^{18}O_{ost}$ and $\delta^{13}C_{ost}$ records. This arises in part because the ostracod profiles reflect bottom-water conditions. Differences between the two may be explained by: (1) differences in temperature between the epilimnion and hypolimnion during the season of carbonate precipitation, which is broadly between late spring and early autumn. The mean difference between the $\delta^{18}O$ values of the ostracods and the authigenic carbonates for the whole sequence is 1.7‰ ± 1.0‰. If this were a function of temperature alone, it would suggest a maximum temperature difference of 4°C for precipitation of authigenic carbonate and ostracod shells once the vital effect had been taken into account (~ 0.26‰ decrease in $\delta^{18}O$ per 1°C rise in water temperature: Craig and Gordon (1965). (2) Seasonal differences in the precipitation of the two types of carbonates, leading to differences in water temperature. (3) Enrichment of the surface waters of the lake by evaporation during the summer season resulting in different isotopic composition in the surface waters compared to deeper waters (Henderson *et al.,* 2003, Fig. 7.12, 7.13). Since there is no isotopic stratification in the modern lake and assuming this to have prevailed throughout the record, the $\delta^{18}O_{ost}$ record will reflect the temperature of calcite precipitation. The $\delta^{18}O_{ost}$ record broadly parallels the $\delta^{18}O_{auth}$ curve suggesting that the lake is thermally stratified and the isotope composition is relatively constant.

This pattern diverges at a number of points where negative excursions occur in the $\delta^{18}O_{ost}$ record suggesting increased bottom-temperatures. The most notable event occurs at 1900 AD suggesting either no thermal stratification of lake waters or early lake overturn during the summer, which is perhaps an indicator of transient increase in wind activity in the catchment and decreasing temperatures (Henderson *et al.*, 2003).

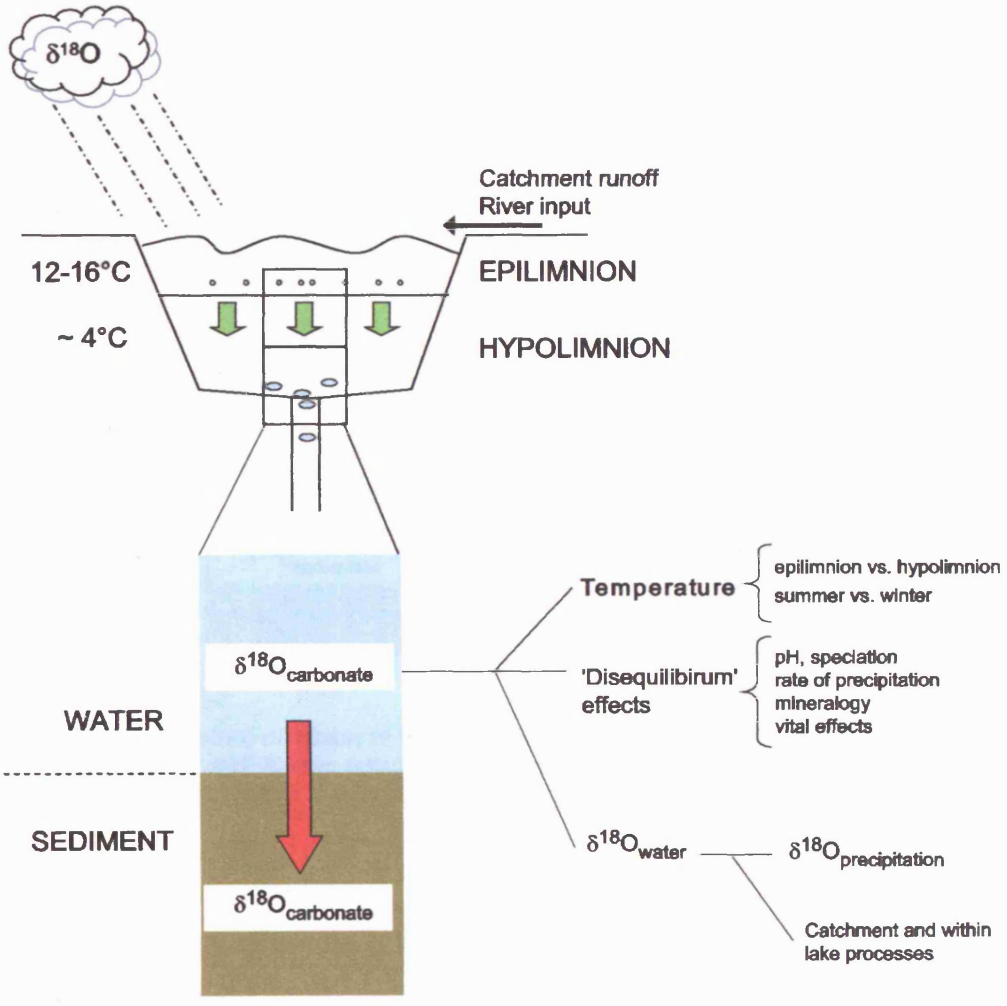

Figure 7.12 – Conceptual diagram of factors effecting the composition of the $\delta^{18}O$ of carbonate. Note precipitation of authigenic precipitates occurs in the epilimnion at a higher temperature than biogenic precipitates in the hypolimnion.

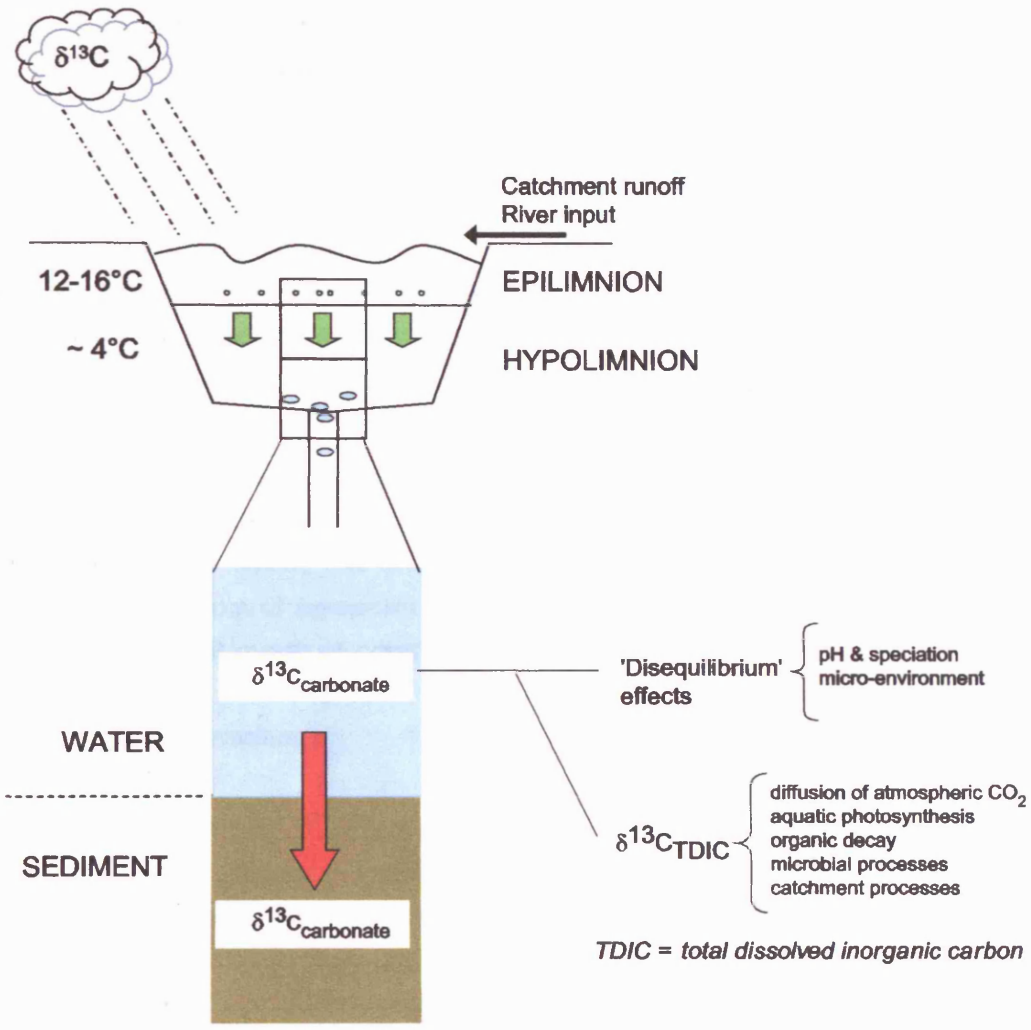

Figure 7.13 – Conceptual diagram of factors effecting the composition of the $\delta^{13}C$ of carbonate. Note precipitation of authigenic precipitates occurs in the epilimnion at a higher temperature than biogenic precipitates in the hypolimnion.

The $\delta^{13}C$ values are higher in $\delta^{13}C_{auth}$ than in $\delta^{13}C_{ost}$, which is a reflection on the degree of enrichment of ^{13}C in the epilimnion TDIC during the summer as a result of phytoplankton activity, compared to depletion in the hypolimnion as a function of organic decay which releases ^{13}C-deplete carbon into the TDIC pool (Kelts and Talbot, 1990; Henderson *et al.*, 2003) of the bottom-waters. Therefore the $\delta^{13}C_{ost}$ is a possible reflection of the amount of decay occurring in organic matter at the bottom of the lake could be linked to the lake condition e.g. length of ice cover and productivity. The $\delta^{13}C_{ost}$ record during this period shows high degree of variability but it indicates that either the decomposition of organic matter has increased under the prevailing limnological conditions or a change in organic input to the lake has occurred. The $\delta^{13}C_{org}$ values become more negative than when the lake was dominated by algae, suggesting a change in organic source, possibly C3 plants within the catchment. This notion is supported by an increase in CN ratios,

suggesting catchment in wash and a change in the vegetation composition of the catchment or the establishment of aquatic submerged plants in the lake as it has become fresher.

7.3.3 Zone A (1920 AD to 0 AD)

There was a large positive shift in $\delta^{18}O_{auth}$ in QING6, QING10 and QHE2 at *c.* 1940 suggesting a change in the effective moisture regime. In some cases, the change is up to *c.* 2‰, similar in magnitude to the negative excursion seen at 1500 AD. Causes of this change may are likely to be opposite to the factors controlling the original excursion at 1500 AD i.e. increasing evaporation. A doubling of evaporation to present day levels of 1217 mm yr^{-1} would produce $\delta^{18}O_{auth}$ = 0.8‰, similar to core top values of 1.0‰. This increase in $\delta^{18}O_{auth}$ values would indicate a reduction in lake level, although this broad pattern is not seen in the $\delta^{13}C_{auth}$ record, which shows an overall decrease in isotope values. This could be linked to the rapidly increasing salinity of the lake or that there is an input of isotopically light carbon from the catchment, which is supported by increased catchment inwash as indicated by C/N ratios at this time.

7.3.4 Isotopic covariance

The covariance between $\delta^{18}O$ and $\delta^{13}C$ values is often seen in stratigraphic sequences of authigenic carbonate formed in hydrologically-closed lakes, where hydrologic balance and vapour exchange are the dominant driving forces behind isotopic change (Talbot, 1990). For QING6 and QING10 this relationship is weak (r^2 = 0.15 and r^2 = 0.29 respectively) (Fig. 7.14, 7.15), while the overall relationship is much stronger for QHE2 (r^2 = 0.49) (Fig. 7.16).

In QING6, the overall weak relationship obscures stronger covariant trends for other parts of the record. Since it is highly improbable that the lake changed from a closed to an open system over such a short timescale it is likely that the differences in the strength of the covariant relationship are due to changing lake water alkalinity. For QING6, Fig. 7.14 shows the relationship between $\delta^{18}O_{auth}$ and $\delta^{13}C_{auth}$ for the whole core (Fig. 7.14a) and the three different zones identified based on the $\delta^{18}O_{auth}$ profile (Fig. 7.14b, c, d). It is immediately apparent that isotopic covariance is much stronger for Zone B compared to both the whole core and to Zones A and C. The isotope values from Zones A and C suggests that the lake water is more evaporated as $\delta^{18}O$ values are higher, suggesting the lake has elevated salinity and alkalinity. Therefore, the lake is likely to have had a much higher dissolved CO_2, which acts to dampen the $\delta^{13}C$ response to changes in freshwater input and lake productivity and so influences the strength of $\delta^{18}O$-$\delta^{13}C$ relationship. On the other hand, Zone B shows increased covariance suggestive of a closed-basin, but it represents a period when the lake was much fresher, with higher lake levels. This means that the $\delta^{13}C$ will have changed in relation to fluctuations in hydrological balances and vapour exchange.

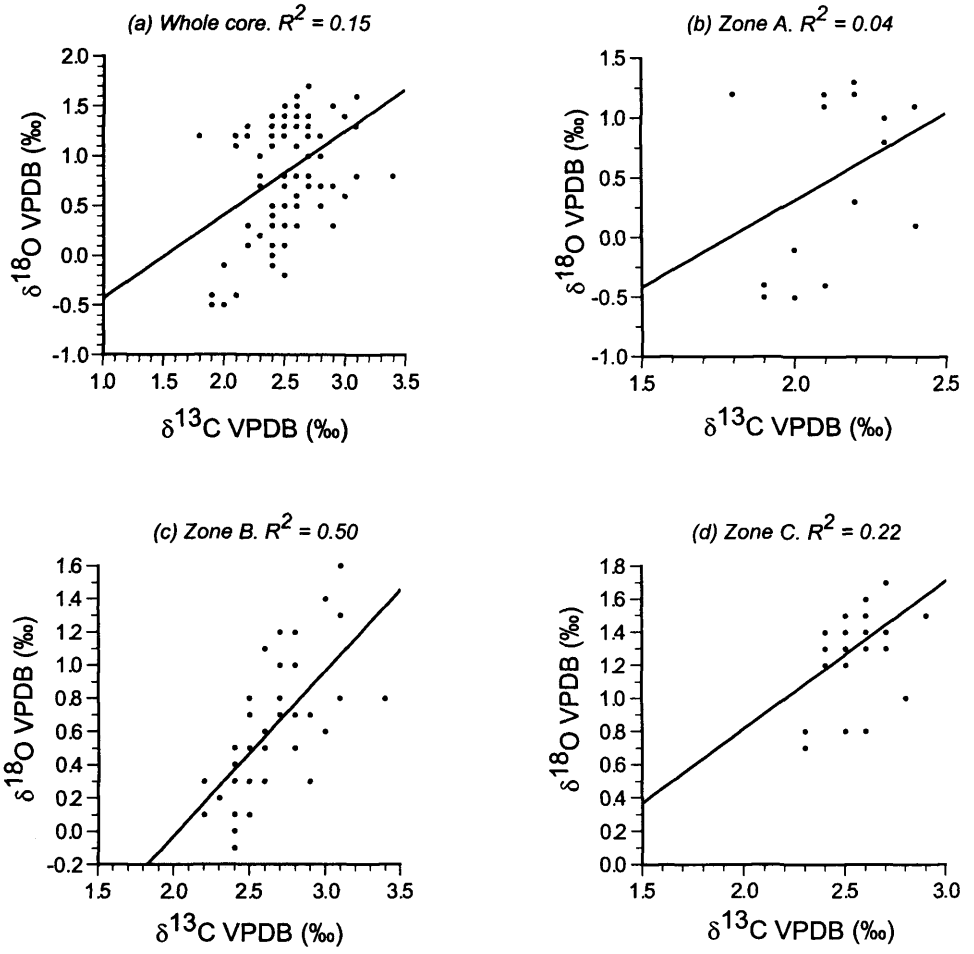

Figure 7.14 – Covariance plots for QING6. (a) $\delta^{18}O$ vs. $\delta^{13}C$ for all QING6 authigenic carbonates, (b) $\delta^{18}O$ vs. $\delta^{13}C$ for Zone A, (c) $\delta^{18}O$ vs. $\delta^{13}C$ for Zone B and (d) $\delta^{18}O$ vs. $\delta^{13}C$ for Zone C.

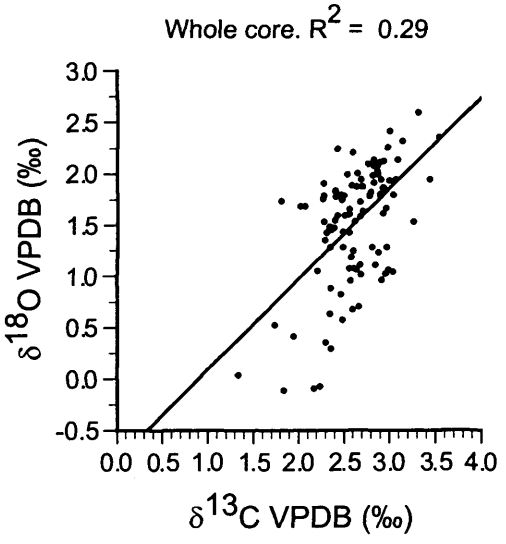

Figure 7.15 – Covariance plot for QING10. $\delta^{18}O$ vs. $\delta^{13}C$ for all QING10 authigenic carbonates.

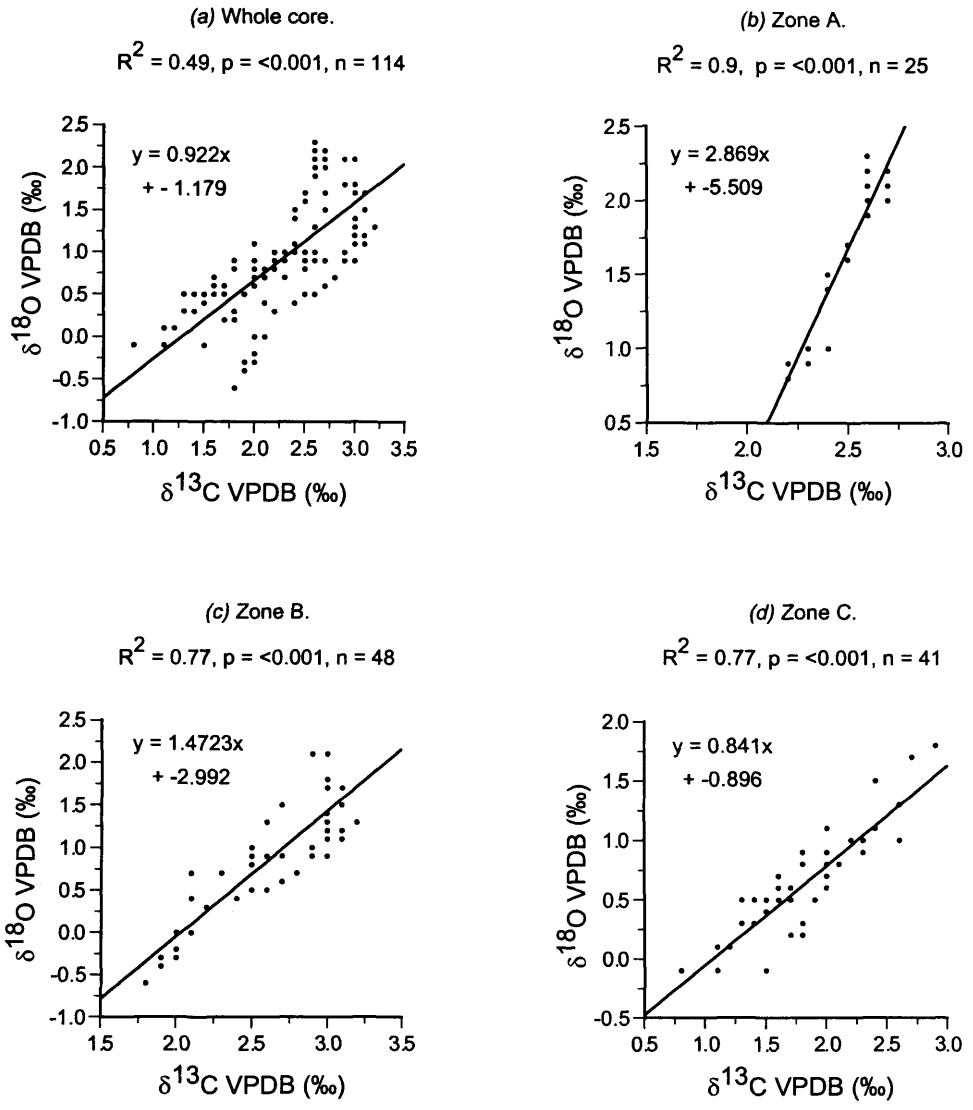

Figure 7.16 – Covariance plots for QHE2. (a) $\delta^{18}O$ vs. $\delta^{13}C$ for all QHE2 authigenic carbonates, (b) $\delta^{18}O$ vs. $\delta^{13}C$ for Zone A, (c) $\delta^{18}O$ vs. $\delta^{13}C$ for Zone B and (d) $\delta^{18}O$ vs. $\delta^{13}C$ for Zone C.

Additionally, pH changes can control the $\delta^{13}C$, as a drop in pH to < 6 would mean CO_2 rather than HCO_3^- becomes the dominant dissolved inorganic carbon ion, causing a higher residual $\delta^{13}C$.

However, for QHE2, the overall relationship is stronger than that seen in QING6 and QING10, but even this obscures the covariant trends of the individual zones, which are even stronger than the overall trend (Fig. 7.16b, c, d). Due to chronological uncertainties in the core, QING10 has not been divided into zones. However, by simply looking at different parts of the core, it suggests that there were periods of increased covariance, similar to the relationships seen in QING6.

7.4 Palaeolimnological interpretation of Lake Gahai

The Lake Gahai record has been divided into three zones (A, B and C) based on the stratigraphy of $\delta^{18}O_{auth}$. There are a number of distinct events occurring within the record and these zones and have been highlighted (Fig. 7.17). Lake Gahai developed from the main body of Lake Qinghai due to the combination of falling lake level and increased aeolian activity in the catchment. The lake is thought to have become isolated from Lake Qinghai *c.* 600 to 1200 years ago (Li *et al.,* 1996) but no specific investigations have been undertaken to verify this. The current record implies (since the evidence is not wholly conclusive) that Lake Gahai became isolated at approximately 760 AD (~ 1240 years ago), as the value of $\delta^{18}O_{ss}$ is close to the $\delta^{18}O_{auth}$ values seen in the Lake Qinghai records and there is a significant change in the behaviour of these proxies i.e. inter-sample variability increases markedly compared to the record below. As the lake has become smaller it is likely to be more responsive to changes in the climate and effective moisture (Leng and Marshall, 2004) when compared to the larger Lake Qinghai. The absence of ostracods also suggests that during the time when the lake was being isolated the waters were extremely turbid (Griffiths and Holmes, 2000) as the water column and volume was being reorganised to reach a new steady-state.

Due to the uncertainty in lake volume (depth) and catchment size isotope mass balance modelling experiments were not done for Lake Gahai, therefore changes seen in the sediment records will be discussed qualitatively.

7.4.1 Zone C (400 AD to 1370 AD)

C3 – The bottom-most sediments of the core (*c.* 400 AD – 760 AD) show distinctly decreased inter-sample variability compared to the rest of the record, although $\delta^{18}O_{auth}$ and $\delta^{13}C_{auth}$ values are similar to those seen in isotope records from Lake Qinghai. These isotope curves occur with a similar smoothness to that seen in the Lake Qinghai suggesting that Lake Gahai was connected to the main water body of Lake Qinghai at this point.

This conclusion is supported by the absence of ostracods, which could have resulted from increased water column turbidity (Griffiths and Holmes, 2000) as a result of reorganisation to a smaller lake. Also, the $\delta^{13}C_{org}$ and C/N ratio suggest that organic matter of algal origin dominates the lake.

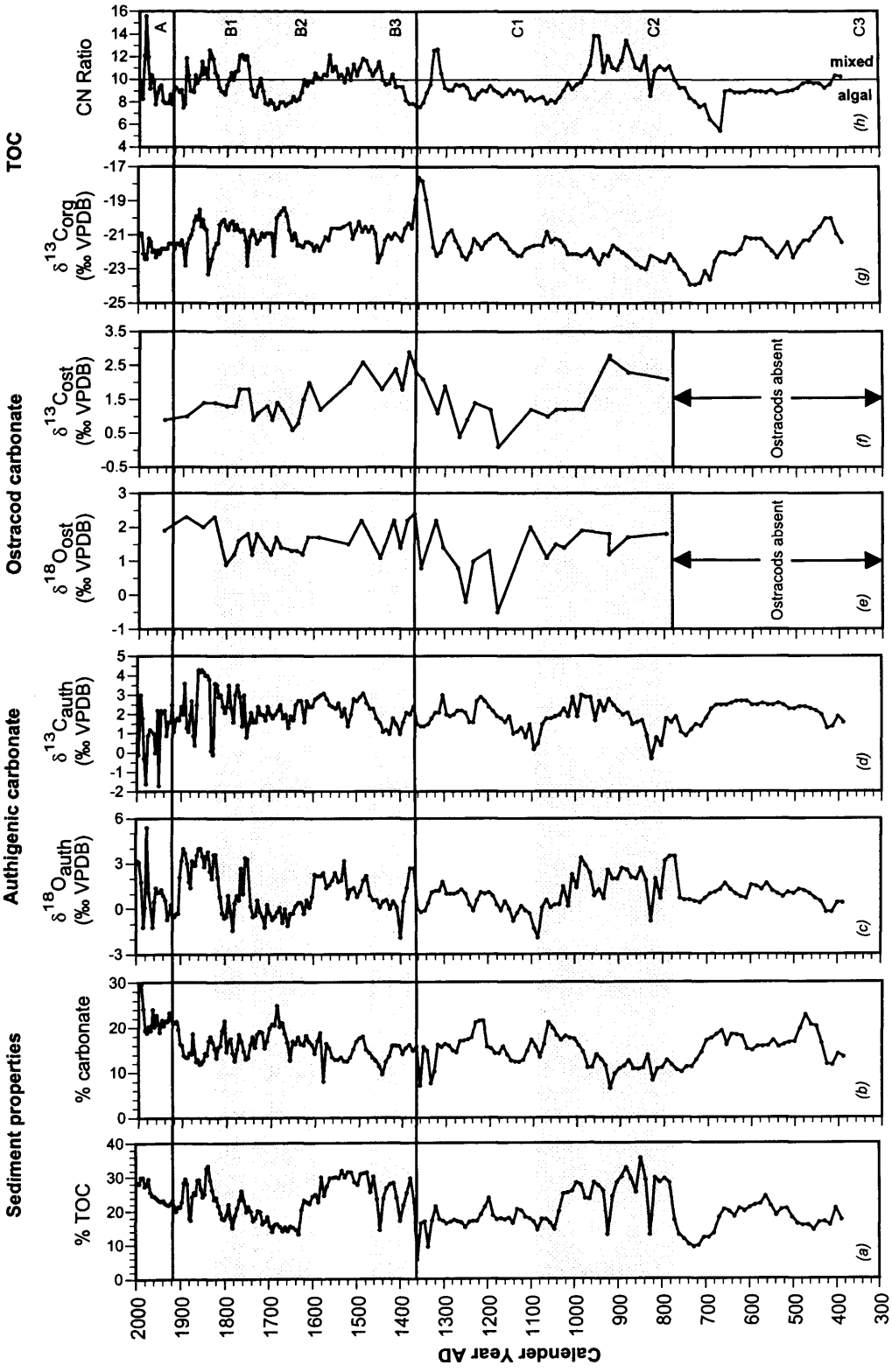

Figure 7.17 – Summary diagram of geochemical proxies plotted using the age model for core GAHA1. Sediment properties: (a) % carbon (b) % carbonate. Isotopic composition of authigenic carbonate: (c) carbon-isotope values (d) oxygen-isotope values. Isotopic composition of ostracode carbonate: (e) carbon-isotope values (f) oxygen-isotope values. Composition of the total organic carbon: (g) carbon-isotope values (h) carbon/nitrogen ratio.

C2 – After 760 AD there was increased variability with the increase in $\delta^{18}O_{auth}$ and $\delta^{13}C_{auth}$ values suggesting the lake had undergone reduced effective moisture, with an associated increase in productivity. Total organic carbon (TOC) also increases significantly, but it is highly variable. Even so, it suggests an increase in C_3 plants or increased catchment in-wash/establishment of aquatic plants in the lake. This period was warmer than the previous one and possibly more humid since there are higher $\delta^{13}C_{auth}$ and C/N values indicating increased higher plants in the catchment (C_3 and C_4). This event was also punctuated with two negative excursions in $\delta^{18}O_{auth}$ after *c.* 800 AD and 920 AD that suggest there are periods of increased effective precipitation, particularly since there is a significant increase in C/N after these events suggesting increased moisture.

C3 – There is overall increasing trends to drier catchment conditions with phytoplankton dominating the organic matter suggests the lake is initially fresher, with the ostracod isotope data broadly reflect this trend. Before the transition into the next zone there is a *c.* 2‰ negative change in $\delta^{18}O_{auth}$ indicating a short-lived increase in effective moisture, perhaps as a result of increased precipitation in the catchment or reduced evaporation. Concomitant with this event is a peak in C/N suggesting a change in the source of organic matter, most likely due to establishment of floating and submergent authigenic plants rather than catchment in-wash.

7.4.2 Zone B (1370 AD to 1920 AD)

There is greater variability within this period suggesting the lake is being more responsive to effective moisture as it has reduced in size. There are three prominent negative excursions (labelled B1, B2, B3, Fig. 7.17) within this period, which suggest that there has been a significant increase in effective precipitation at this time. After each excursion the $\delta^{18}O_{auth}$ values recover back to pre-event levels. These negative shifts occurred at 1380 AD – 1475 AD (B3), 1600 – 1740 AD (B2) and 1760 AD – 1825 AD (B1) with values after 1825 AD increasing to remain much higher compared to those in the rest of the zone. Productivity as indicated by $\delta^{13}C_{auth}$ decreases at the same time as $\delta^{18}O_{auth}$ changes suggesting a link between the changes in the limnology and lake productivity. Organic matter decreases in times of reduced $\delta^{18}O_{auth}$ but it was dominated by an algal input as suggested by CN. In between, there is an increase in and a mixed source for organic matter, however, the $\delta^{13}C_{auth}$ suggest that productivity has decreased; therefore this increase in TOC is best explained by catchment in-wash. This could be linked to either increased precipitation in the catchment, but this is not directly supported by the $\delta^{18}O_{auth}$ curve, or due to melting of permafrost and snow in the catchment that would have built up during the previous cold spells as shown by $\delta^{18}O_{auth}$. $\delta^{18}O_{ost}$ and $\delta^{13}C_{ost}$ records broadly resemble that of their authigenic counterparts, with negative excursions that have been highlighted reflected in the ostracod record. Since Lake Gahai is shallow (maximum recorded depth <9 m) compared to Lake Qinghai thermal stratification does not occur and therefore the ostracods cannot be used to infer bottom-water conditions like as in QING6.

7.4.3 Zone A (1920 AD – 2000 AD)

There are large scale fluctuations in the upper-most sediments of Lake Gahai. $\delta^{18}O_{auth}$ values initially suggest that the lake was fresher than present-day with a relatively high lake level, but since the 1960s has undergone increased evaporation. Conversely the $\delta^{13}C_{auth}$ shows a decreasing trend indicating a reduction in productivity, which is different to previous episodes in the record where an increase in $\delta^{18}O_{auth}$ was accompanied by an increase in $\delta^{13}C_{auth}$. This is possibly a result of the lake reaching modern-day salinities and thereby limiting algal activity and aquatic plant growth.

7.4.4 Isotopic covariance

The overall isotopic covariance for Lake Gahai is weak (r^2 = 0.13) with the strongest covariance seen in the zone C (Fig. 7.18). However if the data before the lake was isolated (up to 800 AD) the relationship becomes even stronger (r^2 = 0.49). The apparent lack of covariance is likely to be due to the lake's salinity and associated alkalinity, which will dampen the effect of $\delta^{13}C_{auth}$ on the covariant trend (Li and Ku, 1997).

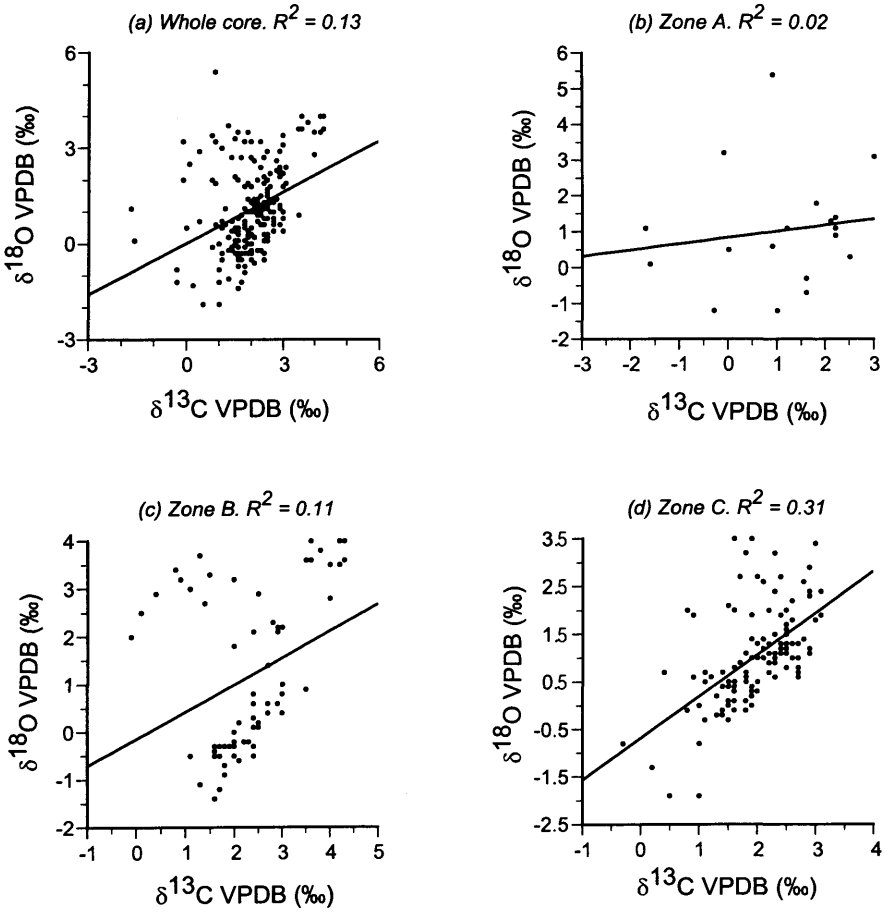

Figure 7.18 – Covariance plots for GAHA1. (a) $\delta^{18}O$ vs. $\delta^{13}C$ for all GAHA1 authigenic carbonates, (b) $\delta^{18}O$ vs. $\delta^{13}C$ for Zone A, (c) $\delta^{18}O$ vs. $\delta^{13}C$ for Zone B and (d) $\delta^{18}O$ vs. $\delta^{13}C$ for Zone C.

7.5 Overall palaeolimnological trends

The records presented here show large isotopic fluctuations related to the balance between precipitation and evaporation and even given the problems with the core chronologies; an outline of climate changes over the last 2000 years can still be tentatively established (summarised in Table 7.2). Most notably, the recent history (*c.* last 100 years) for Lake Qinghai and Lake Gahai has been a period of significant hydrological change. The decreasing lake levels, as documented by the oxygen-isotopes suggest increased aridity in the catchment, likely to be a combination of increased evaporation due to shorter ice-cover periods on the lake (possibly temperature related) and less precipitation recharging the lake.

Preceding this, there was a period of distinct hydrological variability, which is reflected in all the records, perhaps suggesting a single climatic/or other forcing on the lake system. This is particularly prominent in cores QING6 and GAHA1, where a number of excursions were identified. A similar pattern emerges from QHE2, but it is not as clear, possibly as a result of problems in establishing a suitable chronology. Even though an analogous excursion can be seen in QING10 there is no obvious synchroneity to these events, which is more than likely due to a bias introduced by the poor age model. However, this period still represents a distinct shift in the isotope records and it is argued that the changes are being driven by increased effective precipitation as a result of reduced evaporation. This is a result of prolonged periods of ice cover, which reduces the effect of seasonal evaporation (which is seen at the site today). This signal of increased effective moisture is attributed to increased evaporation rather than increased precipitation as this time span is thought to have been colder than present, which would in turn reduce the strength of the monsoon. Therefore, with no obvious mechanism of increasing precipitation on the Tibetan Plateau, more local factors are more important, such as the extent of evaporation from the lake surface.

Before this period of hydrological variability the isotope data suggest that the lake underwent minimal fluctuations in lake level, indicating that the lake's climate was potentially stable. However, QING6 and QING10 suggest that the lake level was comparable or slightly lower than present-day levels, while QHE2 support a higher lake level than today. The cause of this is not clear, but it could suggest that the basin in the east of the lake was possibly larger than it is today, since this part of the lake is slowly shrinking due to aeolian input and encroachment from a dune field, rather directly from a falling lake level.

Calendar years AD

	QING6	QING10	QHE2	GAHA1
2000	Lake levels decreasing, increased aridity	Considerable isotopic variability. Lake levels higher than present day. Increased effective moisture either as a result of increased ppt or decreased evaporation	Lake levels decreasing, increased aridity	Lake levels decreasing, increased aridity
1800				
1600	Fluctuating, but increased lake levels. Caused by increased effective moisture as a result of increased ppt or decreased evaporation		Fluctuating, but increased lake levels due to increased effective moisture as a result of increased ppt or decreased evaporation	Increased lake levels that fluctuate periodically. More effective moisture due to either increase ppt or decreased evaporation
1400				
1200				
1000				
800	Stable isotope values which remain constant, with lake level comparable to modern day. Little or no fluctuation in climate	Low lake levels as indicated by isotopes, with minimal fluctuations.	Decreased lake levels	Increasing lake levels
600				
400			Lake levels higher than in modern lake. Increased ppt in the catchment?	Decreased lake levels and increased aridity due to increased evaporation or decreased ppt
200				
0				

Table 7.2 – Summary of lake levels/climatic changes as inferred from the palaeolimnological data.

7.6 Direct core comparisons

7.6.1 Past 150 years

There are distinct differences between the $\delta^{18}O_{auth}$ and $\delta^{13}C_{auth}$ compositions of carbonates from Lake Qinghai and Lake Gahai. Over the past 150 years (Fig. 7.19), where the chronology is more secure, the isotope stratigraphies are similar, particularly, the $\delta^{18}O_{auth}$ records. Changes within the different cores are broadly parallel, with a large negative excursion in $\delta^{18}O_{auth}$ values between 1880 and 1950 AD. However, the profiles differ as there is a difference in absolute isotope values of *c.* 1.5‰, with an increasing trend within Lake Qinghai from west to east in the lake, QING6 being the most westerly and QHE2 the most easterly. This pattern of spatial variability has also been noted in the $\delta^{18}O_{auth}$ of surface sediments (see section 5.6). GAHA1 differs as the $\delta^{18}O_{auth}$ values are much higher than those seen in the cores from Lake Qinghai (QING, QING10 and QHE2).

The profiles show a negative excursion in $\delta^{13}C_{auth}$ between 1900 and 1950 AD, although this is not mirrored strongly in QING10, it still has a broadly negative trend over this period (Fig. 7.19). Absolute values of $\delta^{13}C_{auth}$ are fairly similar in the cores from Lake Qinghai, while the $\delta^{13}C_{auth}$ values from GAHA1 show much greater variability and range from *c.* – 2‰ to + 4‰, compared to + 1.75‰ to + 3‰ in QING6, QING10 and QHE2.

The spatial variability in the isotopic composition of carbonates, in particular, $\delta^{18}O_{auth}$, is unlikely to be a result of non-equilibrium precipitation of carbonate. Therefore the difference between the cores is likely to be due to gradients in lake water temperature and isotope composition. Spatially, $\delta^{18}O$ values for modern waters are generally similar (see Chapter 5), however, the $\delta^{18}O$ composition near the mouth of the River Buha, in the east of the lake are isotopically lower. Even though the $\delta^{18}O$ values for modern water are similar, apart from this one point, it still suggests that a lighter isotopic signal could have existed in the past.

Importantly, when the modern water samples were taken in May 2001 it was just after the lake had become ice free and was therefore still well mixed (no thermocline). Samples taken in October 2001 also showed no variation in isotope composition either (apart from near the mouth of the River Buha), suggesting the lake had become well mixed again as no thermocline was found. However, when the water samples were collected it was probably outside the period of maximum carbonate precipitation and it is conceivable that a gradient (in both temperature and isotope composition) existed at this time.

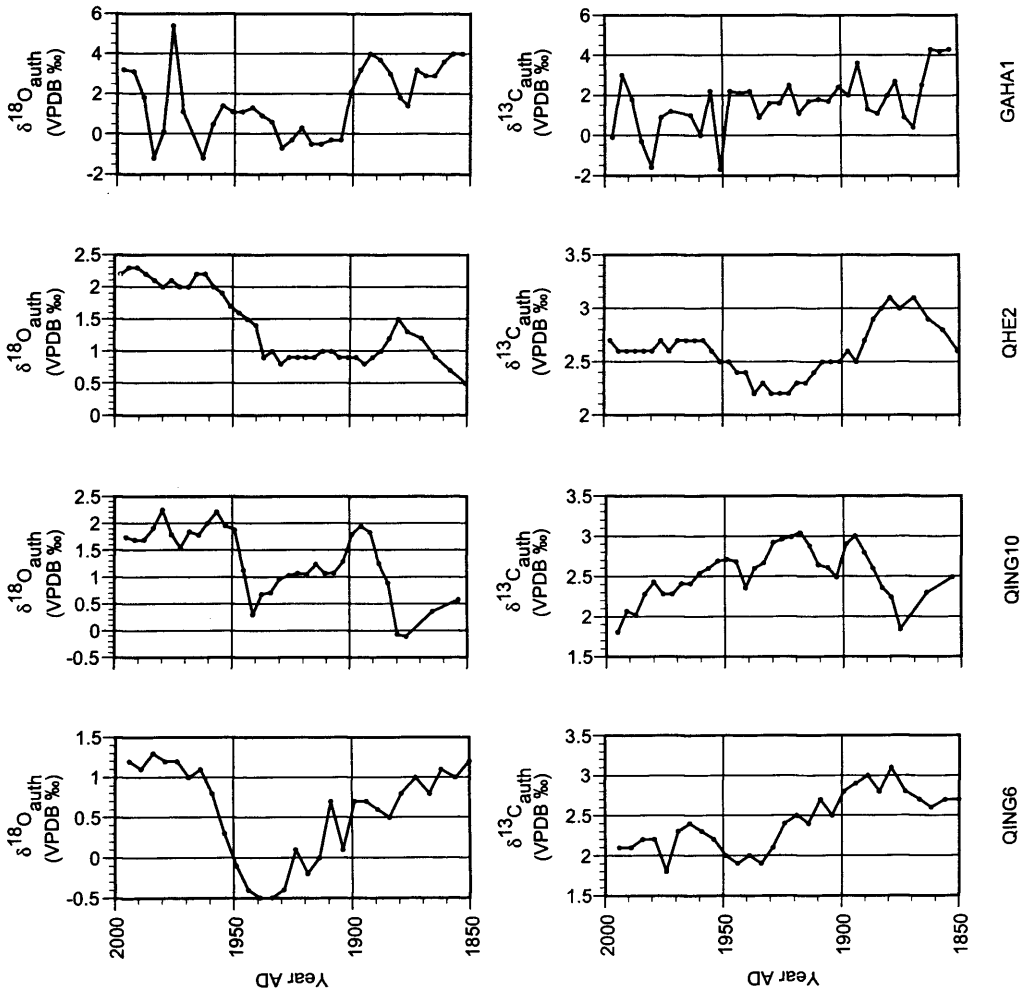

Fig. 7.19 – Comparison of $\delta^{18}O_{auth}$ and $\delta^{13}C_{auth}$ over the past 150 years from Lake Qinghai and Lake Gahai

7.5.1 Past 500 years

This pattern of isotope change is mostly seen in QHE2, with a negative excursion beginning before 1600 AD. $\delta^{18}O_{auth}$ values remain low before increasing at 1750 AD, which is before that seen in QING6 and GAHA1, although they are broadly concurrent. $\delta^{18}O_{auth}$ values in QING10 are relatively high until 1800 AD, before a large negative excursion is seen of a magnitude similar to the events identified at 1600 AD in QING6, QHE2 and GAHA1. This difference between the records therefore could be due to problems already identified in the age model. The QING10 age model is based on a relatively old (for the depth compared to the two other cores from Lake Qinghai) radiocarbon date. This would suggest a decreased sedimentation rate for QING10 compared to QING6 and QHE2, which would affect the apparent chronology of this negative excursion. However, since there are no other dates the core it is impossible to rule out that this part of the lake (northern basin) has lower sedimentation compared to QING6 (southern basin) and QHE2 (east basin).

The $\delta^{13}C_{auth}$ records in QING6, QING10 and GAHA1 are broadly similar, although the difference between these three cores and QING10 is not as great as for $\delta^{18}O_{auth}$. A relatively large negative excursion at approximately 1600 AD is of a similar magnitude in QING6 and QHE2. This event is not particularly pronounced in the GAHA1 record, although there is a slight decreasing trend. QING10 displays a largely decreasing trend in $\delta^{13}C_{auth}$ with a large increase occurring at 1880 AD and a slight isotope fluctuation, but this pattern is either not seen or is not of a similar magnitude in the other three cores to suggest that it is a synchronous event. This leads to the conclusion that either this is a different event not seen in the other cores or it is a result of the age model employed in QING10 (as discussed above).

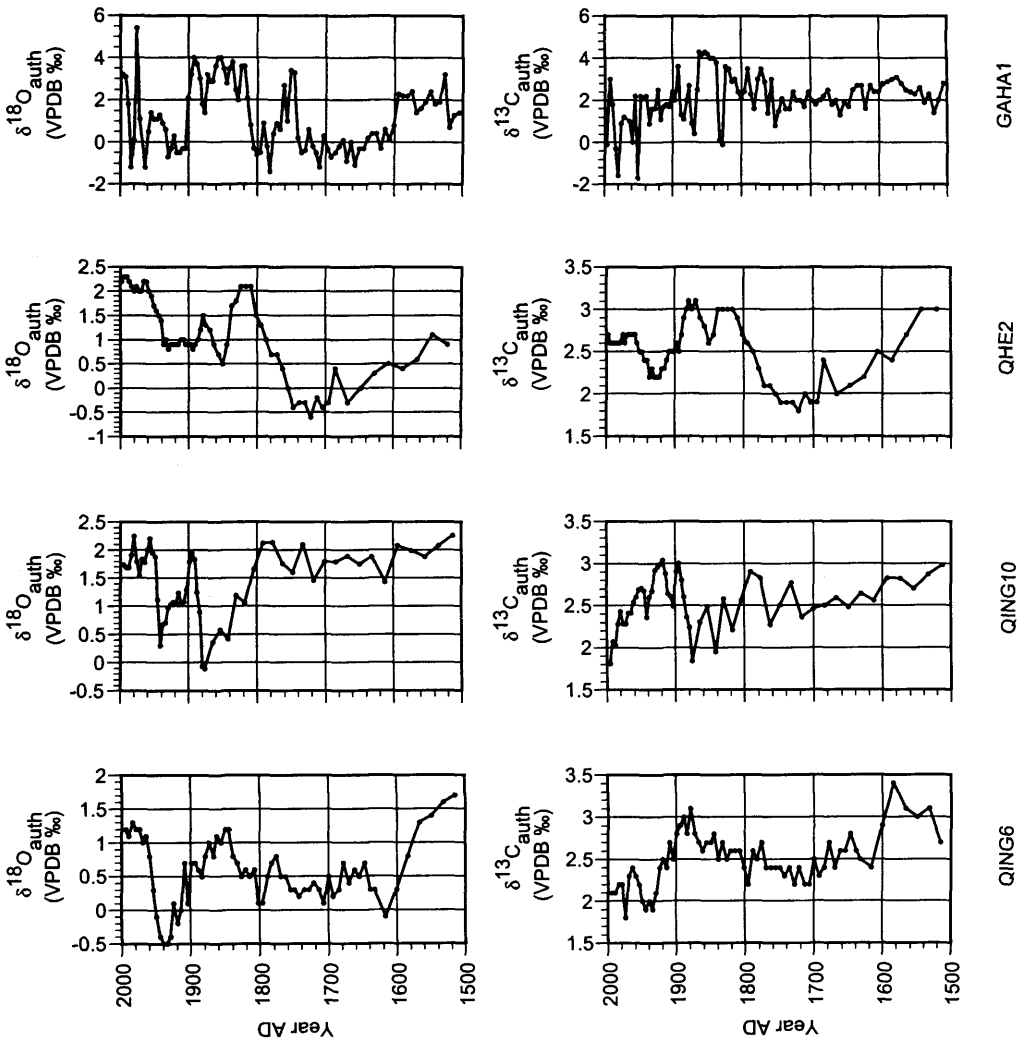

Fig. 7.20 – Comparison of $\delta^{18}O_{auth}$ and $\delta^{13}C_{auth}$ over the past 500 years from Lake Qinghai and Lake Gahai

7.7 Summary

The sediment records presented here show distinct isotopic changes that are indicative of hydrological changes in the lake's catchment. Positive excursions in oxygen-isotopes have been attributed to decreased effective moisture as a result of increased evaporation and associated aridity. Negative excursions correspond to increased effective moisture, however, rather than just being caused by increased precipitation, it is attributed to a decrease in evaporation associated with changing periods of ice cover. Since the major source of moisture to the catchment is associated with the seasonal cycle of the monsoon rains, which in turn is driven by summer heating on the Tibetan Plateau (although not exclusively), the period of higher lake levels in the record coincides with a relatively global cool period that would reduce the strength of the monsoons. Therefore in order to explain increased effective moisture, a mechanism of reduced seasonal evaporation linked to prolonged ice cover was suggested. A simple steady-state model further supports this, as it suggests that lake volume (and subsequent oxygen isotope composition of lake water) is more sensitive to changes in the amount of evaporation (Table 7.1).

Not all the records are directly comparable, largely due to the problems in establishing an appropriate chronology for each core. Of the records presented, QING6 and GAHA1 have basal ages, with the period of age uncertainty between the end of the ^{210}Pb age model and the ^{14}C AMS date(s) inferred by a second order polynomial relationship. With respect to QING10 and QHE2, there are no basal ages, so the bottom of the records are inferred from the age model, however, since no age is known for much of the core this introduces a larger amount of uncertainty about the chronology, more so than for QING6 and GAHA1. As a result of this these two cores will be taken forward and used to make some comparisons with regional records (see next chapter) rather than QING10 and QHE2.

Chapter Eight
Regional comparisons of environmental change and possible forcing mechanisms

Introduction

The sediment records presented in the previous chapter displayed distinct changes in $\delta^{18}O_{auth}$ and $\delta^{13}C_{auth}$ values over the past 1500 years. Simple steady-state models suggest that lake volume (and subsequent oxygen isotope composition of lake water) is sensitive to changes in the amount of evaporation. Down core variations were therefore attributed to changing effective precipitation, most notably between 1600 AD and 1850 AD. Variations observed over the past *c.* 1000 years will be briefly summarised before comparisons of the $\delta^{18}O_{auth}$ records from QING6 and GAHA1 with other palaeoenvironmental archives.

8.1 Recent climate variations

Globally, the last 1000 years experienced considerable climatic variability (Jones *et al.,* 1996; Mann *et al.,* 1999; Crowley, 2000) with three distinct phases of climate in the Northern Hemisphere (NH) during this time: the Medieval Warm Period (MWP) (*c.* 800 – 1200 AD), the Little Ice Age (LIA) (*c.* 1200 – 1850 AD) and the recent warming since *c.* 1850 AD. It has been argued that temperatures in the last decade of 20th Century were the warmest experienced in the last 1000 years (Mann *et al.,* 1999). However, that study fails to identify medieval warming associated with the MWP (Broecker, 2001) and their reconstructions for the LIA do not capture the full range of temperatures experienced in different regions of the NH (Esper *et al.,* 2002).

There is still debate as to the actual causes of the LIA, for example, the relation to relative roles of volcanic (Free and Robock, 1999; Crowley, 2000) and solar forcing (Crowley, 2000; Shindell *et al.,* 2001). One of the coldest periods during the LIA (otherwise known as the Maunder Minimum (MM: 1645 – 1715 AD)) is coincident with reduced sunspot activity and total solar irradiance. Changes in solar forcing causes distinct regional effects in climate (Bradley, 2003), with mid- to high-latitude continental regions experiencing much lower temperatures than sites at similar latitude near to the North Atlantic (Mackay *et al.* in press). Thus while global temperatures were on average slightly lower during the LIA, cooling over the continental region is estimated to be up to five times greater (Shindell *et al.,* 2001).

Synthesis of a number of records has identified an abrupt event at 1300 AD in Chinese palaeoenvironmental records, which marks the transition between the so-called Medieval Warm Period (MWP) and the Little Ice Age (LIA) (Morrill *et al.,* 2003). It was a period of several decadal to multi-decadal warm and cold temperature anomalies, but the exact timing of these events and there extent is highly variable. Additionally, evidence from temperature series data for China

suggest three distinct periods of cold anomalies are synchronous with the increasingly globally identified LIA (Wang *et al.,* 2001; Yang *et al.,* 2002). With this in mind, the palaeolimnology of Lake Qinghai will be discussed in terms of effective precipitation and its link to the climatic changes that have been initially highlighted (see Chapter 3 for a full review).

8.2 Comparisons with regional records

Comparisons of the records from Lake Qinghai and Lake Gahai with other palaeoenvironmental archives from this region would help to establish whether the down core changes seen in the current study are indicative of climate changes in NW China. The Lake Qinghai and Lake Gahai $\delta^{18}O_{auth}$ records represent summer water conditions (extent of evaporation) linked to the seasonal insolation of the Tibetan Plateau. Therefore it would be pertinent to firstly compare them with other lake isotope records from the Tibetan Plateau. However, this study has presented the first high-resolution isotope records from lake sediments over the late Holocene from this region. Other longer term records obtained from lake sediments are not of sufficient resolution to produce direct meaningful comparisons.

Nevertheless, there are further late Holocene isotope records, from non-lake archives in the NE Tibetan Plateau, such as the Dunde ice core (see fig. 3.4). Other palaeoenvironmental archives also exist like tree-ring widths, peat and glacial deposits (e.g. Hong *et al.,* 2000; Su and Shi, 2002; Yang *et al.,* 2003). Furthermore, synthesis of a number of proxies has produced China-wide temperature composites covering the last 2000 years (e.g. Wang *et al.,* 2001; Yang *et al.,* 2002).

8.2.1 NE Tibetan Plateau comparisons – the Dunde ice core

The Dunde ice cap (38°06'N, 96°24'E) on the north eastern side of the Tibetan Plateau has a summit of 5325 m a.s.l and has been subject to a number of studies over the last decade or so (e.g. Thompson *et al.,* 1989; Yao *et al.,* 1991; Yao *et al.,* 1997; Thompson, 2000; Thompson *et al.,* 2003). The ice core record ($\square^{18}O_{ice}$) from Dunde provides a history of the regional isotopic composition of precipitation, changes in which, have been qualitatively attributed to temperature and therefore may be a realistic proxy indicator of lower tropospheric temperatures (Thompson *et al.,* 2003). Since the $\delta^{18}O_{auth}$ stratigraphies from Lake Qinghai and Lake Gahai are sensitive to effective precipitation, the advantage of using $\delta^{18}O_{ice}$ therefore, is when it is corrected for altitude (compared to Lake Qinghai) its value can be used as the isotope composition of input waters.

Past 400 years

Comparisons of the Dunde record over the past 400 years show that there has been much variability in precipitation amount (indicated by accumulation) and isotope composition (Fig. 8.1a and b, 8.2a and b). However, low $\delta^{18}O_{ice}$ values tend to occur concurrently with low $\delta^{18}O_{lake}$ values (Fig 8.1c, 8.2c), indicating reduced regional temperature. Additionally, a relative index of moisture

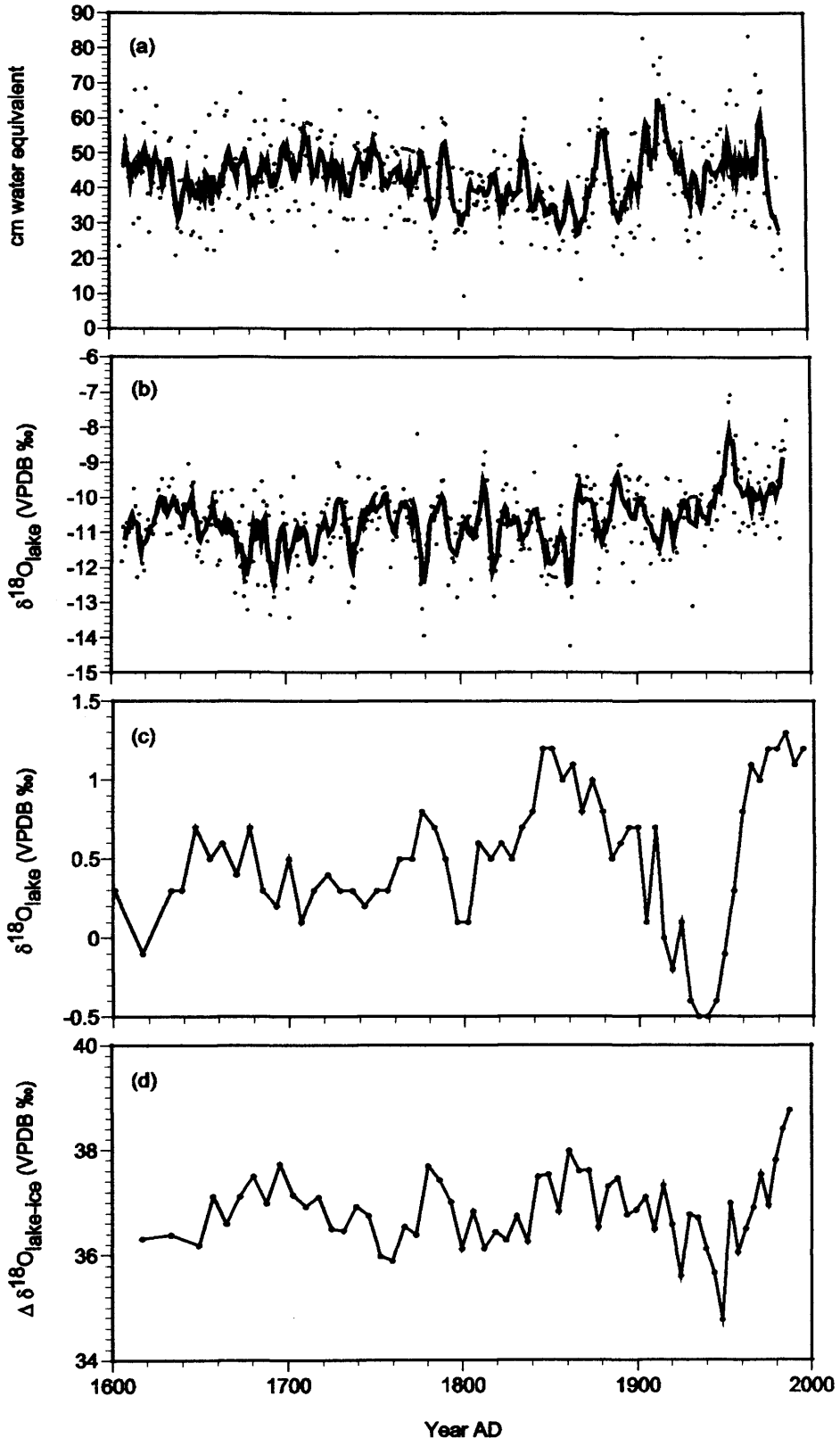

Figure 8.1 – Comparison of QING6 $\delta^{18}O_{auth}$ with Dunde ice core proxies. (a) Dunde ice accumulation, (b) Dunde δ^{18}Oice, (c) QING6 $\delta^{18}O_{auth}$ and (d) QING6 $\Delta\delta^{18}O_{lake-ice}$

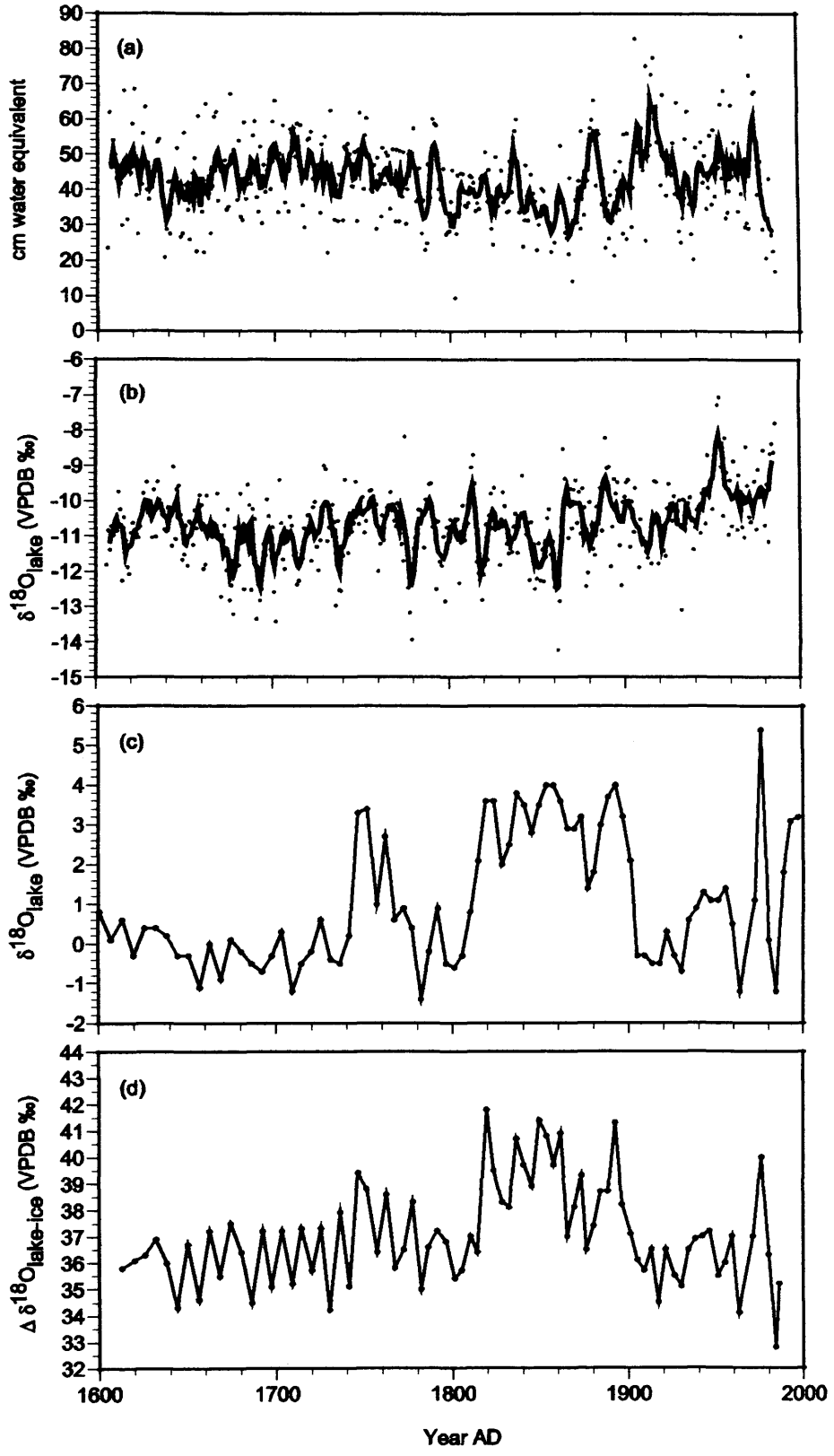

Figure 8.2 – Comparison of GAHA1 $\delta^{18}O_{auth}$ with Dunde ice core proxies. (a) Dunde ice accumulation, (b) Dunde $\delta^{18}O$ice, (c) GAHA1 $\delta^{18}O_{auth}$ and (d) GAHA1 $\Delta\delta^{18}O_{lake-ice}$

– $\Delta\delta^{18}O_{lake\text{-}ice}$ – (Fig. 8.1d, 8.2d) can be calculated using the values of $\delta^{18}O_{ice}$ and $\delta^{18}O_{lake}$, with more positive values indicative of greater isotopic enrichment of lake water and therefore greater evaporation. This index indicates that effective moisture over the Qinghai catchment has been variable, with the least positive values coinciding with the lowest $\delta^{18}O_{lake}$ values, supporting the interpretation that the isotope records of Lake Qinghai and Lake Gahai are controlled by the amount of evaporation (Fig. 8.1, 8.2).

Past 1500 years

Figures 8.3 and 8.4 show the composite temperature anomaly record for China (Yang *et al.*, 2002) compared to $\delta^{18}O_{ice}$, $\delta^{18}O_{lake}$ and $\Delta\delta^{18}O_{lake\text{-}ice}$ from QING6 and GAHA1 respectively, and provide longer term perspective on the trends in climate over the NE Tibetan Plateau. The MWP is clearly identified according to Yang *et al.*, (2002) (Fig. 8.3a, 8.4a) with inter-decadal variability in temperature, but overall the temperature is higher than during the recent centuries. The MWP is not particularly pronounced in the $\delta^{18}O_{lake}$ stratigraphy of QING6 (Fig. 8.4c) although the isotopic composition of precipitation suggests increased temperature (Fig. 8.3b). However, the GAHA1 $\delta^{18}O_{lake}$ stratigraphy (Fig. 8.4c) indicates a MWP as $\delta^{18}O$ values are relatively high during this period. The relative index of moisture also indicates that there was increased evaporation suggesting higher temperatures.

The onset of the LIA is clearly identified in the temperature record (Fig. 8.3a, 8.4a). Initially there is little change in the $\delta^{18}O_{lake}$ values from QING6 (Fig. 8.3c) but there is a significant negative excursion, which then recovers (*c.* 1400 to 1500 AD). At this time there was decreased effective moisture as a result of changes in precipitation input (Fig. 8.3b) as $\delta^{18}O_{ice}$ values indicate initially warm temperatures in the region, so the onset of the LIA was possibly delayed. There then follows a large magnitude shift in $\delta^{18}O$, corresponding to some of the lowest temperatures recorded during the LIA (Fig. 8.3a and c). The LIA is also seen in the $\delta^{18}O_{lake}$ record from GAHA1 (Fig. 8.4c), although there is greater variability compared to QING6, which may be a result of the size of the lake compared to Lake Qinghai. This might account for the apparent delay of the LIA in the QING6 record, as it is clearly identified in GAHA1 and is broadly synchronous (Fig. 8.4).

Three negative excursions are clearly identifiable in the $\delta^{18}O$ records from QING6 and GAHA1 (labelled B1, B2 and B3, see fig. 7.7 and 7.13) and correspond to periods of lowest temperatures during the LIA. The mechanism by which low $\delta^{18}O$ values correspond to times of low temperature is related to evaporation.

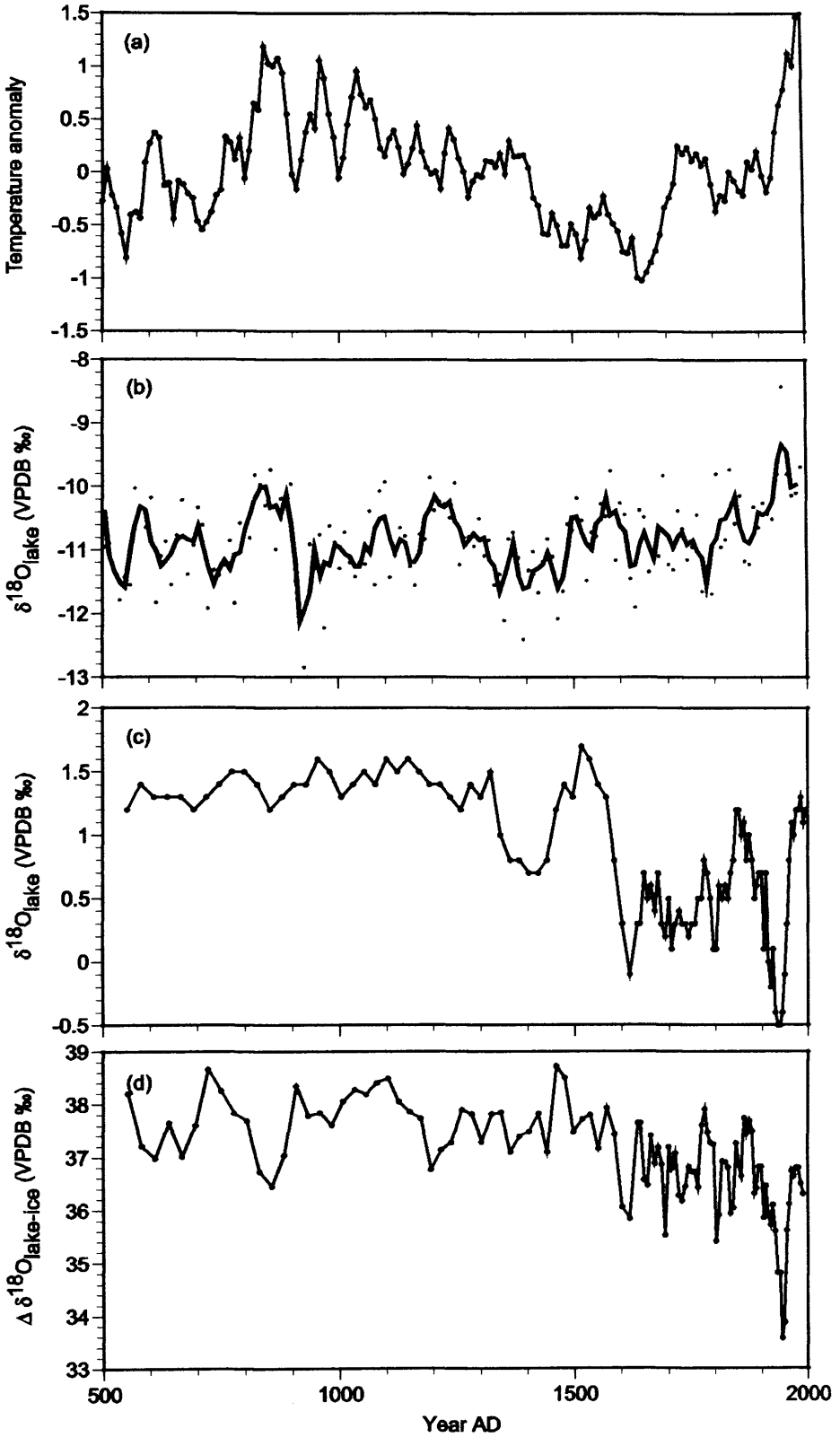

Figure 8.3 – Comparison of QING6 $\delta^{18}O_{auth}$ (c) and QING6 $\Delta\delta^{18}O_{lake-ice}$ (d) with Dunde δ^{18}Oice (b) and reconstructed temperature anomalies (c)

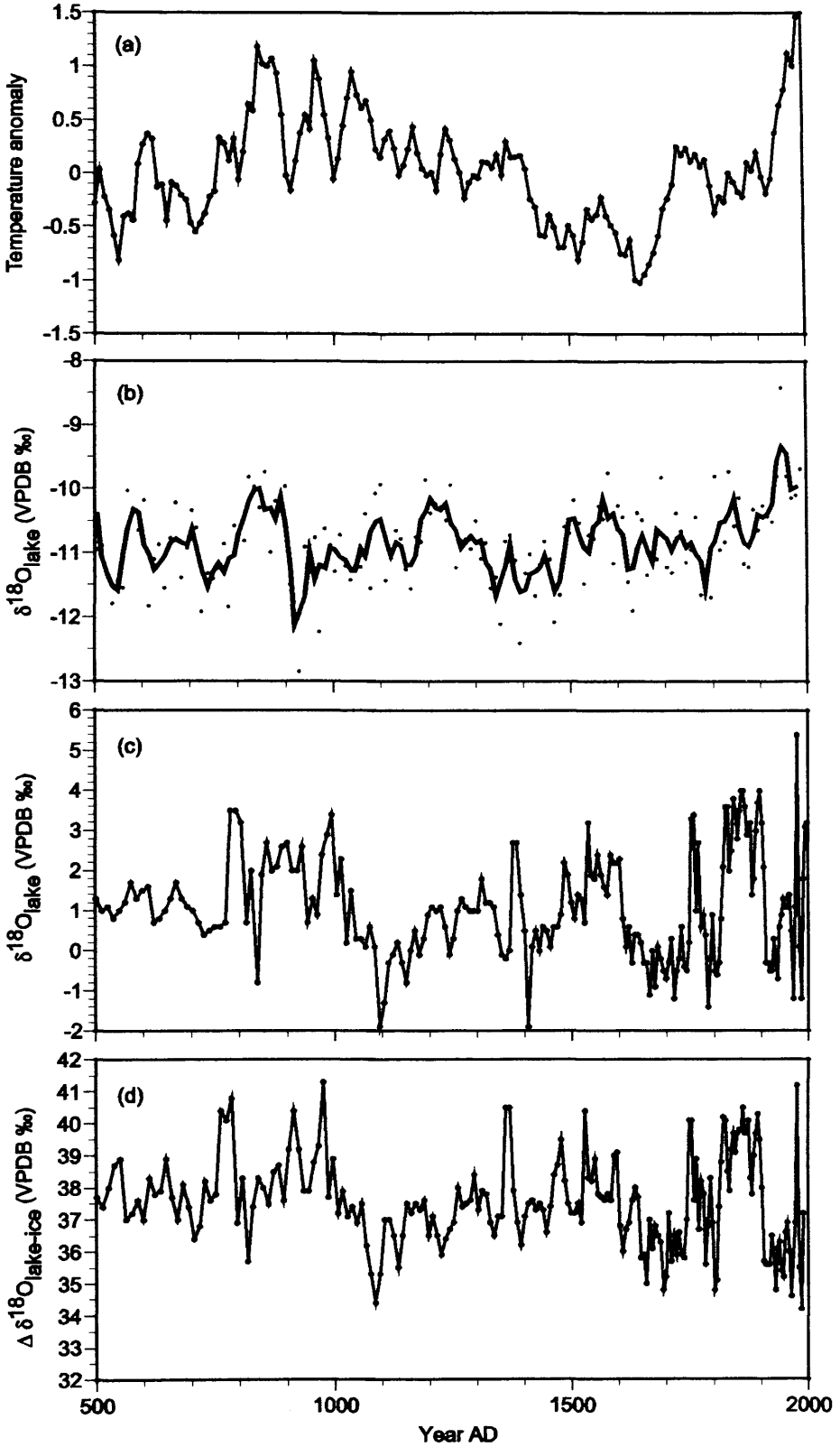

Figure 8.3 – Comparison of GAHA1 $\delta^{18}O_{auth}$ (c) and GAHA1 $\Delta\delta^{18}O_{lake-ice}$ (d) with Dunde δ^{18}Oice (b) and reconstructed temperature anomalies (c)

Colder temperatures during winter would increase the length of ice cover and ice thickness, reducing the amount of time the lake water is subject to seasonal evaporative modification. A prolonged period of colder temperatures would act to reduce the evaporative modification of lake waters and therefore $\delta^{18}O$ values for the lake would be more negative (compared to modern values). The subsequent $\delta^{18}O$ values of carbonate would also be lower; however this effect may be dampened by changes in the fractionation of the oxygen isotopes, as reduced temperatures would enrich the carbonate by 0.24‰/°C.

The recent warming that has been identified in the temperature record (Fig. 8.3a, 8.4a) is supported by the higher $\delta^{18}O_{ice}$ values from the Dunde ice core (Fig. 8.3b, 8.4b). There is a trend for higher $\delta^{18}O_{lake}$ values in QING6 (Fig. 8.3c), although they are not at the same value as the $\delta^{18}O$ before the onset of the LIA. In GAHA1 there appears to be greater variability (Fig. 8.4c) with a generally positive trend, with values approaching those seen before the LIA. A prominent feature of the both $\delta^{18}O_{lake}$ records is the negative excursion at *c.* 1920 AD, which is followed by a sharp rise in $\delta^{18}O$. This is coincident with a sharp rise in temperature (Fig. 8.3a, 8.4a) and $\delta^{18}O_{ice}$ (Fig. 8.3b, 8.4b). This indicates a rapid warming in climate at this time, which is supported by recent tree ring studies that suggest that a two decade period of drought influenced NW China (Liang *et al.,* 2003).

8.2.2 China comparisons – the Buddha cave

Comparison of the Lake Qinghai and Lake Gahai records with other isotope based records from another part of China will help to establish whether the there is a wider signal of climate change. A climate reconstruction based on stable isotopes ($\delta^{18}O_{stal}$, $\delta^{13}C_{stal}$) from a stalagmite in Buddha Cave, central China (Paulsen *et al.,* 2003) provides a record of climate change over the last 1300 years. $\delta^{18}O_{stal}$ values from Buddha cave are positively related to temperature, therefore higher $\delta^{18}O$ reflects a warmer cave temperature or warmer mean annual air temperature outside the cave (Ku and Li, 1998; Li *et al.,* 1998). $\delta^{13}C_{stal}$ values reflects the isotope values of the soil CO_2 and hence that of the vegetation above the cave (Ku and Li, 1998; Li *et al.,* 1998). This is because plants adapted to a relatively cold/wet climate (C_3 type) typically have $\delta^{13}C$ values lighter than those for C_4 type plants that grow in a warm/dry climate (Ku and Li, 1998; Li *et al.,* 1998; Paulsen *et al.,* 2003). Therefore changes in vegetation density and C_3/C_4 plant ratio will lead to changes in soil $\delta^{13}C$ which is recorded by the stalagmite with low $\delta^{13}C$ reflecting wet/cold climates and high $\delta^{13}C$ dry/warm climates (Ku and Li, 1998; Li *et al.,* 1998; Paulsen *et al.,* 2003). Based on these considerations $\delta^{18}O_{stal}$ and $\delta^{13}C_{stal}$ can be used to qualitatively to assess climate variability in terms of warmer/colder (high/low $\delta^{18}O_{stal}$) and wetter/drier (low/high $\delta^{13}C_{stal}$).

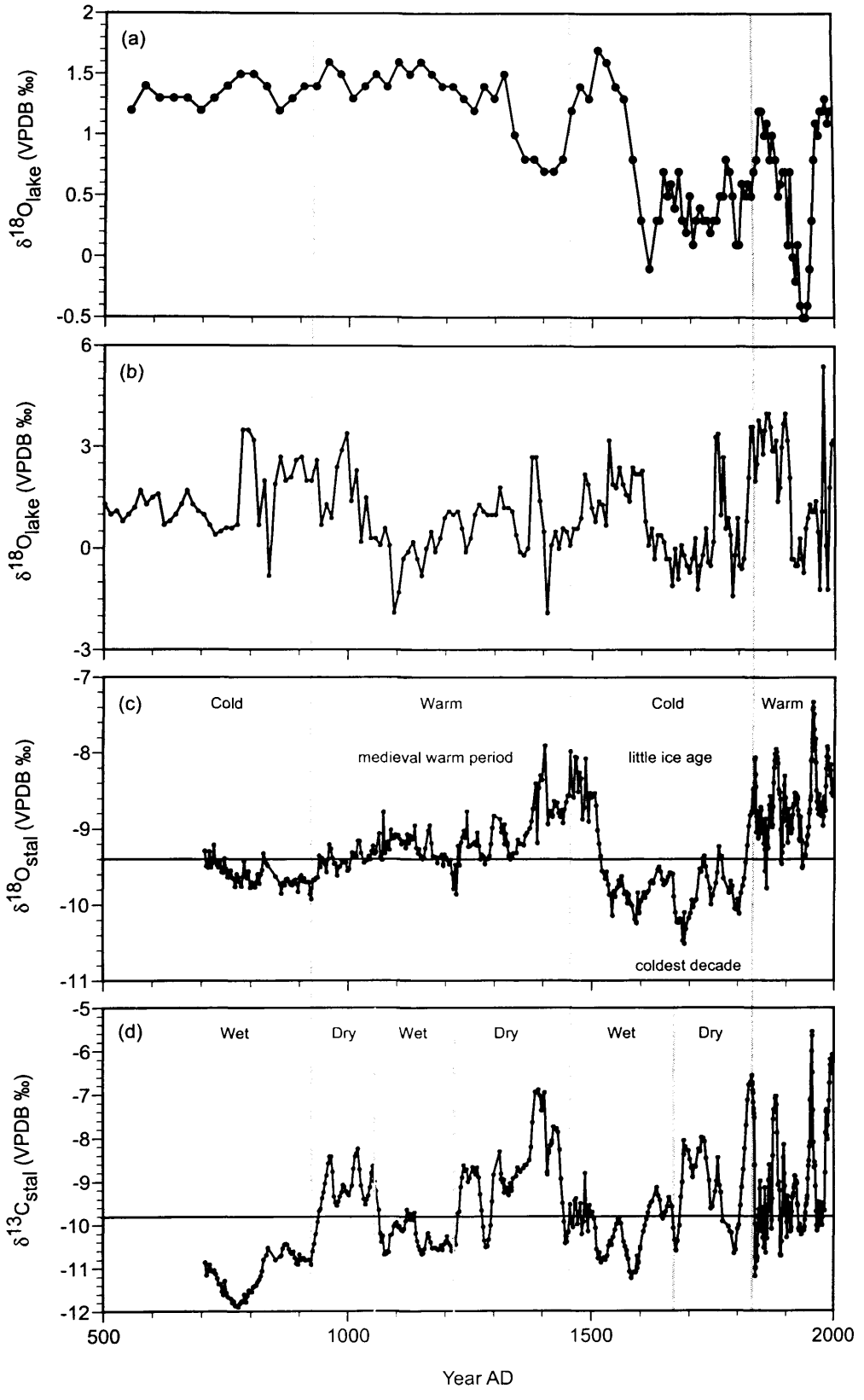

Figure 8.5 – Comparison of QING6 (a) and GAHA1 (b) $\delta^{18}O_{auth}$ with $\delta^{18}O_{stal}$ and $\delta^{13}C_{stal}$ from Buddha Cave (horizontal lines denote mean temperature and moisture conditions respectively) 157

Paulsen *et al.,* (2003) interpret their results in terms of deviations from the mean to indicate the presence of climatic anomalies, namely the Medieval Warm Period (MWP) and the Little Ice Age (LIA). They identify the MWP as the time interval from 965 to 1475 AD when $\delta^{18}O_{stal}$ was heavier than the 1270-year average. This warm period is coincident with some of highest values in $\delta^{18}O_{lake}$ in QING6, while GAHA1 initially starts high, but becomes more variable (Fig. 8.5). The $\delta^{13}C_{stal}$ record indicates changes in moisture during the MWP, suggesting that at the onset it was dry before becoming wet (a pattern observed in GAHA1) before a return to dry conditions. The onset of the LIA is identified at 1475 AD when $\delta^{18}O_{stal}$ values dropped rapidly below their mean. These cold conditions persisted until 1845 AD and are concurrent with the lowest values of $\delta^{18}O_{lake}$ in the QING6 and GAHA1 sediment records. The $\delta^{18}O_{stal}$ record can be divided into three periods: 1545 – 1640 AD, 1675 – 1745 AD and 1790 – 1825 AD (Paulsen *et al.,* 2003).

8.3 The climate history of the last 1500 years

The isotope records from Lake Qinghai and Lake Gahai highlight considerable climatic fluctuations on the Tibetan Plateau as a result of changing effective moisture. Comparisons of the $\delta^{18}O_{lake}$ stratigraphies from QING6 and GAHA1 with other palaeoenvironmental archives have demonstrated that there is some regional synchroniety and similarity between these records. The recent past climate of NW China is broadly consistent with the general northern hemisphere pattern of climate change.

*The medieval warm period (*c. 965 *to 1475 AD)*

The spatial extent, duration and moisture conditions of this climate anomaly are poorly known. However, the records presented here suggest that this period was warm and this is reflected by the high values of $\delta^{18}O_{lake}$, $\delta^{18}O_{ice}$ and $\delta^{18}O_{stal}$. The higher composite records, although variable, provide further evidence for this.

The little ice age (c. 1475 to 1920 AD)

There is growing evidence that the LIA was of global extent and although it varies from region to region, it is clearly evident in these records. Three cold stages have been identified in the lake records (low $\delta^{18}O$ values) and their occurrence coincides with the coldest composite temperatures and three cold phases identified in $\delta^{18}O_{stal}$. The onset of LIA within the catchment of Lake Qinghai is synchronous with these decreasing temperatures in China, which also led to increased glacial activity and extended ice cover (Su and Shi, 2002). The transition from the MWP to LIA is a marked event in Chinese palaeoenviromental records (Morrill *et al.,* 2003), and this is a characteristic of the lake sediment records, as indicated by the marked change in isotope values. There is also a high degree of variability that seems to be coincident with minima in solar variability (see section 8.2.1).

The last 80 years (c. 1920 to 0 AD)

There is clear evidence from all the records that the last 80 years have been warming. This is evidenced by increasingly high values of $\delta^{18}O_{lake}$, $\delta^{18}O_{ice}$ and $\delta^{18}O_{stal}$ suggesting that NW China has been responding to the recent global warming trend. Additionally, there is a pronounced period of drought (from *c.*1920 AD) as indicated by the rising $\delta^{18}O$ values from QING6 and GAHA1. This is supported by drought events identified in the $\delta^{18}O_{stal}$ record (Paulsen *et al.,* 2003).

8.3.1 A possible sun-climate relationship?

The link between long-term climate variability and solar activity has been the focus of a number of recent studies (e.g. Blackford and Chambers, 1995; Chambers and Blackford, 2001; Chambers *et al.,* 1999; Hong *et al.,* 2000; Magny, 2004; van Geel *et al.,* 1999). These investigations highlight the good correspondence between the timing of past major climate (in particular, cold) events and major solar anomalies caused by reduced irradiation. In order to better understand the climate variations inferred from the oxygen-isotope records and to assess the role of solar forcing on Lake Qinghai's catchment, the temporal record of solar irradiance will be compared to the $\delta^{18}O$ of QING6 and GAHA1 (fig. 8.6).

The oxygen-isotope records shown here reflect hydrological variability on the NE Tibetan Plateau, while the cosmosgenic nuclide production record has been interpreted to reflect changes in solar activity (Bard *et al.,* 2000) (fig. 8.6). Even though there are significant issues concerning the dating framework for the lacustrine records, there is a surprising correspondence between hydrological variability and solar irradiation (fig. 8.6). This may imply a relationship between climatic variability (as inferred from the isotope records) and solar output, although they are not completely matching. Where solar minima's are identified there is generally a coincident negative excursion in oxygen isotopes, which have been attributed to reduced evaporation as a result of cooler temperatures. However, this relationship is not particularly synchronous throughout the record, most noticeable during the Oort, Wolf and Spörer minima's (fig. 8.6).

However, given the overall similarity between the curves, especially GAHA1 and cosmosgenic nuclide production, and the approximate timings of the peaks and troughs of the records, suggests the comparison is hampered by dating imprecision, rather the records being out-of-phase.

8.3.2 Possible mechanisms

Even where sun-climate relationships have potentially been identified from proxy records, the mechanism of solar forcing remains controversial. Explaining the physical link on the basis of a relationship between 'solar wind – magnetosphere – ionosphere – atmosphere' is difficult due to

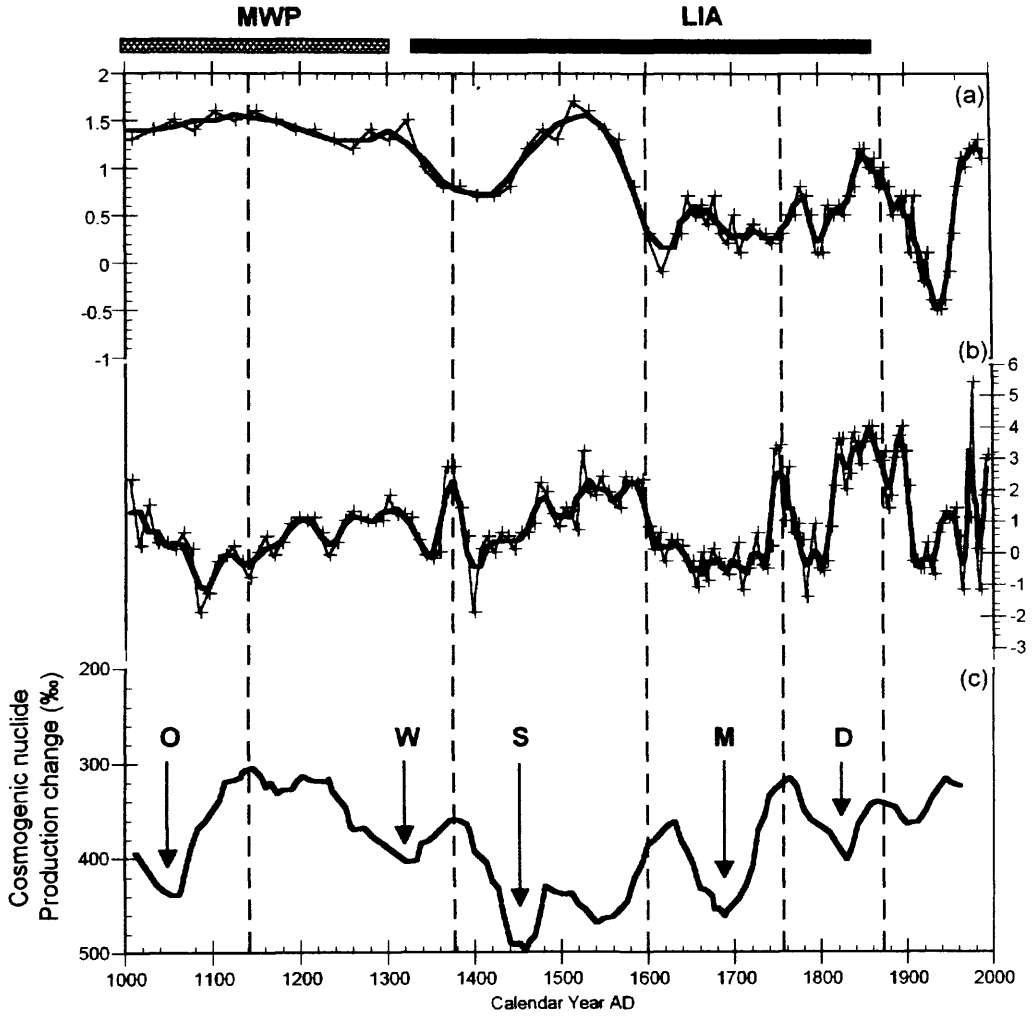

Figure 8.6 – (a) QING6 and (b) GAHA1 $\delta^{18}O$ compared to (c) solar variability, O – Oort (AD 1010 – 1050), W – Wolf (AD 1280 – 1340), S – Spörer (AD 1420 – 1530), M – Maunder (AD 1645 – 1715), D – Dalton (AD 1810) (Bard *et al.*, 2000). Vertical dashed lines denote possible correlations between these proxy records. MWP: Medieval Warm Period; LIA: Little Ice Age.

the difference in magnitude between solar variability and the effect it imparts on the atmosphere (van Geel *et al.,* 1999). Even though the specific mechanisms remain unclear, van Geel *et al.* (1999) propose that variations in UV radiation cause significant shifts in atmospheric circulation through production of ozone. This causes cooler and wetter conditions in mid-latitudes and drier tropics, which correspond to contractions in the Hadley cells, possibly weakening the summer monsoon and shifting mid-latitude storm tracks to the equator, while expanding the polar cells.

In a study by Agnihotri *et al.,* (2002) the role of solar forcing on monsoonal climate was investigated. They proposed that monsoon intensity increases as a result of greater solar output, causing more evaporation over East Africa, which enhanced the net transport of moisture to the sub-continent via the Indian monsoon. Stager and Mayewski (1997) further support the link between solar variability and monsoon behaviour by inferring a early to mid-Holocene transition climatic reorganisation took place analogous to a Maunder-type minima. This climate event led to a weakened monsoon decreased tropical precipitation, precipitation changes at mid-latitudes and a cooling at the poles (Alley *et al.,* 1997).

Based on the above observations, it would seem that reduced solar output corresponds to periods of weakened monsoon conditions. If this is assumed to be correct and the current dating framework for QING6 and GAHA1 are cautiously accepted, the periods of increased effective moisture (as denoted by the negative isotope excursions in the sedimentary records) would coincide with reduced monsoon precipitation. This supports the palaeolimnological interpretation of the isotopes presented in Chapter 7 that evaporation is more important in determining the isotope composition of lake water (and ultimately the composition of lake carbonates) as influenced by prolonged ice cover and cooler temperatures.

8.4 Summary

The oxygen-isotope records from two cores, QING6 and GAHA1 were compared to two key regional records, with a discernable similarity between effective moisture and temperature during the past 1500 years on the NE Tibetan Plateau identified. It is suggested that decreased temperatures in the region caused prolonged periods of lake ice cover, thereby reducing the period of seasonal evaporation. The chronology of these climate events is similar (given the imprecise dating framework) highlighting a regional response to climate changes during the past 1500 years. The down-core climate variability has been tentatively linked to solar output given the similarities between irradiance and hydrological shifts in the sedimentary records, but the precise mechanism of this forcing is unclear, although it is possibly related to temperature rather monsoon changes.

Chapter Nine
Conclusions

Introduction

The effect of man on climate has been debated extensively, with growing evidence supporting a link between anthropogenic impacts and recent climate changes. Climate-driven hydrologic variability has direct socio-economic impacts, particularly in the regions that lie within the East Asian monsoon boundaries, rendering this region susceptible to small changes in the timing and intensity of seasonal precipitation. People of this heavily populated region have adapted key aspects of their society to the subtleties of these rains, but this is potentially threatened by unanticipated decade to century-scale extremes in monsoon behaviour. An understanding of natural climate variability is therefore essential for evaluating anthropogenic impacts on recent and future climate and the consequences that they have for monsoon circulation.

The arid regions of NW China are very sensitive to climate changes and the Tibetan Plateau plays an important role in monsoon generation due to its high-altitude and position at a critical climate boundary. Consequently, the aim of the study was to reconstruct late Holocene hydrologic and climatic variability from the sediments of Lake Qinghai, a hydrologically closed saline water body on the Tibetan Plateau, which lies close to the maximum extent of the present-day monsoon. Previous studies from the site suggest that the lake has responded to changing boundary conditions as documented through lake level fluctuations as a result of changes in effective moisture balance, reflecting shifts in monsoon circulation. However, these studies are limited as they are of coarse resolution and focus on the last glacial-interglacial transition to the mid-Holocene, where significant climate reorganisation is known to have occurred (e.g. Kelts *et al.,* 1989; Lister *et al.,* 1991; Yu and Kelts, 2002). Therefore, the specific focus of the current study was to look at short-term small-scale climate oscillations and how these are represented in the sedimentary record.

9.1 Key outcomes of the current research

Background to isotopes in palaeolimnology

Stable isotopes of oxygen and carbon have been used in a wide range of hydrological contexts and are now more or less commonplace as a palaeolimnological technique. There use is particularly relative to hydrological-closed lakes whose annual evaporation generally exceeds precipitation and since they have little or no outflow are subsequently responsive to moisture balance changes. Depending on their current water balance, these lakes have high ionic concentrations and small changes in precipitation/evaporation (P-E) can result in large lake-level and lake salinity variations. These climate signals are recorded in precipitates (notably carbonate)

geochemically and isotopically, which are deposited at the lake bottom forming the sedimentary record.

The controls on the isotope composition of the carbonates is complex, being determined by a number of inter-linked processes which need to be understood before the full potential of a record is realized. In general though, the $\delta^{18}O$ of precipitated carbonate in hydrologically closed basins will reflect the $\delta^{18}O$ of lake water – which is determined by moisture source, local evaporation and temperature – and the lake water temperature in which the carbonate forms, together with any vital or kinetic effects. The $\delta^{13}C$ composition of precipitated carbonate and organic matter is more complex; although the composition of the lake's total dissolved inorganic carbon (TDIC) pool is the most important. This is due to the environmental process that can effect its eventual isotope composition such as equilibration with atmospheric CO_2, particularly important in lakes with long residence times, and changes in lake productivity through the preferential uptake of ^{12}C by aquatic plants.

Assessing modern isotope hydrology

An important question in any palaeo-isotope study is – what is the relationship between modern climate and lake water isotope composition? To calibrate lake-water response in Lake Qinghai a modern isotope systematic study was undertaken to acquire knowledge of baseline conditions for isotopes in the meteoric and surface water components of the hydrological cycle. This is necessary as the isotope composition of lake-water (together with other effects) is recorded in precipitates such as authigenic and ostracods carbonate.

Chapter 5 presents the most extensive investigation of oxygen, hydrogen and carbon isotope composition of Qinghai lake waters. The most remarkable feature of the modern water isotopes is that the governing environmental process on lake water composition is seasonal evaporation. This is denoted from the position of the isotope composition of lake waters with respect to the global meteoric water line (GMWL) and the values of input waters, which are significantly isotopically lighter. Even though the measurements are constrained to May and October, the data collected shows that isotope composition of lake water is relatively consistent between both sampling periods, highlighting an evaporatively enriched lake, with no obvious isotopic stratification (Fig. 5.3). Spatially, there is little difference between the lake waters except in the west basin where one sample is *c.* 1.1‰ less positive, which perhaps reflects the input of depleted waters from the Buha River that enters the lake here.

Mass balance estimations were attempted to further quantify the controls on current lake water isotope values. Although the techniques are not new, this is the fist time they have been applied to Lake Qinghai and such a large saline system. As a result, it was predicted that the majority of input to the lake was through groundwater (65 – 71% of total input waters) and river input and direct on-lake precipitation accounted for the rest. Since there is no surface outflow, the models

predicted that evaporation from the lake surface was 44 – 54% of the total output, while groundwater outflow accounted for the rest. However, these predictions varied significantly depending on the evaporation model (δ_E) that was employed, which in turn was influenced by assumptions and the quality of the data inputs, thereby hampering any full climate interpretations from this exercise.

Establishing a chronology

Fundamental to the success of any palaeolimnological study is the establishment of good chronological control, so that observed down-core changes can be put into the context of other regional palaeoenvironmental archives. Analysis of the ^{210}Pb profiles from three sites in Lake Qinghai and one from Lake Gahai yields age information about the last 100 – 150 years. Age estimation for these cores was based on the constant flux: constant sedimentation or simple model, derived by the straight-line fit of a graph of $\ln^{210}Pb_{excess}$ versus depth. Average sedimentation rates for the most recent sediments in Lake Qinghai range from 0.1 to 0.15 cm/yr^{-1}, while in Lake Gahai sedimentation is calculated as 0.1 cm/yr^{-1}, although this core displayed a non-exponential characteristic, further complicating its interpretation. The recent sedimentation of these cores was corroborated using ^{137}Cs profiles, an artificial radionuclide produced from above ground nuclear weapons testing. In the absence of large-scale local or regional inputs from nuclear establishments, the main subsurface maximums correspond to 1963. This gives ^{137}Cs-derived sedimentation rates of 0.15 cm/yr^{-1} for two cores from Lake Qinghai and 0.1 cm/yr^{-1} for Lake Gahai. In the case of QING6, there is a considerable disparity between ^{210}Pb- and ^{137}Cs-derived sedimentation rates (0.1 cm/yr^{-1} and 0.04 cm/yr^{-1} respectively), the cause of this remains unclear, but could be due to bioturbation or physical mixing of sediments.

Dating of older sediments was determined by accelerator-mass spectrometry (AMS) methods, based on authigenic inorganic carbonate (fraction <63 μm) and carbonate-free bulk organic samples. Terrestrially derived macroscopic organic fossils were absent from the sediment, causing a problem when encountering hard-water lakes, with the high possibility of reservoir effects on radiocarbon ages. Therefore, paired analysis of authigenic carbonate and bulk organic samples at the same depth were undertaken to assess this.

The results highlight that AMS dates based on carbonate samples was consistently older than their organic counterparts. This apparent offset was attributed to detrital input of carbonate, as the modern surface water of Lake Qinghai is 'post-bomb' indicating no reservoir effect in modern water TDIC. This supports the possibility of reworking of lakeshore deposits rather than the dissolution of old carbonate in the catchment altering the apparent age of lake water. Additionally, the modern dissolved organic carbon (DOC) has a notable radiocarbon age of 661 ± 32 yrs BP, sustaining the notion that detrital carbonate rather than old carbon is being incorporated into the lake sediments. As the degree of detrital contamination in the sediment is difficult to quantify,

radiocarbon dates based on authigenic carbonate were rejected and the bulk organic dates as corrected by modern DOC used.

Age models were then developed based on the ^{210}Pb and ^{137}Cs age estimations and corrected bulk organic AMS radiocarbon ages. The models were derived using a second order polynomial that took into account any possible sedimentation changes/compaction between the ^{210}Pb-derived sedimentation rate and the radiocarbon age estimate (Fig. 6.5). The age-depth models for three cores seem reasonable (QING6, QHE2, GAHA1), as the radiocarbon-derived ages are at least compatible with the ^{210}Pb and ^{137}Cs constraints on the upper sediments. Unfortunately, the age-depth model derived for QING10 predicts negative sedimentation in the upper sediments suggesting that this model is not appropriate for this core, possibly as a result of the AMS date being too old.

Palaeolimnological trends

Given the problems with developing an appropriately viable chronology for the cores from Lake Qinghai (in particular QING10) the cores were compared to see if the general isotope patterns could be independently matched (Fig. 7.7). There are many similar features in the oxygen-isotope records, but the patterns disappear when the age models are applied. Since the dating evidence is weak and there are no independent stratigraphic horizons to aid core correlation, any interpretations based on these records are tentatively suggested.

Overall, the cores show distinct isotopic variability over the last *c.* 1500 years, with a number of events identified that have been associated with changes in effective moisture, most notably between 1600 AD and 1850 AD (based on the preliminary age-depth models). These isotope excursions are evident in two cores from Lake Qinghai (QING6, QHE2) and in Lake Gahai (GAHA1/01), but not in QING10 largely as a result of the problems with its age model, although these events have been identified by wiggle matching to other cores. The excursions suggest that effective moisture may have been a result of increased precipitation in the catchment causing increased lake levels and depleting the isotope composition of lake water. However, the negative excursion in $\delta^{18}O_{auth}$ could be caused not only by an increase in precipitation but also by a decrease in evaporation from the lake, or a combination of both. The controls on lake water isotope composition are a myriad of processes, but given the modern hydrology of the lake, the balance between precipitation/evaporation (P/E) is thought to be the most important. These are complicated further by other more regional influences on the lakes hydrological budget such as local convective precipitation and length of ice cover. A simple isotope steady-state model was therefore used to evaluate the causes of these changes and to assess what is controlling the isotope shifts. The model established that Lake Qinghai was more sensitive to variations in evaporation rather than precipitation, perhaps suggesting that the hydrological variability, as inferred from oxygen-isotopes, is actually a record of evaporative history rather than a balance between P/E. These isotope shifts were tentatively linked to reduced mean annual temperature,

which would not only reduce the amount of evaporation, but also prolong the period of ice cover on the lake shortening the period the lake was exposed to evaporative effects. It is thought to reflect changes in the hydrology of the lake rather than changing temperature fractionations as the direction of the excursion is opposite to any such effect.

Regional trends

The hypothesis that the oxygen-isotope records reflect changing evaporation from Lake Qinghai, rather than a balance between inputs and outputs is supported when put into context of regional records. Comparisons with the Dunde ice core and the temperature anomaly record show that isotope variations in QING6 and GAHA1 are coincident with the onset of the Little Ice Age (LIA), a cooling event that is thought to be global in nature; with all the records indicating the estimated coldest decade during this climate event. This period of cold temperature is consistent with the large negative excursions in the $\delta^{18}O_{lake}$ records, which may have been caused by a weakening in the monsoon system (Agnihotri *et al.,* 2002). Therefore the apparent increased lake levels as inferred from the isotope record did not result from increased precipitation, but occurred due to a reduction in evaporation (direct and from prolonged ice cover) as a result of colder temperatures.

The LIA appears to be a consistent climate phenomenon in China as the comparison between the Buddha Cave and the lake records show (Fig. 9.1). This record suggests that the early part of the LIA was wet followed by a drying, but overall the period was colder than the preceding climate. However the timing of this event is delayed in the lake records, but this may be due to the unreliable chronological framework, so an assessment of the extent of the LIA in China is perhaps not appropriate at this stage.

Is there a sun-climate relationship?

Recent studies had highlighted the possible link between climate variability and solar activity as a result of the good correspondence between timing of past major climate changes and solar anomalies. This was assessed from Lake Qinghai and Lake Gahai by comparison of two oxygen-isotope records (QING6, GAHA1) with a temporal record of solar irradiance. Even though there are significant issues with the dating framework, there is a surprising correspondence between hydrological variability ($\delta^{18}O_{lake}$) and solar irradiation (Fig. 9.1). This may imply a relationship between climatic variability (as inferred from the isotope records) and solar activity, although they are not totally synchronous. However, the remarkably similarity between the curves and the approximate timings of peaks and troughs suggest that observed differences between the records may be a result of dating imprecision rather the records being out-of-phase.

Where possible sun-climate relationships have been identified before, there remains controversy over the mechanism by which solar forcing operates. This is due to the difference in magnitude between solar variability and the effect it has on atmospheric changes. van Geel *et al.,* (1999) proposed that variations in UV radiation could cause significant shifts in atmospheric circulation

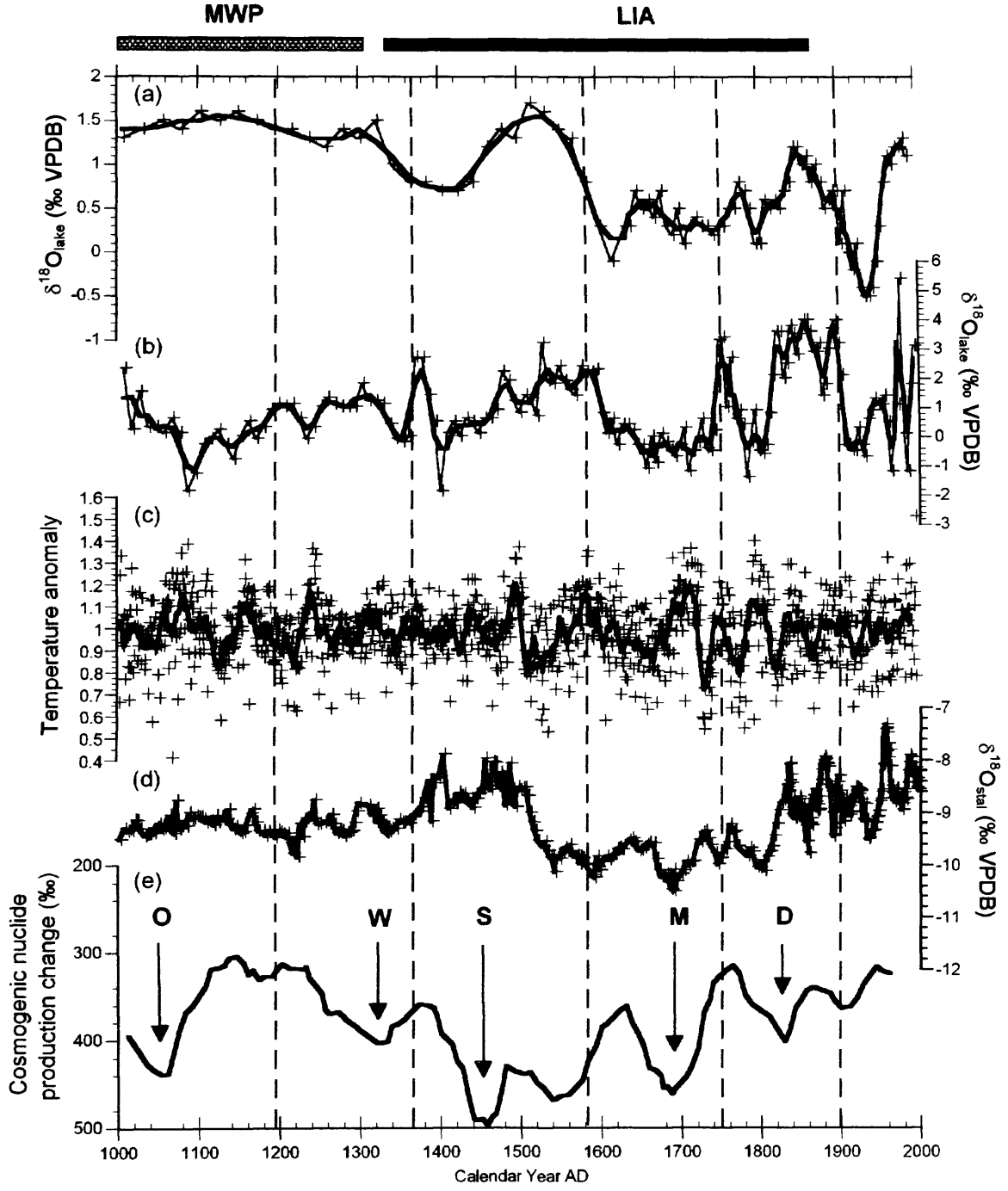

Figure 9.1 – Summary of climate proxies. (a) $\delta^{18}O_{lake}$ for QING6, (b) $\delta^{18}O_{lake}$ for GAHA1, (c) regional tree ring inferred temperature anomalies (Brauning, unpublished data), (d) $\delta^{18}O_{stal}$ from Buddha Cave (Paulsen *et al.*, 2003) and (e) solar proxies O – Oort (AD 1010 – 1050), W – Wolf (AD 1280 – 1340), S – Spörer (AD 1420 – 1530), M – Maunder (AD 1645 – 1715), D – Dalton (AD 1810) (Bard *et al.*, 2000).

that would cause cooler and wetter conditions in the mid-latitudes and drier tropics. This would correspond to a weakening of the summer monsoon and shifting the mid-latitude storm tracks to the equator, while expanding the polar cells. This is further supported by Agnihotri *et al.,* (2002), who observed that monsoon intensity increases as a result of greater solar output, causing more evaporation over East Africa, enhancing the net transport of moisture to the sub-continent.

Based on these observations it seems that reduced solar irradiance corresponds to a weakened monsoon, which if the chronology of QING6 and GAHA1 are accepted, suggests periods of increased effective precipitation coincide with reduced monsoon precipitation. Thus, it supports the hypothesis proposed, that evaporation is the key driver in the hydrological record of Lake Qinghai, and this is reflected in the isotope record.

This thesis makes an important contribution to understanding recent changes in this climatically sensitive region. The records that have been presented demonstrate that Lake Qinghai, even though large, is extremely responsive to changes in regional climate, although the link with the monsoon system is less than straightforward and is perhaps more important on a longer timescale.

9.2 Future work

The aim of the current study was to assess the use of high-resolution sedimentary records from Lake Qinghai in documenting short-term shifts in monsoonal circulation. Even though an attempt at establishing the controls on the isotope composition of carbonate precipitated within the lake (and its relationship to climate) was undertaken, it is obvious that the processes are still poorly understood. Furthermore, this limited understanding hampers full interpretations of down-core data. Therefore improved monitoring of lake waters and carbonate formation within Lake Qinghai would greatly improve our understanding of lake functioning as well as enhance our capability to model changes that occur in the climate and how these are expressed in lake sediments.

A substantial limiting factor of the present study is the poor chronological framework. The chronology of the most recent sediments (*c.* last 150 years) is reasonably secure as determined by ^{210}Pb- and ^{137}Cs-derived sedimentation rates. However, there are obvious problems with AMS ^{14}C dating of sediments from Lake Qinghai, as the carbonates appear too old compared to their bulk organic counterparts. Analysis of modern water DIC and DOC suggest that there is no systematic offset between carbonate and organic dates. This complication warrants a further investigation of the distribution of ^{14}C in modern waters, the catchment and surface sediments, if a reliable chronology is to be obtained.

There are also a host of other proxies that could potentially be used to infer past environmental changes from Lake Qinghai sediments. Isotope analysis of cellulose is fast becoming a reliable indicator of past hydrology (e.g. Wolfe *et al.,* 2001), although concerns over the source of cellulose (e.g. whether it is terrestrially or aquatically derived) can undermine its usefulness. In the case of Lake Qinghai, the CN ratio suggests that the majority of the organic matter in the lake is derived from aquatic productivity. Therefore, oxygen-isotope analysis of cellulose extracted from Lake Qinghai has the potential to provide an independent palaeohydrological indicator. Additionally, analysis of compound-specific organic isotopes is a developing science that shows promise in reconstructing hydrogen-isotopes from palmictic acid (Huang *et al.,* 2004), as well as a newly developing palaeothermometer based on TEX_{86} (Colman *pers comm.*).

Given the importance of Lake Qinghai and its apparent sensitivity to changes in hydrology, longer-term studies to assess monsoon dynamics and the effect of Tibetan Plateau uplift on monsoonal circulation would be pertinent. Although, the success of such a project would depend on understanding the modern system in order to interpret changes down-core. If this could be achieved, then it would be possible to assess the impact of Tibetan Plateau uplift on the monsoon regime. Therefore being able to place monsoon dynamics in the context of other Cenozoic climate shifts as documented by ocean sediment cores.

References

Abell, P.I. and Williams, M.A.J. (1989). Oxygen and carbon isotope ratios in gastropod shells as indicators of paleoenvironments in the Afar region of Ethiopia. Palaeogeography Palaeoclimatology Palaeoecology, 74: 265-278.

Agnihotri, R., Dutta, K., Bhushan, R. and Somayajulu, B.L.K. (2002) Evidence for solar forcing on the Indian monsoon during the last millennium. Earth and Planetary Science Letters, 198: 521-527.

Aizen, V.,Aizen, H., Melack, J., and Martma, T. (1996). Isotopic measurements of precipitation on central Asian glaciers (southeastern Tibet, northeastern Himalayas, central Tien Shan). Journal of Geophysical Research, 101: 9185-9196.

Alley, R.B., Mayewski, P.A., Sowers, T., Stuiver, M., Taylor, K.C. and Clark, P.U. (1997) Holocene climate instability – a prominent widespread event 8200 yr ago. Geology, 25: 483-486.

An, Z.S. (2003). Scientific drilling at Qinghai Lake on the northeastern Tibetan Plateau: high-resolution palaeoenvironmental records of eastern Asia and their significance for global change. (Eds) An, Z.S. Abstracts for Lake Qinghai workshop, Xining, China, 20-24 October 2003. Xian, China, Institute of Earth Environment, Chinese Academy of Sciences.

An, Z.S., Kutzbach, J.E., Prell, W.L., and Porter, S.C. (2001). Evolution of Asian monsoons and phased uplift of the Himalaya- Tibetan plateau since Late Miocene times. Nature, 411: 62-66.

An, Z.S., Porter, S.C., Kutzbach, J.E., Wu, X.H., Wang, S.M., Liu, X.D., Li, X.Q., and Zhou, W.J. (2000). Asynchronous Holocene optimum of the East Asian monsoon. Quaternary Science Reviews, 19: 743-762.

An, Z.S., Porter, S.C., Zhou, W.J., Lu, Y.C., Donahue, D., Head, M.J., Wu, X.H., Ren, J.Z., and Zheng, H.B. (1993). Episode of strengthened summer monsoon climate of Younger Dryas age on the Loess Plateau of Central China. Quaternary Research, 39: 45-55.

Appleby, P.G. (2001). Chronostratigraphic techniques in recent sediments. (Eds) Last, W.M. and Smol, J.P. Tracking Environmental Change Using Lake Sediments. Volume 1: Basin Analysis. Coring and Chronological Techniques. Dordrecht, The Netherlands, Kluwer Academic Publishers. pp. 171-203.

Appleby, P.G. and Oldfield, F. (1992). Applications of ^{210}Pb to sedimentation studies. (Eds) Ivanovich, Ma and Harmon, R.S. Uranium- series disequilibrium. Applications to Earth, Marine and Environmental Sciences. Oxford, Oxford Science.

Araguas- Araguas, L., Froehlich, K., and Rozanski, K. (1998). Stable isotope composition of precipitation over southeast Asia. Journal of Geophysical Research, 103: 28721-28742.

Araguas- Araguas, L., Froehlich, K., and Rozanski, K. (2000). Deuterium and oxygen-18 isotope composition of precipitation and atmospheric moisture. Hydrological Processes, 14: 1341-1355.

Ariztegui, D., Farrimond, P., and McKenzie, J. (1996). Compositional variations in sedimentary lacustrine organic matter and their implications for high alpine Holocene environmental changes: Lake St. Moritz, Switzerland. Organic Geochemistry, 24: 453-461.

Bard, E., G. Raisbeck, F. Yiou, and J. Jouzel, (2000) Solar irradiance during the last 1200 years based on cosmogenic nuclides. Tellus B 52, 985-992.

Bartlein, P.J., Edwards, M.D., Shafer, S.L., and Barker, E.D. (1995). Calibration of radiocarbon ages and the interpretation of palaeoenvironmental records. Quaternary Research 44: 417-424.

Battarbee, R.W. (2000). Palaeolimnological approaches to climate change, with special regard to the biological record. Quaternary Science Reviews, 19: 107-124.

Benn, D.I. and Owen, L.A. (1998). The role of the Indian summer monsoon and the mid-latitude westerlies in Himalayan glaciation: review and speculative discussion. Journal of the Geophysical Society, 155: 353-363.

Bennett, K.D. (1994). Confidence intervals for age estimates and deposition times in late-Quaternary sediment sequences. The Holocene, 4: 337-348.

Bennett, K.D. and Fuller, J.L. (2002). Determining the age of the mid- Holocene *Tsuga canadensis* (hemlock) decline, eastern North America. The Holocene, 14: 421-429.

Benson, L.V. and Paillet, F. (2002). HIBAL: a hydrologic-isotope-balance model for application to paleolake systems. Quaternary Sciences Reviews, 21: 1521-2539.

Benson, L.V. and White, J.W.C. (1994). Stable isotopes of oxygen and hydrogen in the Truckee River-Pyramid Lake surface-water system. 3. Source of water vapor overlying Pyramid Lake. Limnology and Oceanography, 39: 1945-1958.

Binford, M.W. (1990) Calculation and uncertainty analysis of ^{210}Pb dates for PIRLA project lake sediment cores. Journal of Paleolimnology, 3: 253-267.

Björck, S. and Wohlfarth, B. (2001). 14C chronostratigraphic techniques in paleolimnology. (Eds) Last, W.M. and Smol, J.P. Tracking environmental change using lake sediments: Volume 1: Basin Analysis. Coring and Chronological Techniques. Dordrecht, The Netherlands, Kluwer Academic Publishers. pp. 205-245.

Blackford, J.J. and Chambers, F.M. (1995) Proxy climate record for the last 1000 years from Irish blanket peat and a possible link to solar variability. Earth and Planetary Science Letters, 13: 145-150.

Bond, G., Showers, W.J., Cheseby, M., Lotti, R., Almasi, P., deMenocal, P., Priore, P., Cullen, H., Hajda, I, and Bonani, G. (1997). A pervasive millennial-scale cycle in North Atlantic Holocene and glacial climates. Science, 278: 1257-1266.

Bond, G., Showers, W.J., Elliot, M., Evans, M., Lotti, R., Hadjas, I., Bonani, G., and Johnson, S. (1999). The North Atlantic 1-2 kyr climate rhythm: relation to Heinrich events, Dansgaard/Oeschger cycles and the Little Ice Age. (Eds) Clark, P.U., Webb, R.S., and Keigwin, L. Mechanisms of global climate change at millennial time scales. Geophysical Monograph Series 112. Washington, DC, American Geophysical Union. pp. 35-58.

Bowen, G.J. and Wilkinson, B. (2002). Spatial distribution of δ18O in meteoric precipitation. Geology, 30: 315-318.

Boyle, E.A. and Keigwin, L. (1987). North Atlantic thermohaline circulation during the past 20,000 years linked to high- latitude surface temperatures. Nature, 330: 35-40.

Bradbury, J.P., Dean, W.E., and Anderson, R.Y. (1993). Holocene diatom palaeolimnology of Elk Lake, Minnesota: a synthesis. (Eds) Bradbury, J.P. and Dean, W.E. Elk Lake Minnesota: evidence for rapid climate change in the North-central United States. Boulder, Colorado, Geological Society of America Special Paper, Vol. 276. pp 215-237.

Bradley, R.S. (2003). Climate during the Holocene. (Eds) Mackay, A.W., Battarbee, R.W., Birks, H.J.B., and Oldfield, F. Global change in the Holocene. Arnold. pp. 10-19.

Bradley, R.S. and Jones, P.D. (1993). 'Little Ice Age' summer temperature variations: nature and relevance to recent global warming trends. The Holocene, 8: 477-483.

Bradley, R.S., Briffa, K.R., Cole, J.E., Hughes, M.K., and Osborn, T.J. (2002). The climate of the last Millennium. (Eds) Alverson, K.D., Bradley, R.S., and Pedersen, T.F. Paleoclimate, global change and the future. Berlin, Heidelnerg, New York, Springer- Verlag pp. 105-141.

Brenner, M., Schelske, C.L., and Kenney, W.F. (2004). Inputs of dissolved and particulate ^{226}Ra to lakes and implications of ^{210}Pb dating of recent sediments. Journal of Paleolimnology, 32: 53-66.

Brocoli, A.J. and Manabe, S. (1992). The effects of orography on mid-latitude Northern Hemisphere dry climates. Journal of Climate, 5: 1181-1201.

Broecker, W.S. (2001). Was the Medieval Warm Period global? Sciences, 291: 1497- 1499.

Broecker, W.S., Andree, M., Wolfti, W., Oeschger, H., Bonani, G., Kennett, J., and Peteet, D. (1988). The chronology of the last deglaciation: implications to the cause of the Younger Dryas event. Paleooceanography, 3: 1-19.

Chambers, F.M. and Blackford, J.J. (2001) Mid- and Late-Holocene climatic changes: a test of periodicity and solar forcing in proxy-climate data from blanket peat bogs. Journal of Quaternary Science, 16: 329-338.

Chambers, F.M., Ogle, M.I. and Blackford, J.J. (1999) Palaeoenvironmental evidence for solar forcing of Holocene climate: linkages to solar science. Progress in Physical Geography, 23: 181-204.

Charles, C.D., Hunter, D.E., and Fairbanks, R.G. (1997). Interaction between the ENSO and the Asian monsoon in a coral record of tropical climate. Science, 277: 925-928.

Chen, C-T. A., Lan, H-C., Lou, J-Y., and Chen, Y-C. (2003a). The Dry Holocene Megathermal in Inner Mongolia. Palaeogeography Palaeoclimatology Palaeoecology, 193: 181-200.

Chen, F., Wu, W., Holmes, J.A., Madsen, D.B., Zhu, Y., Jon, M., and Oviatt, C.G. (2003b). A mid-Holocene drought interval as evidenced by lake desiccation in the Alashan Plateau, Inner Mongolia, China. Chinese Science Bulletin, 48: 1401-1410.

Clark, C.O., Cole, J.E., and Webster, P.J. (2000). Indian Ocean SST and Indian summer rainfall: predictive relationships and their decadal variability. Journal of Climate, 13: 2503- 2518.

Clark, J.S. and Fritz, I. (1997). Environmental isotopes in hydrogeology. Boca Raton, LA., Lewis.
Clausen, M., Kubatzki, C., Brovkin, V., and Ganopolski, A. (1999). Simulation of an abrupt change in Sahara vegetation in the mid- Holocene. Geophysical Research Letters, 26: 2037-2040.

Cleens, S.C., Murray, D.W., and Prell, W.L. (1996). Non- stationary phase of the Plio- Pleistocene Asian monsoon. Science, 274: 943-948.

Clemans, S.C., Wang, P.X., and Prell, W.L. (2003). Monsoons and global linkages on Milankovitch and sub- Milankovitch timescales. Marine Geology, 201: 1-3.
Coplen, T.B., Kendall, C., and Hopple, J. (1983). Comparison of stable isotope reference samples. Nature, 302: 236-239.

Craig, H. (1961). Isotope variations in meteoric waters. Science, 133: 1833-1834.

Craig, H. (1965). The measurement of oxygen isotope paleotemperatures. (Eds) Tongiorgi, E. Stable isotopes in oceanographic studies and paleotemperatures. Pisa, Consigilio Nazionale della Ricerche, Laboratorio Nucleare. pp. 161-182.

Cross, S.L., Baker, P.A., Seltzer, G.O., Fritz, S.C., and Dunbar, R.B. (2001). Late Quaternary climate and hydrology of Tropical South America inferred from an isotopic and chemical model of Lake Titicaca, Bolivia and Peru. Quaternary Research, 56: 1-9.

Crowley, T.J. (2000). Causes of climate change over the past 1000 years. Science, 289: 270-277.

Crowley, T.J. and Lowert, T.S. (2000). How warm was the Medieval Warm Period? Ambio, 29: 51-54.

Cundy, A.B. and Croudace, I.W. (1996). Sediment accretion and recent sea level rise in the Solent, southern England: inferences from radiometric and geochemical studies. Estuarine, Coastal and Shelf Science, 43: 449-467.

Cushing, E.J. and Wright, H.E. (1965). Hand operated piston corers for lake sediments. Ecology, 46: 360-384.

Dansgaard, W. (1964). Stable isotopes in precipitation. Tellus, 16: 436-468.

Dean, W.E. (1974). Determination of carbonate and organic matter in calcareous sediments and sedimentary rocks by loss on ignition: comparison with other methods. Journal of Sedimentary Petrology, 44: 242-248.

DeDecker, P. (1988). An account of the techniques using ostracods in palaeolimnology in Australia. Palaeogeography Palaeoclimatology Palaeoecology, 463-475.

Deines, P. (1980). The isotopic composition of reduced organic carbon. (Eds) Fritz, P. and Fontes, J.C. Handbook of environmental isotope geochemistry. 1- The terrestrial environment. Netherlands, Elsevier Scientific Publishing Company. pp. 329-406.

Dincer, T. (1968). The use of oxygen-18 and deuterium concentrations in the water balance of lakes. Water Resources Research, 4: 1289-1306.

Edwards, T.W.D., Wolfe, B.B., Gibson, J.J., and Hammarlund, D. (2004). Use of water isotope tracers in high- latitude hydrology and paleohydrology. (Eds) Pienitz, R., Douglas, M.S.V., and Smol, J.P. Long-term environmental change in Arctic and Antarctic lakes. Dordrecht, The Netherlands, Kluwer Academic Publishers.

Esper, J., Cook, E.R., and Schweingruber, F.H. (2002). Low-frequency signals in long tree- ring chronologies for reconstructing past temperature variability. Science 295: 2250-2253.

Eugster, H.P. and Hardie, L.A. (1978). Saline lakes. (Eds) Lerman, A. Lakes: Chemistry, Geology, Physics. New York, Springer- Verlag. pp. 237-293.

Fairbanks, R.G. (1989). A 17,000 year glacio-eustatic sea level record: influence of glacial melting rates on the Younger Dryas event and deep- ocean circulation. Nature, 342: 637-642.

Fan, H., Gasse, F., Huc, A., Li, Y.F., Sifeddine, A., and Soulie-Marsche, I. (1996). Holocene environmental changes in Bangong Co basin (western Tibet). 3. Biogenic remains. Palaeogeography Palaeoclimatology Palaeoecology, 120: 65-78.

Fontes, J.C., Gasse, F., and Gibert, E., (1996). Holocene environmental changes in Lake Bangong Co basin (western Tibet). 1. Chronology and stable isotopes of carbonates of a Holocene lacustrine core. Palaeogeography Palaeoclimatology Palaeoecology, 120: 25-47.

Fontes, J.C., Melieres, F., Gibert, E., Qing, L., and Gasse, F. (1993). Stable- Isotope and radiocarbon Balances of two Tibetan lakes (Sumxi Co, Longmu Co) from 13,000-BP. Quaternary Science Reviews, 12: 875-887.

Free, M. and Robock, A. (1999). Global warming in the context of the Little Ice Age. Journal of Geophysical Research, 104: 19057-19070.

Gasse, F. and Van Campo, E. (1994). Abrupt Postglacial Climate Events in West Asia and North-Africa Monsoon Domains. Earth and Planetary Science Letters, 126: 435-456.

Gasse, F., Arnold, M., Fontes, J.C., Fort, M., Gibert, E., Huc, A., Li, B.Y., Li, Y.F., Lju, Q., Melieres, F., Van Compo, E., Wang, F.B., and Zhang, Q.S. (1991). A 13,000- Year Climate Record from Western Tibet. Nature, 353: 742-745.

Gasse, F., M., Fontes, J.C., Van Compo, E., and Wei, K. (1996). Holocene environmental changes in Bangong Co basin (western Tibet). 4. Discussion and conclusions. Palaeogeography Palaeoclimatology Palaeoecology, 120: 79-92.

Gat, J.R. (1981). Lakes. (Eds) Gat, J.R. and Gonfiantini, R. Stable Isotope Hydrology: Deuterium and Oxygen -18 in the Water Cycle. Vienna, International Atomic Energy Agency. pp. 203-222.

Gat, J.R. and Lister, G.S. (1995). The 'catchment effect' on the isotopic composition of lake waters; its importance in palaeolimnological interpretations. (Eds) Frenzel, B. Problems of Stable Isotopes in Tree- Rings, Lake Sediments and Peat-Bogs as Climatic Evidence for the Holocene. Mainz, Akademie der Wissenschaften und der Literatur.

Gibson, J.J., Edwards, T.W.D., and Prowse, T.D. (1999). Pan- derived isotopic composition of water vapour and its variability in northern Canada. Journal of Hydrology, 217: 55-74.

Gibson, J.J., Edwards, T.W.D., Bursey, G.C., and Prowse, T.D. (1993). Estimating evaporation using stable isotopes: quantitative results and sensitivity analysis for two catchments in northern Canada. Nordic Hydrology, 24: 29-94.

Glew, J.R. (1991). Miniature gravity corer for recovering short sediment cores. Journal of Paleolimnology, 5: 285-287.

Gonfiantini, R. (1986). Environmental isotopes in lake studies. (Eds) Fritz, P. and Fontes, J.C. Handbook of Environmental Isotope Geochemistry, Volume 2: The terrestrial environment. Amsterdam, pp. 113-168, Elsevier.

Griffiths, H.I. and Holmes, J.A. (2000). Non- marine ostracods and Quaternary palaeoenvironments. Quaternary Research Association Technical Guide No. 8. London, Quaternary Research Association.

GRIP Project Members. (1993). Climate instability during the last interglacial period recorded in the GRIP ice core. Nature, 364: 203-207.

Grootes, P.M., Stuiver, M., White, J.W.C., Johnsen, S., and Jouzel, J. (1993). Comparison of oxygen isotope records from GISP2 and GRIP Greenland ice cores. Nature, 366: 552-554.

Grossman, E.L. (1984). Carbon isotopic fractionation in live benthic foraminfera- comparison with inorganic precipitate studies. Geochimica et Cosmochimica Acta, 48: 1505-1512.

Grossman, E.L. and Ku, T-L. (1986). Oxygen and carbon isotope fractionation in biogenic aragonite: temperature effects. Chemical Geology, 59: 59-74.

Grove, J.M. (1988). The Little Ice Age. New York, Methuen.

Guo, Z.T., Liu, T.S., Fedoroff, N., Wei, L.Y., Ding, Z.L., Wu, N.Q., Lu, H.Y., Jiang, W.Y., and An, Z.S. (1998). Climate extremes in Loess of China coupled with the strength of deep-water formation in the North Atlantic. Global and Planetary Change, 18: 113-128.

Guo, Z.T., Petit-Maire, N., and Kropelin, S. (2000). Holocene non- orbital climatic events in present-day arid areas of northern Africa and China. Global and Planetary Change, 26: 97-103.

Harrison, T.M., Copeland, P., Kidd, W.S., and Yin, A. (1992). Raising Tibet. Science, 255: 1663-1670.

Heaton, T.H.E. (1992). Procedure and notes on zinc reduction of water for D/H analysis and aluminum-bronze hot-block. Unpublished Report Series Number 43, NERC Isotope Geosciences Laboratory.

Heaton, T.H.E., Holmes, J.A., and Bridgewater, N.D. (1995). Carbon and oxygen isotope variations among lacustrine ostracods: Implications for palaeoclimatic studies. Holocene, 5: 428-434.

Henderson, A.C.G. (1999) Detecting climate change using a high resolution record from the recent lake sediments of Qinghai Hu, NE Tibetan Plateau, China. Unpublished M.Res. thesis. University of London.

Henderson, A.C.G., Holmes, J.A., Zhang, J.W., Leng, M.J., and Carvalho, L.R. (2003). A carbon- and oxygen- isotope record of recent environmental change from Qinghai Lake, NE Tibetan Plateau. Chinese Science Bulletin, 48: 1463- 1468.

Hewitt, C.D. and Mitchell, J.F.B. (1998). A fully coupled GCM simulation of the climate of the mid-Holocene. Geophysical Research Letters, 25: 361-364.

Hoffman, G. and Heimann, M. (1997). Water isotope modelling in the Asian monsoon region. Quaternary International, 37: 115-128.

Holmes, J.A. and Chivas, A.R. (2002). Ostracod shell chemistry- overview. (Eds) Holmes, J.A. and Chivas, A.R. The Ostracoda: applications in Quaternary research. Washington. pp. 185-204, Geophysical Union.

Holmes, J.A., Street- Perrott, F.A., Allen, M.J., Fothergill, P.A., Harkness, D.D., Kroon, D., and Perrott, R.A. (1997). Holocene palaeolimnology of Kajemarum Oasis, Northern Nigeria: An isotopic study of ostracods, bulk carbonates and organic carbon. Journal of the Geological Society, 154: 311-319.

Holmes, J.A., Street- Perrott, F.A., Perrott, R.A., Stokes, S., Waller, M.P., Huang, Y., Eglinton, G., and Ivaniovich, M. (1999). Holocene landscape evolution of the Manga grasslands, N.E. Nigeria: evidence from palaeolimnology and dune chronology. Journal of Geological Society, 156: 357-368.

Hong, Y.T., Jiang, H.B., Liu, T.S., Zhou, L.P., Li, H.D., Leng, X.T., Hong, B., and Qin, X.G. (2000). Response of climate to solar forcing recorded in a 6000- year $\delta^{18}O$ time-series of Chinese peat cellulose. The Holocene, 10: 1-7.

Horita, J. and Wesolowski, D. (1994). Liquid- vapour fractionation of oxygen and hydrogen isotopes of water from freezing to the critical temperature. Geochimica et Cosmochimica Acta, 58: 3425-3437.

Houghton, J.T., Ding, Y., Griggs, D.J., Noguer, M., van der Linden, P.J., Dai, X., Maskill, K., and Johnson, C.A. (2001). Climate Change 2001: the scientific basis. Cambridge, Cambridge University Press.

Huang, C.C., Pang, J.L., and Zhao, J.P. (2000). Chinese loess and the evolution of the east Asian monsoon. Progress in Physical Geography, 24: 75-96.

Huang, Y., Shuman, B., Wang, Y. and Webb, T. (2004) Hydrogen isotopes of individual lipids in lake sediments as novel tracers of climatic and environmental change: a surface sediment test. Journal of Paleolimnology, 31: 363-375.

Hughen, K.A., Southon, J.R., Lehman, S.J., and Overpeck, J.T. (2000). Synchronous radiocarbon and climate shifts during the last deglaciation. Science, 290: 1951-1954.

Hughes, M.K. and Diaz, H.F. (1994). Was there a 'Medieval Warm Period', and if so, where and when? Climatic Change, 26: 109-142.

IAEA. (2001). GNIP Maps and Animations, International Atomic Energy Agency, Vienna. Accessible at http://isohis.iaea.org.

Jennings, A.E., Knudsen, K.L., Hald, M., Hansen, C.V., and Andrews, J.T. (2002). A mid-Holocene shift in Arctic sea ice variability on the East Greenland shelf. The Holocene, 12: 49-58.

Johnson, K.R. and Ingram, B.L. (2004). Spatial and temporal variability in the stable isotope systematics of modern precipitation in China: implications for palaeoclimate reconstruction. Earth and Planetary Science Letters, 220: 365-377.

Jones, B.F. and Browser, C.J. (1978). The Mineralogy and related chemistry of lake sediments. (Eds) Lerman, A. Lakes: chemistry, geology, physics. New York, USA, Springer- Verlag. pp 180-235.

Jones, P.D., Bradley, R.S., and Jouzel, J. (1996). Climate variations and forcing mechanisms of the last 2000 years. New York, Springer.

Jones, P.D., New, M., Parker, D.E., Martin, S., and Rigor, I.G. (1999). Surface air temperature and its changes over the past 150 years. Review of Geophysics, 37: 173-199.

Karpuz, N.K. and Jansen, E.A. (1992). A high-resolution diatom record of the last deglaciation from the SE Norwegian Sea: documentation of rapid climate changes. Paleooceanography, 7: 499-520.

Keatings, K.W., Heaton, T.H.E., and Holmes, J.A. (2002). Carbon and oxygen isotope fractionation in non-marine ostracods: Results from a ' natural culture' environment. Geochimic et Cosmochimica Acta, 66: 1701-1711.

Kebede, S., Lamb, H.F., Telford, R.J., Leng, M.J., and Umer, M. (2002). Lake- groundwater relationships, oxygen isotope balance and climate sensitivity of the Bishoftu Crater Lakes, Ethiopia. (Eds) Odada, E.O. and Olago, D.O. The East African Great Lakes: limnology, palaeolimnology and biodiversity. Netherlands, Kluwer. pp 261-275.

Keeley, J.E. and Sandquist, D.R. (1992). Carbon: freshwater plants . Plant, Cell and Environment, 1021- 1035.

Keigwin, L.D. (1996). The little ice age and medieval warm period in the Sargasso Sea. Science, 274: 1504-1508.

Kelts, K. and Talbot, M.R. (1990). Lacustrine carbonates as geochemical archives of environmental change and biotic- abiotic interactions. 290-317. (Eds) Tilzer, M. M. and Serruya, C. Ecological structure and function in large lakes. Madison, WI, Science and Technology Publications.

Kelts, K., Zao, C.K., Lister, G., Qing, Y.J., Hong, G.Z., Niessen, F., and Bonani, G. (1989). Geological Fingerprints of Climate History- A Cooperative Study of Qinghai Lake, China. Eclogae Geologicae Helvetiae, 82: 167-182.

Kim, S-T. and O'Neil, J.R. (1997). Equilibrium and non- equilibrium oxygen isotope effects in synthetic carbonates. Geochimica et Cosmochimica Acta, 61: 3461-3475.

Ku, T.-L. and Li, H.-C. (1998). Speleotherms as high- resolution paleoenvironment archives: records from northeastern China. Proceedings of the Indian Academy of Sciences. Earth and Planetary Sciences, 107: 321-330.

Kudrass, H.R., Hofmann, A., Doose, H., Emeis, K., and Erlenkeuser, H. (2001). Modulation and amplification of climate changes in the Northern Hemisphere by the Indian summer monsoon during the past 80 k.y. Geology, 29: 63-66.

Kutzbach, J.E. and Liu, Z. (1997). Response of the African monsoon to orbital forcing and ocean feedbacks. Science, 278: 440-443.

Kutzbach, J.E., Gutter, P., Behling, P.J., and Selin, R. (1993a). Simulated climate changes: results of the COHMAP climate- model experiments. (Eds) Wright, H.E., Kutzbach, J.E., Webb III, T., Ruddiman, W.F., Street-Perrott, F.A., and Bartlein, P.J. Global climates since the Last Glacial Maximum. London, University of Minnesota Press. pp. 24-93.

Kutzbach, J.E., Prell, W.L. and Ruddiman, W.F. (1993b). Sensitivity of Eurasian climate to surface uplift of the Tibetan Plateau. Journal of Geology, 101: 177-190.

Kutzbach, J.E., Ruddiman, W.F., and Prell, W.L. (1997) Tectonic Uplift and Climate Change. New York, Plenum.

Laird, K.R., Fritz, S.C., Maasch, K.A., and Cumming, B.F. (1996). Greater drought intensity and frequency before AD 1200 in the Northern Great Plains, USA. Nature, 384: 552-554.

Lehmkuhl, F. and Haselein, F. (2000). Quaternary palaeoenvironmental change on the Tibetan Plateau and adjacent areas (Western China and Western Mongolia). Quaternary International, 65/66: 121-145.

Lehmkuhl, F., Owen, L.A., and Derbyshire, E. (1998). Late Quaternary glacial history of Northeast Tibet. Quaternary Proceedings, 6: 121-142.

Leng, M.J. (2003). Stable isotopes in lakes and lake sediment archives. (Eds) Mackay, A.W., Battarbee, R.W., Birks, H.J.B., and Oldfield, F. Global change in the Holocene. London., Arnold. pp. 124-139.

Leng, M.J. and Marshall, J.D. (2004). Palaeoclimate interpretation of stable isotope data from lake sediment archives. Quaternary Science Reviews, 23: 811-831.

Li, H.-C. and Ku, T.-L. (1997). $\delta^{13}C$-$\delta^{18}O$covariance as a palaeohydrological indicator for closed-basin lakes. Palaeogeography Palaeoclimatology Palaeoecology, 133: 69-80.

LI, H.-C., Ku, T.-L.., Stott, L.D., and Chen, W.-J. (1998). Applications of interannual- resolution stable isotope records of speleotherms: climatic changes in Beijing and Tianjin, China during the past 500 years- the $\delta^{18}O$ record. Science in China (Series D), 41: 362- 368.

Liang, E., Shao, X., Kong, Z., and Lin, J. (2003). The extreme drought in the 1920s and its effect on tree growth deduced from tree ring analysis: a case study in North China. Annals of Forest Science, 60: 145-152.

Lister, G.S., Kelts, K., Zao, C.K., Yu, J.Q., and Niessen, F. (1991). Lake Qinghai, China- Closed-Basin Lake Levels and the Oxygen Isotope Record for Ostracoda Since the Latest Pleistocene. Palaeogeography Palaeoclimatology Palaeoecology, 84: 141-162.

Liu, X.D. and Chen, B. (2002). Climate warming in the Tibetan Plateau during recent decades. International Journal of Climatology, 20: 1729-1742.

Liu, X.Q., Shen, J., and Wang, S.M. (2002). A 16,000 year pollen record of Qinghai Lake and its paleoclimate and paleoenvironment. Chinese Science Bulletin, 47: 1931-1936.

Lowe, J.J. (1991) Radiocarbon dating: recent applications and future potential. Quaternary Proceedings, 1: 1-89.

Lowe, J.J. and Walker, M.J.C. (1997). Reconstructing Quaternary environments. Longman.

Mackay, A.W., Ryves, D.B., Battarbee, R.W., Flower, R.J., Granin, N., Jewson, D., Rioual, P.M.J., and Sturm, M. (In press). 1000 years of climate variability in central Asia: assessing the evidence

using Lake Baikal (Russia) diatom assemblages and the application of a diatom-inferred model of snow cover on the lake. Global and Planetary Change.

Mackereth, F.J.H. (1969). A short core sampler for sub aqueous deposits. Limnology and Oceanography, 14: 145-151.

Magny, M. (1994) Solar influences on Holocene climatic changes illustrated by correlations between past lake-level fluctuations and the atmospheric ^{14}C record. Quaternary Research, 40: 1-9.

Magny, M. (2004) Holocene climate variability as reflected by mid-European lake-level fluctuations and its probable impact on prehistoric human settlements. Quaternary International, 113: 65-79.

Mann, M.E., Bradley, R.S., and Hughes, M.K. (1988). Global- scale temperature patterns and climate forcing over the past six centuries. Nature, 392: 779-787.

Mann, M.E., Bradley, R.S., and Hughes, M.K. (1999). Northern hemisphere temperatures during the past millennium: inferences, uncertainties, and limitations. Geophysical Research Letters, 26: 759-762.

Marchitto, T.M., Curry, W.B., and Oppo, D.W. (1998). Millennial-scale changes in North Atlantic circulation since the last glaciation. Nature, 393: 557-581.

McKenzie, J. (1985). Carbon isotopes and productivity in the lacustrine and marine environment. (Eds) Stumm, W. Chemical processes in lakes. London, Wiley.

McKenzie, J. and Hollander, D. (1993). Oxygen-isotope record in recent carbonate sediments from Lake Greifen, Switzerland (1750-1986): application of continental isotopic indicator for evaluation of changes in climate and atmospheric circulation patterns. Climate change in the continental isotope records. Washington, AGU.PP. 101-111.

Meehl, G.A. (1997). The South Asian monsoon and the tropospheric biennal oscillation. Journal of Climate, 10: 1921-1943.

Merlivat, L. and Jouzel, J. (1979). Global climate interpretation of the deuterium- oxygen 18 relationship for precipitation. Journal of Geophysical Research, 84: 5029-5033.

Meyers, P. A. and Teranes, J. (2001). Sediment organic matter. (Eds) Last, W.M. and Smol, J.P. Tracking environmental change using lake sediments: physical and geochemical methods, Kluwer pp. 239-269.

Meyers, P.A. and Lallier- Vergas, E. (1999). Lacustrine sedimentary organic matter records of Late Quaternary paleoclimates. Journal of Paleolimnology, 21: 345-372.

Mischke, S. (2001). Mid and Late Holocene palaeoenvironment of the lakes Eastern Juyanze and Sogo Nur in NW China, based on ostracod species assemblages and shell chemistry. Berliner Geowissenschaftliche Abhandlungen, 35: 1-31.

Mischke, S., Demske, D., and Schudack, M.E. (2003). Hydrologic and climate implications of a multi-disciplinary study of the mid to late Holocene Lake Eastern Juyanze. Chinese Science Bulletin, 48: 1411-1417.

Molnar, P., England, P., and Martiod, J. (1993). Mantle dynamics, uplift of the Tibetan Plateau and the Indian Monsoon development. Review of Geophysics, 34: 357-396.

Mook, W.G. (1986). Recommendations/ resolutions adopted by the 12th International Radiocarbon Conference. Radiocarbon, 28: 799.

Morrill, C., Overpeck, J.T., and Cole, J.E. (2003). A synthesis of abrupt changes in the Asian summer monsoon since the last deglaciation. The Holocene, 13: 465-476.

Murray, F.W. (1967). On the computation of saturation vapor pressure. Journal of Applied Meteorology, 6: 203-204.

Olsson, I. (1991). Accuracy and precision in sediment chronology. Hydrobiologia 214: 25-34.

Olsson, I. (1986). Radiometric dating. (Eds) Berglund, B.E. Handbook of Holocene palaeoecology and palaeohydrology. New York, Wiley. pp. 273-312.

Overpeck, J.T., Anderson, D., Trumbore, S., and Prell, W. L. (1996). The southwest Indian monsoon over the last 18,000 years. Climate Dynamics, 12: 213-225.

Paulsen, D.E., Li, H.-C., and Ku, T.-L. (2003) Climate variability in central China over the last 1270 years revealed by high- resolution stalagmite records. Quaternary Science Reviews, 22: 691-701.

Perry, A.H. and Walker, J.M. (1977). The ocean- atmosphere systems. White Plains, NY, Longman.

Porter, S.C. (2001). Chinese loess record of monsoon climate during the last glacial- interglacial cycle. Earth- Science Reviews, 54: 115-128.

Porter, S.C. (2003) Eolian, alluvial, lacustrine, glacial and periglacial geology along the southern margin of Qinghai Lake. (Eds) Porter, S.C. Guidebook for Qinghai Lake Field Excursion. Workshop on Scientific Drilling at Qinghai Lake, Xining, P.R. China.

Porter, S.C. and An, Z.S. (1995). Correlation between climate events in the North Atlantic and China during the last glaciation. Nature, 375: 305-308.

Porter, S.C., Singhvi, A., An, Z.S., and Lai, Z. P. (2001). Luminescence age and palaeoenvironmental implications of a Late Pleistocene ground wedge on the northeastern Tibetan Plateau. Permafrost and Periglacial Processes, 12: 203-210.

Prell, W.L. and Kutzbach, J.E., (1987). Monsoon variability over the past 150,000 years. Journal of Geophysical Research, 92: 8411-8426.

Pye, K. and Zhou, L.P. (1989). Late Pleistocene and Holocene aeolian dust deposition in North China and the Northwest Pacific Ocean. Palaeogeography Palaeoclimatology Palaeoecology, 73: 11-23.

Qian, Y.F., Zheng, Y.Q., Zhang, Y., and Miao, M.Q. (2003). Responses of China's summer monsoon climate to snow anomaly over the Tibetan Plateau. International Journal of Climatology, 23: 593-613.

Qin, B. and Huang, Q. (1998). Evaluation of the climatic change impacts on the inland lake- a case study of Lake Qinghai, China. Climatic Change, 39: 695-714.

Rea, D.K. and Leinen, M. (1988). Asian aridity and the zonal westerlies: late Pleistocene and Holocene record of eolian deposition in the northwest Pacific Ocean. Palaeogeography Palaeoclimatology Palaeoecology, 66: 1-8.

Rea, D.K., Snoeck, H., and Joseph, L.H. (1998). Late Cenozoic eolian deposition in the North Pacific: Asian drying, Tibetan Uplift, and cooling of the Northern Hemisphere. Paleooceanography, 13: 215-224.

Ricketts, R.D. and Johnson, T.C. (1996). Climate change in the Turkana basin as deduced from a 4000 year long delta O-18 record. Earth and Planetary Science Letters, 142: 7-17.

Rochen, A., de Vernal, A., Sejrup, H.-P., and Haflidason, H. (1998). Palynological evidence of climate and oceanographic change in the North Sea during the last deglaciation. Quaternary Research, 49: 197-207.

Romanek, C.S., Grossman, E.L., and Morse, J. W. (1992). Carbon isotopes fractionation in synthetic aragonite and calcite: effects of temperature and precipitation rate. Geochimica et Cosmochimica Acta, 56: 419-430.

Rosenmeier, M.F., Brenner, M., Hodell, D.A., Martin, J.B., and Binford, M.W. (In press). Quantitative assessments of Holocene environmental change in Peten, Guatemala: predictive models of Catchment hydrology and lake water $\delta^{18}O$ values.

Rost, K.T. (2000). Pleistocene palaeoenvironmental changes in the high mountain ranges of central China and adjacent regions. Quaternary International, 65/66: 147-160.

Rozanski, K., Araguas- Araguas, L., and Gonfiantini, R. (1992). Relation between long-term trends of oxygen-18 isotope composition of precipitation and climate. Science, 258: 981-985.

Rozanski, K., Araguas-Araguas, L., and Gonfiantini, R. (1993). Isotopic patterns in modern global precipitation. (Eds) Swart, P.K., Lohmann, K.C., McKenzie, J., and Savin, S. Climate Change in Continental Isotopic Records. Washington, American Geophysical Union. pp. 1-36.

Severinghaus, J.P., Sowers, T., Brook, E.J., Alley, R.B., and Bender, M.L. (1998). Timing of abrupt climate change at the end of the Younger Dryas interval from thermally fractioned gases in polar ice. Nature, 391: 141-146.

Shi, P. and Song, C. (2003). Palynological records of environmental changes in the middle part of Inner Mongolia, China. Chinese Science Bulletin, 48: 1433-1438.

Shi, Y.F. (2002). Characteristics of late Quaternary monsoonal glaciation on the Tibetan Plateau and in East Asia. Quaternary International, 97-98: 79-91.

Shi, Y.F. and Liu, S. (2001). Estimation on the response of glaciers in China to the global warming in the 21st century. Chinese Science Bulletin, 45: 668-672.

Shi, Y.F., Kong, Z.C., and Wang, S.M. (1993). Mid-Holocene climates and environment in China. Global and Planetary Change, 7: 219-233.

Shi, Y.F., Kong, Z.C., and Wang, S.M. (1994). The climate fluctuation and important events of Holocene Megathermal in China. Science in China Series B- Chemistry Life Sciences & Earth Sciences, 37: 353-365.

Shi, Y.F., Zheng, B.X., and Li, S. (1992). Last glaciation and maximum glaciation in the Qinghai-Xizhang (Tibet) Plateau: a controversy to M. Kuhle's ice sheet hypothesis. Zeitschrift fur Geomorpholqie Band 84, 19-35.

Shindell, D.T., Schmidt, G.A., Mann, M.E., Rind, D., and Waple, A. (2001). Solar forcing of regional climate change during the maunder minimum. Science, 294: 2149-2152.

Silliman, J.E., Meyers, P.A., and Bourbonniere, R.A. (1996). Record of post glacial organic matter delivery and burial in sediments of Lake Ontario. Organic Geochemistry, 24: 463-472.

Sirocko, F., Garbe-Schonber, D., McIntyre, A., and Molfino, B. (1996). Teleconnections between the subtropical monsoons and high- Latitude climate during the Last Deglaciation. Science, 272: 526-529.

Smart, P.L. and Frances, P.D. (1992). Quaternary dating methods. London, Quaternary Research Association.

Smith, B.N. and Epstein, S. (1971). Two categories of $^{13}C/^{12}C$ ratios for higher plants. Plant Physiology, 47: 380-384.

Stager, J.C. and Mayewski, P.A. (1997) Abrupt early to mid-Holocene climatic transition registered at the equator and the poles. Science, 276: 1834-1836.

Steig, E.J. (1999). Palaeoclimate- Mid- Holocene climate change. Science, 286: 1485-1487.

Street-Perrott, F.A., Huang, Y.S., Perrott, R.A., Eglinton, G., Barker, P., Ben Khelifa, L., Harkness, D.D., and Olago, D.O. (1997). Impact of lower atmospheric carbon dioxide on tropical mountain ecosystem. Science, 278: 1422-1426.

Stuiver, M. and Reimer, P.J. (1993). Extended ^{14}C data base and revised CALIB 3.0 ^{14}C age calibration program 1993. Radiocarbon, 35: 215-230.

Stuiver, M., Reimer, P.J., Bard, J., Beck, J.W., Burr, G.S., Hughenm K.A., Kromer, B., McCormac, G., van der Plicht, J., and Spurk, M. (1998). INTCAL98 Radiocarbon age calibration, 24,000-0 BP. Radiocarbon, 40: 1041-1083.

Su, Z. and Shi, Y.F. (2002). Response of monsoonal temperature glaciers to global warming since the Little Ice Age. Quaternary International, 97-8: 123-131.

Suli, N.H., Goswani, B.N., Vinayachandra, P.N., and Yamagata, T. (1999). A dipole mode in the tropical Indian Ocean. Nature, 401: 360-363.

Sun, D.P., Tang, Y., Xu, Z.Q., and Han, Z.M. (1992). A preliminary investigation on chemical evolution of the Qinghai Lake water. Bulletin of Chinese Science, 3: 507-511.

Talbot, M.R. (1990). A review of the palaeohydrological interpretation of carbon and oxygen ratios in primary lacustrine carbonates. Chemical Geology (Isotope Geosciences Section), 80: 261-279.

Tao, S.Y. and Chen, L.X. (1987). A review of recent research on the East Asian summer monsoon in China. 60-92. (Eds) Change, C.P. and Krishnamurti, T. N. Oxford University Press.

Tarutani, T., Clayton, R.M., and Mageda, T.K. (1969). The effect of polymorphism and magnesium substitution on oxygen isotope fractionation between calcium carbonate and water. Geochimica et Cosmochimica Acta, 33: 987-996.

Taylor, K.C., Lamorey, G.W., Doyle, G.A., Alley, R.B., Grootes, P.M., Mayewski, P.A., White, J.W.C., and Barlow, L.K. (1993). The flickering switch of Late Pleistocene climate change. Nature, 361: 432-436.

Telford, R.J., Heegaard, E., and Birks, H.J.B (2004). All age-depth models are wrong: but how badly? Quaternary Science Reviews, 23: 1-5.

Thompson, L.G. (2000). Ice core evidence for climate change in the Tropics: implications for our future. Quaternary Science Reviews, 19: 19-35.

Thompson, L.G., Mosley-Thompson, E., Davis, M.E., Bolzan, J.F., Dai, J., Yao, T., Gundestrup, N., Wu, X., Klein, L., and Xie, Z. (1989). Holocene Late Pleistocene Climatic Ice core Records from Qinghai- Tibetan Plateau. Science, 246: 474-477.

Thompson, L.G., Mosley-Thompson, E., Davis, M.E., Lin, P.N., Henderson, K.A., and Mishiotta, T.A. (2003). Tropical glacier and ice core evidence of climate change on annual to millennial timescales. Climatic Change, 59: 137-155.

Thompson, L.G., Yao, T., Davis, M.E., Henderson, K.A., Mosley-Thompson, E., Lin, P.N., Beer, J., Synal, H.A., Coledai, J., and Bolzan, J.F. (1997). Tropical climate instability: The last glacial cycle from a Qinghai- Tibetan ice core. Science 276: 1821-1825.

Thompson, L.G., Yao, T., Mosley-Thompson, E., Davis, M.E., Henderson, K.A., and Lin, P.N. (2000). A high- resolution millennial record of the South Asian Monsoon from Himalayan ice cores. Science, 289: 1916-1919.

Tian, L., Yao, T., Schuster, P.F., White, J.W.C., Ichiyanagi, K., Pendall, E., Pu, J., and Yu, W. (2003). Oxygen 18 concentrations in recent precipitation and ice cores on the Tibetan Plateau. Journal of Geophysical Research, 108:16-10.

Tian, L., Yao, T., Sun, W., Stievenard, M., and Jouzel, J. (2001). Relationship between □D and □^{18}O in precipitation on north and south of the Tibetan Plateau and moisture recycling. Science in China (Series D), 44: 789-796.

Tucker, M.E. and Wright, V.P. (1990). Carbonate sedimentology. Oxford, Blackwell Scientific Publications.

Turpen, J.B. and Angell, F.W. (1971). Aspects of moulting and calcification in the ostracode Heterocypris. Biological Bulletin, 140: 331-338.

Van Campo, E. and Gasse, F. (1993). Pollen- Inferred and Diatom- Inferred Climatic and Hydrological Changes in Sumxi Co Basin (Western Tibet) since 13,000 Yr BP. Quaternary Research, 39: 300-313.

Van Campo, E., Cour, P., and Hang, S.X. (1996). Holocene environmental changes in Bangong Co basin (Western Tibet). Part 2: The pollen record. Palaeogeography Palaeoclimatology Palaeoecology, 120: 49-63.

van Geel, B., Raspopov, O.M., Renssen, H., ven der Plicht, J., Dergachev, V.A. and Meijer, H.A.J. (1999) The role of solar forcing upon climate change. Quaternary Science Reviews, 18: 331-338.

Verschuren, D., Laird, K.R., and Cumming, B.F. (2000). Rainfall and drought in equatorial east Africa during the past 1100 years. Nature, 403: 410-414.

von Grafenstein, U., Erlenkeuser, H., and Trimborn, P. (1999). Oxygen and carbon isotopes in modern freshwater ostracod valves: assessing vital offsets and autoecological effects of interest for palaeoclimate studies. Palaeogeography Palaeoclimatology Palaeoecology, 152: 133-152.

Wang, B., Wu, R., and Lau, K.-M. (2001a). Interannual variability of the Asian summer monsoon: contrasts between the Indian and the Western North Pacific- East Asian monsoons. Journal of Climate, 14: 4073-4090.

Wang, R.L., Scarpitta, S.C., Zhang, S.C., and Zheng, M.P. (2002). Later Pleistocene/ Holocene climate conditions of Qinghai- Xizhang Plateau (Tibet) based on carbon and oxygen stable isotopes of Zabuye Lake sediments. Earth and Planetary Science Letters, 203: 461-477.

Wang, S., Gong, D., and Zhu, J.H., (2001b). Twentieth –century climatic warming in China in the context of the Holocene. The Holocene, 11: 313-321.

Webster, P.J. (1998). Monsoons: processes, predictability and the prospects for predication. Journal of Geophysical Research, 103: 14451-144510.

Webster, P.J., Moore, A.M., Loschigg, J.P., and Leben, R.R. (1999). Coupled ocean-atmosphere dynamics in the Indian Ocean during 1997-98. Nature, 401: 356-360.

Wei, K. and Gasse, F. 91999). Oxygen isotopes in lacustrine carbonates of West China revisited: implications for post glacial changes in summer monsoon circulation. Quaternary Science Reviews, 18: 1315-1334.

Winkler, M.G. and Wang, P.K. (1993). The late Quaternary vegetation and climate of China. 221-261. (Eds) Wright, H.E. Global climates since the last glacial maximum. Minneapolis, University of Minnesota Press.

Wolfe, B.B., Aravena, R., Abbott, M.B., Seltzer, G.O., and Gibson, J.J. (2001). Reconstruction of paleohydrology and palaeohumidity from oxygen isotope records in the Bolivian Andes. Palaeogeography Palaeoclimatology Palaeoecology, 176: 177-192.

Woodhouse, C.A. and Overpeck, J.T. (998). 2000 years of drought variability in the central United States. Bulletin of the American Meteorological Society, 79: 2693-2714.

Xia, J., Ito, E., and Engstrom, D.R. (1997). Geochemistry of ostracode calcite: Part 1: an experimental determination of oxygen isotope fractionation. Geochimica et Cosmochimica Acta, 61: 377-382.

Yan, G., Wang, F.B., Shi, G.R., and Li, S.F. (1999). Palynological and stable isotopic study of palaeoenvironmental changes on the northeastern Tibetan Plateau in the last 30,000 years. Palaeogeography Palaeoclimatology Palaeoecology, 153: 147-159.

Yan, J.P. (1998). Numerical modelling of topographically-closed lakes: impact of climate on lake level, hydrochemistry and chemical sedimentation. Tubinger Geowissenschaftliche Arbeiten (TGA), 46: 1-145.

Yan, J.P., Hinderer, M and Einsele, G. (2001). Geochemical evolution of closed basin lakes: general model and application to Lakes Qinghai and Turkana. Sedimentary Geology,

Yang, B., Braeuning, A., and Shi, Y.F. (2003a). Late Holocene temperature fluctuations on the Tibetan Plateau. Quaternary Science Reviews, 22: 2335-2344.

Yang, B., Braeuning, A., Johnson, K.R., and Yafeng, S. (2002). General characteristics of temperature variation in China during the last two millennia. Geophysical Research Letters, 29: 38-1-38-4.

Yang, S. (1996). ENSO- snow-monsoon associations and seasonal –interannual predictions. International Journal of Climatology, 16: 125-134.

Yang, S. and Xu, L. (1994). Linkage between Eurasian winter snow cover and regional Chinese summer rainfall. International Journal of Climatology, 14: 739-750.

Yang, W., Spencer, R.J., Krouse, H.R., Lowenstein, T.K., and Casa, E. (1995). Stable isotopes of lake and fluid inclusion brines, Dabusun Lake, Qaidam Basin, western China: hydrology and palaeoclimatology in arid environments. Palaeogeography Palaeoclimatology Palaeoecology, 117: 279-290.

Yang, X.D., Kamenik, C., Schmidt, R., and Wang, S.M. (2003b). Diatom-based conductivity and water-level inference models from Eastern Tibetan (Qinghai- Xizang) Plateau lakes. Journal of Paleolimnology, 30: 1-19.

Yang, X.P., Liu, T.S., and Xiao, H.L. (2003c). Evolution of megadunes and lakes in the Badain Jaran Desert, Inner Mongolia, China during the last 31,000 years. Quaternary International, 104: 99-112.

Yao, T.D., Shi, Y.F., and Thompson, L.G. (1997a). High resolution record of paleoclimate since the little ice age from the Tibetan ice cores. Quaternary International, 37: 19-23.

Yao, T.D., Thompson, L.G., and Shi, Y.F. (1997b). Climate variation since the last deglaciation recorded in the Guliya ice core. Science in China, Series D, 40: 662-668.

Yao, T.D., Xie, Z.C., Wu, X.L. and Thompson, L.G. (1991). Climate- Change Since the Little Ice-Age Recorded by Dunde Ice Cap. Science in China Series B- Chemistry Life Sciences & Earth Sciences, 34: 760-767.

Yu, J.Q. and Kelts, K.R. (2002). Abrupt changes in climatic conditions across the late-glacial/ Holocene transition on the N.E. Tibet- Qinghai Plateau: evidence from Lake Qinghai, China. Journal of Paleolimnology, 28: 195-206.

Yuan, F. (2003). Late Holocene hydrologic and climate variability in the Walker Lake Basin, Nevada and California. Unpublished Ph.D. Thesis. pp. 167.

Yurtsever, Y. and Gat, J.R. (1981). Atmospheric waters. (Eds) Gatand, J.R. and Gonfiantini, R. Stable-isotope hydrology. IAEA Technical report series 210, pp. 103-142.

Zeebe, R.E. (1999). An explanation of the effects of seawater carbonate concentration on foraminiferal oxygen isotopes. Geochimica et Cosmochimica Acta, 13/14: 2001-2007.

Zhang, J.W., Ming, J., Chen, F., Battarbee, R.W., and Henderson, A.C.G. (2003). High- resolution precipitation variations in the Northeast Tibetan Plateau over the last 800 years documented by sediment cores of Qinghai Lake. *Chinese Science Bulletin*, 48: 1451-1456.

Zhang, X., Nakawo, M., Yao, T., Han, J., and Xie, Z. (2002). Variations of stable isotopic compositions in precipitation on the Tibetan Plateau and its adjacent regions. Science in China (Series D), 45: 481-493.

Zheng, B.X., Xu, Q., and Shen, Y.P. (2002). The relationship between climate change and Quaternary glacial cycles on the Qinghai- Tibetan Plateau: review and speculation. Quaternary International, 93-101.

Zhou, W.J., Donahue, D., Porter, S.C., Jull, A.J.T., Li, X.Q., Stuiver, M., An, Z., Matsumota, E., and Dong, G. (1996). Variability of Monsoon Climate in East Asia at the end of the Last Glaciation. Quaternary Research, 46: 219-229.

Zhou, W.J., Head, M.J., An, Z.S., De Deckker, P., Liu, Z.Y., Liu, X.D., Lu, X.F., Donahue, D., Jull, A.J.T., and Beck, J.W. (2001a). Terrestrial evidence for a spatial structure of tropical-polar interconnections during the Younger Dryas episode. Earth and Planetary Science Letters, 191: 231-239.

Zhou, W.J., Head, M.J., and Deng, L. (2001b). Climate changes in northern China since the late Pleistocene and its response to global change. Quaternary International, 83-85: 285-292.

Zhou, W.J., Head, M.J., Lu, X.F., An, Z.S., Jull, A.J.T., and Donahue, D. (1999). Teleconnection of climatic events between East Asia and polar, high latitude areas during the last deglaciation. Palaeogeography Palaeoclimatology Palaeoecology, 152: 163-172.

Zhou, Z., Chen, F., Pan, B.T., and Derbyshire, E. (1991). Environmental changes during the Holocene in the western China on millennial timescale. The Holocene, 1: 151-156.

Zhu, Y. (2001). The Holocene Pollen from the lake sediments and environmental changes in the Shiyang river drainage, arid China. Lanzhou University, Unpup. Ph.D. Thesis.

Zhu, Y., Chen, F., and Madsen, D.B. (2001). Environmental signal of early Holocene pollen record from Shiyang River basin lake sediments, NW China. Chinese Science Bulletin, 47: 267-273.

Zuber, A. (1983). On the environmental isotope method for determining the water balance components of some lakes. Journal of Hydrology, 61: 409-427.

Appendix 1
XRD Results

XRD for QING6 (Fig. I)
XRD for QING10 (Fig. II)
XRD for QHE2 (Fig. III)
XRD for GAHA1 (Fig. IV)

SEM photographs

Calcite (Fig. V)
Aragonite (Fig. VI)

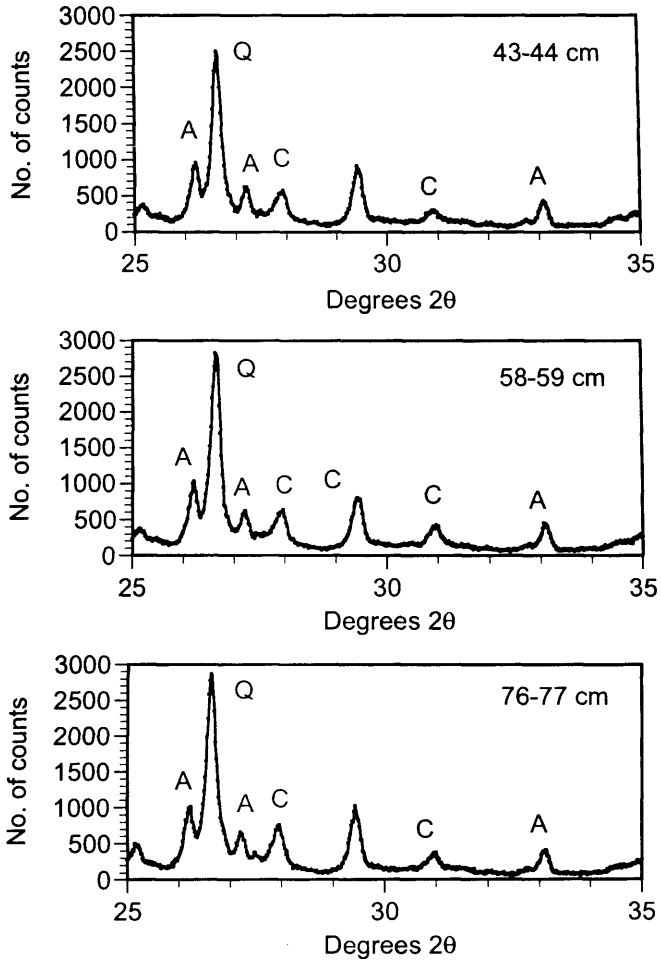

Figure I – XRD results for QING6. Q = quartz, C = calcite, A = aragonite

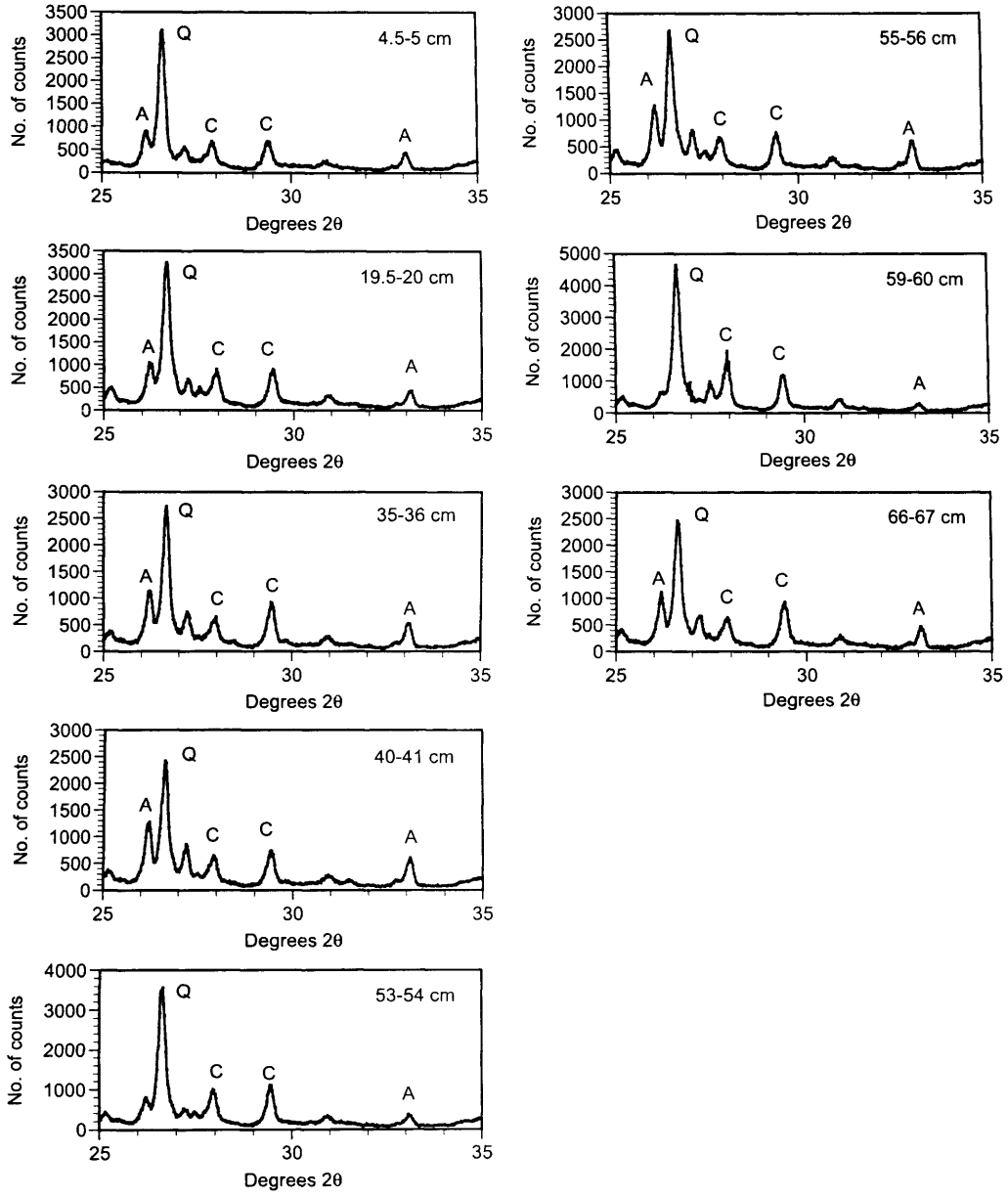

Figure II – XRD results for QING10. Q = quartz, C = calcite, A = aragonite

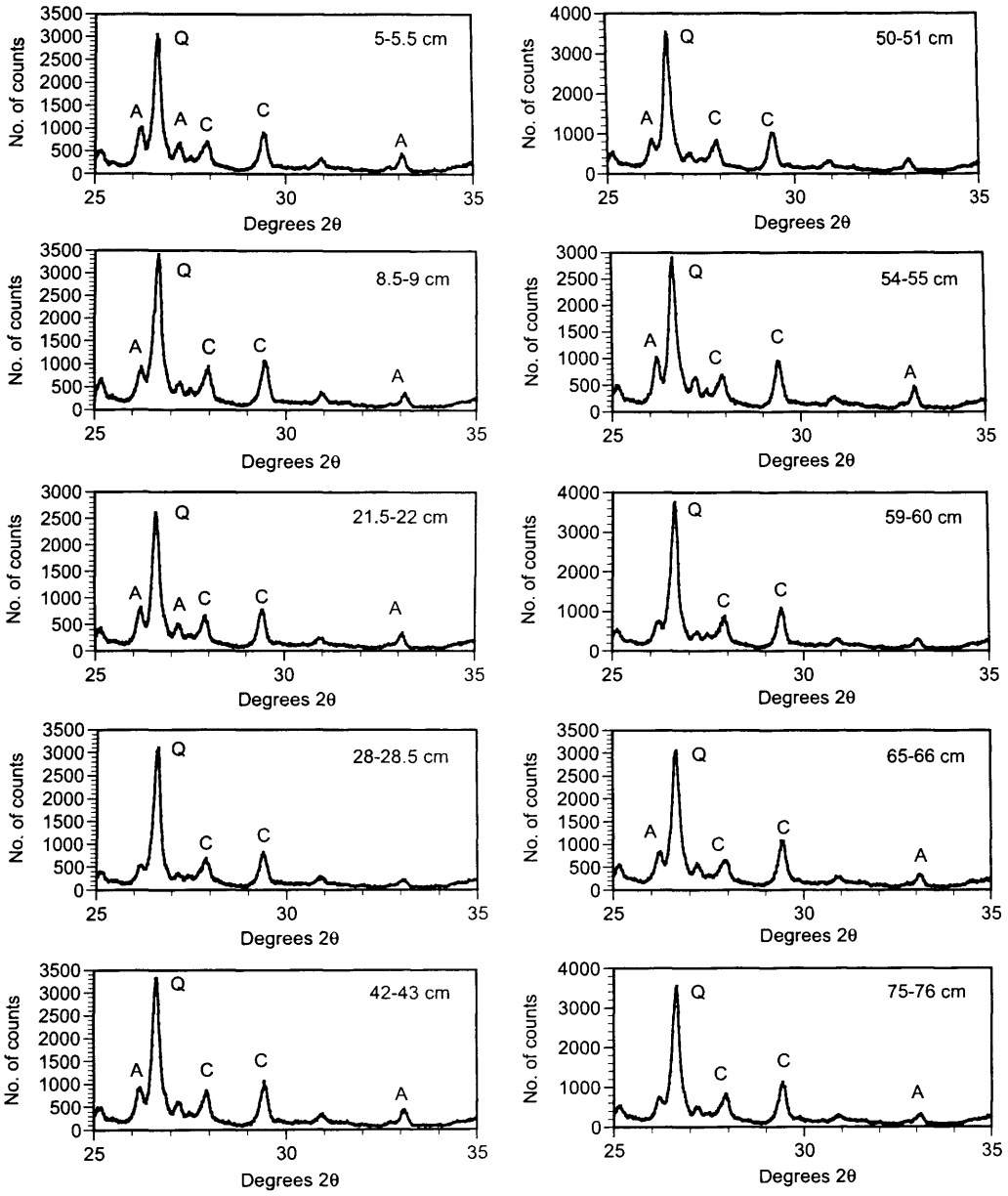

Figure III – XRD results for QHE2. Q = quartz, C = calcite, A = aragonite

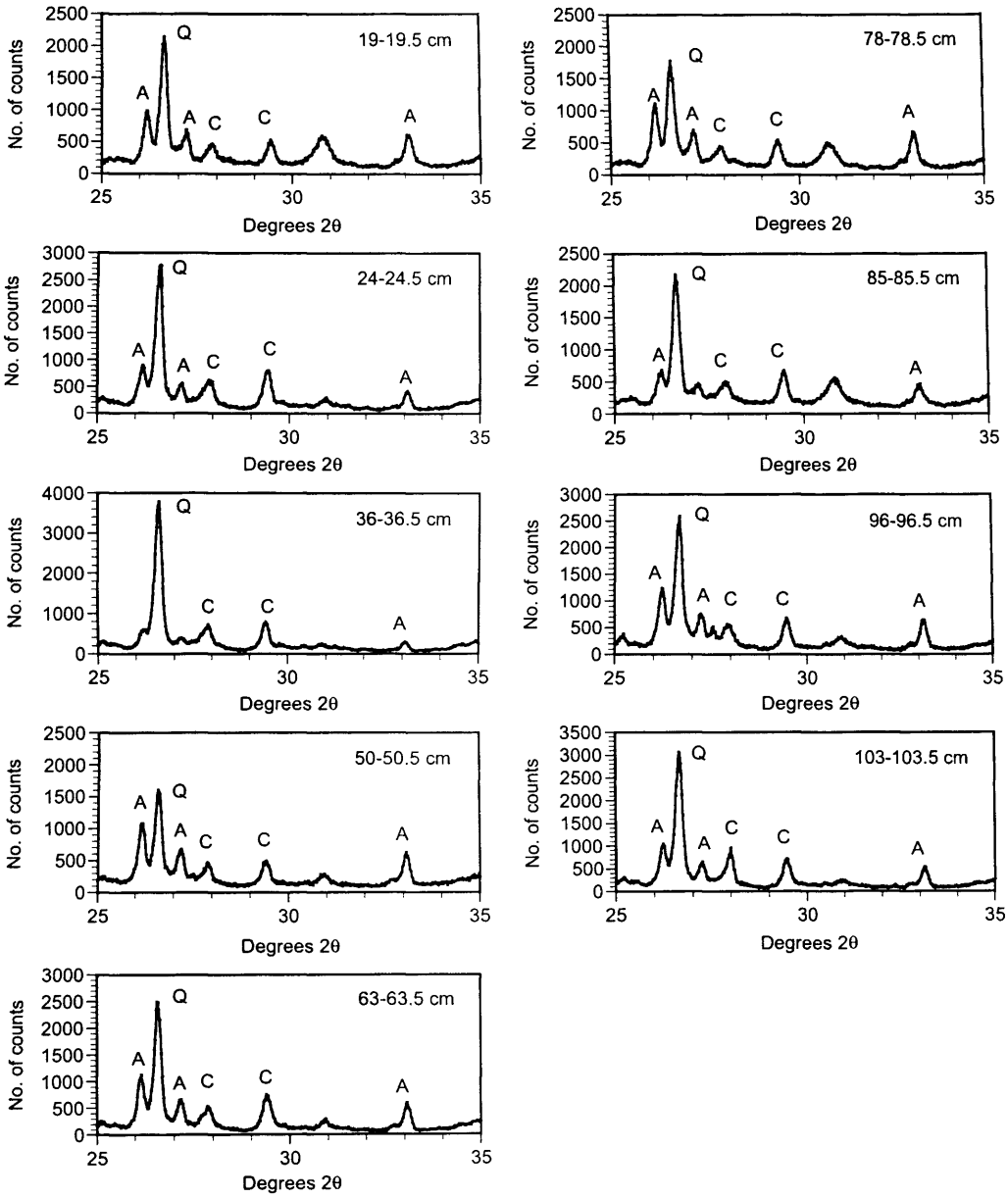

Figure IV – XRD results for GAHA1. Q = quartz, C = calcite, A = aragonite

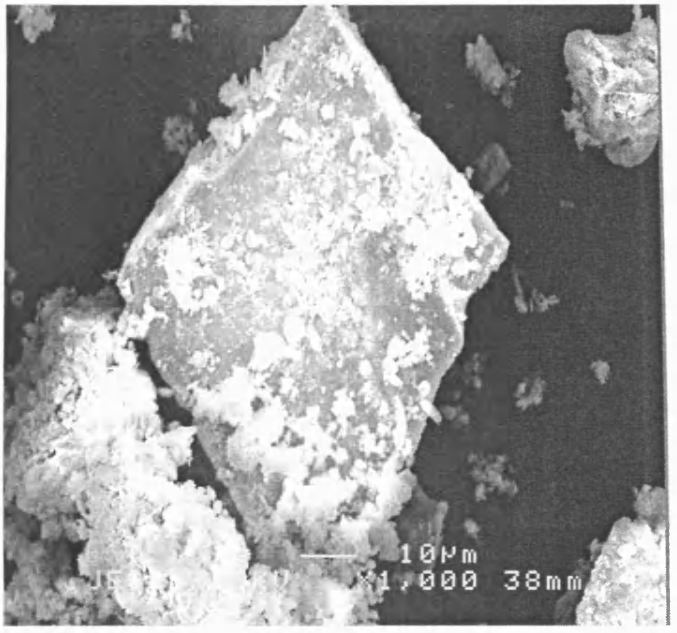

Figure V – SEM picture of calcite

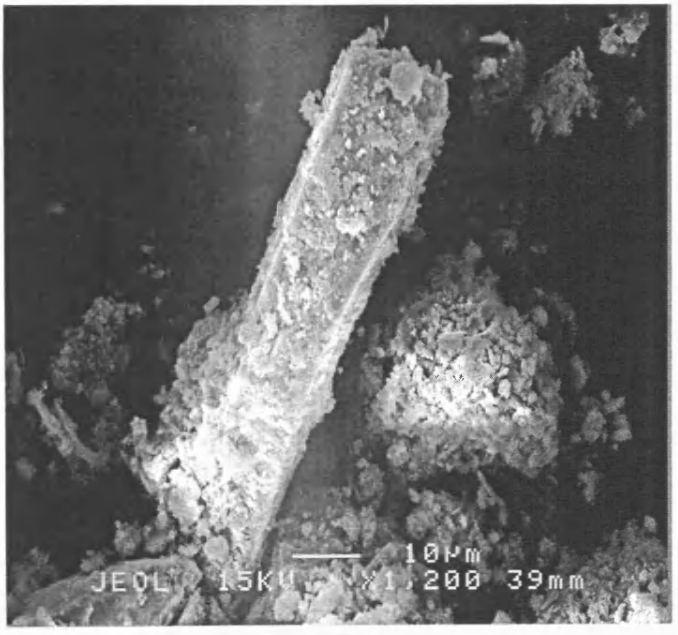

Figure VI – SEM picture of aragonite

Appendix II

Other results

CD includes: QING6 isotope data

QING10 isotope data

QHE2 isotope data

GAHA1 isotope data

Modern waters and surface sediment isotope data

Age models for QING6, QING10, QHE2 and GAHA1